Development of a Chemoenzymatic (-)-Menthol Synthesis

Entwicklung einer chemoenzymatischen (-)-Menthol Synthese

Von der Fakultät 3: Chemie der Universität Stuttgart zur Erlangung der Würde eines Doktors der Naturwissenschaften (Dr. rer. nat.) genehmigte Abhandlung

Vorgelegt von

Nico Kreß

aus Stuttgart

Hauptberichter:	Prof. Dr. Bernhard Hauer
Mitberichter:	Prof. Dr. René Peters
Vorsitzender:	Prof. Dr. Elias Klemm
Tag der mündlichen Prüfung:	18.06.2018

Institut für Biochemie und Technische Biochemie der Universität Stuttgart

Abteilung für Technische Biochemie

2018

Opening statement

The presented work was developed at the suggestion and under supervision of Prof. Dr. Bernhard Hauer from January 2015 to April 2018 at the Institute of Biochemistry and Technical Biochemistry, Department of Technical Biochemistry at the University of Stuttgart.

Within the scope of this work the following publications have been released or are submitted:

Halter, W., **Kress**, **N.**, Otte, K., Reich, S., Hauer, B. & Allgöwer, F. Yield-Analysis of Different Coupling Schemes for Interconnected Bio-Reactors. *Proc. SIAM Conf. Control and its Applications* 384-391(Society for Industrial and Applied Mathematics, 2015).

Kress, **N.**, Rapp, J. & Hauer, B. Enantioselective Reduction of Citral Isomers in NCR Ene Reductase: Analysis of an Active-Site Mutant Library. *ChemBioChem* **18**, 717-720 (2017).

Bastian, S.A., Hammer, S.C., **Kreß**, **N.**, Nestl, B.M. & Hauer, B. Enabling New Selectivities in the Cyclization of Citronellal by Squalene Hopene Cyclase Variants. *ChemCatChem*, **9**, 4364–4368 (2017).

Kreß, **N.** & Hauer, B. Biologische und mechanistische Diversität von Enzymen als Basis für die Entwicklung artifizieller Biosynthesen. *BioSpektrum*, **7**, 836-838 (2017).

Kress, **N.**, Halder, J.M., Rapp, L.R. & Hauer, B. Unlocked potential of dynamic elements in protein structures: channels and loops. *Curr. Op. Chem. Biol.*, submitted.

Declaration of authorship

I hereby certify that the dissertation entitled "*Development of a Chemoenzymatic (-)-Menthol Synthesis*" is entirely my own work except where otherwise indicated. Passages and ideas from other sources have been clearly indicated.

Erklärung über die Eigenständigkeit der Dissertation

Ich versichere, dass ich die vorliegende Arbeit mit dem Titel „*Entwicklung einer chemoenzymatischen (-)-Menthol Synthese*" selbständig verfasst und keine anderen als die angegebenen Quellen und Hilfsmittel benutzt habe; aus fremden Quellen entnommene Passagen und Gedanken sind als solche kenntlich gemacht.

Name/Name: Nico Kreß

Signed/Unterschrift: _____

Date/Datum: Stuttgart, 09.04.2018

Acknowledgements

Mein besonderer Dank gilt Herrn Prof. Dr. Bernhard Hauer. Nicht allein, weil er mir die Durchführung meines spannenden Dissertations-Themas ermöglichte, sondern auch aufgrund seines Vertrauens in meine Arbeit und seine fortwährende Unterstützung. Dies ermöglichte mir große Freiheiten in der Erstellung dieser Arbeit.

Für die Übernahme des Nebengutachtens bedanke ich mich recht freundlich bei Prof. Dr. René Peters sowie auch bei Prof. Dr. Elias Klemm für die Übernahme des Prüfungsvorsitzes.

Ich möchte mich weiterhin herzlich bei Wolfgang Halter und Prof. Dr. Frank Allgöwer für die gemeinsame Arbeit zur Berechnung eines mathematischen Modells bedanken. Weiterhin bin ich PD Dr. Wolfgang Brandt für seine umfangreiche Unterstützung in der Einführung computerchemischer Berechnungen während meines Forschungsaufenthaltes in seiner Arbeitsgruppe sehr dankbar.

Ich möchte mich auch beim Fonds der Chemischen Industrie für die Unterstützung durch das Chemiefonds-Stipendium bedanken.

Zu Beginn der Dissertation hatte ich das Glück von der Erfahrung vieler hilfsbereiter Mitglieder der Abteilung der Technischen Biochemie profitieren zu können. Zuvorderst möchte ich mich hier bei Dr. Sabrina Reich bedanken, die mich all jenes lehrte, was mir den Weg zur erfolgreichen Durchführung meiner Doktorarbeit bereitete. Diesbezüglich gilt mein weiterer Dank insbesondere Dr. Stephan Hammer, Dr. Martin Weissenborn, Dr. Konrad Otte, Dr. Sandra Facey, Dr. Janosch Klebensberger und Dr. Silke Bastian.

Besonders dankbar bin ich auch für die durchgehende sowohl fachliche als auch moralische Unterstützung durch Dr. Bernd Nebel und Dr. Bettina Nestl, sowie für allgemeine Unterhaltungen im Laboralltag. Bei Bettina Nestl möchte ich mich insbesondere für die wertvolle Unterstützung bei der kritischen Durchsicht dieses Manuskripts bedanken, um nur eines von vielen Beispielen zu nennen.

Für wertvolle Hilfen organisatorischer Art gilt mein großer Dank auch Frau Christine Klumpp-Klug.

Ich hatte das Glück, im Rahmen dieser Arbeit Unterstützung durch sehr fähige Studenten zu erhalten. Dafür möchte ich mich sehr herzlich bei Johanna Rapp,

Friederike Dehli, Ira Lauer, Marie-Sophie Russ und Dennis Reil bedanken. Auch bei Julian Wissner möchte ich mich für seinen Einsatz bedanken.

Für die umfangreiche Korrektur dieser Arbeit spreche ich auch Sabrina Henche meinen besonderen Dank aus. Ihr, Svenja Kaspari und Jens Schmid bin ich allerdings viel dankbarer für die Freundschaft, die während unserer Zeit am ITB erwachsen ist. Diese bedeutet mir viel und trug sicher auch zum Gelingen einer erfolgreichen Arbeit bei. Insbesondere möchte ich mich bei Jens Schmid für die ganze Zeit seit dem Beginn unseres Studiums, seine Engagiertheit und seine große Unterstützung vielfältigster Art bedanken. Für die prägende gemeinsame Zeit während des Studiums danke ich auch meinen weiteren Studienkollegen des AK Mensa, allen voran Dennis Ergenzinger und den Mitgliedern der Fachschaft Chemie.

Für die gemeinsame Zeit und manch lustigen Moment bedanke ich mich auch bei Lars Hinner, Pascal Reis, meiner besten Nebensitzerin Maike Lenz, sowie auch bei Julia Halder und Sara Hoffmann. Für ein unterhaltsames, lehrreiches und hilfsbereites Arbeitsklima möchte ich mich zudem bei Lisa Steiner, Stefanie Kummer, Miriam Kuhn, Rebecca Demming, Max-Phillipp Fischer, Andreas Hunold, Dr. Sven Richter, Niels Borlinghaus, Sebastian Gergel, Dr. Juliane Stahmer, Dr. Sandra Notonier, Jörg Domenicus, Dr. Sebastian Löw, Matthias Wehrmann, Dr. Lisa Kühnel, Dr. Wendy Escobedo, Benjamin Aberle, Ludwig Bengel, Andreas Schneider, Lea Rapp, Peter Heinemann, Jan Klenk, Thorsten Henkes, Dr, Christine Gally, Dr. Daniel Scheps, Phillipp Trauzettel, Dr. Sandra Vlahovic, Leonie Schön, Dr. Jennifer Bolsinger, Dominique Darimont, Melanie Allgaier, Dr. Mihaela Antonovici und auch bei Dr. Tobias Kulschewski, Dr. Silvia Fademrecht, Prof. Dr. Jürgen Pleiss, Dr. Valerio Ferrario, Dr. Sven Benson, Patrick Buchholz, Catharina Zeil sowie Dr. Henrique Carvalho bedanken.

An dieser Stelle danke ich auch Adrian für die Unterstützung durch seine Freundschaft. Weiterhin bedanke ich mich bei meiner Familie, die mich stets bei allen meinen Vorhaben unterstützt hat. Meli, dir gilt mein besonderer Dank für all die Kraft und Nerven, die du mir stets gespendet hast als du mit mir gemeinsam durch all die Höhen und Tiefen, auch beim Verfassen dieser Arbeit, gegangen bist. Mein größter Dank gilt allerdings meinen Eltern, die es mir überhaupt erst ermöglicht haben, dass ich nach einem langen Weg nun diese Arbeit beenden kann. Das werde ich euch niemals vergessen.

Table of contents

List of abbreviations

°C	degree Celsius
D	dextro from lat. *dexter* = right
L	laevo from lat. l*aevus* = left
%	percent sign
% (*v*/*v*)	volume concentration
% (*w*/*v*)	mass concentration
% (*w*/*w*)	mass fraction
µ	micro
A	ampere; or: adenine; or: alanine
Å	Ångström
a.u.	arbitrary unit
Aac	*Alicyclobacillus acidocaldarius*
*Aac*SHC	squalene-hopene cyclase from *Alicyclobacillus acidocaldarius*
acac	acetylacetonate
ADH	alcohol dehydrogenase
A-H	amino acid acting as Brønsted acid
Amp	ampicillin
Ap.	appendix
APS	ammonium persulfate
aq.	aqueous
Ar	aryl
Arg variant	NCR variant W66A/I231R/F269V
*At*OYE1	ene reductase 1 from *Arabidopsis thaliana*
*At*OYE3	ene reductase 3 from *Arabidopsis thaliana*
ATR	attenuated total reflection
BFGS	Broyden–Fletcher–Goldfarb–Shanno algorithm
BINAP	2,2'-bis(diphenylphosphino)-1,1'-binaphthyl
bom	basis of mobility
BSA	bovine serum albumin
BVMO	Bayer-Villiger monooxygenase
c	concentration
cat.	catalyst
CHAPS	3-[(3-cholamidopropyl)dimethylammonio]-1-propanesulfonate
*Cm*OYE	ene reductase from *Corynebacterium aquaticum*
COD	1,5-cyclooctadiene
cww	cell wet weight
CYE	ene reductase from *Kluyveromyces marxianus*
d.r.	diastereomeric ratio
ddH_2O	double distilled water
DEAE	diethylaminoethyl
DMAPP	dimethylallyl pyrophosphate
DMSO	dimethyl sulfoxide
DNA	deoxyribonucleic acid
dNTP	deoxyribonucleotide
DpnI	a restriction endonuclease
*Dr*ER	ene reductase from *Deinococcus radiodurans*

DTT	dithiothreitol
DWP	deep-well plate
E	ger. *entgegen* = *trans*; or: energy
E. coli	*Escherichia coli*
e.e.	enantiomeric excess
e.g.	lat. *exempli gratia* = for example
E_a	activation barrier
EBP1	estrogen binding protein from *Candida albicans*
EDTA	ethylenediaminetetraacetic acid
Elu	elution
$E_{reaction}$	reaction energy
ERED	ene reductase
ERED_*R*	NCR variant W66A/I231R/F269V
et al.	lat. *et alii* = and others
EWG	electron withdrawing group
FID	flame ionization detector
FMN	flavin mononucleotide
fr. transf.	freshly transformed
FT	Fourier transform
fw	forward
g	gram; or: gravitational acceleration; or: gas
G	guanine; or: glycine
GC	gas chromatography
GC/MS	gas chromatography–mass spectrometry
GDH	glucose dehydrogenase
ger.	German
*Glu*ER	ene reductase from *Gluconobacter oxidans*
gly. stock	glycerol stock
GPP	geranyl pyrophosphate
h	hour
H-BEA	acidic form of zeolite Beta
H-MCM-41	acidic form of mobile composition of matter No. 41(mesoporous material)
HPLC	high performance liquid chromatography
H-Y	acidic form of zeolite type Y
i.e.	lat. *id est* = that is to say
IBTB	Institute of Biochemistry and Technical Biochemistry
IPP	isopentenyl pyrophosphate
IPTG	isopropyl-β-D-thiogalactopyranoside
IR	infrared
ISM	iterative site-saturation mutagenesis
isom.	isomerization
J	Joule
K	encodes nucleobases T and G; or: lysine; or: Kelvin
KAc	potassium acetate
Kan	kanamycin
kb	kilo base
kDa	kilo Dalton
L	liter
l	liquid
lat.	Latin
LB	lysogeny (Lauria-Bertani) broth

*Le*OPR1	ene reductase 1 from *Solanum lycopersicum*
*Le*OPR3	ene reductase 3 from *Solanum lycopersicum*
m	milli; or: meter
M	encodes nucleobases A and C; or: marker; or: moiety, or: molar
m	meta, or: mass
MD	molecular dynamics
MeO_2Ph	methyl benzoate
MEP	methylerythritol phosphate
MES	2-(*N*-morpholino)ethanesulfonic acid
MEV	mevalonate
MHz	megahertz
min	minute
MKII	mark II
MM	molecular mechanics
MMOK	molecular mechanics correction
MMR	menthone reductase from *Mentha piperita*
MOE	Molecular Operating Environment
MOPAC	Molecular Orbital PACkage
MOPS	3-(N-morpholino)propanesulfonic acid
MR	morphinone reductase from *Pseudomonas putida* M10
MTBE	methyl *tert*-butylether
n	nano
N	encodes nucleobases A, T, G and C; or: asparagine
n	amount of substance
NAD(P)H	nicotinamide adenine dinucleotide (phosphate)
NCR	2-cyclohexen-1-one reductase from *Zymomonas mobilis*
NemA	ene reductase from *E. coli*
NMR	nuclear magnetic resonance
*Nt*DBR	ene reductase from *Nicotiana tabacum*
OD	optical density
OYE	Old Yellow Enzyme
OYE1	Old yellow enzyme 1 from *Saccharomyces pastorianus*
OYE2	Old yellow enzyme 2 from *Saccharomyces cerevisiae*
OYE2.6	ene reductase from *Scheffersomyces stipitis* CBS 6054
OYE3	Old yellow enzyme 3 from *Saccharomyces cerevisiae*
p	pico
p	pressure
Pa	pascal
PCR	polymerase chain reaction
Pd/C	palladium on charcoal
pdb	protein data bank
PEG	polyethylene glycol
PETNR	Pentaerythritol tetranitrate reductase from *Enterobacter chloacae* PB2
pH	lat. *potentia hydrogenii*
Ph	phenyl
P_i	inorganic phosphate
pK_a	logarithmic form of acid dissociation constant
PMSF	phenylmethylsulfonyl fluoride
PP	pyrophosphate
Pro variant	NCR variant W66A/I231P/F269V
pur.	purified

QM	quantum mechanics
R	lat. *rectus* = right
R	residue; or: ideal gas constant
R^2	coefficient of determination
red.	reduction
rel. act.	relative activity
rev	reverse
rhaB	rhamnose promoter
*Rm*ER	ene reductase from *Ralstonia metallidurans*
rpm	revolutions per minute
RT	room temperature
S	lat. *sinister* = left
s	second; or: solid
SDS-PAGE	sodium dodecyl sulfate – polyacrylamide gel electrophoresis
SHC	squalene-hopene cyclase
SHC_*R*	*Aac*SHC variant A419G/Y420C/G600A
SOC	super optimal broth
T	thymine; or: threonine
T	temperature
t	time
TAE	Tris-acetate-EDTA
TB	terrific broth
TEMED	tetramethylethylenediamine
Tfb	transformation buffer
THF	tetrahydrofuran
TIC	total ion current
TIM	triosephosphate isomerase
TMS	tetramethylsilane
TOF	turnover frequency
TOYE	ene reductase from *Thermoanaerobacter pseudethanolicus* E3993
Tris	tris-(hydroxymethyl)-aminomethane
*Ts*OYE	ene reductase from *Thermus scotoductus*
U	uracil
uV	microvolt
UV/VIS	ultraviolet/visible
V	volt
V_{Gas}	gas volume
VOC	volatile organic compound
vs.	versus
wc	whole cell
wt	wild-type
WT	wild-type
YersER	ene reductase from *Yersinia bercovieri*
YqiG	ene reductase from *Bacillus subtilis* strain 168
YqjM	ene reductase from *Bacillus subtilis* strain 168
Z	ger. *zusammen = cis*
z. B.	zum Beispiel
*Zmo*SHC	squalene-hopene cyclase from *Zymomonas mobilis*

Abstract

Biocatalysis is an emergent research area for the development of efficient and sustainable synthesis processes. A crucial milestone for the better applicability of biocatalysts thereby consists of the increasing knowledge of the adaptability of enzymes for distinct synthetic needs like the conversion of specific molecular structures with defined selectivity. In addition, it is equally important to demonstrate that such novel catalysts are combinable among themselves and with established non-enzymatic catalysts to enable unexplored synthetic routes. Using the example of the chemoenzymatic synthesis of (-)-menthol from citral, this work therefore addresses the development and applicability of such evolved enzyme catalysts for the synthesis of an industrially relevant molecule.

In this complementary synthetic route inspired from an existing industrial process, a mixture of citral isomers is reduced to citronellal using an *R*-selective ene reductase. In a subsequent Prins reaction, the selective cyclization of *R*-citronellal to (-)-isopulegol is achieved by the application of an engineered squalene-hopene cyclase variant. The final reduction to (-)-menthol proceeds by hydrogenation on a palladium catalyst.

Especially the first catalytic step enables an immediate synthetic advantage in comparison to the currently performed industrial process. So far, no catalyst is applied converting *both* isomers of citral *R*-selectively at the same time. Both isomers have to be separated under high energy expenditure by distillation prior to reduction. No enzymatic catalyst is described displaying this reactivity yet. As, however, the opposite enantioconvergent *S*-selective citral reduction by ene reductases is known, the development of an enzyme catalyst constituted an attractive solution for this limitation. Hence, a focus of the work laid on the inversion of the *S*-selectivity of the citral reduction by NCR ene reductase from *Zymomonas mobilis* by enzyme engineering.

The studies started by characterization of the citral reduction by NCR wild-type. Next to the determination of the course of the reaction over time, semi-empiric quantum mechanics calculations on the oxidative half reaction of this conversion were carried out. The calculations suggest a so far undescribed catalytic role of an arginine at position 224 for a facilitated hydride transfer and a more complex proton shift involving water molecules in the reaction.

The subsequently performed engineering comprised the identification of selectivity determining amino acid positions W66, Y177, I231 and F269 in the active site of the enzyme followed by their variation in an iterative combinatorial fashion. In order to enable the analysis of the multitude of generated enzyme variants, a whole cell screening was developed using chiral gas chromatography. Thereby, the triple variant W66A/I231R/F269V was created converting *E*/*Z*-citral in the whole system to *R*-citronellal with an enantiomeric excess of 89 %. It could be determined that a cell-induced citral isomerization leads to increased enantioselectivity in comparison to using purified enzyme.

Especially for the influence of the selectivity-determining positions W66 and I231 an increased understanding of structure-function relations was achieved during the course of semi-rational enzyme evolution by the separated analysis of single citral isomers and by supportive *in silico* analyses like docking and molecular dynamics simulations.

The subsequent integration of the established variant A419G/Y420C/G600A of the squalene-hopene cyclase from *Alicyclobacillus acidocaldarius* is remarkable catalyzing the Prins cyclization to (-)-isopulegol with an enantiomeric excess of 99 % and a diastereoselectivity of 90 %. In this context, the enzyme's underlying Brønsted acid chemistry could be evolved towards the in nature unknown Prins reaction reactivity. In this work it could be shown that enzyme catalysts acquired by such chemical inspection can be implemented in application-oriented synthetic routes. In combination with the developed selective ene reductase, the bienzymatic cascade to (-)-isopulegol was successfully performed and characterized. For the final reduction to (-)-menthol an established heterogeneous catalyst like palladium on charcoal could be applied under hydrogen atmosphere. This demonstrates nicely that novel biocatalysts can be combined with approved synthetic processes. With the attained insights, highly valuable (-)-menthol was made accessible for the first time by a chemoenzymatic cascade using an isomeric mixture of citral on preparative scale with 7 % isolated yield. This work not only highlights different strategies for the development of novel biocatalysts, but also contributes to their possible synthetic applicability in the synthesis of industrially relevant molecules.

Zusammenfassung

Die Biokatalyse ist ein aufstrebendes Forschungsgebiet für die Entwicklung von effizienten und nachhaltigen Syntheseprozessen. Ein entscheidender Meilenstein für die breitere Anwendung von Biokatalysatoren besteht dabei im zunehmenden Verständnis der Anpassung von Enzymen an bestimmte synthetische Vorgaben wie z. B. die Umsetzung bestimmter Molekülstrukturen in einer definierten Selektivität. Daneben ist es ebenso entscheidend zu zeigen, dass solche neuartigen Katalysatoren untereinander und mit etablierten nicht-enzymatischen Katalysatoren kombiniert werden können, um unerforschte Syntheserouten zu ermöglichen. Am Beispiel der chemoenzymatischen Darstellung des (-)-Menthols aus Citral beschäftigt sich diese Arbeit daher mit der Entwicklung und Anwendbarkeit von solch evolvierten Enzymkatalysatoren für die Synthese eines industriell relevanten Moleküls.

In dieser an einen existierenden industriellen Prozess angelehnten komplementären Syntheseroute wird unter Verwendung einer evolvierten *R*-selektiven En-Reduktase zunächst ein Citral-Isomerengemisch zu Citronellal reduziert. In einer anschließenden Prins-Reaktion wird die selektive Zyklisierung des *R*-Citronellals zu (-)-Isopulegol durch Anwendung einer hierfür entwickelten Squalen-Hopen Zyklase erreicht. Die abschließende Reduktion zum (-)-Menthol erfolgt durch Hydrierung an einem Palladiumkatalysator.

Insbesondere im ersten katalytischen Schritt eröffnet sich ein unmittelbarer synthetischer Vorteil im Vergleich zum heute industriell durchgeführten Prozess. Da bisher kein Katalysator verwendet wird, welcher *beide* Isomere des Citrals zugleich *R*-selektiv umsetzt, werden die Isomere vor Beginn der Reduktion unter hohem Energieaufwand destillativ getrennt. Bisher ist kein enzymatischer Katalysator beschrieben, welcher diese Reaktivität aufweist. Da allerdings die umgekehrte enantiokonvergente *S*-selektive Citral-Reduktion für En-Reduktasen bekannt ist, stellte die Entwicklung eines Enzymkatalysators eine attraktive Lösung zur Beseitigung dieser Limitation dar. So lag ein Schwerpunkt der Arbeit in der Umkehrung der *S*-Selektivität der Citral-Reduktion durch die NCR En-Reduktase aus *Zymomonas mobilis* durch Enzym-Engineering.

Zunächst wurde hierfür die Reduktion des Citrals durch den NCR Wild-Typ charakterisiert. Neben der Bestimmung des zeitlichen Verlaufs der Reaktion wurden auch semiempirische quantenmechanische Berechnungen zur oxidativen Halbreaktion dieser Umsetzung durchgeführt. Die Berechnungen legen eine bisher nicht beschriebene katalytische Rolle eines Arginins an Position 224 für einen erleichterten Hydrid-Transfer sowie eine komplexere Protonen-Übertragung unter Einbeziehung von Wasser-Molekülen in der Reaktion nahe.

Das anschließend durchgeführte Engineering umfasste zu Beginn die Identifizierung der Selektivitäts-bestimmenden Aminosäurepositionen W66, Y177, I231 und F269 in der aktiven Tasche des Enzyms, die anschließend in iterativer Weise kombinatorisch variiert worden sind. Um die Analyse der Vielzahl an generierten Enzym-Varianten zu ermöglichen, wurde ein Ganzzell-Screening in Kombination mit gaschromatographischer Enantiomerentrennung entwickelt. Dabei konnte die NCR Dreifachvariante W66A/I231R/F269V generiert werden, die im Ganzzell-System *E*/*Z*-Citral mit einem Enantiomerenüberschuss von 89 % zu *R*-Citronellal umsetzt. Es konnte festgestellt werden, dass eine Zell-induzierte Citral-Isomerisierung zu einer erhöhten Enantioselektivität im Vergleich zur Verwendung von gereinigten Enzymen führt.

Insbesondere für den Einfluss der Selektivitäts-bestimmenden Positionen W66 und I231 konnte ein Verständnis der Struktur-Funktions-Beziehungen im Verlauf der semi-rationalen Enzym-Evolution durch die getrennte Analyse der einzelnen Citral-Isomere und durch unterstützende *in silico* Analysen wie Docking- und Molekulardynamik-Simulationen gewonnen werden.

Bemerkenswert ist auch die anschließende Einbindung der literaturbekannten Variante A419G/Y420C/G600A der Squalen-Hopen Zyklase aus *Alicyclobacillus acidocaldarius*, welche die Prins-Zyklisierung zum (-)-Isopulegol mit einem Enantiomerenüberschuss von 99 % und einer Diasteroselektivität von 90 % katalysiert. Hierbei konnte die dem Enzym zugrundeliegende Brønstedsäure-Chemie für die in der Natur unbekannte Reaktivität der Prins-Reaktion evolviert werden. In dieser Arbeit konnte gezeigt werden, dass solche durch chemische Betrachtungsweise gewonnenen Enzym-Katalysatoren in anwendungsorientierte Syntheserouten implementiert werden können. In Kombination mit der entwickelten selektiven En-Reduktase wurde zunächst die bienzymatische Kaskade zum (-)-Isopulegol erfolgreich durchgeführt und

charakterisiert. Für die abschließende Reduktion zum (-)-Menthol konnte ein gängiger heterogener Katalysator wie z.B. Palladium auf Aktivkohle in Wasserstoffatmosphäre angewandt werden. Dies demonstriert in geeigneter Weise, dass neue Biokatalysatoren mit bewährten Syntheseprozessen kombiniert werden können. Mit den gewonnenen Erkenntnissen konnte (-)-Menthol anschließend erstmals präparativ in 7 % isolierter Ausbeute über eine chemoenzymatische Kaskade aus dem Isomerengemisch des Citrals zugänglich gemacht werden. Abschließend beleuchtet diese Arbeit damit nicht nur unterschiedliche Strategien zur Entwicklung neuartiger Biokatalysatoren, sondern leistet auch einen Beitrag zu deren möglichen synthetischen Anwendbarkeit in der Darstellung industriell relevanter Moleküle.

1. Introduction

Life depends on the unique precision and molecular adaptability of enzymes.[1] These are the catalysts of nature enabling reactions under ambient conditions. The three-dimensional protein structure of these biocatalysts enables reactions with remarkable reaction rates and high selectivity (chemo-, regio- and stereoselectivity) - features often unmatched by man-made homogeneous and heterogeneous catalysts.[2] This is promising from a chemical point of view. Many valuable molecules that are for instance important in the fragrance (e.g. (-)-menthol, vanillin or ambroxan) and the healthcare (e.g. ragasalin, atorvastatin, artesiminin) industry require highly controlled reactions to maintain their stereochemical demand and degree of functionalization.[3] It has been demonstrated in the last years that microorganisms and enzymes are a true alternative to provide this molecular control.[4–8] These fascinating aspects of nature's catalysts trigger an intriguing question: can we use and adopt them for the synthesis of valuable molecules through innovative biosynthetic processes?

Despite these aspects, newest developments in the field of biocatalysis promise yet unexplored potential.[7,9,10] Intriguing examples of 'classical' chemistry show that the implementation of cascade reactions that overcome intermediary purification can provide significant synthetic simplifications.[11,12] From nature we are well aware of the puzzling complexity of multienzymatic cascades that, however, are not directly suited for high-titer production of specific compounds but are designed to provide a cell's need for regulation.[13] Nevertheless, it has been shown that such cascades can be reprogrammed[14], that efficient multienzymatic cascades can be designed outside of cells[15] and that they can also be combined with 'classical' chemical steps in chemoenzymatic reactions.[16] A second powerful improvement lies in the mutagenic adaption of enzymes by application of advanced molecular biology techniques, a procedure, which is known as 'enzyme engineering'.[9,10] Thereby, enzyme properties can be elevated from the existent limitations of natural activities to be theoretically tailored to whatever synthetic needs. It has been shown that it is not only possible to alter properties like selectivity, stability and substrate specificity based on the existent biological diversity of reactions. It is also possible to exploit the inherent chemical diversity that lies within the basic mechanisms of enzymes to induce reactions that nature did not evolve.[17] However, examples that study the application of such evolved

catalysts in chemoenzymatic cascades are still scarce.[18] This work was motivated by the desire to probe the potential of implementing such evolved enzymes concurrently with 'classical' chemistry in chemoenzymatic cascade synthetic routes for the synthesis of industrially relevant molecules like the aroma chemical (-)-menthol from the monoterpene aldehyde *E*/*Z*-citral. This work provides important insights in the potentials and remaining challenges of such novel biosynthetic routes.

1.1 Synthetic routes to (-)-menthol

Worldwide, (-)-menthol (also (1*R*, 3*R*, 4*S*)-(-)-menthol or L-menthol) is one of the industrially most relevant flavor and fragrance compounds.[19] Its characteristic peppermint smell as well as the perceived cooling effect is applied in various cosmetic and pharmaceutical products. However, these beneficial properties are only obtained for one of eight possible stereoisomers of menthol, namely (-)-menthol (Figure 1). The other seven stereoisomers cause bitter tastes or musty off-notes to varying degrees, which is undesirable for an aroma chemical.[20] In consequence, the production requires maintenance of a high optical purity of this molecule.

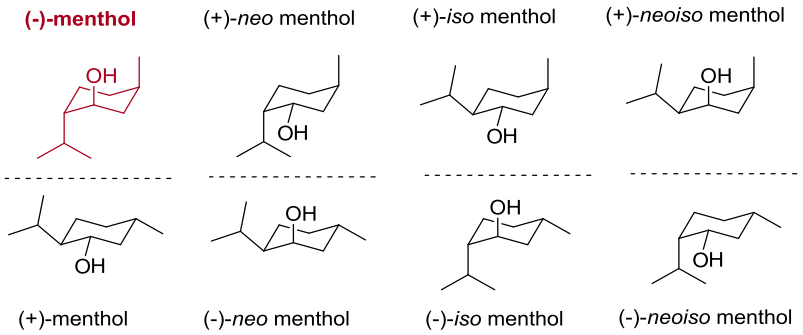

Figure 1: Menthol stereoisomers. Due to its three chiral centers, eight stereoisomers of menthol can be distinguished, which consist of four pairs of enantiomers or in other words two pairs of diastereomers. The industrially important (-)-menthol is highlighted red. Dashed lines indicate mirror planes of enantiomer pairs.

Until today large amounts of (-)-menthol are therefore still provided by extracting the *Mentha arvensis* plant (corn mint) relying on the organism's natural biosynthesis of (-)-menthol (Figure 2).[21] The general natural terpene precursors dimethylallyl pyrophosphate (DMAPP) and isopentenyl pyrophosphate (IPP) are converted in eight enzymatic steps *via* limonene to (-)-menthol. It's a complex cascade of redox and isomerization reactions. Pure (-)-menthol is isolated by several process steps from plant-derived cornmint oil involving freeze crystallization as the final one.[22] Metabolic

engineering strategies showed that the overall (-)-menthol yield in the plant biosynthesis can be increased.[23] Nevertheless, one of the main issues of plant-derived menthol production is the dependence on seasonal fluctuations causing harvest losses.[24] This has fueled the demand for a more reliable supply of synthetic (-)-menthol and consequently, different synthetic routes have been evaluated.

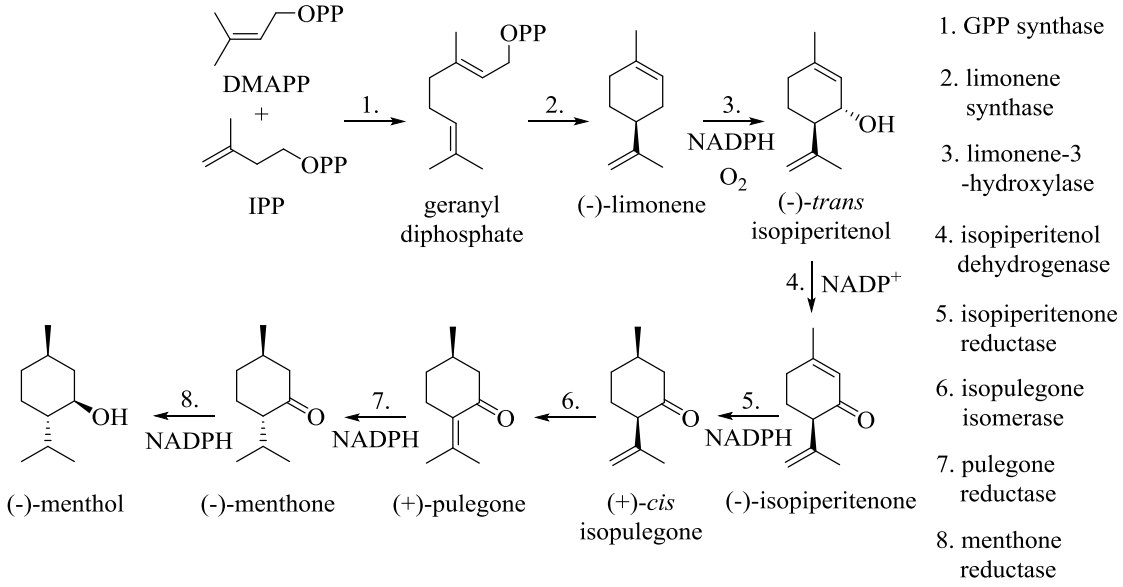

Figure 2: Natural (-)-menthol synthesis from dimethylallyl pyrophosphate (DMAPP) and isopentenyl pyrophosphate (IPP).[21] Depending on the organism, IPP and DMAPP are either provided from the mevalonate (MEV) pathway or the methylerythritol phosphate (MEP) pathway.[25]

Inspired by the natural biosynthesis, synthetic biologists discussed the use of the much simpler and better understood bacterium *Escherichia coli* (*E. coli*) as production strain for menthol by implementation of the plant biosynthetic pathway.[26] However, it appears that complete transfer of this pathway starting from IPP and DMAPP did not succeed yet.[27] Though, in one proof of concept study, (-)-menthol was synthesized from *R*-pulegone in 79.1 % purity (referring to overall product formation) using *E. coli* cell lysate by cloning and overexpressing genes encoding for the ene reductase *Nt*DBR from *Nicotiana tabacum* and the menthone reductase MMR from *Mentha piperita*.[28] The same group proposed most recently that they might soon be able to adopt the complete biosynthetic pathway upon finding a potential isopulegol isomerase, which was yet missing to achieve this.[29] A different enzymatic approach showed that lipases are an option to enrich (-)-menthol from racemic (+/-)-menthol by interesterification or by hydrolysis of an existing menthyl ester.[30,31]

There have also been numerous efforts to implement heterogeneous solid-state catalysts for the one-pot conversion of various precursors (e.g. the monoterpene citral) to

diastereomers of menthol.[32–34] For example, Ni-supported H-Y zeolite catalysts or Ni-supported H-MCM-41 (another silicate-based mesoporous solid-state catalyst) provided menthols in up to 54 % chemoselectivity, however, these catalysts struggle in terms of stereoselectivity (71 % (+/-)-menthol).[33] In another study, a Ru/H-BEA zeolite catalyst was applied to show that citronellal can be converted efficiently with up to 87 % chemoselectivity and 73 % diastereomeric ratio to (+/-)-menthol, however, no chiral differentiation was possible.[35]

Today, synthetic (-)-menthol is provided by three major industrial processes (Figure 3). These are the Haarmann & Reimer (or Symrise) process, the Takasago process and the BASF process.[19,36]

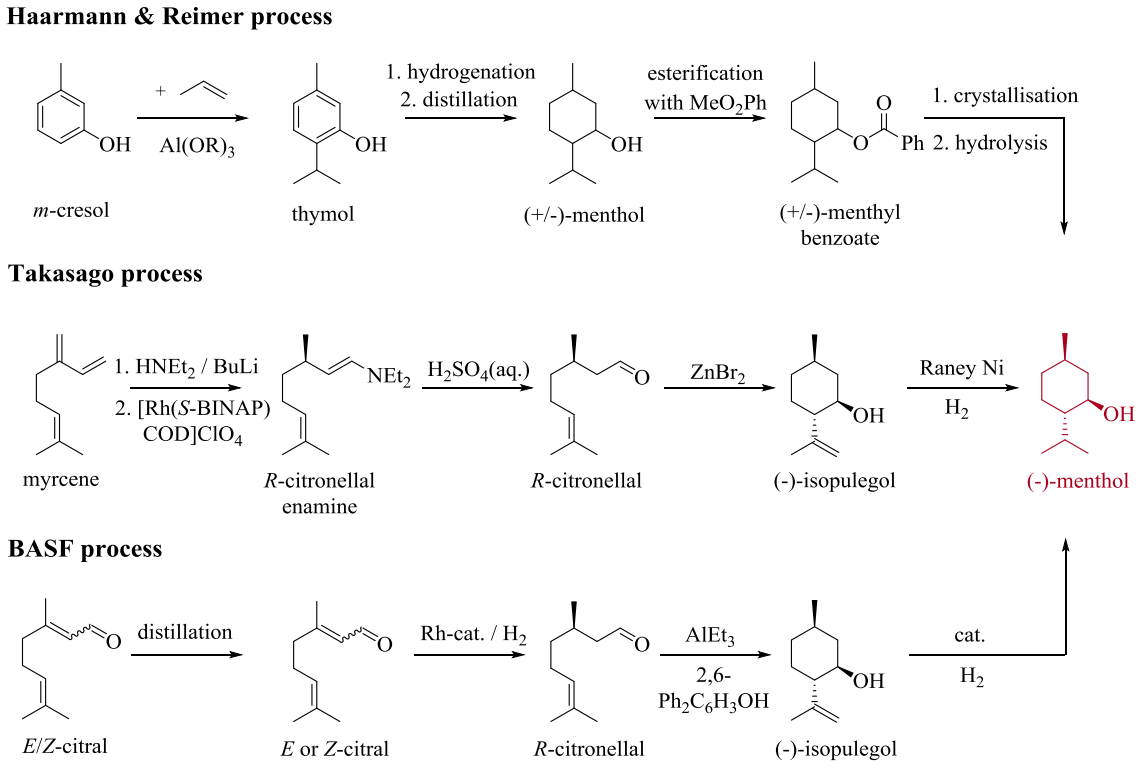

Figure 3: Overview of the three actual industrial (-)-menthol synthetic routes, the Haarmann & Reimer (or Symrise) process, the Takasago process and the BASF process.[19,36]

From these, the Haarmann & Reimer process is the oldest starting in the seventies of the twentieth century.[37] It relies on fractional crystallization of menthyl benzoate, which is produced from *m*-cresol and propene *via* a thymol intermediate. Roughly one decade later the Japanese Takasago company started to use a distinctly different process relying on asymmetric organocatalytic isomerization that was developed in collaboration with Nobel laureate Noyori.[38] The process starts from myrcene and makes use of a BINAP-rhodium-catalyzed isomerization to form *R*-citronellal enamine, which provides *R*-citronellal after acidification. Then, an enantioselective Lewis acid-catalyzed

cyclization to (-)-isopulegol follows and the reaction pathway is finally completed by heterogeneous-catalyzed hydrogenation to (-)-menthol. The last two reaction steps are principally also applied in the BASF process with alternative catalysts, however, *R*-citronellal is obtained by asymmetric hydrogenation of citral.[19,36] The process requires an additional isomer separation step and performs two separate hydrogenation reactions to provide *R*-citronellal from both isomers.

1.2 Asymmetric reduction of citral

The BASF process expanded the Takasago route by implementing citral as an alternative feed to provide *R*-citronellal that can subsequently be converted to (-)-menthol.[19,36] This chapter highlights the synthetic value of citral and focuses on synthetic aspects of the asymmetric hydrogenation of citral. The volatility of these compounds is an essential feature of the involved monoterpene educts and products and for a start this feature is therefore explained in a prior excursion.

1.2.1 Excursion: volatility of monoterpenes

The herein described monoterpenes are "volatile organic compounds" (VOC) and tend to evaporate easily into the air.[39] Biologically, this can be important for signaling and the physical phenomenon substantiates the olfactory accessibility of such compounds that are often recognized by distinct smells. Due to the implications on the small scale analytical reactions in this work, this long known physical phenomenon[40,41] shall be defined further. Vaporization, hence the transition from liquid to gas phase, is subdivided in evaporation and boiling (Figure 4).[42]

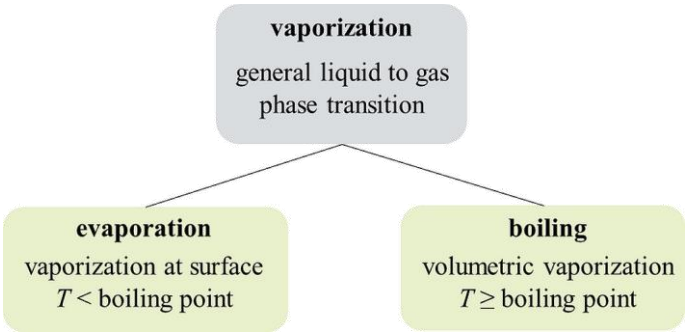

Figure 4: Terminologies of liquid to gas phase transitions. The general phase transition is denoted vaporization, which is distinguished as evaporation at the surface of a liquid that happens at temperatures *T* below the boiling point and boiling, which is a volumetric phase transfer happening at or above the boiling point.

While evaporation solely happens at the surface of a liquid and below the boiling point, boiling affects the complete volume of the liquid above the boiling point. According to the Boltzmann distribution a finite fraction of molecules at a liquid surface will have enough kinetic energy to overcome the intermolecular forces that constitute the liquid phase and are transferring into the gaseous. This process is called evaporation. In contrast, at the boiling temperature, the bulk of liquid molecules possesses enough kinetic energy to form gas bubbles within the liquid, which starts the process of boiling.

If that boiling is imagined to happen in a closed vessel, a significant pressure increase can be observed if the vessel does not provide the necessary space for the expanding gas. In contrast, in a closed vessel, evaporation will achieve equilibrium with condensation, the reverse process, at which a certain partial pressure of the evaporating/condensating molecule is achieved in the confined gas volume. Then, the same number of molecules that leave the liquid phase (evaporation), reenters the gas phase (condensation).

1.2.2 Synthetic methods for the asymmetric reduction of citral

Citral is a linear monoterpene aldehyde that is naturally found in the essential oils of many citrus plants.[43] This volatile molecule consists naturally as a 3:2 mixture of its isomers, which are *E*-citral and *Z*-citral (also known as geranial and neral) and exhibits a pleasant citrus odor. From a synthetic point of view citral can be regarded as a platform chemical that serves for the synthesis of various flavors and fragrances as well as vitamins.[44] Citral itself is for example cheaply available from the abundant precursors isobutene, formaldehyde and oxygen (Figure 5).[45]

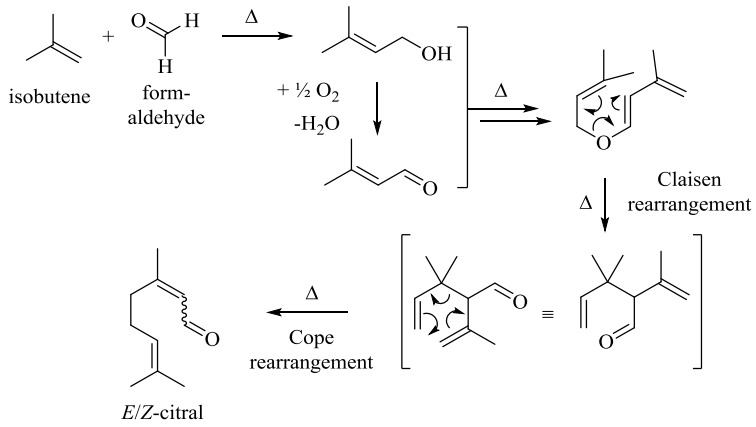

Figure 5: Synthesis of citral from isobutene, formaldehyde and oxygen.[45] The process exploits a heat-induced Claisen-Cope rearrangement domino reaction. Water is the only by-product.

This industrial synthetic process makes use of a sequential Claisen-Cope rearrangement reaction. This provides citral with water as the only by-product. Citral is well-suited for demonstrating the significance of chemoselectivity.[46] In theory, a non-selective hydrogenation can address the isoprene C=C double bond as well as the activated C=C double bond and the C=O double bond of the enal moiety. This entails a variety of possible reduction products of which citronellal is one (Figure 6).[47] This reduction has

experienced significant attention in all domains of catalysis because of its potential in menthol synthesis.

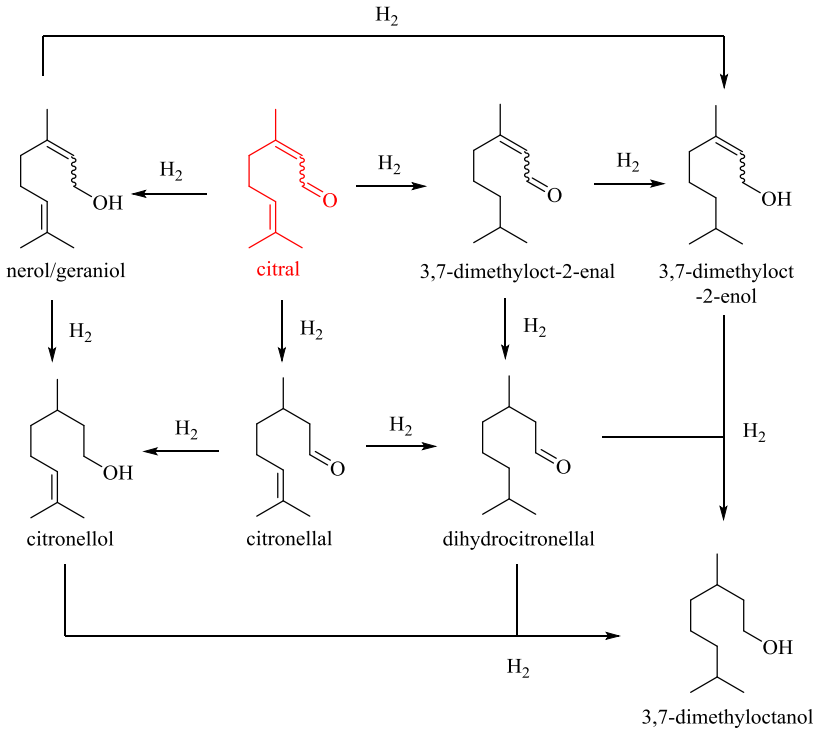

Figure 6: Various products in the general hydrogenation of citral.[47] A general hydrogenation can address both the olefin and the carbonyl function to finally produce 3,7-dimethyloctanol. Intermediate products are obtainable by chemoselective hydrogenation. Wavy bonds indicate *cis-trans* isomerism.

In terms of production scale, the industrial hydrogenation as carried out in the BASF process for (-)-menthol synthesis is one of the largest existing applications of homogeneous asymmetric catalysis (Figure 7).[44,48] This has been realized by groundbreaking research in the field of transition-metal asymmetric catalysis, which is nowadays a standard-procedure of chiral catalysis.[49,50] The chiral control of the hydrogenation is required to subsequently make (-)-menthol with high optical purity (chapter 1.1). This hydrogenation, which uses a homogeneous rhodium catalyst complex with chiral chiraphos ligands was inspired by studies from Dang et al. and Chapius et al.. They investigated several chiral ligands for asymmetric hydrogenations of this kind.[51,52]

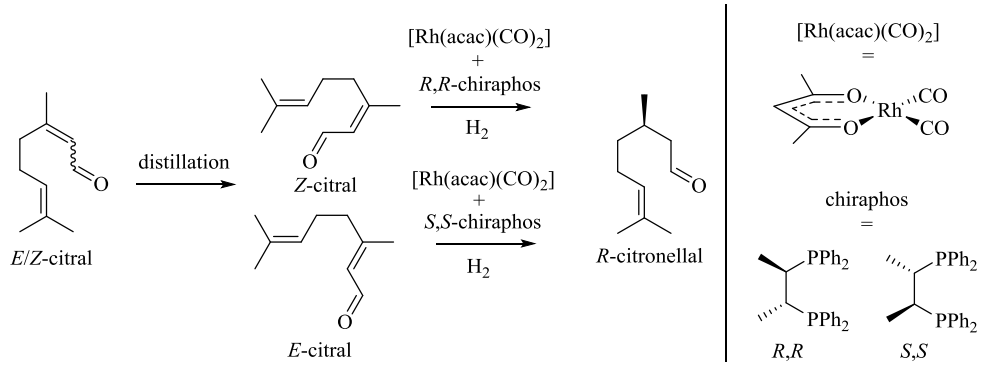

Figure 7: Asymmetric hydrogenation of *E*/*Z*-citral to *R*-citronellal as performed in the BASF process to (-)-menthol.[44,48] First, the isomers of citral are separated by distillation. Each isomer is reduced by rhodium-catalyzed hydrogenation. The chiral organocatalyst forms *in situ* by a dicarbonyl(acetylacetonato)rhodium(I) precursor and chiral chiraphos ligands.[19] *R*-selective hydrogenation is ensured for *Z*-citral by addition of *R*,*R*-configured chiraphos ligands, while for *E*-citral *S*,*S*-configuration is required. The industrial process supplies the reaction with additional carbon monoxide, which leads to more stable catalysts.[48]

The industrial process exploits the chirality of chiraphos ligands that form complexes with a rhodium catalyst. Different stereoisomers of the ligands are required to provide desired *R*-selectivity for both citral isomers because they display mirrored selectivities for the isomers.[52] This behavior explains the necessary previous separation of citral isomers, which is achieved by a rather energy-intense distillation. Hence, direct enantioconvergent reduction of both citral isomers to *R*-citronellal would be appealing from a synthetic point of view.

Controlling the selectivity of the hydrogenation reaction is, however, rather challenging. This is further described schematically displaying a *trans*-hydrogenation process *via* hydride and proton transfer (Figure 8). It considers different orientations of the *Z*- and *E*-isomer of citral leading to opposite enantioselectivities. The hydride attachment is guided to olefin Cβ position due to mesomeric carbonyl polarization. In this case this attachment consequently guides the reaction's selectivity. The selectivity is determined by the relative orientation of a smaller methyl group and the larger hydrophobic moiety M to the hydride. One orientation will deliver *S*-selectivity (A and C) and the other *R*-selectivity (B and D). Both are in principle accessible for each of the two isomers. However, the respective binding modes of *Z*- and *E*-citral, which deliver the same selectivity, for instance *R*-selectivity, inherently result in opposite orientation of the aldehyde functional group. This is a critical aspect for metal-catalyzed asymmetric hydrogenations because here, the metal surrounded by its chiral ligands appears to bind to the carbonyl oxygen in a defined geometry that hinders above mentioned opposite

aldehyde orientation.[44] Consequently, the relative orientation at Cβ is reversed and thus, opposite enantioselectivities are obtained due to this substrate control.

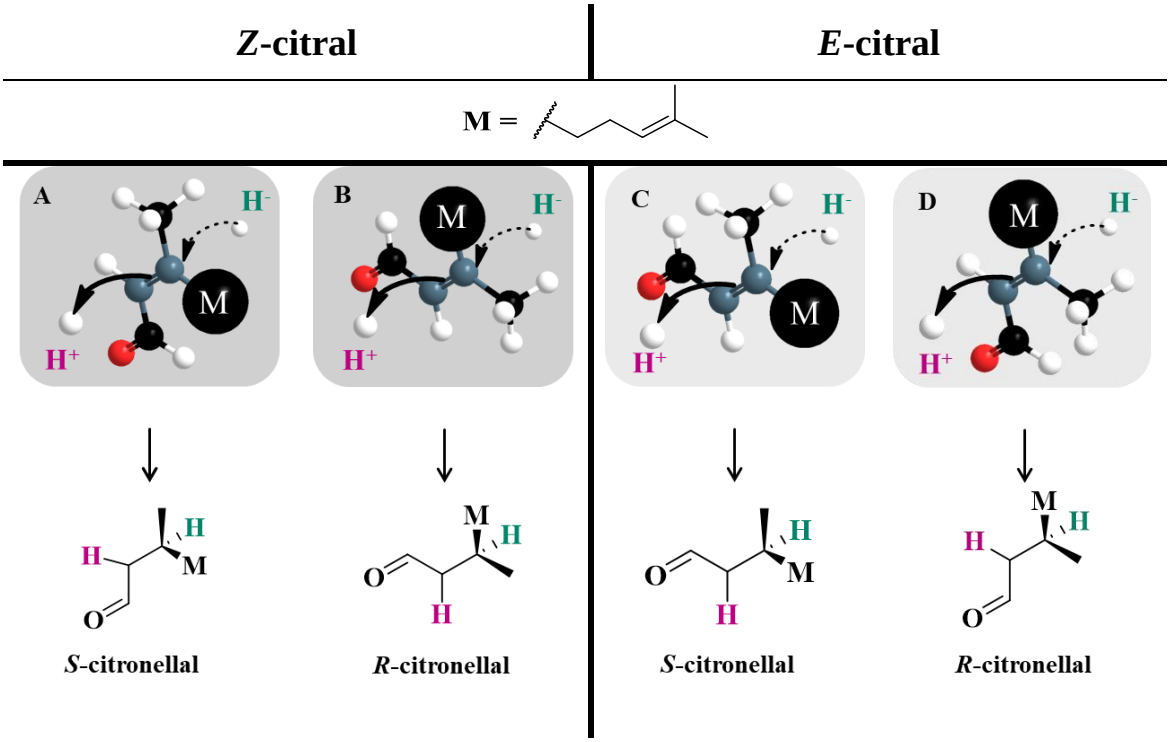

Figure 8: Schematic representation of different *Z*-citral or *E*-citral orientations relative to an attaching hydride during a hydrogenation reaction explaining either the formation of *R*-citronellal or *S*-citronellal. The scheme highlights the theoretical accessibility of both citronellal enantiomers from both citral isomers A: *Z*→*S*, B: *Z*→R, C: *E*→S, D: *E*→*R*. In the respective representations the large moiety M needs to adopt the same orientation for both isomers to provide *R*-selectivity, while then the carbonyl is inherently oriented opposite. Likewise, opposite enantioselectivity is obtained for two isomers if the carbonyl adopts similar orientation. For representative reasons, a hydrogenation reaction *via* a hydride attack is assumed and here the additional proton transfer happens *trans*-selective not influencing the stereoselective outcome. The methylprenyl tail of citral is abbreviated as moiety M.

A method that seeks to achieve enantioconvergent reduction for both isomers is thus not easily achieved. An isomerization-based shift towards one isomer can be one solution to this issue. In this regard, Hori et al. described one potential alternative combining heterogeneous and homogeneous catalysis.[53] They found that dual catalyst systems consisting of $Pd/BaSO_4$ and derivatives of the catalytic auxiliary 2-(diphenyl)methylpyrrolidine can reduce both isomers of citral yielding high enantiomeric excess up to 89 % *R*. Apparently, the isomerization of an *in situ* formed iminium species between citral aldehyde and the amine auxiliary is responsible for the achieved high selectivities.

1.3 Enzymatic asymmetric reduction by EREDs

A different approach for directing selectivity is to provide a steric bulk that only allows for a specific relative orientation of the large moiety M to the small methyl residue relative to the transferred hydride. In this regard, the three-dimensional protein structure of enzymes might be a valuable alternative and can be found in the enzymatic asymmetric reduction using ene reductases (EREDs) of the Old Yellow Enzyme family.

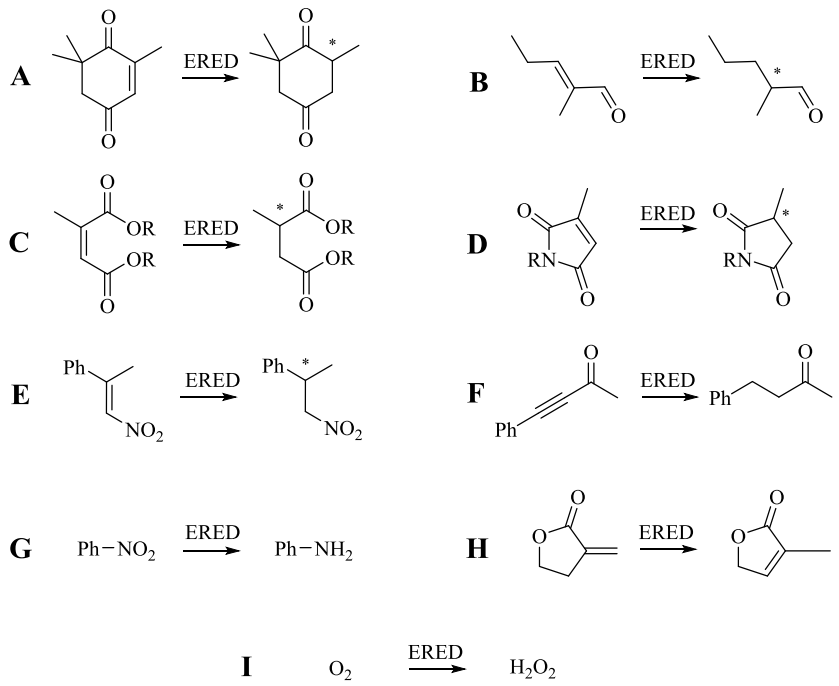

Figure 9: Various selected ERED-catalyzed reduction reactions.[8,54,55] **A-E**: Reduction of C=C double bonds adjacent to various electron withdrawing groups like ketones (**A**), aldehydes (**B**), carboxylic acids and esters (**C**), imides (**D**) and nitro groups (**E**); **F**: reduction of ynone to ketone; **G**: Reduction of nitro group to amine; **H**: Isomerization of exo alkenes to endo alkenes; **I**: Oxygen reduction to hydrogen peroxide, which is regarded as uncoupling reaction. Different EREDs catalyze mentioned reactions to various extent and often stereoselectively in case of prochiral molecules. They require redox equivalents, typically in the form of NAD(P)H.

The asymmetric reduction of C=C double bonds is found in many bacteria, yeasts, fungi and plants.[56] EREDs from the Old Yellow Enzyme family are considered an emerging enzyme class for potential industrial application.[8,57] This is reasoned by their chemical versatility and usefulness (Figure 9).[8,54,55] As an often inherent property of enzyme catalysis these reductions usually proceed with high chemo-, regio- and stereoselectivity forming up to two stereocenters.[54] Typically, these NAD(P)H-dependent enzymes catalyze the reduction of olefins, however, they are required to be electron-deficient by means of an adjacent electron withdrawing group.[54] This activation can for example be provided by ketones, aldehydes, carboxylic acids and esters, imides or also nitro groups to name prominent examples. As a rule of thumb, substitutions at olefinic Cα are better

accepted by the majority of EREDs than those at Cβ, though, both are in principle possible.[58] It has been shown that activated C≡C triple bonds can be reduced to respective saturated molecules[59] and that some EREDs can reduce aromatic nitro groups to aromatic amines.[60] As shown for many other enzymes, EREDs can display catalytic promiscuity, which is the ability to catalyze different reaction types, namely the isomerization of exo-alkenes to endo-alkenes could be demonstrated.[61] It is relevant to mention that some EREDs tend to be air-sensitive reducing oxygen to hydrogen peroxide.[62] This can lead to a potentially undesired Weitz-Scheffer reaction. This refers to the epoxidation of electron-deficient olefins at usually alkaline conditions.[63]

Though, EREDs are not yet used in industrial processes, a recent study successfully proofed their applicability at a 70 g scale for the reduction of dimethylcitraconate to dimethyl-2-methylsuccinate.[64]

1.3.1 Protein structure of EREDs

The first structural elucidation of an ERED from the Old Yellow Enzyme family was performed 1994 by Fox and Karplus.[65] There was a considerable time gap between this first structural elucidation and the actual identification of these Old Yellow Enzymes. In fact, these previously called ‘ferments’ were the first characterized flavin-containing enzymes.[66] A first isolation from the bottom of brewer’s yeast was reported by Warburg and Christian in 1932 and called ‘yellow ferment”.[67] After the isolation of a different ‘new yellow ferment’ by Haas in 1938, the previous was considered as ‘old yellow ferment’ (today known as OYE1), a name that adhered to this enzyme family until today.[68] The use of unsaturated ketones or aldehydes as oxidants for these isolated enzymes was then reported by Massey et al. in 1993.[69] It is interesting to note, however, that Wiedemann and Fischer already reported a biochemical hydrogenation of various olefins (amongst them citral) using fermenting yeast in 1934.[70] It is likely that the reactivity can be deduced to the old yellow enzymes that were isolated from such yeast.

Since this first structural elucidation of OYE1, many more ERED structures have been solved (at present apparently > 60 different EREDs).[56] This includes NCR (NADH-dependent 2-cyclohexen-1-one reductase) ERED from *Zymomonas mobilis*, an enzyme that efficiently reduces citral as a substrate (compare following chapter).[59] They all share a conserved structural fold (Figure 10).[54]

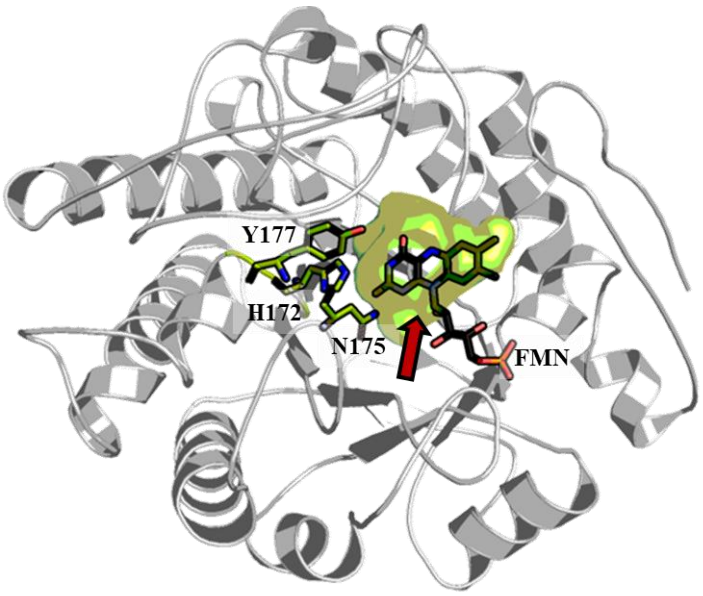

Figure 10: Shared $(\alpha,\beta)_8$-TIM-barrel motif, flavin mononucleotide (FMN) and catalytic key residues (H172, N175 and Y177) in ERED structures as well as green highlighted active site pocket. Exemplary, the crystal structure of NCR ERED from *Zymomonas mobilis* (pdb ID: 4A3U) is shown because it was chosen as target enzyme. A red arrow marks a possible entrance to the active site pocket. Each neighboring α-helix and β-sheet is connected by loop regions that mainly constitute the entrance to the active site.

The proteins form a $(\alpha,\beta)_8$-TIM-barrel motif, which is widespread in nature. A characteristic feature of this motif is the presence of eight more or less dynamic loop secondary structure elements that connect the eight α-helices and β-sheets that form this motif. This is relevant because the entrance to the active site pocket as well as the active site pocket itself is mainly formed by these loop structures. Especially the entrance loops are highly dynamic. It has been shown that this has implications on the catalytic features of these enzymes and on their stability.[71–74] Another common feature is the non-covalent but fixed incorporation of a flavin mononucleotide (FMN) prosthetic group above the β-barrel. This is achieved by various interactions between the flavin and protein amino acids (Figure 11). Some of these amino acids like T37 and Q114 (in OYE1 ERED) are also described to modulate the redox potential of the flavin, which is relevant because next to its structural function it is important for the enzyme's mechanism.[65,75,76] The mainly hydrophobic active site pocket of these enzymes additionally harbors three widely conserved and catalytic relevant amino acids, namely a His/His or His/Asn pair together with a Tyr residue.[77,78] In NCR ERED from *Zymomonas mobilis* these are for example H172, N175 and Y177 (Figure 10).

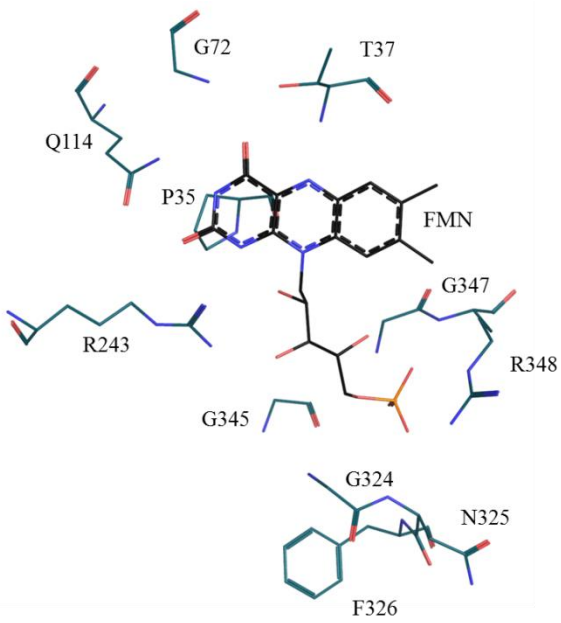

Figure 11: Amino acids providing non-covalent interactions between ERED protein and prosthetic flavin mononucleotide (FMN) as described by Karplus et al. upon their crystallization of the ERED OYE1.[65] Intermolecular interactions to the FMN were found for OYE1 amino acids P35, T37, G72, Q114, R243, G324, N325, F326, G345, G347 and R348. Relevant residues in familiar EREDs can be deduced by sequence alignments (e.g. for OYE1 and NCR in Figure Ap. 1).

Most EREDs are functional monomers or dimers, however, a distinct subclass called "thermophilic-like" EREDs forms higher order quaternary structures.[54]

1.3.2 Mechanism of ERED-catalyzed asymmetric hydrogenation

The hydrogenation reaction of EREDs proceeds in a so called ping-pong bi-bi mechanism (Figure 12).[54,77] This refers to a two-step mechanism consisting of a reductive and an oxidative half reaction with respect to the flavin prosthetic group. In the reductive half reaction oxidized FMN is reduced by a transient NAD(P)H cofactor. The cofactor transfers a hydride to the N5 position of the isoalloxazine ring. Because of steric reasons it needs to leave the catalytic site afterwards before the substrate (typically an olefin) can enter the active site pocket. In the following reductive half reaction, the NAD(P)H-derived hydride at the flavin adds to the C=C double bond and the reduction is then completed by a proton transfer, which is derived from a catalytic tyrosine (e.g. Y177 in NCR ERED).[77]

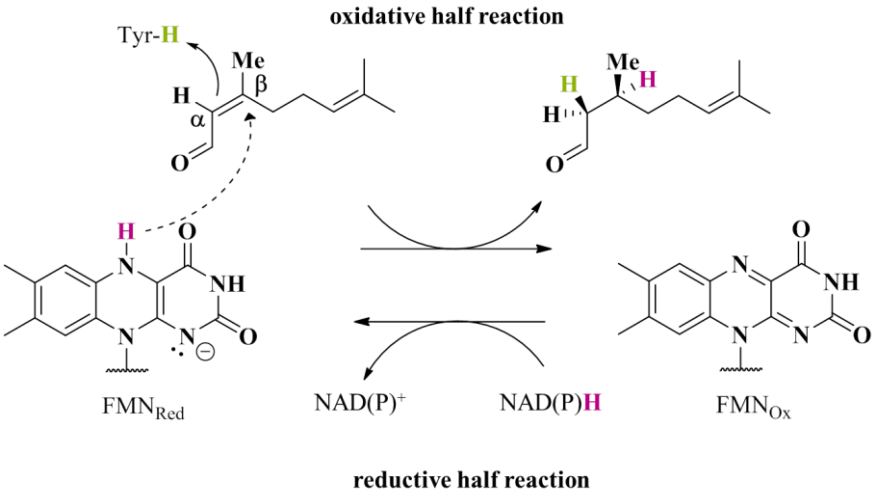

Figure 12: Ping-pong bi-bi mechanism of EREDs. The mechanism consists of two distinct sequential half reactions. Oxidized prosthetic FMN is reduced by a transient NAD(P)H cofactor *via* hydride transfer in a reductive half reaction. After NAD(P)$^+$ leaves the active site pocket an α,β-unsaturated electron-deficient olefin serves as oxidant in a separate oxidative half reaction. Here, the NAD(P)H-derived hydride is further transferred to the olefin Cβ position while a proton, which is derived from a catalytic tyrosine is attached to the Cα position. The reaction, which is shown for citral as oxidant happens *trans*-selective.

While the reductive half reaction adds to the overall reaction rate, from a stereochemical point of view the oxidative half reaction, hence the reduction of the olefin, is crucial. The three-dimensional course of the reaction is highly controlled (Figure 13).[77] For reactive binding, the oxidant's C=C double bond adopts a stacked conformation above the flavin isoalloxazine ring allowing for π-π interactions. A conserved His/His or His/Asn pair (e.g. H172 and N175 in NCR ERED) facilitates this orientation by hydrogen bridging to the electron withdrawing group that is required for olefin activation.[78,76] The electron pull of this group, for example an aldehyde, causes a partially negative charge at the olefin Cβ making this position electrophilic. Thus, the hydride nucleophile attaches to this carbon atom. The final proton transfer to the Cα olefin position is believed to derive from a conserved tyrosine residue.[77] As the flavin and the tyrosine are located on opposite faces of the olefin plane, the reduction proceeds *trans*-selective. Due to the nature of this reaction, the hydride addition will directly influence a prochirality at Cβ and the proton transfer at Cα. Different enantioselective outcomes are consequently determined by opposite binding modes as generally introduced for the substrate citral in chapter 1.2 (Figure 8). The specific shape of ERED active site pockets often favors a specific binding mode or even renders some impossible to adopt, explaining their often high enantioselectivities.[79]

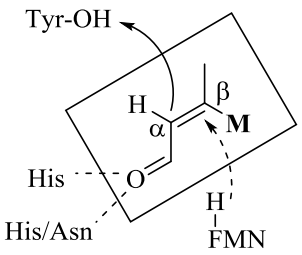

Figure 13: Spatial course of ERED-catalyzed hydrogenation. The figure highlights that the flavin-derived hydride and the tyrosine-derived (e.g. Y177 in NCR) proton are added to the substrate's α,β-unsaturated C=C double bond from opposite sides of the olefin plane causing an overall *trans*-selective hydrogenation. The electron withdrawing group of ERED oxidants is positioned *via* hydrogen bonds to a conserved His-His/Asn pair (e.g. H172 and N175 in NCR ERED). Citral is depicted as exemplary activated olefin (enal) with M being the methylprenyl moiety.

Most of today's mechanistic understanding of EREDs is derived from studies of Massey et al. performing diverse spectral and knock-out experiments using OYE1.[65,75,77,78] This involves the presented tyrosine proton donor (Y196 in OYE1).[77] An Y196F variant rendered the variant catalytically inactive, which together with structural elucidations led to the generally accepted role of this conserved tyrosine as proton donor. However, recent studies involving variations at homologous tyrosine residues in familiar EREDs surprisingly observed retained activity, though being diminished.[76,80,81] In consequence, the proton donor function of this tyrosine is partially up for discussion considering that the proton might also be water-derived.

Novel insights into the ERED mechanism were provided by detailed kinetic studies from Scrutton et al. unveiling that quantum tunneling plays a significant role in the hydride transfers of the reductive and oxidative half reaction.[82,83] Quantum tunneling is a non-classical effect based on the wave properties of particles (wave-particle duality of matter) that at room temperature can be significant for light atoms like hydrogen.[84] The consequence of atom tunneling is that reactions can proceed with higher reaction rates although classically the majority of atoms do not possess enough kinetic energy to cross the activation barrier of a certain chemical reaction.

1.3.3 ERED-catalyzed reduction of citral

Already in 1934, Wiedemann and Fischer observed citral reduction in fermenting yeast, which nowadays can be ascribed to ERED activity.[70] Today, several EREDs from this enzyme family have been characterized biochemically and also, their crystal structure is known.[56] Some of these reductases have also been tested with regard to their ability to convert citral. From the currently available data of those studies from which both,

product selectivities and the isomeric nature of the applied citral can be retrieved, two selectivity patterns can be distinguished (Table 1).

Table 1: Present selectivity types of characterized EREDs in the reduction of *E*- or *Z*-citral to *R*- or *S*-citronellal. Data is retrieved from various publications that allowed insight into which citral isomer or whether the isomeric mixture was used. Identified type I citral reductases are *R*-selective for *E*-citral reduction but produce racemic mixtures or *S*-citronellal for *Z*-citral reduction and all so far identified representatives are yeast-derived. In contrast, type II citral reductases are exclusively *S*-selective for both citral isomers and all so far known representatives are either plant- or bacterial-derived.

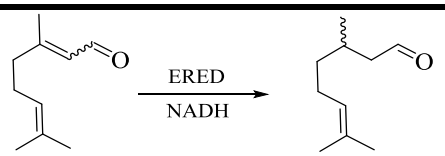

E- or *Z*-citral *R*- or *S*-citronellal

Type I enantio*divergent* reduction of citral isomers yeast-derived **trend: *E* → *R* & *Z* → *S***	**Type II** enantio*convergent* reduction of citral isomers bacterial- or plant-derived **trend: *E*/*Z* → *S***
OYE1 from *Saccharomyces pastorianus*[85]	**NCR** from *Zymomonas mobilis*[85]
OYE2 & OYE3 from *Saccharomyces cerevisiae*[85]	***Le*OPR1 & *Le*OPR3** from *Solanum lycopersicum*[86]
EBP1 from *Candida albicans*[87]	***At*OYE1 & *At*OYE3** from *Arabidopsis thaliana*[88]
CYE from *Kluyveromyces marxianus*[89]	***Glu*ER** from *Gluconobacter oxidans*[90]
KYE1 from *Kluyveromyces lactis*[91]	**MR** from *Pseudomonas putida* M10[87]
OYE2.6 from *Scheffersomyces stipitis* CBS 6054[88]	**PETNR** from *Enterobacter chloacae* PB2[87]
	NemA from *Escherichia coli*[87]
	YersER from *Yersinia bercovieri*[91]
	YqjM from *Bacillus subtilis* strain 168[86]
	YqiG from *Bacillus subtilis* strain 168[92]
	TOYE from *Thermoanaerobacter pseudethanolicus* E39[93]

Some EREDs like *Ts*OYE from *Thermus scotoductus* did not convert citral.[80] Others exerted only minor activity due to the challenging substrate's Cβ substitution.[54] From the available data, roughly two selectivity behaviors of EREDs, which in this regard can also be regarded as 'citral reductases', are distinguishable. The first behavior, arbitrarily denoted as type I citral reductase, is exclusively found for all yeast-derived EREDs.

They reduce *E*-citral with high, but not exclusive *R*-selectivity, while the reduction of *Z*-citral tends to proceed racemic or shows opposite selectivity. In contrast, a distinctly differing selectivity pattern, denoted as type II citral reductases, is found for all plant- and bacterial-derived EREDs. They are *S*-selective regardless of the citral isomer that is used as substrate and most representatives even display enantiomeric excess values ≥ 99 %. Such a distinction has been previously suggested and is herein confirmed.[89]

An especially relevant contribution for the ERED-catalyzed reduction of citral has been reported by Stewart et al. successfully probing the preparative-scale application of this reaction. Both, *S*- and *R*-citronellal were obtained in high optical purity by applying the type I citral reductase OYE2.6 for *E*-citral reduction and the type II citral reductase NemA for *Z*-citral reduction.[88]

This preparative-scale demonstration made use of the purified enzymes. This is caused by a limiting side reactivity that is typically observed in whole cells or their respective lysates. Ubiquitous non-specific alcohol dehydrogenases reduce carbonyl moieties to the respective alcohols.[89] While product reduction to citronellol might be undesired for possible further reaction steps, the reduction of citral to nerol and geraniol represents a dead-end for the ene reduction. Alcohols do not provide enough olefin activation for the reduction with EREDs.[54] Other potential side reactivities were reported under alkaline conditions in the presence of amino acids or the protein bovine serum albumin.[94] Then, partial deacetylation to sulcatone as well as citral isomerization was observed.

In light of the presented issues in chemical asymmetric hydrogenation, the enantioconvergent citral reduction of type II citral reductases is appealing. It proves that these enzymes can indeed provide enantioconvergent selectivity. A property that would potentially facilitate (-)-menthol synthesis rendering citral separation redundant. However, the process requires the opposite *R*-selectivity that, so far has not yet been identified for natural EREDs. Nevertheless, type I citral reductases also highlight the principally possible *R*-selective citral reduction with those enzymes. One potential strategy to close this selectivity gap is the continuous characterization of the vast majority of yet uncharacterized EREDs in nature. On the other hand, the recent advances in enzyme engineering provide another promising strategy.

1.4 Creating enzymes beyond nature – tools in enzyme engineering

One motivation of the present work is to demonstrate the methodological value of molecular biology for creating novel synthetic pathways. Due to the fact that the protein structure of enzymes is encoded genetically by its underlying DNA, it is relatively simple to change one or more enzyme amino acids by DNA mutagenesis. This is known as enzyme engineering because with these alterations enzymatic features can be directly adapted.[9] Typical features that are addressed are for example catalytic activity, selectivity, substrate scope, enzyme stability but also mechanistic diversity.

1.4.1 Enzyme engineering strategies

Enzyme engineering is considerably affected by the question how to cope with the enormous sequence space that arises of the possible protein alterations.[95] Three major strategies can be distinguished that address this issue.[96,97] Directed evolution adopts nature's strategy of evolution by natural selection.[98] Herein, usually large enzyme libraries are generated and screened with high-throughput assays.[96] The development of a suitable assay is often not trivial and a limiting factor. In contrast, the rational design strategy can be regarded as an opposite approach.[97] It aims to predict certain sequence-structure-function relations on the basis of structural and mechanistic information to select for defined amino acid exchanges creating very small enzyme libraries that are screened easily. Due to our still limited understanding of enzyme catalysis, optimizations in proof of concept directed evolution examples are often higher compared to purely rational approaches.[99]

The so called semi-rational design is a third strategy that combines features of the first two strategies.[100] A very prominent and often successful strategy that generates medium-sized enzyme libraries (hundreds to thousands of variants) is iterative site-saturation mutagenesis, or short ISM.[101] ISM can be regarded as a semi-rational approach. It uses preliminary information as known from the rational design approach to select single or clustered amino acids, which should hypothetically influence a desired enzyme function that one wants to engineer. At these so called "hot-spots" diversity is introduced by varying these hot-spots with up to all of the twenty canonical amino acids. The thus generated libraries are then analyzed and "hits" with improved

feature are selected. Then, this hit is used as template for consecutive diversifications at residual hot-spot regions or positions. This process is continued in an iterative fashion until the desired feature is engineered. It has been shown that choosing a limited amount of hot-spot sites but exchanging those against all 20 canonical amino acids is a strategy as viable as doing the opposite, selecting a large amount of hot-spots, which are, however, only exchanged against a limited set of amino acids.[102] Both strategies can provide sufficient diversity.

Due to the limited library-sizes, the method is especially suited for enantioselectivity engineering because of the limited ability to quickly distinguish chiral information in a high-throughput assay.[103] Examples of effective screening assays like UV/VIS spectroscopy-based detection of more selective lipases and others have been reported.[104] However, these assays require certain molecular motifs and are thus not generally applicable. This explains why most studies rely on chiral GC or HPLC analysis.[105] In consequence, the screenable library sizes are then limited.

A recent ERED-focused review highlights that many features like activity, substrate scope, stability and also selectivity could be optimized successfully by different enzyme engineering approaches.[79] For the present work, two specific ISM examples of engineered ERED selectivities are especially relevant to mention. Reetz et al. demonstrated the usefulness of the ISM strategy by engineering both, the *R*- and *S*-selective reduction of 3-methylcyclohexenone to 3-methylcyclohexanone in the thermophilic ERED YqjM.[106] Furthermore, Stewart et al. were also successful in the engineering of stereoselective OYE1 variants for the synthesis of the building block methyl 3-hydroxy-2-methylpropionate (Roche ester) from the respective Baylis-Hillman adduct.[107] Despite these efforts, so far no report is known that tried to engineer an enantioconvergent *R*-selective citral reduction. This might be explained by the fact that in contrast to other selectivity engineering studies, the selectivity towards both citral isomers needs to be engineered concomitantly, which is complicated by a possible opposite substrate control as described before (Figure 8).

1.4.2 *In silico* methods for understanding and guiding enzyme engineering

Many computational tools have been developed that can be used to guide enzyme engineering.[108] They enable visualizations of enzymatically relevant situations and processes that are experimentally difficult to achieve. In a so called *de novo* design approach, it is even possible to design new enzyme functions from scratch.[109] The concepts of three in this work applied *in silico* methods are introduced (Figure 14).

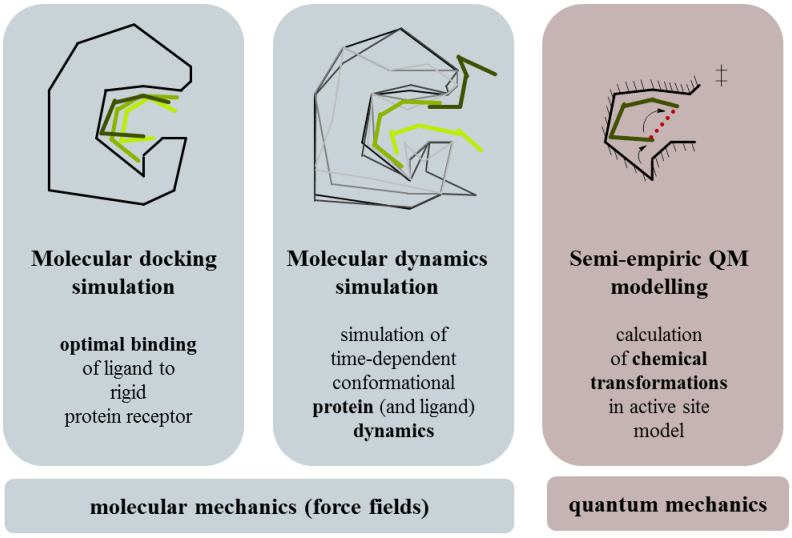

Figure 14: Conceptual representation of selected *in silico* methods from the view point of enzyme catalysis. The figure highlights basic differences in the application of these methods as described in this work. QM is referring to quantum mechanics.

Molecular docking simulation

The objective of ligand-receptor docking is to computationally predict the binding of rigid or flexible small molecules to a rigid protein.[110] The computation aims to find optimal non-covalent interactions between a receptor (protein) and a ligand (inhibitor or substrate), which it does by the calculation of binding energies. The fact that protein dynamics are usually not accounted for in this method makes this technique fast and relatively easy to apply, but one should also be aware that the lacking protein dynamics might conceal interactions that are in fact essential.[111] The probably most valuable feature of this method is that it allows a graphical representation of ligand-receptor binding that can be useful together with experimental verifications. Concisely spoken, the method relies on force field calculations, which simplify atoms and bonds as point charges and springs that span a force field in which a ligand is set randomly and thus exposed to these forces.[112]

Molecular dynamics simulation

In principle, molecular docking and molecular dynamics (MD) simulations are related methods because usually both apply force field calculations.[113] The main advantage over docking simulations is the consideration of protein dynamics, which increases the meaningfulness of these calculations but also complicates the computation significantly.[108,114] Because of the sheer size of proteins, a lot more interactions need to be calculated. Further on, in contrast to docking, laws of kinetic motion are added to the calculations that are needed to explicitly describe motion. The thus present kinetic energy allows the switch between different conformational states. Usually, such simulations include a solvent, so for proteins an aqueous buffer solution. The simulation time is an essential parameter in MD simulations and depends on the nature of the questions that such a calculation tries to answer.[114] Short simulations in the picosecond to nanosecond scale allow for bond vibrations and some side chain rotations. After a docking simulation this can be regarded as MD refinement. However, microsecond- to second-simulations are needed to simulate various degrees of secondary structure and domain movements.

Semi-empirical quantum mechanics modelling

The described force field calculations are usually not suited for the simulation of chemical reactions, which in enzyme catalysis might be valuable for understanding mechanistic details or potential mechanistic promiscuity.[115] Chemistry is basically the breaking and formation of bonds, which is guided by the interaction of electrons. For an accurate representation of these interactions the quantum mechanical nature of these small particles like the wave-particle duality cannot be neglected.[112] Quantum mechanical simulations that reproduce chemical reactions and their transition states solve the Schrödinger equation, which describes these interactions. Due to a trade-off of calculation accuracy and effort, so called semi-empirical methods like PM7 proved their applicability to simulate an enzyme's underlying chemistry.[115] They are suitable for a system accounting several hundreds of atoms, which is the typical size of an enzyme's active site. Hence, an active site model is generated, which is for example retrieved from an available crystal structure or previous force field simulations. A common simplification is to fix the backbone of selected model amino acids in space to account for the limited degrees of backbone atoms.

1.5 Promiscuous Prins monocyclization by *Aac*SHC

Squalene-hopene cyclases (SHCs) are enzymatic Brønsted acid catalysts that naturally catalyze the cyclization of the triterpene squalene to the pentacyclic products hopene and hopanol (Figure 15 A) for the cyclization of terpenoids.[118]

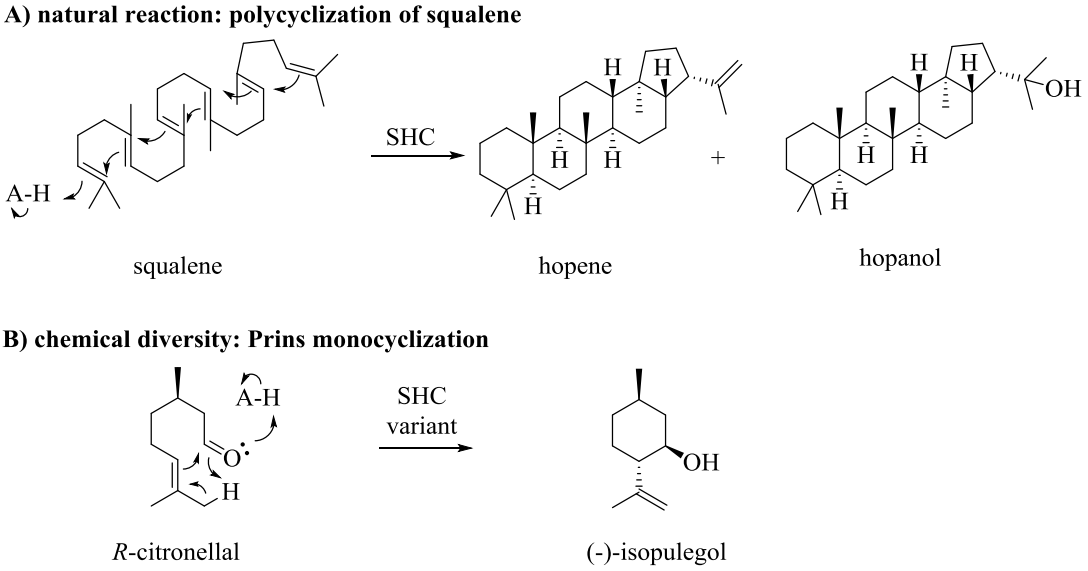

Figure 15: Promiscuous catalytic activities of squalene-hopene cyclase. A) The natural polycyclization of squalene is a Brønsted acid-initiated domino reaction that is either quenched by elimination to form hopene or by water addition to form hopanol in a highly selective manner.[116] B) The catalytic promiscuity of the general Brønsted acid character of the *Aac*SHC could be exploited by enzyme engineering to generate an *Aac*SHC variant for the Prins monocyclization of *R*-citronellal to (-)-isopulegol.[117] Herein, A-H refers to an amino acid acting as Brønsted acid.

In this reaction, a cyclization cascade starts by initial protonation of a terminal isoprene C=C double bond with intermediate carbocations forming that are finally either quenched by elimination to hopene or by water addition to hopanol.[116,118–121] Studies on the squalene-hopene cyclase from *Alicyclobacillus acidocaldarius* (*Aac*SHC) are a powerful example of the potential that lies in enzyme engineering.[117,122–126] Inspired by the potential of Brønsted acid chemistry, it was thereby demonstrated that *Aac*SHC can indeed catalyze a set of chemically diverse reactions with various substrate specificities and selectivities.[125,127]

One intriguing example of this catalytic promiscuity is the Prins cyclization of citronellal to isopulegol (Figure 15 B).[117,122,124] Apart from the fact that the monoterpene is roughly 1/3 of the squalene size, it is most remarkable that the cyclization initiation of citronellal requires the protonation of the C=O bond instead of the also present C=C double bond.[122] While another wild-type SHC from *Zymomonas mobilis* (*Zmo*SHC 1) was able to catalyze this conversion, though, unselective, the natural *Aac*SHC was

initially reported to be inactive in this conversion.[122] A mutational study could increase the citronellal cyclization activity of the *Zmo*SHC and also induce this activity in the *Aac*SHC, but the conversions remained unselective.[122,123] However, in a broader enzyme engineering project centered on the *Aac*SHC it was then shown that already by introduction of single amino acid variations highly selective Prins monocyclization of *S*-citronellal could be engineered.[124] It should be noted that during these studies, a more detailed analytics also enabled the identification of citronellal traces when using the wild-type.[128] It was somewhat surprising that the engineering of selective *R*-citronellal cyclization was less facile. An additional engineering project, however, succeeded to close this gap and also generated the *Aac*SHC triple variant A419G/Y420C/G600A with *e.e.* ≥ 99 % and *d.r.*= 90 % towards (-)-isopulegol.[117,129]

The underlying thermostable wild-type SHC is a membrane protein originally derived from the thermophilic organism *Alicyclobacillus acidocaldarius* (Figure 16).[118] The crystal structure revealed an α-helix that serves as membrane anchor as well as a long hydrophobic active site pocket that is formed at the interface of two separate protein domains, which each form a $(\alpha/\alpha)_6$-barrel structure. The SHC is a class II triterpene cyclase. In contrast to class I cyclases, these enzymes do not require a magnesium cofactor and a diphosphate leaving group.[130,131] Instead, the enzyme acts as a Brønsted acid due to a defined hydrogen network that orients the catalytic acid Asp376 (for *Aac*SHC) in an *anti*-conformation, which is up to 10,000-fold more acidic than the *syn*-conformation.[132]

Next to presented alternative enzymatic hydrogenation in the reduction of *E*/*Z*-citral to *R*-citronellal, cyclase variant A419G/Y420C/G600A might be exploited for the synthesis of (-)-menthol. As the variant achieves high selectivity in the cyclization of *R*-citronellal to (-)-isopulegol it might be an interesting alternative to so far applied chemical methods. Recent examples also highlighted that high selectivities can be achieved with homogeneous Lewis acid catalysts.[133] However, the recovery of these metal-based catalysts is complex.[134] Furthermore, other approaches based on heterogeneous catalysis[35,135] or supramolecular catalysis[136] often struggle with providing sufficient selectivity and unwanted side reactions, although for example heterogeneous catalysts are easier to recycle.[134] The cyclase enzyme offers a highly selective metal-free alternative to be studied.

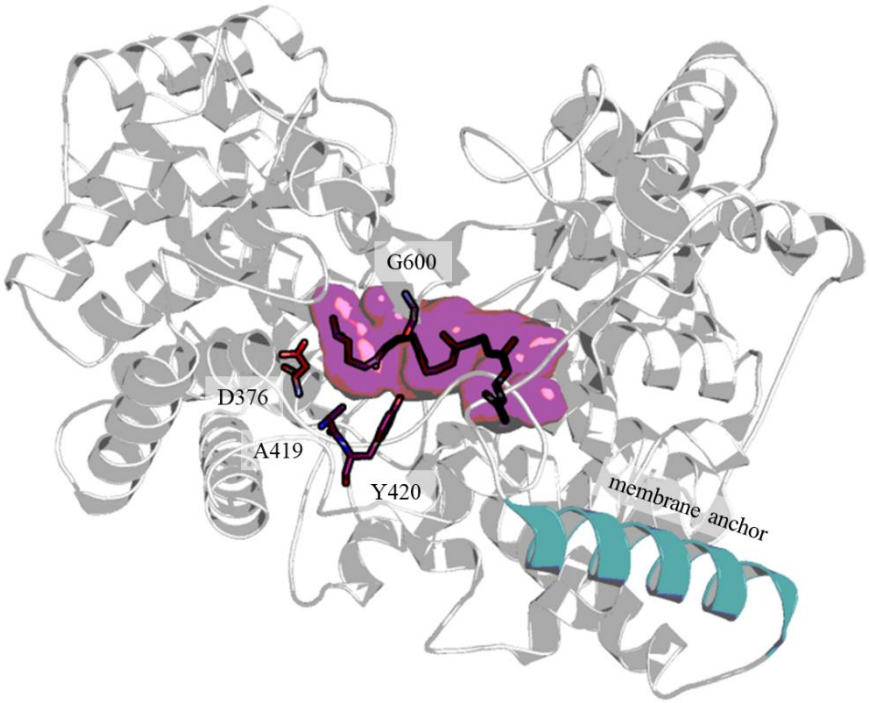

Figure 16: Crystal structure (pdb ID: 1UMP) of squalene-hopene cyclase from *Alicyclobacillus acidocaldarius* with highlighted active site in purple surface color. Aspartic acid D376 in red stick representation acts as catalytic Brønsted acid. In purple stick representation highlighted residues A419, Y420 and G600 were key positions for the generation of an SHC variant that catalyzes the Prins monocyclization of *R*-citronellal to (-)-isopulegol.[117] The crystal structure contains azasqualene (black) for identification of the substrate's binding site. The membrane anchor α-helix of the SHC is colored petrol.

While such squalene-hopene cyclases are in nature often part of enzymatic cascades at the starting point of generating molecular diversity, so far no report of their use in man-made cascade reactions is known despite their huge synthetic potential.

1.6 New synthetic concepts by implementation of multienzymatic and chemoenzymatic cascades

Cascade reactions are „[…]sequences of chemical transformations in which the starting substrate is designed so as to […] undergo a reaction whose product becomes the substrate for the next step […] and so on […]" (Figure 17).[11] This is a definition from Nicolaou et al. in a review about cascade reactions in 'classical' organic chemistry. He described one of the key features that are found in natural metabolism. Here, vast sequences of enzymatic conversions generate the molecular diversity cells require for survival.[18] This highlights that it might be of value to adopt nature's catalysts in such synthetic cascade reactions.

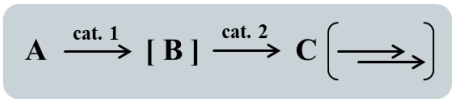

Figure 17: Concept of a general (linear) catalytic cascade reaction. At least two reactions, the conversion of A to B as catalyzed by catalyst 1 (cat. 1) and the conversion B to C as catalyzed by catalyst 2 (cat. 2) are coupled in one reaction environment. Intermediate B is not isolated in between. A, B and C represent either single or several reactants/products. Any number of additional reaction steps could follow.

It should be considered that these natural cascades are designed to fulfill a cell's need for high regulation rather than providing high yields that is desired in a synthetic process.[13] Hence, a fruitful strategy might be to dissect the synthetically useful elements from those that are unnecessary for a desired synthesis to finally assemble new synthetic pathways. And indeed, increasing efforts provide numerous multienzymatic cascade reactions that demonstrate the synthetic value of this concept.[137–139] The successful implementation of EREDs is for example demonstrated by a linear trienzymatic cascade also involving an alcohol dehydrogenase (ADH) and a Baeyer-Villiger monooxygenase (BVMO).[140] First, an ADH oxidizes a cyclic enol to the respective enone to sufficiently activate the olefin to be directly reduced by the ERED and the thereby formed saturated cyclic ketone can finally be oxidized by a BVMO to the respective lactone (Figure 18).

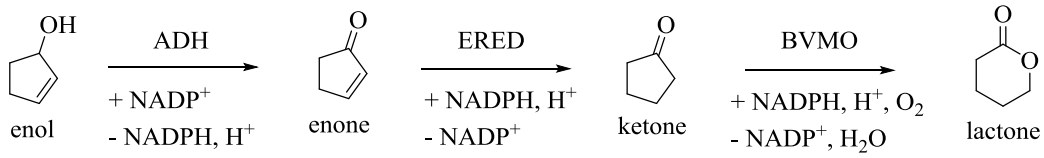

Figure 18: Exemplary trienzymatic cascade of a pentacyclic enol to a hexacyclic lactone. It employs $NADP^+$-dependent alcohol dehydrogenase (ADH), NADPH-dependent ERED and NADPH- and oxygen-dependent Baeyer-Villiger monooxygenase (BVMO).[140]

This cascade was initially implemented *in vitro*, hence isolated enzymes have been applied. It was, however, later also realized *in vivo*[141], which refers to the realization of the cascade within a usually living cell.[142] The advantages of *in vitro* cascades are their better controllability, the independence from cell viability and possible unpredictable side reactivity within the cellular environment and a usually easier analytical workup.[142] In contrast, *in vivo* cascades do not require enzymes to be purified, can provide internal cofactor regeneration and the cascades might be coupled to the cells central metabolism (metabolic engineering) allowing the use of renewable resources as substrates (e.g. glucose). In addition, unviable cells or lysates thereof are often also applied. The selection of the reaction system mainly depends on the requirements and purpose of the cascade to be assembled and the advantages and disadvantages need to be considered case by case. Due to the inherent better controllability, often novel cascades are in fact initially assembled *in vitro*.[16]

Generally, the synthetic appeal of using such reaction cascades derives from the potential to design more efficient and cleaner syntheses, which save physical resources, intermediate workup and purification steps as well as time.[12] Such cascades also enable the handling of otherwise unstable or toxic intermediates and provide the opportunity to shift equilibrium conversions by addition of irreversible reaction steps.[16] These are advantages of both, economic and ecologic nature. In this regard, it is tried to implement reactions under similar conditions, which is then called a "one-pot" reaction. Potential limitations of such cascade reactions are potentially divergent reaction conditions and the therefore relatively complex matrix of parameters (e.g. pH, temperature, solvent, concentrations etc.) that needs to be adapted. This implies a necessary trade-off between sometimes competing parameters.

Typically, reaction cascades are assembled linearly.[15] However, such cascades can also contain orthogonal elements. Using oxidoreductases can for example require the additional implementation of cofactor regenerating enzymes like a glucose dehydrogenase.[143] Moreover, concurrent cascades initially mixing all reactants and catalysts of a cascade can be distinguished from a sequential fashion adding additional reactants and catalysts after the completion of prior reaction steps.[16]

While the creation of novel biosynthetic pathways inside cellular factories is one major trend in biocatalysis, the conceptual similarities of such cascades with counterparts in 'classical' chemistry also triggered a combination in so called "chemoenzymatic"

cascades.[16,144] This is not a new concept and the first example was presented in 1980 when D-mannitol synthesis from D-glucose demonstrated that a metal-catalyzed hydrogenation in aqueous solution can be fruitfully combined with enzyme-catalyzed isomerization (Figure 19-A).[145] A newer example successfully combined a C=C double bond-forming Wittig reaction with a subsequent reduction of the *in situ* formed olefin by employing EREDs (Figure 19-B).[146]

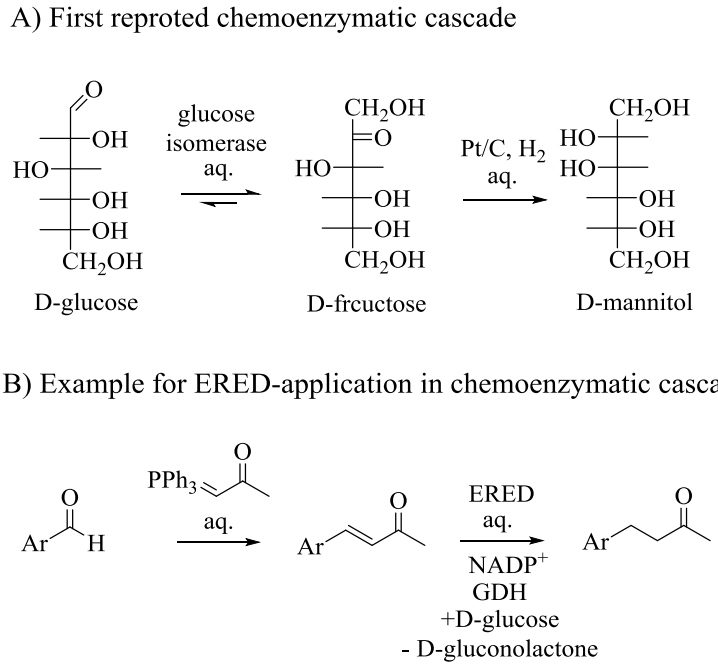

Figure 19: Selected examples of one-pot chemoenzymatic cascades. A) First published chemoenzymatic cascade from van Bekkum et al. reporting on the concurrent use of glucose isomerase for interconversion of a invert sugar mixture to enrich D-fructose from D-glucose for subsequent hydrogenation to D-mannitol by supported platinum catalyst.[145] B) Concurrent C=C double bond formation by means of Wittig reaction and subsequent C=C double bond reduction using an ERED. Required $NADP^+$ is regenerated by glucose dehydrogenase (GDH) at the expanse of D-glucose forming D-gluconolactone.[146]

While nowadays also more and more of such chemoenzymatic cascade examples are published, it is expected that enzyme engineering will provide even greater adaptations and synthetic applications.[16,138] However, the study of such engineered enzymes in chemoenzymatic cascades is still scarce. In one inspiring example, a typical Hoveyda-Grubbs metathesis catalyst was successfully combined in a one-pot reaction system with an engineered monooxygenase.[147] The subsequent enzymatic epoxidation reaction favored the formation of a specific olefin intermediate by the metathesis catalyst. In the following description of this thesis's motivation a novel chemoenzymatic cascade employing engineered enzymes is envisioned to provide an alternative synthetic route to (-)-menthol from *E*/*Z*-citral.

1.7 Motivation and aim of the thesis

The aim of the present thesis was the implementation and study of a novel chemoenzymatic cascade for the synthesis of the industrially relevant aroma chemical (-)-menthol (Figure 20). Based on an existent production route from *E*/*Z*-citral, the synthesis should combine the stereocontrol of highly selective engineered ERED and SHC biocatalysts with a well-established heterogeneous hydrogenation catalyst in one-pot.

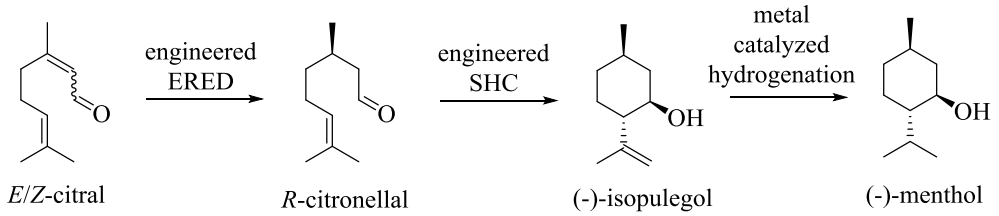

Figure 20: Envisioned aqueous one-pot chemoenzymatic cascade from *E*/*Z*-citral to (-)-menthol. The cascade aims to exploit an initial *R*-selective asymmetric hydrogenation to *R*-citronellal by an engineered ERED as well as a subsequent selective promiscuous Prins monocyclization by an engineered SHC to (-)-isopulegol. Final unselective metal-catalyzed hydrogenation provides (-)-menthol.

Specifically, this work was divided in two major challenges:

1) The creation of a so far unknown *R*-selective ERED biocatalyst for the reduction of both citral isomers by enzyme engineering to provide an alternative to the currently required costly isomer separation. Engineering of ERED-catalyzed citral reduction selectivity has not been reported before.

2) The evaluation and optimization of the combined use of thus engineered ERED biocatalyst with a previously engineered SHC triple variant. This is the first study that implements an engineered SHC in a man-made cascade reaction. Finally, a sequential Pd-catalyzed hydrogenation should be added without intermediate purification to show as proof of principle that (-)-menthol can be synthesized with the envisioned one-pot chemoenzymatic cascade.

This work is generally motivated to contribute to a broader applicability of enzymes in novel man-made biosynthetic pathways. To this end, it shall be highlighted how newest developments in enzyme engineering can realize new kinds of chemoenzymatic cascades. This shall showcase how enzymes can complement established chemical methods to close existent synthetic gaps in the synthesis of industrially relevant molecules. On the long run this research will provide more economic and ecologic processes that are much-needed for a more reasonable resource handling.

2. Materials and methods

If possible, stock solutions of chemicals as well as aliquot solutions (pooling of components in master mixes) were applied in order to reduce pipetting effort and error.

2.1 Materials

2.1.1 Chemicals

Table 2: Used chemicals with supplier information.

supplier	chemical
VWR (Darmstadt, Germany)	NaOH, IPTG
ThermoFisher Scientific Inc. (Waltham, USA)	10 mM dNTP mix, Gene Ruler™ 1 kb Prestained DNA Ladder, PageRuler™ Prestained Protein Ladder, Pierce™ Coomassie Assay Reagent, 2 mg/mL Albumin Standard Ampules
Sigma-Aldrich (St. Louis, USA)	tryptone enzymatic digest from casein, RbCl, MOPS, *R*-citronellal, *S*-citronellal, BSA, EDTA, bromophenol blue sodium salt, Coomassie® brilliant Blue R 250, KAc, $CaCl_2$ dehydrated, $MnCl_2 \cdot 4\ H_2O$, sucrose, $MgCl_2$ dehydrated, $MgSO_4$ anhydrous, KCl, 5 % (*w*/*w*) Pd/C, L-rhamnose monohydrate, α-D-glucose, *E*/*Z*-citral, *R*/*S*-citronellal, *R*/*S*-citronellol, *R*-citronellol, *S*-citronellol, nerol, geraniol, (+)-isopulegol, (-)-isopulegol, (-)-menthol, (+)-menthol, tetracycline hydrochloride, spectinomycin dihydrochloride, 30 % acrylamide solution, DEAE-Sephacel©, β-NAD reduced sodium salt, TEMED, MES, $CDCl_3$, 1-octanol, imidazole, Triton X-100, sulfuric acid, citric acid monohydrate, PEG 8000, KOH
Carl Roth GmbH + Co. KG (Karlsruhe, Germany)	yeast extract, ampicillin sodium salt, glycerol, kanamycin sulfate, agarose NEEO Ultra-Quality, Orange G, MTBE, NADH disodium salt, KH_2PO_4, K_2HPO_4, ethanol, DTT, DMSO, APS, isopropanol, 37 % HCl, agar-agar, NaCl, D(+)-lactose monohydrate, chloramphenicol, Tris, PMSF, SDS, ethyl acetate, *n*-heptane, isooctane, acetone, celite 545, vanillin, sea sand, CHAPS, acetic acid 100 %, methanol
Merck Millipore (Billerica, USA)	ethanol, 1-decanol , silica gel (0.040-0.063 mm)
Expedeon LTD (Cambridgeshire, UK)	BradfordUltra™
Air Liquide S.A. (Paris, France)	N_2(l)
abcr GmbH (Karlsruhe, Germany)	isopulegol mixture of isomers
BASF SE (Ludwigshafen, Germany)	*Z*-citral (~94 % purity), *E*-citral (~85 % purity)

2.1.2 Enzymes

Enzymes applied for cloning and expression are displayed (Table 3). All enzymes were stored at -20 °C.

Table 3: Applied enzymes for cloning and expression with supplier information.

supplier	enzyme
VWR (Darmstadt, Germany)	*Dpn*I restriction enzyme
Sigma-Aldrich (St. Louis, USA)	deoxyribonuclease, KOD Hot Start DNA polymerase
Agilent Technologies (Santa Clara, USA)	*PfuUltra* II Fusion HS DNA polymerase
New England Biolabs GmbH (Frankfurt, Germany)	T5 exonuclease, Taq DNA ligase

2.1.3 Designed primers

All primers were purchased from metabion international AG (Planegg, Germany).

Primers applied for site-directed mutagenesis:

Primer design followed rules as outlined in the QuikChange II Site-Directed Mutagenesis Kit (Agilent Technologies, Santa Clara, USA). For site-directed mutagenesis in the *ncr* and *oye*1 genes, defined triplet codon exchanges were performed (Table 4 and Table 5). In the case of codon redundancy, the codon with highest use in *E. coli* K12 was applied.

Table 4: List of utilized forward and reverse primers for the creation of site-directed mutants in the *ncr* wild-type gene.

mutation	forward primer (5'→3') / reverse primer (5'→3')
T25A	GATGGCGCCTCTGGCGCGTGGCCGTGCCAC GTGGCACGGCCACGCGCCAGAGGCGCCATC
T25F	GATGGCGCCTCTGTTTCGTGGCCGTGCCAC GTGGCACGGCCACGAAACAGAGGCGCCATC
A56G	CTGATTATTTCAGAAGGCACTGGCATTAGTC GACTAATGCCAGTGCCTTCTGAAATAATCAG
A56F	CTGATTATTTCAGAATTTACTGGCATTAGTCAGG CCTGACTAATGCCAGTAAATTCTGAAATAATCAG
W66A	CAGGAAGGTTTGGGCGCGCCTTATGCTCCGG CCGGAGCATAAGGCGCGCCCAAACCTTCCTG
W66V	GTCAGGAAGGTTTGGGCGTTCCTTATGCTCCGG CCGGAGCATAAGGAACGCCCAAACCTTCCTGAC
W66I	GTCAGGAAGGTTTGGGCATTCCTTATGCTCCGG CCGGAGCATAAGGAATGCCCAAACCTTCCTGAC
W66L	CAGGAAGGTTTGGGCCTGCCTTATGCTCCG CGGAGCATAAGGCAGGCCCAAACCTTCCTG
W66M	GTCAGGAAGGTTTGGGCATGCCTTATGCTCCG CGGAGCATAAGGCATGCCCAAACCTTCCTGAC
W66S	GTCAGGAAGGTTTGGGCAGCCCTTATGCTCCG CGGAGCATAAGGGCTGCCCAAACCTTCCTGAC
W66N	GTCAGGAAGGTTTGGGCAACCCTTATGCTCCG CGGAGCATAAGGGTTGCCCAAACCTTCCTGAC
W66Q	GTCAGGAAGGTTTGGGCCAGCCTTATGCTCCG CGGAGCATAAGGCTGGCCCAAACCTTCCTGAC
W66C	CAGGAAGGTTTGGGCTGCCCTTATGCTCC GGAGCATAAGGGCAGCCCAAACCTTCCTG
W66G	CAGGAAGGTTTGGGCGGCCCTTATGCTCCG CGGAGCATAAGGGCCGCCCAAACCTTCCTG
W66P	CAGGAAGGTTTGGGCCCGCCTTATGCTCCG CGGAGCATAAGGCGGGCCCAAACCTTCCTG
W66R	CAGGAAGGTTTGGGCCGCCCTTATGCTCCG CGGAGCATAAGGGCGGCCCAAACCTTCCTG
W66H	GTCAGGAAGGTTTGGGCCATCCTTATGCTCCGG CCGGAGCATAAGGATGGCCCAAACCTTCCTGAC
W66K	GTCAGGAAGGTTTGGGCAAACCTTATGCTCCGG CCGGAGCATAAGGTTTGCCCAAACCTTCCTGAC
W66D	GTCAGGAAGGTTTGGGCGATCCTTATGCTCCGG CCGGAGCATAAGGATCGCCCAAACCTTCCTGAC
W66E	GTCAGGAAGGTTTGGGCGAACCTTATGCTCCGG CCGGAGCATAAGGTTCGCCCAAACCTTCCTGAC
W66F[a]	GTCAGGAAGGTTTGGGCTTTCCTTATGCTCCGG CCGGAGCATAAGGAAAGCCCAAACCTTCCTGAC
W66T[a]	GTCAGGAAGGTTTGGGCACCCCTTATGCTCCGG CCGGAGCATAAGGGGTGCCCAAACCTTCCTGAC
W66Y[a]	GTCAGGAAGGTTTGGGCTATCCTTATGCTCCGG CCGGAGCATAAGGATAGCCCAAACCTTCCTGAC
W100A	CTTATCTTTGCCCAGCTAGCGCACATGGGACGTATGGTG CACCATACGTCCCATGTGCGCTAGCTGGGCAAAGATAAG
W100F	CTTATCTTTGCCCAGCTATTTCACATGGGACGTATGGTG CACCATACGTCCCATGTGAAATAGCTGGGCAAAGATAAG
H128A	GCACCCGGATTGGGGGCGACCTATGATGGTAAAAAG CTTTTTACCATCATAGGTCGCCCCCAATCCGGGTGC
H128F	CCCGGATTGGGGTTTACCTATGATGGTAAAAAG CTTTTTACCATCATAGGTAAACCCCAATCCGGG

H172A	GATGGCGTACAGATCGCGGCCGCTAATGGT ACCATTAGCGGCCGCGATCTGTACGCCATC
H172F	GATGGCGTACAGATCTTTGCCGCTAATGGT ACCATTAGCGGCAAAGATCTGTACGCCATC
N175A	CAGATCCATGCCGCTGCGGGTTATTTGATTGACG CGTCAATCAAATAACCCGCAGCGGCATGGATCTG
N175F	CAGATCCATGCCGCTTTTGGTTATTTGATTGACG CGTCAATCAAATAACCAAAAGCGGCATGGATCTG
Y177A[a]	CATGCCGCTAATGGTGCGTTGATTGACGAATTTA TAAATTCGTCAATCAACGCACCATTAGCGGCATG
Y177W	CATGCCGCTAATGGTTGGTTGATTGACGAATTTA TAAATTCGTCAATCAACCAACCATTAGCGGCATG
I231A	CACCGAATGGTGAAGCGCAGGGGACGGTTGATAG CTATCAACCGTCCCCTGCGCTTCACCATTCGGTG
I231F	GGTTATCACCGAATGGTGAATTTCAGGGGACGGTTGATAGTC GACTATCAACCGTCCCCTGAAATTCACCATTCGGTGATAACC
Q232A	CGAATGGTGAAATAGCGGGGACGGTTGATAGTC GACTATCAACCGTCCCCGCTATTTCACCATTCG
Q232F	CACCGAATGGTGAAATATTTGGGACGGTTGATAGTCATCCCG CGGGATGACTATCAACCGTCCCAAATATTTCACCATTCGGTG
R261A	GCCTTTTTAGGGATGGCGGAAGGGGCTGTTGATGGC GCCATCAACAGCCCCTTCCGCCATCCCTAAAAAGGC
R261F	GATATTGCCTTTTTAGGGATGTTTGAAGGGGCTGTTGATGGCACC GGTGCCATCAACAGCCCCTTCAAACATCCCTAAAAAGGCAATATC
F269A	GGGCTGTTGATGGCACCGCGGGCAAAACAGATCAG CTGATCTGTTTTGCCCGCGGTGCCATCAACAGCCC
F269W	GGCTGTTGATGGCACCTGGGGCAAAACAGATCAG CTGATCTGTTTTGCCCCAGGTGCCATCAACAGCC
W342A	CAAAGATGTGATTGAGACTGCGTATACCCAAACCCCCAAG CTTGGGGGTTTGGGTATACGCAGTCTCAATCACATCTTTG
W342F	GATGTGATTGAGACTTTTTATACCCAAACCC GGGTTTGGGTATAAAAGTCTCAATCACATC
Y343A	GATGTGATTGAGACTTGGGCTACCCAAACCCCCAAG CTTGGGGGTTTGGGTAGCCCAAGTCTCAATCACATC
Y343W	GATGTGATTGAGACTTGGTGGACCCAAACCCCCAAG CTTGGGGGTTTGGGTCCACCAAGTCTCAATCACATC

[a] These mutations were obtained from previous work.[74]

Table 5: List of utilized forward and reverse primers for the creation of site-directed mutants in the *oye*1 wild-type gene as used in the supervised Bachelor thesis of F. Dehli.[148]

mutation	**forward primer (5'→3') / reverse primer (5'→3')**
T37A	GATTCCGCCGCTGGCGCGCATGCGCGCG CGCGCGCATGCGCGCCAGCGGCGGAATC
T37F	GTGATTCCGCCGCTGTTTCGCATGCGCGCGC GCGCGCGCATGCGAAACAGCGGCGGAATCAC
G72A	CCATGATTATTACCGAAGCGGCGTTTATTAGCCCG CGGGCTAATAAACGCCGCTTCGGTAATAATCATGG
G72F	CCATGATTATTACCGAATTTGCGTTTATTAGCCCGC GCGGGCTAATAAACGCAAATTCGGTAATAATCATGG
Y82A	CAGGCGGGCGGCGCGGATAACGCGCCG CGGCGCGTTATCCGCGCCGCCCGCCTG
Y82W	CAGGCGGGCGGCTGGGATAACGCGCCG CGGCGCGTTATCCCAGCCGCCCGCCTG

W116A	TGTGTGGGTGCAGCTGGCGGTGCTGGGCTG CAGCCCAGCACCGCCAGCTGCACCCACACA
W116F	CTTTGTGTGGGTGCAGCTGTTTGTGCTGGGCTGGGC GCCCAGCCCAGCACAAACAGCTGCACCCACACAAAG
Q147A	GTTTATGGATGCGGAAGCGGAAGCGAAAGCG CGCTTTCGCTTCCGCTTCCGCATCCATAAAC
Q147F	CGTGTTTATGGATGCGGAATTTGAAGCGAAAGCGAAAAAAGC GCTTTTTTCGCTTTCGCTTCAAATTCCGCATCCATAAACACG
H191A	GATGGCGTGGAAATTGCGAGCGCGAACGGCTAT ATAGCCGTTCGCGCTCGCAATTTCCACGCCATC
H191F	GATGGCGTGGAAATTTTTAGCGCGAACGGC GCCGTTCGCGCTAAAAATTTCCACGCCATC
N194A	GAAATTCATAGCGCGGCGGGCTATCTGCTG CAGCAGATAGCCCGCCGCGCTATGAATTTC
N194F	GGAAATTCATAGCGCGTTTGGCTATCTGCTGAAC GTTCAGCAGATAGCCAAACGCGCTATGAATTTCC
Y196A	TAGCGCGAACGGCGCGCTGCTGAACCAG CTGGTTCAGCAGCGCGCCGTTCGCGCTA
Y196F	CATAGCGCGAACGGCTTTCTGCTGAACCAGTTTC GAAACTGGTTCAGCAGAAAGCCGTTCGCGCTATG
Y196W	GCGCGAACGGCTGGCTGCTGAACCAGTTTC GAAACTGGTTCAGCAGCCAGCCGTTCGCGC
F250A	GAGCCCGTATGGCGTGGCGAACAGCATGAGC GCTCATGCTGTTCGCCACGCCATACGGGCTC
F250W	GAGCCCGTATGGCGTGTGGAACAGCATGAGCG CGCTCATGCTGTTCCACACGCCATACGGGCTC
N251A	CGTATGGCGTGTTTGCGAGCATGAGCGGCG CGCCGCTCATGCTCGCAAACACGCCATACG
N251F	CGTATGGCGTGTTTTTTAGCATGAGCGGCGGCG CGCCGCCGCTCATGCTAAAAAAACACGCCATACG
V288A	GCGTTTGTGCATCTGGCGGAACCGCGCGTG CACGCGCGGTTCCGCCAGATGCACAAACGC
V288F	GCGTTTGTGCATCTGTTTGAACCGCGCGTG CACGCGCGGTTCAAACAGATGCACAAACGC
F296A	GCGTGACCAACCCGGCGCTGACCGAAGGC GCCTTCGGTCAGCGCCGGGTTGGTCACGC
F296W	GCGTGACCAACCCGTGGCTGACCGAAGGC GCCTTCGGTCAGCCACGGGTTGGTCACGC
F374A	GATCGCGATACCGCGTATCAGATGAGCGCG CGCGCTCATCTGATACGCGGTATCGCGATC
F374W	GATCGCGATACCTGGTATCAGATGAGCGCG CGCGCTCATCTGATACCAGGTATCGCGATC
Y375A	GATCGCGATACCTTTGCGCAGATGAGCGCGC GCGCGCTCATCTGCGCAAAGGTATCGCGATC
Y375W	GATCGCGATACCTTTTGGCAGATGAGCGCGC GCGCGCTCATCTGCCAAAAGGTATCGCGATC

Primers applied for iterative site-saturation mutagenesis:

Primers containing degenerate NNK codons were used for semi-rational iterative site-saturation mutagenesis (Table 6).

Table 6: List of utilized forward and reverse primers for the creation of semi-rational site-saturation mutants in the *ncr* wild-type gene using NNK codon degeneracy. X refers to one of the 20 canonical proteinogenic amino acids.

mutation	forward primer (5'→3') / reverse primer (5'→3')
W66X	GTCAGGAAGGTTTGGGCNNKCCTTATGCTCCGG CCGGAGCATAAGGMNNGCCCAAACCTTCCTGAC
Y177X	CATGCCGCTAATGGTNNKTTGATTGACGAATTTA TAAATTCGTCAATCAAMNNACCATTAGCGGCATG
I231X	CACCGAATGGTGAANNKCAGGGGACGGTTG CAACCGTCCCCTGMNNTTCACCATTCGGTG
F269X	GCTGTTGATGGCACCNNKGGCAAAACAGATCAG CTGATCTGTTTTGCCMNNGGTGCCATCAACAGC

Primers for Gibson assembly:

Custom primers for inserting an N-terminal poly-His_6 tag into the pDHE_*ncr* plasmid (chapter 2.1.6) were designed by following instructions of the SnapGene 3.1.4 software from GSL Biotech (Chicago, USA) available at 'snapgene.com' (Table 7).

Table 7: Designed Gibson assembly primers for inserting an N-terminal poly-His_6 tag into the pDHE_NCR gene.

name	forward primer (5'→3') / reverse primer (5'→3')
NCRHis_from_pET28	CGCCAAAACAGCCGGTACCCTCAATCCCCAAGCAAAGGA CTTAAGAAGGAGATATACATATGGGCAGCAGCCATCATCA
pDHE_linearization	ATCCTTTGCTTGGGGATTGAGGGTACCGGCTGTTTTGG TGATGATGGCTGCTGCCCATATGTATATCTCC

Sequencing primers:

Commercial GATC Biotech AG (Konstanz, Germany) sequencing service was used. If applicable, genes were sequenced by application of GATC in-house primers. In this regard, T7 and pET-RP primers were used for sequencing genes contained in pET vector systems, while pGL3-1 and pTI2-1-2 primers were used for sequencing genes contained in pDHE vector systems (Table 8). Due to gene length, sequencing of the *Aac*SHC gene required an additional custom-made primer called In_Primer.

Table 8: The Primers that were used for gene sequencing.

name	primer (5'→3')
T7	TAATACGACTCACTATAGGG
pET-RP	CTAGTTATTGCTCAGCGG
pGL3-1	GAGCTGACTGGGTTGAAG
pTI2-1-2	GCGTTTCACTTCTGAGTTCG
In_Primer	CGCTGAGCATTGTGATGAGCCGC

2.1.4 Strains

For DNA cloning and mutagenesis using genes in pET-28a(+) or pET-22b(+) vectors either the *E. coli* XL-1 Blue or the *E. coli* DH5α strain was applied. The *E. coli* BL21(DE3) strain was subsequently used as gene expression strain for protein production. In contrast, the *E. coli* TG20+ strain was applied for cloning, mutagenesis as well as expression of genes contained in the pDHE vector system.
Available stock solutions of listed strains at the IBTB, department of Technical Biochemistry (University of Stuttgart) were used to produce corresponding competent cells.

The *E. coli* TG20+ strain was initially provided by the BASF SE company (Ludwigshafen, Germany). The strain is based on the commercial TG1 strain[149] and contains additional features. *E. coli* TG20+ is deficient of L-rhamnose isomerase. Thus, it does not metabolize rhamnose making the strain amenable towards rhamnose-induced promotors. In fact, the isomerase gene is replaced by a tetracycline resistance gene. In addition, the strain contains two gene deletions Δ*yahk*$^-$ and Δ*yisb*$^-$ both encoding for unspecific *E. coli* dehydrogenases.[150] The *E. coli* TG20+ strain also incorporates the two chaperone plasmids pHSG and pAgro4 (chapter 2.1.6).

2.1.5 Antibiotics

For strains containing the pDHE vector, ampicillin was applied with a working concentration of 100 µg/mL. For pET-28a(+) vector constructs, kanamycin with 50 µg/mL working concentration was utilized. Respective aqueous stock solutions were stored at -20 °C. Spectinomycin was applied with a working concentration of 50 µg/mL,

chloramphenicol with 5 µg/mL and tetracycline with 15 µg/mL. While the three beforehand mentioned antibiotics were added as aqueous 1000x stock solutions, tetracycline was added as 5 mg/mL stock solution dissolved in 70 % ethanol and chloramphenicol as 1000x stock solution dissolved in pure ethanol.

2.1.6 Plasmids

During the scope of the presented thesis several plasmids were either used or produced (Table 9-10). Construction of the pET-28a(+) plasmid containing the *ncr* wild-type gene from *Zymomonas mobilis* with an N-terminal poly-His_6 tag is described elsewhere.[72] The pDHE vector containing the *oye*1 gene from *Saccharomyces pastorianus* was obtained from an IBTB in-house plasmid library.

Table 9: List of pET-28a(+) vectors containing the *ncr* gene from *Zymomonas mobilis* with an N-terminal poly-His_6 tag with one of the listed *ncr* mutations.

T25A	T25F	A56G	A56F	W66A
W66V	W66I	W66L	W66M	W66S
W66N	W66Q	W66C	W66G	W66P
W66R	W66H	W66K	W66D	W66E
W66F[a]	W66T[a]	W66Y[a]	W100A	W100F
H128A	H128F	H172A	H172F	N175A
N175F	Y177A[a]	Y177W	I231A	I231F
Q232A	Q232F	R261A	R261F	F269A
F269W	W342A	W342F	Y343A	Y343W
W66A/T25A	W66A/T25F	W66A/A56G	W66A/A56F	W66A/W100A
W66A/W100F	W66A/H128A	W66A/H128F	W66A/H172A	W66A/H172F
W66A/N175A	W66A/N175F	W66A/Y177A	W66A/Y177W	W66A/I231A
W66A/I231F	W66A/Q232F	W66A/R261A	W66A/R261F	W66A/F269A
W66A/F269W	W66A/W342A	W66A/W342F	W66A/Y343A	W66A/Y343W
loop 6* W66A[b]				

[a] These mutations were contained from previous work.[74]
[b] Loop 6* corresponds to the exchange of NCR amino acids T268-F269 against OYE1 N295-E302 (amino acid sequence NPFLTEGE) as described elsewhere.[74]

Additionally, the W66A mutation comprising *ncr* gene contained in the pDHE vector system without N-terminal poly-His_6 tag was generated. The vector construct pDHE_*ncr* containing an N-terminal poly-His_6 tag was constructed in the course of combinatorial iterative site-saturation by Gibson assembly (chapter 2.2.5).

Table 10: List of pDHE vectors that contain the *oye*1 gene from *Saccharomyces pastorianus*. The genes do not incorporate a poly-His_6 tag. All genes were prepared in the scope of the supervised Bachelor thesis of F. Dehli.[148]

T37A	T37F	G72A	G72F	Y82A
Y82W	W116A	W116F	Q147A	Q147F
H191A	H191F	N194A	N194F	Y196A
Y196F	Y196W	F250A	F250W	N251A
N251W	V288A	V288F	F269A	F269W
F374A	F374W	Y375A	Y375W	

Throughout the performed site-saturation screening, several hits have been selected for plasmid isolation and sequencing (Table 11).

Table 11: List of pDHE vectors containing the *ncr* gene from *Zymomonas mobilis* with an N-terminal poly-His_6 tag and one of the listed *ncr* mutations. A selection of mutations beneficial for an increased *R*-selectivity in the citral reduction is presented.

W66A	W66A/I231P	W66A/I231R	W66A/I231W	W66A/I231Y
W66A/I231K	W66A/I231D	W66A/I231H	W66A/I231L	W66A/Y177A
W66A/Y177T	W66A/Y177N	W66A/Y177H	W66A/Y177D	W66A/Y177M
W66A/Y177C	W66A/F269S	W66A/F269C	W66A/F269L	W66A/F269K
W66A/F269V	W66A/F269G	W66A/I231P/F269V	W66A/I231P/F269H	W66A/I231P/F269Q
W66A/I231P/F269P	W66A/I231P/F269Y	W66A/I231P/Y177R	W66A/I231P/Y177K	W66A/I231P/Y177F
W66A/I231R/F269V	W66A/I231P/F269V/Y177D			

Regarding squalene-hopene cyclases, several variants from previous studies have been assessed in this work (Table 12).

Table 12: List of pET-22b(+) vectors containing the *shc* gene from *Alicyclobacillus acidocaldarius* and one of the listed *shc* mutations. All genes were obtained from an IBTB in-house plasmid library.

wild-type[a]	D376A[a]	I261A[a]	A419G/Y420A[b]	A419G/Y420C[b]
A419G/Y420G[b]	A419G/G600A[b]	Y420A/G600A[b]	Y420C/G600A[b]	Y420G/G600A[b]
A419G/Y420A/G600A[b]	A419G/Y420C/G600A[b]	A419G/Y420G/G600A[b]		

[a] Plasmids were generated during the PhD thesis of Dr. Stephan Hammer.[128]
[b] Plasmids were generated during the PhD thesis of Dr. Silke Bastian.[129]

Both, the pET-28a(+) and the pET-22b(+) plasmid contain a *lac* operon, a T7 promoter and a multiple cloning site (Figure 21 A and B). While the first vector contains a kanamycin resistance (*Kan*), the second contains an ampicillin resistance (*Amp*). The pDHE plasmid is derived from the pJOE2702 plasmid, which is a pBR322 descendant (Figure 21 C).[151,152] It contains an ampicillin resistance (*Amp*), a rhamnose promoter (*rhaB*), diverse restriction sites, a basis of mobility region (*bom*) for horizontal gene transfer and a *rop* site for low copy maintenance.

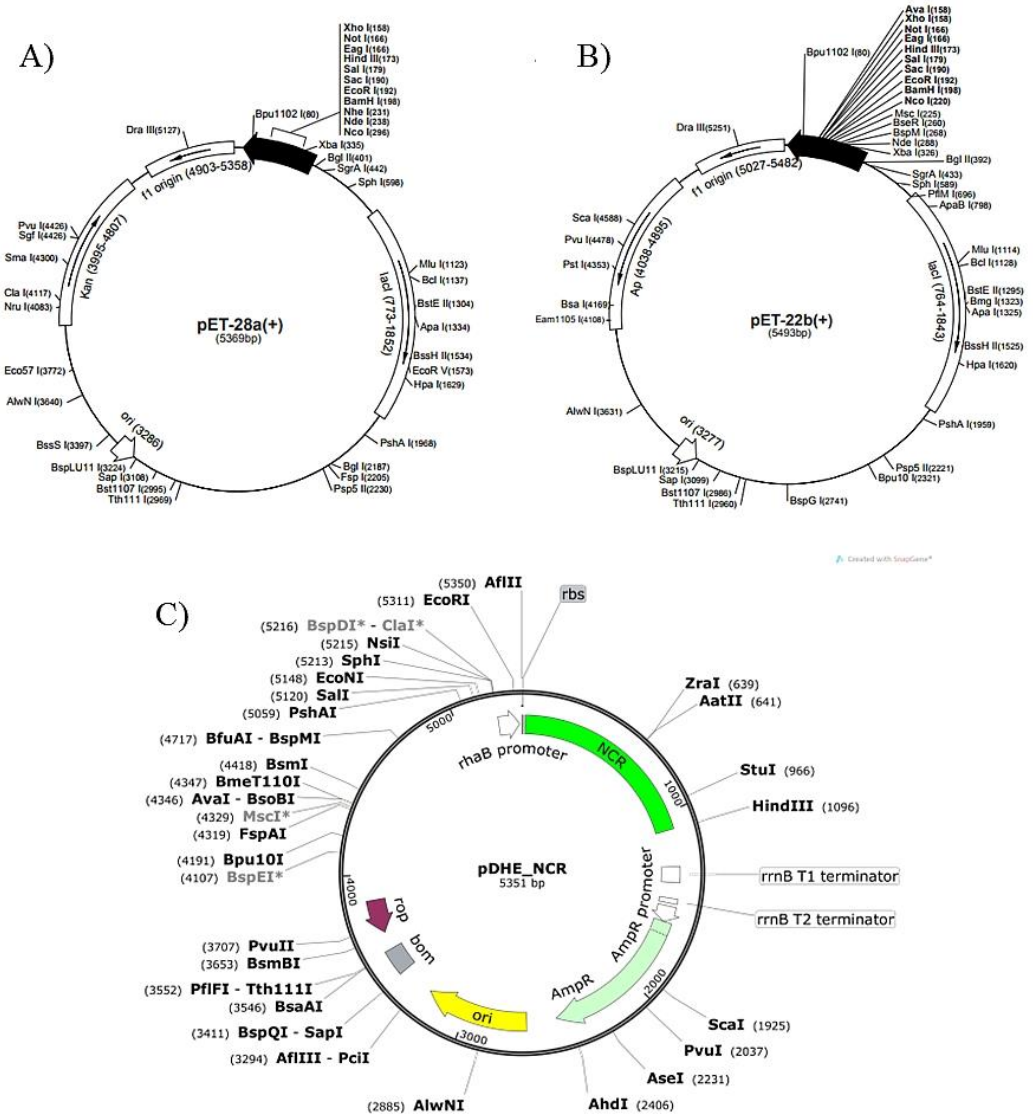

Figure 21: Vector systems used for cloning and expression of ERED and SHC genes; A) map of pET-28a(+) containing a kanamycin resistance, a *lac* operon, a T7 promoter and the displayed restriction sites; B) map of pET-22b(+) containing an ampicillin resistance, a *lac* operon, a T7 promoter and the displayed restriction sites; C) exemplary map of pDHE_NCR containing an ampicillin resistance, a rhamnose promoter and the displayed restriction sites; the pDHE vector map was generated using the SnapGene 3.1.4 software from GSL Biotech (Chicago, USA) available at 'snapgene.com'.

The plasmids pAgro and pHSG contain genes for GroES/GroEL chaperonins, a *lac* operon and a gene for the *lacIq* repressor.[152] Furthermore, pAgro contains a spectinomycin and pHSG a chloramphenicol resistance gene.

2.1.7 Buffers and media

Molecular biology and expression:

DNA- and RNA-free sterile ddH_2O obtained by Milli-Q® Integral Water Purification System (Merck Millipore, Billerica, USA) was used.

10x PCR buffer for KOD Hot Start polymerase (Sigma-Aldrich, St. Louis, USA) and 10x *PfuUltra* II reaction buffer (Agilent Technologies, Santa Clara, USA) were used as received from the supplier.

3 % (*w*/*v*) Agarose gel was produced by dissolving 3 g Agarose NEEO Ultra Quality in 300 mL TAE buffer by microwave heating. After complete dissolution, 3 µL Midori Green were added to 50 mL agarose gel, mixed gently and subsequently poured into an agarose gel chamber for hardening. Before hardening, a comb was added for pocket formation.

TAE buffer (50x)	
Tris acetate (pH 8.0)	2 M
EDTA	100 mM

5x DNA loading buffer	
sucrose	2 g
Orange G	10 mg
ddH_2O	fill up to 5 mL

TfbI buffer	
KAc	0.59 g
RbCl	2.42 g
$CaCl_2$	0.29 g
$MnCl_2 \cdot 4\ H_2O$	2.0 g
glycerol	30 mL
ddH_2O	fill up to 200 mL
pH 5.8 with 1 % acetic acid	
Sterile filtration (0.45 µM)	

TfbII buffer	
MOPS	0.21 g
RbCl	0.12 g
$CaCl_2$	1.1 g
glycerol	15 mL
ddH_2O	fill up to 100 mL
pH 6.5 with 1 M NaOH	
Sterile filtration (0.45 µM)	

The following media were sterilized at 121 °C and 1.3 bar for 20 min.

LB medium (per liter)	
NaCl	5 g
yeast extract	5 g
tryptone	10 g
ddH_2O	1000 mL

LB agar plate medium (per liter)	
NaCl	5 g
yeast extract	5 g
tryptone	10 g
agar-agar	15 g
ddH_2O	1000 mL

Desired antibiotics were only added to media < 50 °C. Dissolved LB agar plate medium was poured into Petri dishes for hardening and afterwards stored at 4 °C.

TB medium (per liter)	
tryptone	12 g
yeast extract	24 g
glycerol	4 mL
ddH_2O	900 mL
phosphate buffer	100 mL

phosphate buffer (per 500 mL)	
KH_2PO_4	11.57 g
K_2HPO_4	62.70 g
ddH_2O	500 mL
pH 7 with HCl (37 %)	

TB medium and phosphate buffer were sterilized separately to hinder phosphate precipitation.

SOC medium (per 100 mL)	
tryptone	2 g
yeast extract	0.5 g
1 M NaCl (final: 10 mM)	1 mL
1 M KCl (final: 2.5 mM)	0.25 mL
1 M $MgCl_2$ (final: 10 mM)	1 mL
1 M $MgSO_4$ (final: 10 mM)	1 mL
1 M glucose (final: 20 mM)	2 mL
ddH2O	fill up to 100 mL

5x ISO reaction buffer	
25 % (*w*/*v*) PEG-8000	1.5 g
500 mM Tris-HCl (pH 7.5)	3 mL
50 mM $MgCl_2$	150 µL
50 mM DTT	300 µL
1 mM dNTP mix	240 µL
5 mM NAD	300 µL

Protein purification:

For affinity chromatography protein purification 50 mM Tris-HCl (pH 7.5) buffers with varying imidazole concentrations, namely 0 mM, 5 mM, 10 mM, 50 mM and 300 mM were used.

Several surfactant-containing buffers as listed in the following were applied for purification of squalene-hopene cyclases.

lysis buffer (per liter)	
citric acid (final: 200 mM)	38.4 g
EDTA (final: 0.1 mM)	37 mg
pH 6 with 1 M NaOH	

solubilization buffer (per liter)	
citric acid (final: 60 mM)	11.5 g
detergent (final: 1 % (*w*/*v*))	10 g
pH 6 with 1 M NaOH	

regeneration buffer (per liter)	
citric acid (final: 12 mM)	2.31 g
NaCl (final: 500 mM)	29.22 g
detergent (final: 0.1 % (*w*/*v*))	1 g
pH 6 with 1 M NaOH	

wash buffer (per liter)	
citric acid (final: 12 mM)	2.31 g
detergent (final: 0.1 % (*w*/*v*))	1 g
pH 6 with 1 M NaOH	

elution buffer (per liter)	
citric acid (final: 12 mM)	2.31 g
NaCl (final: 200 mM)	11.69 g
detergent (final: 0.1 % (*w*/*v*))	1 g
pH 6 with 1 M NaOH	

Regarding above mentioned lysis, solubilization, regeneration, wash and elution buffer: Triton X-100 or CHAPS were used as detergent. As described in the results part, the detergent concentration was varied in some experiments (chapter 3.2.1). The buffers were filled up with ddH_2O.

SDS gels:

running gel 12 % (20 mL)	
ddH_2O	6.6 mL
30 % acrylamide mix	8.0 mL
1.5 M Tris-HCl (pH 8.8)	5.0 mL
10 % SDS (aq.)	0.2 mL
10 % APS (aq.)	0.2 mL
TEMED	8 µL

stacking gel 5 % (4 mL)	
ddH_2O	2.7 mL
30 % acrylamide mix	0.67 mL
1 M Tris-HCl (pH 6.8)	0.5 mL
10 % SDS (aq.)	40 µL
10 % APS (aq.)	40 µL
TEMED	4 µL

First, the running gel was prepared and poured for hardening directly after final APS addition. Afterwards, stacking gel was poured on top accordingly followed by comb addition for pocket formation.

At a later stage of the thesis, commercially available ExpressPlus™ PAGE Gels (ready-to-use SDS-PAGE gels) from Genscript Biotech Corp. (Hongkong, China) were applied according to manufacturer's instructions including Tris-MOPS SDS running buffer powder. The Mini-PROTEAN® Tetra system from Bio-Rad Laboratories Inc. (Hercules, USA) was used for performing the SDS-PAGE.

Lämmli loading buffer (20 mL)	
1 M Tris-HCl (pH 6.8)	2 mL
$MgCl_2$	190 mg
glycerol	1 mL
SDS	0.8 g
bromophenol blue	2 mg
DTT	0.31 g
ddH_2O	fill up to 20 mL

5x SDS gel running buffer (2 L)	
Tris	30 g
glycerol	144 g
SDS	10 g
ddH_2O	fill up to 2 L

staining solution (per liter)	
Coomassie®-Blue G-250	60-80 mg
30 % HCl (aq.)	35 mM
ddH_2O	1 L

destaining solution (per liter)	
methanol	300 mL
acetic acid, 100 %	100 mL
ddH_2O	600 mL

Biotransformations:

Elution buffer used for squalene-hopene cyclase purification as described above was also used as reaction buffer for any reaction applying squalene-hopene cyclase including all cascade reactions that were conducted concurrently with EREDs.

ERED reactions were either carried out in 12 mM citrate buffer (pH 6) or in 50 mM MES/KOH buffer (pH 6.8).

2.2 Molecular biology

2.2.1 Standard procedures

Agarose gel electrophoresis

The method was used to separate DNA and to qualitatively assess their amount. Gene Ruler™ 1 kb Prestained DNA Ladder was used as marker. Marker (5 µL) and samples mixed with 5x DNA loading buffer (5-25 µL) were loaded on a hardened agarose gel (chapter 2.1.7) that was overlaid with 1x TAE buffer beforehand. A voltage was applied to the gel for 45 min (120 mV) in TAE buffer. DNA visualization was accomplished by UV light.

DNA clean-up procedures

Different DNA clean-up procedures were utilized in this thesis: i) the DNA Clean & Concentrator^{TM}-5 kit (ZYMO Research Corp, Irvine, USA) was used to clean DNA fragments according to the manufacturers instruction, except an additional centrifugation step after the last washing step and before elution. DNA was eluted with 10 µL ddH_2O; ii) nitrocellulose membranes (0.025 µm VSWP02500, Merck Millipore, Billerica, USA) were used to purify DNA by means of dialysis. The membrane was placed carefully on top of a ddH_2O reservoir and 10-20 µL DNA-containing sample were added as one drop on top of the membrane. After 20 min up to 15 µL purified DNA was used subsequently; iii) DNA was isolated after separation by gel electrophoresis cutting out the band of interest and applying the Zymoclean™ Gel DNA Recovery Kit (ZYMO Research Corp, Irvine, USA) according to the manufacturer's instruction; iv) plasmid DNA was purified from cell pellets by the application of the Zyppy^{TM} Plasmid Miniprep Kit (ZYMO Research Corp, Irvine, USA) according to the manufacturer's instruction, except a prolonged centrifugation after neutralization for 10 min and an additional centrifugation step after the last washing step and before elution. DNA was eluted with 30 µL ddH_2O.

Concentration determination

DNA concentration and purity were determined using a Nanodrop ND 1000 Spectrophotometer (Agilent Technologies, Santa Clara, USA). 1 µL per sample was transferred onto the spectrophotometer.

DNA sequencing

Commercial GATC Biotech AG (Konstanz, Germany) sequencing service was used. 20 µL of a 30-50 ng/µL purified DNA sample were sent.

Cell growth monitoring

Cell growth was monitored by measuring optical density (OD) values at 600 nm using a Amersham Biosciences Ultrospec 3100 pro UV/VIS-spectrometer (GE Healthcare, Chicago, USA).

2.2.2 Preparation of competent cells

Competent cells were evaluated before use by transforming them with an appropriate positive control and ddH_2O as negative control.

RbCl competent cells

RbCl competent cells were prepared for transformation of cells with plasmid DNA by heat-shock. After inoculation of a LB preculture over night at 37 °C and 180 rpm with the desired *E. coli* strain (DH5α, XL1-Blue or BL21(DE3)), a 200 mL LB culture was inoculated with 1 mL of the preculture. Cell growth was maintained at 37 °C and 180 rpm until an OD value of 0.5-0.7 (chapter 2.2.1). In the following, the culture was first cooled on ice for 15 min and afterwards centrifuged for 10 min at 3220 rpm and 4 °C. Isolated pellet was resuspended gently in 20 mL TfbI buffer, the solution cooled on ice for 15 min, centrifuged as before and the newly obtained pellet gently resuspended in 2 mL TfbII buffer. Again, the solution was cooled on ice for 15 min before finally shock-frosting 50 µL aliquots with liquid nitrogen that were stored at -80 °C.

Electrocompetent cells

Electrocompetent *E. coli* TG20+ cells were prepared for transformation of cells with plasmid DNA by electroporation. The preparation made use of the strain's inherent tetracycline resistance and ensured the essential cooling chain maintenance. After inoculation of a LB preculture over night at 37 °C and 200 rpm with the *E. coli* TG20+ strain, a 500 mL LB culture was inoculated to an OD value of 0.05. Cell growth was maintained at 37 °C and 200 rpm until achieving an OD value of 0.5-0.7. In the

following, the culture was first cooled on ice for 30 min with repeated slow hand-shaking and afterwards centrifuged for 10 min at 7800 rpm and 4 °C. First, the isolated pellet was resuspended gently in 5 mL ice-cold ddH_2O, filled up to 500 mL with ddH_2O and centrifuged as before. Secondly, the obtained pellet was gently resuspended in 5 mL ice-cold ddH_2O, filled up to 250 mL with ddH_2O and centrifuged as before. Third, the obtained pellet was gently resuspended in 5 mL ice-cold 10 % (*v*/*v*) glycerol, filled up to 25 mL with 10 % (*v*/*v*) glycerol and centrifuged as before. Finally, the pellet was resuspended in 2 mL 10 % (*v*/*v*) glycerol before shock-frosting 50 µL aliquots with liquid nitrogen that were stored at -80 °C.

2.2.3 Cell transformation

Heat-shock transformation

Depending on the material source, 1-10 µL of purified DNA (linear or cyclic) was added to a 50 µL aliquot of RbCl competent cells (chapter 2.2.2) thawed on ice and then incubated for 30 min on ice before the heat-shock was performed at 42 °C for 45-60 seconds. After immediate cooling on ice for 2-3 min, the cells were mixed with 500 µL LB medium and cell growth was stimulated at 37 °C and 180 rpm for 45 min. A 100 µL fraction of the obtained solution was plated on LB agar plates directly. From the residual solution cells were harvested by centrifugation for 1 min at 7000 rpm and 4 °C, resuspended in 100 µL of the supernatant and plated completely on an additional LB agar plate. All plates were incubated overnight at 37 °C. To select for cells with successful DNA uptake, LB agar plates contained antibiotic according to the resistance gene encoded by the utilized DNA (pET-22b(+) vector: ampicillin, pET-28a(+) vector: kanamycin; pDHE vector: ampicillin).

Electroporation

Depending on the material source, 1-10 µL of purified DNA (linear or cyclic) was added to a 50 µL aliquot of electrocompetent cells (chapter 2.2.2) thawed on ice. The mixture was gently mixed and transferred into the bottom of a suitable electrocuvette (2 mm gap) preventing any bubble formation before electroporation was initiated at 2.5 volts using the H132507 GenePulser™ 1652076 electroporation system from Bio-Rad Laboratories Inc. (Hercules, USA). Immediately, 1 mL warm SOC medium (pre-heated at 37 °C) was added and the electroporated cells were regenerated for

30 min at 37 °C and 180 rpm. A 100 µL fraction of the obtained solution was plated on LB agar plates directly. From the residual solution cells were harvested by centrifugation for 1 min at 7000 rpm and 4 °C, resuspended in 100 µL of the supernatant and plated completely on an additional LB agar plate. All plates were incubated overnight at 37 °C. To select for cells with successful DNA uptake, LB agar plates contained antibiotic according to the resistance gene encoded by the utilized DNA.

2.2.4 Site-directed and site-saturation mutagenesis

Sample reaction

The QuikChange II Site-Directed Mutagenesis Kit (Agilent Technologies, Santa Clara, USA) was used for site-directed mutagenesis or site-saturation mutagenesis (the latter uses degenerate codons, chapter 2.1.3). First, the sample reaction was prepared (Table 13) using complement pairs of forward and reverse primers (chapter 2.1.3). pET-28a(+) vector containing *ncr* ERED gene or pDHE vector containing *oye*1 ERED gene served as templates for site-directed mutagenesis. pDHE vector containing *ncr* ERED gene was used as template for site-saturation mutagenesis. The following described methodological differences between mutant generation for site-directed mutagenesis *vs.* site-saturation mutagenesis are the result of an optimization process (chapter 3.1.3) aiming to generate enough mutant gene containing colonies after transformation. The use of degenerate codons like NNK does not result in distinctly separable genes but rather generates a mixture of all those genes. After cell transformation, each colony contains one of those genes. For statistical reasons, the number of colonies screened is linked to the probability of actually assessing all possible amino acid variants (all 20 in case of NNK), which can for example be assessed by the freely available CASTER tool from Reetz et al..[101] As applied in this work, the screening of 95 colonies for a single NNK codon theoretically provides 95 % coverage.

Table 13: 50 µL sample reaction for QuikChange site-directed mutagenesis using the KOD Hot Start DNA polymerase. The enzyme was added as last component.

components*	amounts (example)
ddH_2O	32 µL
10x PCR buffer for KOD Hot Start polymerase	5 µL
2 mM dNTP mix (final: 0.2 mM)	5 µL
25 mM $MgSO_4$ (final: 1.5 mM)	3 µL
30 ng/µL template vector (final: 30 ng)	1 µL
10 pmol forward primer	1.5 µL
10 pmol reverse primer	1.5 µL
KOD Hot Start DNA polymerase	1 µL

*up to 2 % (*v*/*v*) DMSO was added to the sample reaction if the GC content of the primers exceeded 70 %

The sample reaction was performed using an appropriate thermocycler (e.g. Mastercycler EP S from Eppendorf AG, Hamburg, Germany) with repeated heating and cooling steps (Table 14).

Table 14: Thermocycler program that was applied to the QuikChange reaction sample. The applied temperature and time of each step as well as the number of repeated cycles are displayed. The annealing temperature was adapted according to the primer GC content.

step	program		
initial denaturation	95 °C	2 min	1x
denaturation	95 °C	1 min	
annealing	50-65 °C	1 min	20x
elongation	72 °C	3 min	
final elongation	72 °C	3 min	1x

Agarose gel electrophoresis

For QuikChange trouble shooting, the annealing temperature was varied as indicated or up to 2 % (*v*/*v*) DMSO was added to the reaction samples. For evaluation of different reactions for the same mutation, 8 µL of the reacted sample were analyzed by agarose gel electrophoresis (chapter 2.2.1). The sample indicating highest DNA amount was selected for further processing.

Restriction digest

Parental methylated DNA was disposed of by addition of 1 µL *Dpn*I restriction enzyme incubated for 1 h at 37 °C. For site-saturation mutagenesis additional 1 µL were added afterwards and incubated over night at 37 °C.

DNA purification

For site-directed mutagenesis, DNA was purified by DNA Clean & Concentrator^{TM}-5 kit, while dialysis was applied for site-saturation mutagenesis (chapter 2.2.1).

Cell transformation

RbCl competent *E. coli* DH5α cells or *E. coli* XL1-Blue cells were transformed using 10 µL of purified DNA by means of heat-shock transformation in the case of site-directed mutagenesis, while electrocompetent *E. coli* TG20+ cells were transformed using 10 µL of purified DNA by means of electroporation (chapter 2.2.3). Plasmid isolation and sequencing followed for mutants generated by site-directed mutagenesis. In the case of site-saturation libraries, the obtained colonies were used for direct inoculation (chapter 2.3.1)

Plasmid isolation and sequencing

A grown colony from the incubated LB agar plates was picked to inoculate a LB preculture containing appropriate antibiotic (chapter 2.1.5). After incubation at 37 °C and 180 rpm overnight, the culture was centrifuged and the plasmid was isolated from the obtained pellet using the Zyppy^{TM} Plasmid Miniprep Kit and subsequently sent for sequencing to control successful mutagenesis after concentration determination by NanoDrop (chapter 2.2.1).

2.2.5 Gibson assembly

Insert amplification and vector linearization

Gibson assembly represents an alternative for classical restriction digestion-ligation-cloning allowing for insertion and deletion of gene fragments into a plasmid. First, two separate polymerase chain reactions (PCR) are performed to produce amplified copies

of the desired insert and linearized vector containing overlapping gene sequences that are introduced by the designed primers (Table 15).

Table 15: 50 µL PCR sample reaction for amplification of the desired insert or linearization of the vector using the *PfuUltra* II Fusion HS DNA polymerase. The enzyme was added as last component.

components	amounts
template DNA*	50-200 ng
10x *PfuUltra* II reaction buffer	5 µL
10 mM dNTP mix	1.3 µL
10 pmol forward primer*	1 µL
10 pmol reverse primer*	1 µL
***PfuUltra* II Fusion HS DNA polymerase**	1 µL
ddH_2O	fill up to 50 µL

*Template was selected according to the primers applied (chapter 2.1.3). As two PCR reactions are performed, suitable plasmids for insert and vector amplification were used and four different primers are needed in total.

The PCR reactions were performed using an appropriate thermocycler (e.g. Mastercycler EP S from Eppendorf AG, Hamburg, Germany) with repeated heating and cooling steps (Table 16).

Table 16: Thermocycler program that was applied to the PCR reactions for insert amplification and vector linearization. The applied temperature and time of each step as well as the number of repeated cycles are displayed.

step	program		
initial denaturation	95 °C	120 s	1x
denaturation	95 °C	20 s	
annealing	60-70 °C*	20 s	30x
elongation	72 °C	90 s	
final elongation	72 °C	180 s	1x

*Annealing temperature was applied as suggested for primers used by the SnapGene 3.1.4 software from GSL Biotech (Chicago, USA) available at ‘snapgene.com’.

DNA purification

The PCR sample was separated by agarose gel electrophoresis, the DNA of interest purified using the Zymoclean™ Gel DNA Recovery Kit and the concentration determined by NanoDrop (chapter 2.2.1).

Assembly reaction

The molar ratio of insert to vector should be 5:1 and can be calculated using DNA concentrations and length (e.g. NEBioCalculator v1.7.1; source: 'https://nebiocalculator.neb.com'). 200 ng vector DNA was used and the insert adjusted accordingly. Assembly reaction contained 15 µL of Gibson master mix solution (Table 17) and 5 µL of the 5:1 vector-insert mix (filled up with ddH_2O if necessary) and was initiated by incubation at 50 °C for 1 h. Gibson master mix contains T5 exonuclease to generate sticky ends causing annealing of insert and vector, a polymerase to fill up missing gaps and a ligase to combine them to a cyclic plasmid.

Table 17: Preparation of Gibson master mix.

components	amounts
5 x ISO reaction buffer	100 µL
T5 exonuclease	0.2 µL
***Taq* DNA ligase**	50 µL
***PfuUltra* II Fusion HS DNA polymerase**	6.25 µL
ddH_2O	fill up to 375 µL

The solution was separated in 15 µl aliquots and stored at -20 °C for further use.

Cell transformation

RbCl competent *E. coli* XL1-Blue cells were transformed using 2 µL of reacted Gibson assembly sample by means of heat-shock transformation (chapter 2.2.3).

Plasmid isolation and sequencing

A grown colony from the incubated LB agar plates was picked to inoculate a LB preculture containing appropriate antibiotic (chapter 2.1.5). After incubation at 37 °C and 180 rpm overnight, the culture was centrifuged and the plasmid was isolated from the obtained pellet using the Zyppy^{TM} Plasmid Miniprep Kit and subsequently sent for sequencing to control successful mutagenesis after concentration determination by NanoDrop (chapter 2.2.1).

2.3 Protein production and purification

Different gene expression and protein purification protocols depending on the applied enzyme, strain and purpose were applied in this thesis. For EREDs and cyclases different conditions and methods were necessary. In the case of EREDs, additionally different expression systems were used, depending on the ERED-containing vector, pET-28a(+) or pDHE. Furthermore, an expression system in 96-deep-well plates (96-DWP) (Ritter GmbH, Schwabmünchen, Germany) was developed for screening larger mutant libraries.

2.3.1 Gene expression and cell harvesting

ERED gene expression using pET-28a(+) vector

All media contained kanamycin for selection purposes. RbCl competent *E. coli* BL21(DE3) cells were transformed with purified pET-28a(+) vectors containing either wild-type *ncr* gene from *Zymomonas mobilis* or variants thereof, namely all variants created by site-directed mutagenesis with defined codon exchange (chapter 2.2.3). A single colony or a glycerol stock solution was used to inoculate a 5 mL LB preculture (37 °C, 180 rpm, overnight), which in turn was used to inoculate a larger TB culture (100 or 400 mL) in a 1:5000 dilution. 500 µL of the preculture were mixed with 50 % (*v*/*v*) glycerol to prepare a glycerol cell stock solution stored at -80 °C. Overexpression was induced by addition of IPTG (end concentration: 0.2 mM) at 30 °C and 180 rpm after an initial cell growth stimulation at 37 °C and 180 rpm up to an OD value of 0.5-0.7 (chapter 2.2.1). After roughly 20 h cells were harvested by centrifugation at 8000 rpm and 4 °C for 30 min and the obtained pellet was either further processed or stored at -18 °C.

ERED gene expression using pDHE vector

All media contained ampicillin for selection purposes and in some cases also tetracycline, spectinomycin and chloramphenicol (the latter three were only used during method development being omitted for later standard expression of genes encoding enzyme variants). Electrocompetent *E. coli* TG20+ cells were transformed with purified pDHE vectors containing either wild-type *ncr* or *oye*1 gene from *Zymomonas mobilis* and *Saccharomyces pastorianus*, respectively or variants thereof, namely all NCR

variants created by site-saturation mutagenesis, some NCR variants created by site-directed mutagenesis and all OYE1 variants (chapter 2.2.3). A single colony or a glycerol stock solution was used to inoculate a 5 mL LB preculture (37 °C, 180 rpm, overnight), which in turn was used to inoculate a larger TB culture (100 or 400 mL) containing 0.5 g/L rhamnose (overexpression inductor) in a 1:5000 dilution. Overexpression and growth were simultaneously triggered at 37 °C and 180 rpm. Except for the characterization of hits as described in the following expression method, 500 µL of the preculture were mixed with 50 % (*v*/*v*) glycerol to prepare a glycerol cell stock solution stored at -80 °C for back-up. After 22-24 h cells were harvested by centrifugation at 8000 rpm and 4 °C for 30 min and the obtained pellet was either further processed or stored at -18 °C.

ERED gene expression using pDHE vector in 96-DWP scale

Ampicillin was used as antibiotic in all media solutions and transformation of *E. coli* TG20+ cells using *ncr* genes modified by site-saturation mutagenesis was performed as described in the beforehand expression method. For 95 out of 96 wells of a 96-DWP a colony was picked and added to 1 mL LB preculture solution in each well. One well served as negative control. To limit media evaporation, but allow for oxygen input, the 96-DWP was sealed with an air-permeable membrane and wrapped in a plastic bag containing small punctures and a wet paper cloth beneath the plate. After incubation of this "preculture 96-DWP" at 37 °C and 350 rpm, 50 µL of the grown preculture were used to inoculate 950 µL per well of LB medium containing 0.5 g/L rhamnose inductor. Growth and overexpression in the "expression 96-DWP" was stimulated under the same conditions as the "preculture 96-DWP" was grown. For long-time storage, well per well, 500 µL from the "preculture 96-DWP" were used to mix with 50 % (*v*/*v*) glycerol in an additional "glycerol 96-DWP". This stock plate was sealed with an impermeable aluminum lid and stored at -80 °C for further use. After 22-24 h cells were harvested by centrifugation at 4000 rpm and 4 °C for 10 min, the supernatant was discarded and the pellet-containing 96-DWP was either further processed or stored at -80 °C.

SHC gene expression using pET-22b(+) vector

All media contained ampicillin for selection purposes. RbCl competent *E. coli* BL21(DE3) cells were transformed with purified pET-22b(+) vectors containing either wild-type *shc* gene from *Alicyclobacillus acidocaldarius* or variants thereof

(chapter 2.2.3). A single colony was used to inoculate a 5 mL LB preculture (37 °C, 180 rpm, overnight), which in turn was used completely to inoculate a larger TB culture (400 mL) containing 0.5 g/L lactose (dissolved by heating). After simultaneous cell growth and gene overexpression stimulation at 37 °C and 100 rpm for roughly 20 h, cells were harvested by centrifugation at 6000 rpm and 4 °C for 30 min and the obtained pellet was either further processed or stored at -18 °C.

2.3.2 Cell disruption

Harvested cell pellets were resuspended in 5 mL/1 g pellet 50 mM Tris-HCl pH 7.5 buffer (for EREDs) or lysis buffer (for cyclases; chapter 2.1.7; here a spatula-tip full of deoxyribonuclease and 10 µL/1 g pellet PMSF were added). Cell disruption was achieved on ice by sonication for 4 min using Branson Sonifier 250 (G. Heinemann Ultraschall- und Labortechnik, Schwäbisch Gmünd, Germany). The cell debris was pelleted by centrifugation at 17000-23000 rpm and 4 °C for 25 min. For ERED workup, the lysate supernatant was either used for reactions, freeze-dried over night to obtain lyophilizate or was further purified without delay. For the membrane-bound cyclase, the supernatant was discarded and the pelleted cell debris was further processed.

2.3.3 Protein purification

Affinity chromatography

EREDs containing an N-terminal Poly-His_6 tag were purified *via* metal affinity chromatography using His GraviTrap TALON columns (GE Healthcare, Chicago, USA). Filtered solutions and buffers were used for column application. The columns were prepared by washing with water and 50 mM Tris-HCl pH 7.5 buffer. The lysate was filtered through a 0.45 µm filter before it was poured onto the column. Elution was performed using imidazole in rising concentrations contained in 50 mM Tris-HCl pH 7.5 to get rid of proteins binding non-specifically to the column. First, up to 2 mL buffer containing 5 mM and 10 mM imidazole were used, then the tagged enzyme was eluted with 50 mM imidazole (2-4 mL). Residual binders were removed using 300 mM imidazole and discarded. The columns were regenerated by washing with 50 mM Tris-HCl pH 7.5, ddH_2O and 20 % ethanol in which they were stored at 4 °C. The purified enzyme solution was concentrated and desalted with Vivaspin ultrafiltration

spin columns (Vivaspin 10 kDa from Sartorius AG, Göttingen, Germany) using 50 mM Tris-HCl pH 7.5 buffer. Remaining 2-3 mL were aliquoted and stored at -18 °C for further use.

Heat-shock and ion exchange chromatography

*Aac*SHC is a thermostable protein and could be purified by heat-shock denaturation of other proteins. The enzyme-containing cell debris was solubilized over night at 4 °C with solubilization buffer (chapter 2.1.7) (1 mL/1 g pellet) using the Intelli-Mixer RM-2M (ELMI Ltd., Riga, Latvia). Afterwards, the heat-shock was applied at 50 °C for 30 min. The treated solution was centrifuged at 23000 rpm and 4 °C for 30 min and the supernatant was filtered (0.2 µM) before application onto ion exchange columns. DEAE-Sephacel© was used as solid ion exchange material that was freshly packed into a column (2-3 mL) *in vacuo* before use. Before addition of the filtered supernatant, the column was washed with 5 column volumes of regeneration and wash buffer (chapter 2.1.7). After protein binding, again 5 column volumes wash buffer were added before elution with 2-3 column volumes using elution buffer (chapter 2.1.7). The purified cyclase solution was stored at 4 °C for further use.

2.3.4 SDS-PAGE

Control of expression and purification was performed by SDS polyacrylamide gel electrophoresis (PAGE). For expression, samples before and during expression induction as well as shortly before cell harvest were taken. The pelleted samples correlated to an optical density of 0.25 (when diluted with buffer to 1 mL) and were resuspended in 15 µL ddH_2O. Purified enzyme solutions were used directly. Each sample was diluted appropriately to 15 µL and mixed with 15 µL Lämmli loading buffer (chapter 2.1.7). After denaturation for 10 min at 95 °C and centrifugation, 15-30 µL of supernatant were cast onto a polyacrylamide gel (chapter 2.1.7). 5 µL PageRuler^{TM} Prestained Protein ladder (5 µL) was used as marker in a separate gel pocket. The gel electrophoresis was performed at 10 mA per gel for 10 min and then 25 mA per gel for 55 min. The gel was developed by application of staining and destaining solution (chapter 2.1.7).

2.3.5 Determination of protein concentration

Enzyme concentrations were measured by Bradford assay.[153]

For EREDs, 200 µL Coomassie®-Blue G-250 dye is added to 800 µL 1:1000-1:5000 diluted enzyme solution (with ddH_2O). After a 5 min incubation time, the binding of Coomassie to protein was determined by measuring the absorption at 595 nm. The concentration was calculated by comparison to a calibration curve that was obtained by measuring the absorption of BSA samples of known concentrations (10, 8, 6, 4 und 1 µg/mL). Samples were measured as triplicates.

For cyclases, the detergent-compatible BradfordUltra™ reagent was used. Protein samples were diluted 1:10 with elution buffer. 10 µL sample were mixed with 150 µL Bradford reagent and the absorption at 595 nm was measured immediately. The concentration was calculated by comparison to a calibration curve that was determined by measuring the absorption of BSA samples of known concentrations (1, 0.8, 0.6, 0.4, 0.2 and 0 mg/mL). Samples were measured as triplicates.

2.4 Analytical biotransformations and product analysis

In the following, standard procedures for analytical biotransformations are described. Experiments leading to those methods as well as specific analyses and unique negative controls are mentioned in the results part. The specification of different conditions, e.g. buffer concentrations, indicates that, depending on the purpose of the experiment, different variations of the same method was used, which is further specified in the related results part. Extraction of samples (chapter 2.4.6) and their analysis (chapter 2.6.1) are described in separate chapters. If not specified further, duplicate or triplicate measurements refer to similarly, but separately prepared reaction approaches using the same stock of either a purified enzyme preparation or the enzyme-containing cell culture.

2.4.1 Biotransformations using purified NCR ERED

The isomers *E*- and *Z*-citral were used as substrates for all analytical biotransformations and in some cases the isomeric mixture was utilized additionally. The 1 mL-scaled reactions contained 2 mM substrate, 2.5 mM NADH, 1 % (*v*/*v*) DMSO and 50 µg/mL purified enzyme solution (purity > 90 %) in 12 mM citrate buffer at pH 6. The reactions were started by final enzyme addition and incubation at 30 °C and 180 rpm for 4 h. Reactions were performed as triplicates and carried out in 2 mL plastic tubes.

2.4.2 Whole cell biotransformations

The isomers *E*- and *Z*-citral were used as substrates for all analytical biotransformations and in some cases the isomeric mixture was utilized additionally. Conditions were used for OYE1 library screening and NCR hit characterization as mentioned accordingly. The 1 mL-scaled reactions contained 2 mM substrate, 2.5 mM NADH, 5 % (*v*/*v*) isopropanol and 5 g/L enzyme containing *E. coli* TG20+ cells resuspended in 50 mM MES/KOH buffer at pH 6.8. The reactions were started by final substrate addition and incubation at 30 °C and 180 rpm for 4 h. For OYE1 library screening, reactions were performed as duplicates in 2 mL plastic tubes, but active variants were rescreened in duplicates under the same reaction conditions except using 5 mM substrate and 6 mM NADH.

2.4.3 96-DWP screening of NCR variants

The isomers *E*- and *Z*-citral were used as separate substrates for each screened variant. In fact, for each "preculture 96-DWP", two "expression 96-DWPs" have been inoculated to enable parallel screening of both substrate isomers separately (chapter 2.3.1). For screening, the cells from a harvested "expression 96-DWP" were resuspended in 50 mM MES/KOH buffer at pH 6.8 containing NADH (2.5 mM final concentration). Thus, whole cells were used for screening. The cell suspension was transferred to a separate DWP containing glass inlets from Hirschmann Laborgeräte GmbH & Co. KG (Eberstadt, Germany). The reaction was started by addition of citral stock solution in isopropanol to achieve final concentrations of 2 mM substrate and 5 % (*v*/*v*) isopropanol in 500 µL total reaction volume per well. The glass inlets not only ensured inert surrounding but also allowed for prevention of evaporation by using tight-fitting cap mats by Hirschmann. The reactions were performed at 30 °C and 500 rpm for 4 h using the plate shaker TiMix5control equipped with a T30 Incubator hood from Edmund Bühler GmbH (Hechingen, Germany).

2.4.4 Biotransformations using purified *Aac*SHC

Either *S*-citronellal or *R*-citronellal was used as substrate. The 500 µL-scaled reactions consisted of 2 mM substrate, 1 % (*v*/*v*) DMSO and 2 mg/mL purified enzyme solution (purity > 80 %) in elution buffer (chapter 2.1.7; contains 0.2 % (*w*/*v*) Triton X-100 if not mentioned otherwise). The reactions were started by final enzyme addition and incubation at 30 °C and 600 rpm for 5 h or 40 h. Reactions were performed as triplicates in 2.5 mL glass vials.

2.4.5 Biotransformation for cascade reactions

E/*Z*-citral was used as substrate for cascade reactions towards isopulegol using an ERED and an SHC concurrently. For cascade evaluation, several parameters were changed (chapter 3.2.2) in comparison to following chosen reference conditions: A 500 µL-scaled reaction in 2.5 mL glass vials contained 2 mM substrate, 1 % (*v*/*v*) DMSO, 0.5 mg/mL purified ERED and 2.5 mg/mL purified SHC enzyme in elution buffer. The reactions were started by final substrate addition and incubation at 20 °C and 600 rpm for 5 h and performed as triplicates. From these experiments following so

far optimized conditions are proposed: The 1100 µL-scaled reactions are performed in 1.1 mL glass vials and consist of 2 mM substrate, 5 % (*v*/*v*) isopropanol, 4 mg/mL purified SHC enzyme solution and 10 g/L *E. coli* TG20+ cells containing ERED in elution buffer (chapter 2.1.7). The reactions were started by final substrate addition and incubation at 20 °C and 600 rpm for 5-20 h.

2.4.6 Extraction methods

ERED biotransformations

Biotransformation samples were extracted by thorough mixing for 10 s using two times 500 µL MTBE containing 2 mM 1-octanol as internal standard. After the two centrifugation steps at about 13000 rpm for 2 min, first, 200 µL of the organic layer and secondly, 400 µL were combined in a gas chromatography glass vial for further analysis (chapter 2.6).

ERED 96-DWP screening

Biotransformation samples were extracted once by thorough mixing for 60 s using 500 µL MTBE per well. Separation of the organic layer was achieved by centrifugation at 4000 rpm for 5 min. 150 µL of organic layer was transferred in an inlet-containing gas chromatography glass vial for further analysis (chapter 2.6).

SHC and cascade biotransformations

Biotransformation samples were extracted by thorough mixing for 40 s using two times 500 µL ethyl acetate containing 2 mM 1-decanol as internal standard. After the two centrifugation steps at 7000 rpm for 2 min, first, 200 µL of the organic layer and secondly, 400 µL were combined in a gas chromatography glass vial for further analysis (chapter 2.6).

2.5 Preparative biotransformation for (-)-menthol synthesis

The preparation of (-)-menthol from *E*/*Z*-citral was performed in a two-step process (Figure 22). First, (-)-isopulegol was produced in a bienzymatic cascade and subsequently the crude reaction mixture was supplied with heterogeneous 5 % (*w*/*w*) Pd/C catalyst and hydrogen gas for reduction to (-)-menthol.

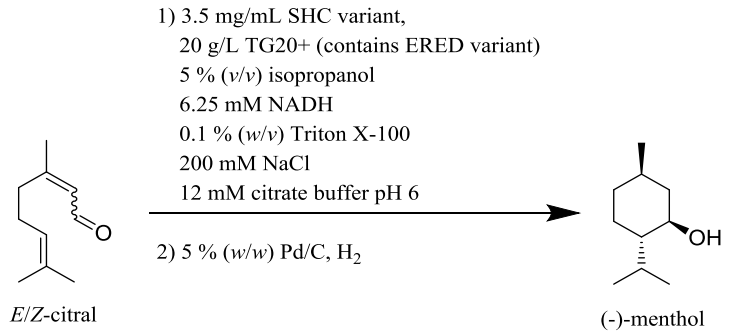

Figure 22: Preparative biotransformation of *E*/*Z*-citral to (-)-menthol. First, citral is converted in a bienzymatic cascade of an ERED and an SHC followed by addition of 5 % (*w*/*w*) Pd/C and hydrogen gas for final reduction to menthol.

Bienzymatic cascade

The bienzymatic cascade using ERED and SHC was carried out in 120 mL total volume. The reaction, however, was split in six 20 mL reactions carried out in 20 mL septum screw cap glass vials. In total, 0.6 mmol citral were used as starting material. To 19 mL elution buffer (12 mM citrate, 200 mM NaCl, 0.1 % (*w*/*v*) Triton X-100, pH 6) containing 3.5 mg/mL *Aac*SHC variant A419G/Y420C/G600A, 20 g/L NCR variant W66A/I231R/F269V comprising *E. coli* TG20+ cells, 6.25 mM NADH and 1 mL *E*/*Z*-citral dissolved in isopropanol (final concentrations: 5 mM citral and 5 % (*v*/*v*) isopropanol) were added. The reaction was carried out for 22 h at 20 °C and 250 rpm using a Multitron shaker from Infors AG (Bottmingen, Swiss). The reaction progress was followed by taking 250 µL samples that were extracted (chapter 2.4.6) and analyzed by gas chromatography (chapter 2.6.1).

Hydrogenation

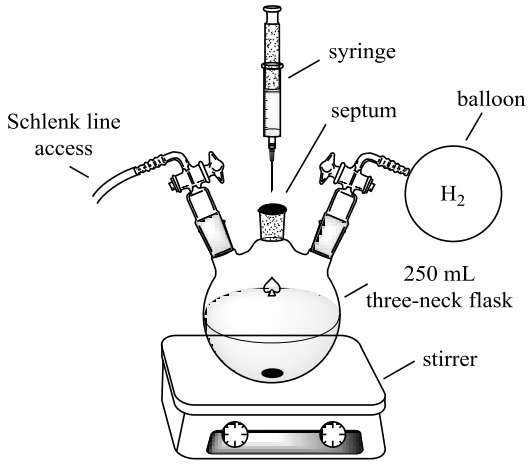

Figure 23: Experimental hydrogenation setup. A 250 mL three-neck flask equipped with septum, gas inlet adapters for Schlenk line connection and hydrogen balloon connection as well as a magnetic stirrer were used. The reaction solution from the previous bienzymatic cascade was added using a syringe.

For the hydrogenation reaction, inert conditions within a 250 mL three-neck flask were generated by alternating heating *in vacuo* and flooding with nitrogen gas for three times. 86 mg of 5 % (*w*/*w*) Pd/C suspended in 5 mL elution buffer were added under nitrogen flow before the flask was flooded with hydrogen. Afterwards, the 120 mL crude reaction solution from the bienzymatic cascade was added dropwise to the flask *via* a septum using a syringe. The reaction was carried out under vigorous magnetic stirring maintaining a constant hydrogen atmosphere. The reaction progress was followed by taking 250 µL samples that were extracted (chapter 2.4.6) and analyzed by gas chromatography (chapter 2.6.1). The reaction was finished after 44 h. The reaction solution was filtered over celite *in vacuo* to remove the heterogeneous catalyst, washed with isopropanol and water and then extracted three times with 120 mL MTBE per extraction. Phase separation was achieved by centrifugation. Combined organic layers were washed with brine, dried over magnesium sulfate and the solvent was removed under reduced pressure. The raw product was purified by flash column chromatography over silica gel using a gradient elution from pure *n*-heptane to a 19:1 *n*-heptane/ethyl acetate mixture. Elution progress was followed by thin layer chromatography (9:1 *n*-heptane/ethyl acetate) using a vanillin development solution (8.6 g vanillin, 2.5 mL sulfuric acid, 200 mL ethanol). Menthol was identified at an R_f value of 0.18. After solvent removal under reduced pressure, (-)-menthol (0.63 mg, 0.04 mmol, 6.7 % yield) was obtained in 93 % purity (chapter 3.2.3) as colorless crystals. ^{1}H-NMR (500 MHz, $CDCl_3$): δ (ppm) 3.41 (td, 1H), 2.17 (sd, 1H), 1.97 (dddd, 1H), 1.66 (dddd, 1H), 1.61 (dq, 1H), 1.42 (m, 1H), 1.26 (s, OH), 1.11 (dddd, 1H), 0.98 (m, 2H), 0.92 (t, 6H), 0.81

(d, 3H). ^{13}C-NMR (126 MHz, $CDCl_3$): δ (ppm) 71.56, 50.14, 45.05, 34.53, 31.63, 25.84, 23.14, 22.20, 21.00, 16.10. The shifts are in accordance to literature.[154] As a side product, 3,7-dimethyloctanol (15.5 mg, 0.1 mmol, 16.3 % yield) was obtained as colorless oil in another fraction. ^{1}H-NMR (500 MHz, $CDCl_3$): δ (ppm) 3.68 (m, 2H), 1.62 (m, 1H), 1.36-1.55 (m, 3H), 1.10-1.32 (m, 6H), 0.89 (d, 3H), 0.87 (d, 3H). ^{13}C-NMR (126 MHz, $CDCl_3$): δ (ppm) 61.27, 40.01, 39.27, 37.38, 29.52, 27.98, 24.69, 22.70, 22.60, 19.65.

2.6 Analytical methods

2.6.1 Gas chromatography

GC/FID

A GC-2010 gas chromatograph from Shimadzu (Kyoto, Japan) equipped with an AOC-20i auto injector, an FID detector and either an HP-1 column (30 m x 0.25 mm ID, 0.25 µm film) from Agilent Technologies (Santa Clara, USA), a chiral β-DEX 225 column (30 m x 0.25 mm ID, 0.25 µm film) from Supelco/Sigma-Aldrich (St. Louis, USA) or a chiral HP-Chiral-20B column (30 m x 0.32 mm ID, 0.25 µm film) from Agilent Technologies was used with hydrogen as carrier gas (30 cm/s if not mentioned otherwise). Depending on the measurement purpose and analytes used, the different columns were used (Table 18).

Table 18: Applied GC programs for Shimadzu GC/FID with injector and FID detector temperatures for different columns and objectives. If not mentioned otherwise the linear velocity of the hydrogen carrier gas was 30 cm/s. Split injection mode was applied in all cases and 1 µL was injected.

column	objective	GC program
Agilent HP-1	determination of product formation for citral to citronellal conversions	60 °C for 3 min, 10 °C/min to 105 °C, hold 4.5 min, 30 °C/min to 135 °C, 50 °C/min to 325 °C, hold 2 min; injector temperature: 325 °C; FID temperature: 325 °C; split ratio 1:10
Supelco β-DEX 225	base-line separation of citronellal enantiomers	90 °C for 25 min, 50 °C/min to 220 °C, hold 3 min; injector temperature: 220 °C; FID temperature: 230 °C; split ratio 1:20; linear velocity of carrier gas: 40 cm/s
Supelco β-DEX 225	rough separation of citronellal enantiomers for screening	100 °C for 8.4 min, injector temperature: 220 °C; FID temperature: 230 °C; split ratio 1:20; linear velocity of carrier gas: 70 cm/s
HP-Chiral-20B	enantiomer-separation for isopulegol and menthol	40 °C for 5 min, 1 °C/min to 130 °C, hold 1 min, 2 °C/min to 200 °C, hold 3 min; injector temperature: 225 °C; FID temperature: 225 °C; split ratio 1:20

GC/MS

A 7890A GC/MS gas chromatograph from Agilent Technologies (Santa Clara, USA) equipped with a 5975 series MSD mass detector (ionization by electron impact; 70 eV) as well as an FID detector and a HP-5 column (30 m x 0.25 mm ID, 0.25 µm film) from Agilent Technologies was used with helium as carrier gas (17.937 psi constant pressure). The chromatograph was used with a single method for the analysis of SHC-derived reactions (Table 19).

Headspace measurements were performed using a GC-2010 gas chromatograph from Shimadzu (Kyoto, Japan) equipped with a QP2010 mass spectrometer, an AOC-5000 auto injector and an FID detector and an HP-5msi column (30 m x 0.25 mm ID, 0.25 µm film) from Agilent Technologies (Santa Clara, USA). Helium served as carrier gas (30 cm/s). Split injection mode was applied in all cases and 1 µL was injected. The applied headspace vial was not heated before measurement.

Table 19: Applied GC/MS programs for Agilent Technologies GC/MS (first entry) and Shimadzu GC/MS (second entry). Split injection mode was applied in all cases and 1 µL was injected.

column	objective	GC program
Agilent HP-5	determination of product formation for isopulegol and menthol	50 °C for 3 min, 6 °C/min to 120 °C, 10 °C/min to 138.5 °C, 120 °C/min to 310 °C, hold 1 min; injector temperature: 250 °C; FID temperature: 310 °C; split ratio 1:5
Agilent HP-5msi	determination of citronellal in the gas phase	60 °C for 3 min, 10 °C/min to 105 °C, hold 4.5 min, 30 °C/min to 135 °C, 50 °C/min to 285 °C, hold 3 min; injector temperature: 250 °C; ion source temperature: 200 °C; split ratio 1:20; headspace measurement

Quantification

Standard quantification for variant characterization was performed by comparison of analyte and internal standard peak areas. Due to their relative nature, enantioselectivity values were determined with suitable accuracy. In this case, product formation values were consequently calculated relative to enzyme wild-type. For all experiments aiming to determine non-relative product formation values, quantification was achieved by additionally comparing to an externally measured calibration line for the analyte of interest. For the characterization of two of the generated most *R*-selective ERED variants (chapter 3.1.5), two separate cell cultures containing the respective variant were used to independently perform reaction triplicates with each of these biological duplicates (six reactions for each variant).

2.6.2 NMR spectroscopy

For nuclear magnetic resonance (NMR) spectroscopy experiments, an Avance 500 spectrometer from Bruker (Billerica, USA) has been used. For ^{1}H-NMR and ^{13}C-NMR analysis, 500 MHz and 126 MHz magnetic fields were applied, respectively. Tetramethylsilane (TMS) was added to samples as standard for calibration of chemical shifts δ in ppm with δ(TMS) = 0 ppm.

2.6.3 IR spectroscopy

For infrared spectroscopy (IR) spectroscopy, a Vector 22 FT-IR spectrometer (equipped with a MKII golden gate single reflection diamond ATR system) from Bruker (Billerica, USA) has been used. The samples were analyzed as liquid films between sodium chloride plates resulting in absorption bands presented as wave numbers (cm^{-1}).

2.7 *In silico* methods

2.7.1 Molecular docking simulation

Molecular docking simulates substrate binding in a rigid protein surrounding within a defined simulation cell. The YASARA software from YASARA Biosciences GmbH (Vienna, Austria) was utilized to perform flexible molecular docking simulation.[155] Protein templates were loaded as pdb files from solved crystal structures (NCR: 4A3U; OYE1: 1OYA). If necessary, the software internal *in silico* variation tool was used to simulate an enzyme variant. Before docking, a simulation cell was defined around the complete protein and water was added followed by application of the YASARA energy minimization script. After removal of water, the simulation cell was defined around the active site cavity and docking simulation was performed by application of the dock_run.mcr macro using VINA as docking method and the AMBER03 force field. Further processing of resulting substrate-enzyme complexes were performed using the PyMOL software from Schrödinger LLC (New York, USA). The obtained binding modes were assessed by meeting certain demands for successful catalysis known from literature (chapter 1.3.2): The activated C=C double bond is stacked above the hydride-donating isoalloxazine moiety of FMN and the electron withdrawing group is in hydrogen bonding distance towards the stabilizing His/Asn pair.[54]

2.7.2 Molecular dynamics simulation

Molecular dynamics simulation allows for the calculation of protein dynamics, thus side chain and domain movements of proteins. Molecular dynamics simulations were performed in collaboration with Dr. Wolfgang Brandt from the Leibniz Institute of Plant Biochemistry (Halle (Saale), Germany) using the YASARA software from YASARA Biosciences GmbH (Vienna, Austria). Protein templates were loaded as pdb files from solved crystal structures (NCR: 4A3U; OYE1: 1OYA). If necessary, the software internal *in silico* variation tool was used to simulate an enzyme variant. Simulations were either performed for single enzymes or substrate-enzyme complexes after docking simulation as described above. Two different YASARA simulation scripts have been used. The md_refinement.mcr macro performed a short 0.5 ns simulation and was primarily used to allow for side chain adjustments after docking simulation. The

md_run.mcr macro performed a 5 ns simulation and was used to simulate the effect of amino acid variations on the active site dynamics. Both scripts simulated the complete protein under periodic boundary conditions in aqueous solution at pH 7.4 and 298 K (standard conditions of the macro). While the MD refinement used the YAMBER03 force field, the MD simulation was performed with the AMBER03 force field. Further processing of the simulation results were performed using the PyMOL software from Schrödinger LLC (New York, USA).

2.7.3 Semi-empirical quantum mechanics calculation

Quantum mechanics calculations solve the Schrödinger equation enabling the calculation of electron properties that are for example completely neglected in molecular dynamics simulations. Thus, transition states and chemical reactions can be calculated. Semi-empirical methods make use of several empirically determined parameters and simplifications in order to also simulate larger reaction systems like an enzyme active site. Semi-empirical quantum mechanics calculations were performed in collaboration with Dr. Wolfgang Brandt from the Leibniz Institute of Plant Biochemistry (Halle (Saale), Germany). Grid calculations of two coordinates were carried out by the use of the PM7 Hamiltonian as implemented in the MOPAC2016 (Version 16.276L, James J. P. Stewart, Stewart Computational Chemistry, 'HTTP://OpenMOPAC.net') program. Each grid point calculation applied MMOK corrections and the BFGS algorithm for geometry optimization. The "Molecular Operating Environment", short MOE from the Chemical Computing Group (Montreal, Canada) was used as software platform for visualization and set up of the calculations. Atoms defining the enzymatic active site have been selected for calculation (chapter 3.1.1). Remaining atoms were removed. Additionally, several atoms were defined as fixed to reduce calculation effort.

3. Results

In contrast to ‘classical’ organic chemistry, biocatalysis is a young and emerging discipline. Due to the tremendous scientific and industrial efforts, it evolves into a serious complement for organic chemistry.[8,10,16,156] The possibility of genetically modifying biocatalysts has shown that enzyme preferences can be altered to overcome existing limitations like stability, narrow reactivities, selectivities and substrate specificities.[9,10] While this has been shown frequently for specific showcases, it is also important to investigate these techniques for the synthesis of specific valuable products. This is achieved by considering enzyme catalysis in retrosynthetic analysis to provide certain missing reactivities or selectivities involving the adaptation opportunity by genetic engineering. In this work, this research is expanded taking the example of the industrially important aroma chemical (-)-menthol. In the following it is described how the envisioned alternative chemoenzymatic synthesis of this molecule (chapter 1.7) is realized and assessed. The first part focuses on engineering of an *R*-selective ERED to provide the necessary selectivity for (-)-menthol synthesis. The second part describes the application of this novel catalyst in a chemoenzymatic synthesis in combination with an engineered SHC and a heterogeneous hydrogenation catalyst.

3.1 ERED engineering towards *R*-selective citral reduction

The envisioned chemoenzymatic synthesis of (-)-menthol is based on an existing large-scale industrial process, which makes use of the easily available starting material *E*/*Z*-citral.[36] One major synthetic advantage that could be achieved by the alternative use of enzymes is based on the challenging stereochemical reduction of citral to *R*-citronellal. The process requires chiral control in the reduction of both isomers of citral, *E* and *Z*, because *S*-citronellal cannot be further converted to produce (-)-menthol, which is the only diastereomer that matches consumer products demands. However, no catalyst has yet been described to catalyze the enantioconvergent reduction of both citral isomers to *R*-citronellal. It appears, though, that the market for (-)-menthol is valuable enough to reason the energetically costly separation of citral isomers that is necessary to apply two different homogeneous catalysts that provide the necessary chiral

conversions. From this point of view, assessing alternative enzyme catalysts constitutes a fascinating object of study. Although, also no enzyme has been described yet that provides the described *R*-selectivity in the reduction of both isomers of citral, the opposite reactivity to the *S*-enantiomer with remarkable enantioselectivity (> 99 % *S*) is widespread as a classification of existent EREDs unveils (chapter 1.3.3). From these data it is also apparent that *R*-selective citral reduction is in principle possible as shown for yeast-derived reductases although only for the *E*-isomer. Ongoing screening and characterization of novel EREDs would be a possible strategy to find a suitable enzyme. But motivated by the inspiring recent advances in enzyme engineering, this work describes a mutagenesis approach to provide the desired *R*-selectivity for both citral isomers.

Finding a suitable target enzyme gene preceded the enzyme engineering strategy that is described in the following. In principle, an ERED either belonging to the identified type I or type II citral reductases could serve as mutagenesis template (chapter 3.1.3). Although type I enzymes already are partially *R*-selective, type II enzymes have the advantage that they already enable enantioconvergent reduction for both isomers. As this is so far unachieved by any 'classical' chemical catalyst, this might be the more challenging feature to address. Due to these considerations, a type II ERED was selected as mutagenesis target in the beginning. Thus, it might also be elucidated how the enzyme maintains its enantioconvergent character. Regarding citral, previous studies rendered NCR ERED from *Zymomonas mobilis* as efficient catalyst for the reduction to citronellal, although it is a challenging substrate for many other EREDs.[85,89] Therefore, it represents the model enzyme in this thesis. Nevertheless, an analogous mutagenesis approach using the type I ERED OYE1 from *Saccharomyces pastorianus* was performed in comparison (chapter 3.1.4). OYE1 is the oldest and best characterized ERED present.[67,69,77,157]

3.1.1 Characterization of NCR ERED-catalyzed citral reduction

The NCR ERED from *Zymomonas mobilis* was chosen for further characterization and as mutagenesis target for the reduction of both isomers of citral (Figure 24).[85]

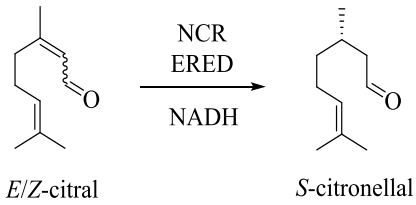

Figure 24: General reaction scheme of the NADH-dependent NCR ERED-catalyzed reduction of *E*/*Z*-citral to *S*-citronellal.

In the following some experiments preceding the later on described mutagenic approaches are described in which citral was converted using NCR wild-type. The deliberation was to characterize some aspects of the reaction that might be crucial for later application. For instance, important implications might derive from the molecular nature of citral and citronellal. On the one hand both structures bear an aldehyde moiety, which is generally a rather reactive functional group and on the other hand, both molecules are regarded as volatile monoterpenes.

Initial reaction and analysis setup

To achieve catalysis, simple access to the catalysts is desirable. Wild-type NCR ERED gene and all later mutants thereof were expressed in *E. coli* BL21(DE3). *E. coli* is the most widespread applied microorganism for molecular biology applications.[158] Enzymes were readily expressed and purified by affinity chromatography (Figure Ap. 2). Purified enzymes displayed a characteristic yellow color. Following experiments and all later NCR-based site-directed mutagenesis approaches employed purified enzyme preparations due to known cellular side reactions in whole cells or its lysate (further specified in chapter 1.3.3 and chapter 3.1.3).

For a start, suitable reaction conditions for the reduction of citral using NCR ERED were chosen on the basis of preceding projects.[72,74] Due to its less polar character, the solubility of citral in water is limited. The addition of 1 % (*v*/*v*) DMSO cosolvent was sufficient to overcome this issue in the scope of analytical conversions using 2 mM substrate in 1 mL reactions. NCR ERED also accepts the presence of other organic solvents (mostly polar protic) that can be used as cosolvents.[71] Furthermore, an excess of NADH (2.5 mM) was added to prevent a limited supply of reduced enzyme. Citrate buffer at pH 6 proved to be suitable buffer conditions for this reaction.[74]

The applied chromatographic methods for achiral and chiral analysis of the reduction reactions realized a sufficient separation of educt and product peaks (Figure Ap. 3-5). For achiral analysis, three minor additional peaks were identified close to the citronellal

product peak. They could be ascribed to citral as they were also found in the respective standards (including the separate isomer standards). Notably, NMR analysis of the citral standards revealed no impurity. No hints for significant uncoupling, meaning the ERED-catalyzed oxygen reduction to hydrogen peroxide, was found. The presence of hydrogen peroxide would cause spontaneous Weitz-Scheffer epoxidation of citral to form epoxides.[63] However, no epoxides were found in the NCR ERED-catalyzed reactions.

Several control experiments were conducted in order to test if certain reaction compounds led to background citral reduction or if other side reactivities were observable with either citral or citronellal (Table 20).

Table 20: Conditions for negative controls performed to link citral reduction activity to the ERED activity and to probe for side reactivities. Samples were tested as triplicates at two time points. First, the sample was mixed and directly extracted and second, the sample was mixed, incubated for 2.5 h at 30 °C and 180 rpm and then extracted to compare the effect of reaction conditions.

probed conditions in buffer solution
citral only
citronellal only
citral and NADH (no enzyme)
citral and enzyme (no NADH)
NADH and enzyme (no substrate)
citronellal and NADH (no enzyme)
citronellal and enzyme (no NADH)

According to the above listed entries, 1 mL samples in 2 mL plastic vials contained one or more of the following additives: 2 mM citral or 2 mM citronellal in 12 mM citrate buffer at pH 6 with 1 % (*v*/*v*) DMSO, 2.5 mM NADH, 10 µg/mL NCR WT.

In none of the citral-based negative controls citronellal formation was found. The reduction depends on the NADH-driven reduction by the ERED. No side products were identified in the samples. However, it was found that under reaction conditions after 2.5 h only a fraction of the initially used substrate amount could be identified when compared to directly extracted samples. This was supposed to be a consequence of the volatility of the monoterpene. This potentially volatility-derived substance loss will be described in more detail in following experiments.

Some insights into the NCR ERED-catalyzed reduction of citral were obtained by determining reaction progress at different time points (Figure 25). It should be noted that each time point represents an individual triplicate analytical sample reaction.

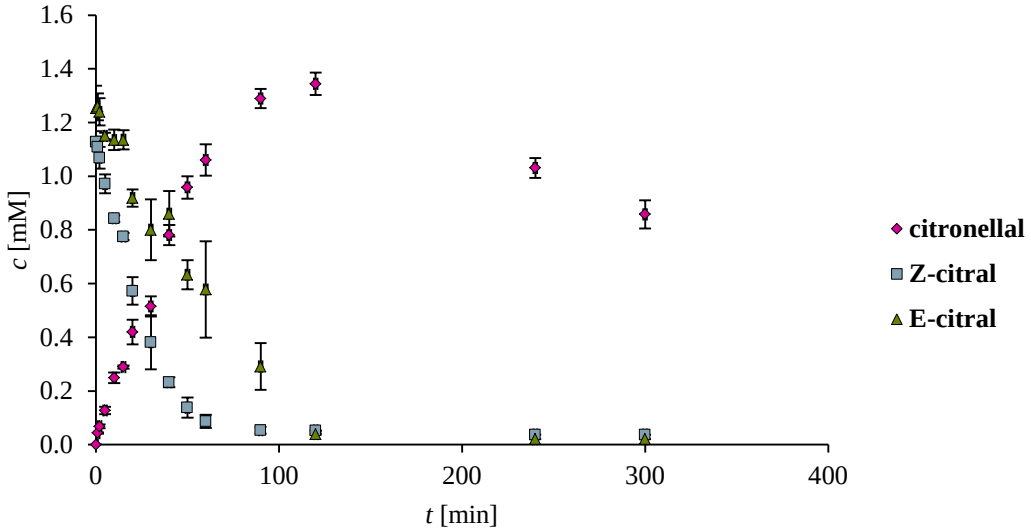

Figure 25: Time-dependent reduction of *E*/*Z*-citral by NCR ERED. Analytical reactions as described in chapter 2.4.1 were performed as triplicates for each displayed time point using 2 mM substrate. The calculated concentrations *c* [mM] of citronellal, *Z*-citral and *E*-citral are plotted against the time *t* [min].

The time-dependent reduction measurements reveal that both isomers of citral are almost completely consumed after 120 min. The *Z*-isomer is depleted faster than the *E*-isomer. This reflects a slight preference of NCR ERED for the reduction of *Z*-citral, which was described previously.[85] Furthermore, after 120 min a maximal product concentration of 1.4 mM citronellal is achieved. Taking into account that for these measurements, 10 µg/mL enzyme was used, a TOF (turnover frequency) of 1.32 s^{-1} can be calculated for the given substrate concentration. Moreover, the product concentration decreases after 2 h. The mentioned volatility of citronellal or further interactions, for instance with the protein or the reaction vessel, were considered possible causes. As this behavior will directly affect all analytical and also preparative reactions, additional investigations were conducted to study this depletion further.

Influence of citronellal volatility

To verify product loss due to evaporation, headspace measurement was performed after reaction incubation for 6 h (Figure 26). It should be noted that for the headspace measurement no preheating of the sample was conducted in order to link identified substances in the gas phase to evaporation during the reaction.

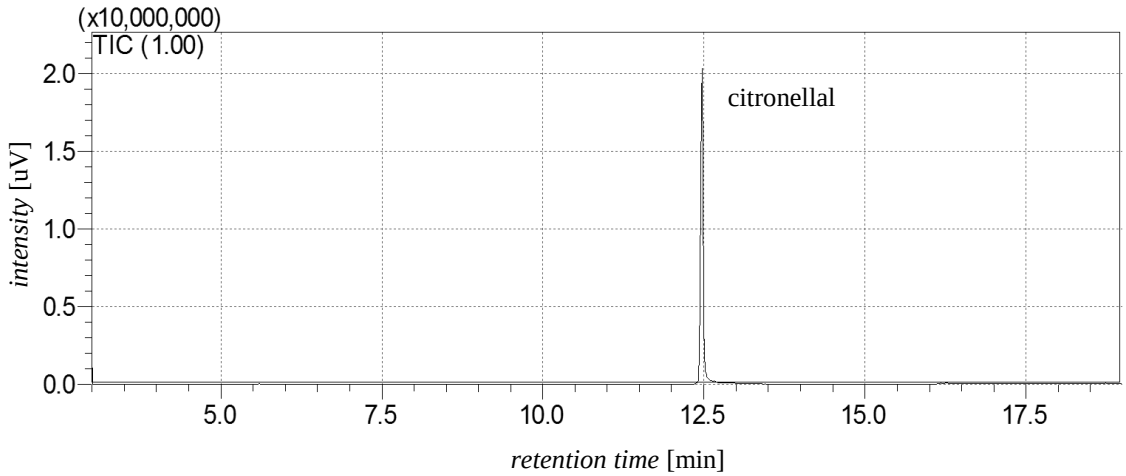

Figure 26: Chromatogram of a headspace measurement after reaction of citral in the presence of NCR wild-type and NADH for 6 h under standard conditions as described in chapter 2.4.1. The sample was not heated to account for evaporation. By its mass spectrum the sole peak could be identified as citronellal.

Indeed, the product citronellal was found in the gas phase, while a reference blank contained no citronellal. As citronellal has a boiling point of 208 °C and reactions were performed at 30 °C, no boiling process explains these observations. Evaporation is a surface effect that happens below the boiling point until the gas phase is saturated with the evaporating substance.[41] Interestingly, no citral was found in the gas phase although it is also a volatile compound. A simple weighing experiment showed that citronellal evaporates faster than citral (Figure Ap. 6). Both compounds were soaked on a filter paper and the loss of weight was followed. In this open system, citronellal evaporated four times faster than citral. In another experiment, 1 mL reactions (10 µg/mL NCR wild-type with 2 mM *E*/*Z*-citral as described in chapter 2.4.1) in different closed reaction vessels were compared, namely 2 mL plastic tubes (1 mL gas volume) and 5 mL glass vials (4 mL gas volume). A reaction time of 15 h was chosen assuming that evaporation would then cause gas phase saturation. The result was that the four-fold higher gas phase volume in the glass vials was correlated to a four-fold decrease in citronellal concentration in the liquid phase (Figure Ap. 7). The results suggested that evaporation is the main cause of the observed product loss and that putative other processes are negligible (chapter 4.2.2).

Computational analysis of NCR ERED-catalyzed citral reduction

As part of this project, NCR ERED was also characterized *in silico*. These studies resulted as part of a research stay at the Leibniz Institute of Plant Biochemistry in Halle (Saale), Germany under supervision of Dr. Wolfgang Brandt. The initial

motivation was to calculate activation barriers of the citral reduction in NCR ERED for different prochiral binding modes aiming to find correlations to achieved selectivities. Interestingly, these calculations led to novel insights into the oxidative half reaction of NCR ERED. A semi-empirical quantum mechanical calculation using the PM7 method was applied to obtain these results. The PM7 method is suited for simulating reactions in catalytic pockets of enzymes.[115] Due to simplifications and implemented empirical parameters, systems with several hundred atoms can be calculated within several hours. With respect to enzymatic reactions, this allows the calculation of active site models.

The generation of this active site model was proceeded as follows: As no crystal structure of NCR in its reduced form was available, $FMNH_2$ was modelled based on the available crystal structure of the oxidized FMN form (pdb ID: 4A3U) and the resulting structure was geometry-optimized using the Amber12EHT force field. As model substrate, *E*-citral was docked into the resulting structure followed by molecular dynamics refinement. Subsequently, the calculation model was extracted (Figure 27). It contained amino acids H172, N175 and Y177, which are described as catalytically relevant amino acids as well as T25, Q98 and R224, which interact with the flavin mononucleotide.[54,159] In order to account for the hydrophobic nature of the binding pocket, residues W66, W100, I231, F269, W342 and Y343 were included in the model. Furthermore, the flavin mononucleotide and the substrate *E*-citral were included. Later calculations also considered a modelled water molecule derived from the refinement structure as described below. All main chain atoms of the amino acids, the flavin ribityl phosphate moiety and the side chains of W66, W100, W342 and Y343 were held fixed during the calculations (chapter 1.6). Side chains I231 and F269 are positioned on especially flexible surface loop regions and thus, these atoms were not fixed.

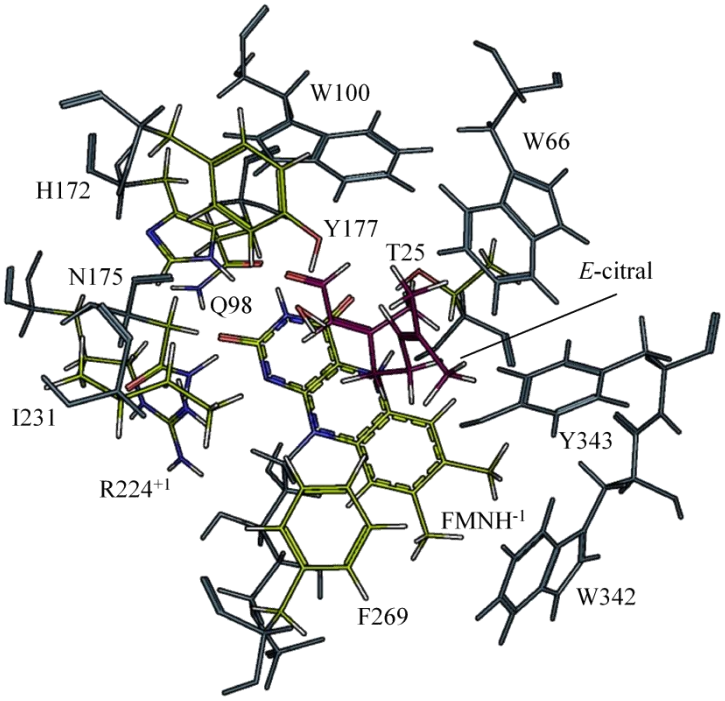

Figure 27: NCR active site model for semi-empirical PM7 calculations of the citral reduction. Atoms are color coded: carbon (green for enzyme and purple for citral), hydrogen (white), oxygen (red) and nitrogen (blue). Gray atoms were considered but defined as fixed during calculations. The representation depicts the catalytic flavin in the $FMNH^{-1}$ state after proton transfer from FMN N1 to R224. The model was extracted based on a molecular-dynamics refined docking structure of *E*-citral in NCR ERED. Before docking, NCR crystal structure (pdb code: 4A3U) was modified to its reduced $FMNH_2$ form and geometry-optimized using the Amber12EHT force field. A modelled water molecule was considered, based on the molecular dynamics refinement.

The preliminary calculation approach was based on the mechanism of the oxidative half reaction as described in literature.[54,160] In this mechanism the main trajectories are a hydride transfer from a $FMNH^{-1}$ species to the Cβ atom of the activated alkene and a proton transfer from Y177 to Cα. In literature, no details were presented why the negatively charged $FMNH^{-1}$ rather than the neutral $FMNH_2$ species was described as the hydride donor. From a mechanistic point of view, the negative charge at N1 of the $FMNH^{-1}$ species would indeed facilitate the hydride transfer by a mesomeric effect. In NCR, amino acid R224, described to stabilize the flavin residue, was identified to be in close proximity to the N1 position. It was suspected that it might act as a base to form the $FMNH^{-1}$ species from $FMNH_2$. The according PM7 calculation could indeed verify this assumption. The reaction proceeded with a low activation barrier of 1.9 kcal/mol and was exergonic resulting in a free energy release of 10.8 kcal/mol. The result reasoned to use the $FMNH^{-1}$ species for further calculations.

Surprisingly, assuming the trajectories of the mechanism described in literature resulted in a highly endergonic reaction (+21.9 kcal/mol) and thus was found to be unfavorable

and unlikely to happen (Figure Ap. 8). As consequence, new trajectories have been evaluated to probe alternative mechanisms in order to result an exergonic reaction. The so far Y177-based protonation was considered as a potential energetic issue because direct protonation gives a negatively charged tyrosine species. Therefore, alternative protonation mechanisms were probed based on residue H172 and a catalytically involved water molecule. Different protonation states of H172 (δ- and ε-tautomers and protonated species) were tested with and without a modelled water molecule. The water molecule was derived from the molecular dynamics refinement that simulates the structure in water. From these calculations an alternative exergonic mechanism could be derived (Figure 28). The respective energy scheme is provided in the appendix (Figure Ap. 8).

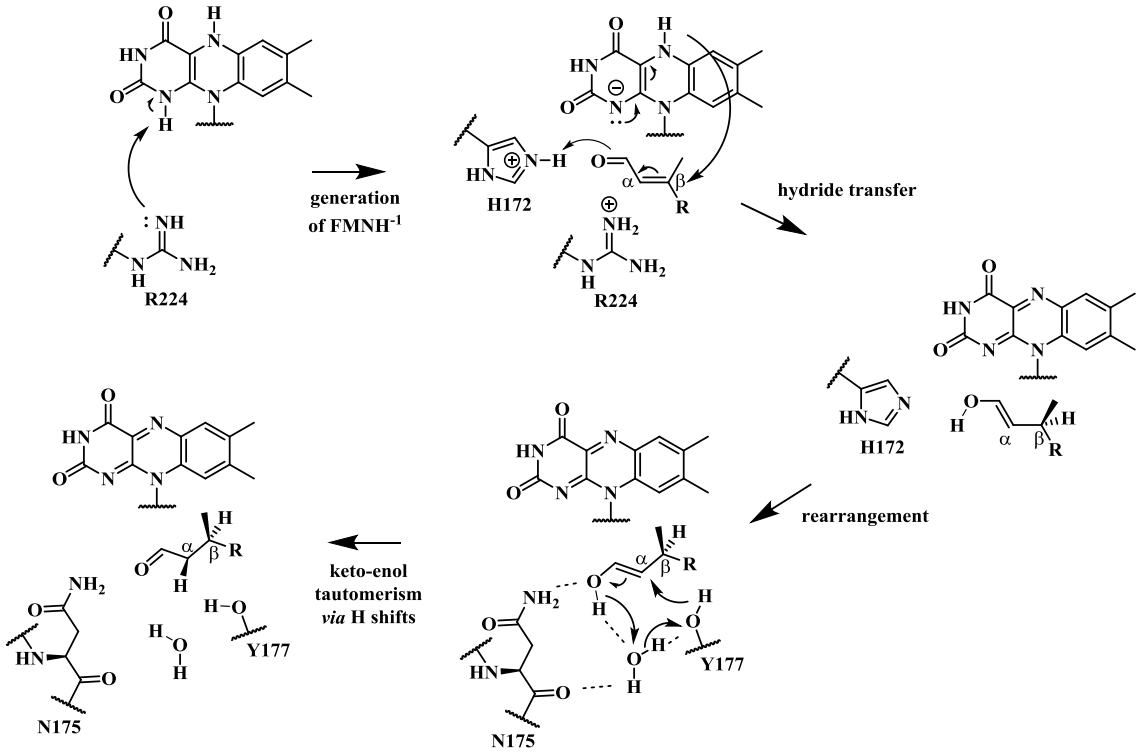

Figure 28: Calculated alternative mechanism for the oxidative half reaction in NCR ERED for the reduction of citral. The $FMNH^{-1}$ species is formed by protonation of R224 to prepare hydride transfer form flavin N5 to citral Cβ, which in combination with protonation by a positively charged H172 species results in an enol intermediate. This intermediate rearranges in the active site pocket to adopt a hydrogen network with residues N175 and Y177 as well as the modelled water molecule. This orientation triggers a final H shift reaction to form the citronellal product in a keto-enol tautomer reaction. Overall, the reaction proceeded *trans*-selective. The first step was calculated separately. Citral methylprenyl residue is denoted residue R.

The previous calculated protonation of R224 to provide $FMNH^{-1}$ can be considered as a first step facilitating the following hydride transfer to the substrates Cβ position. Upon hydride transfer, the carbonyl moiety gets protonated by a positively charged H172 to

form an enol intermediate. The enol rearranges in the active site to adopt new hydrogen bonds to N175 and the modeled water molecule. The water molecule simultaneously adopts hydrogen bonds to N175 and Y177. This rearrangement prepares a last concerted hydrogen shift reaction that releases the citronellal product and is equal to an enzyme-catalyzed keto-enol tautomerism. It is noteworthy that in the calculated mechanism residue Y177 retains its previously ascribed proton donor function, but the calculation hints at the probable necessity of a more complex protonation cascade. The calculated mechanism remained *trans*-selective. The calculated Gibbs free reaction energy is -3.4 kcal/mol and thus the reaction is exergonic. For the hydride transfer, still a high activation barrier is derived (30.1 kcal/mol).

3.1.2 Focused NCR active site engineering

Active site mutagenesis strategy

After basic characteristics of the NCR ERED-catalyzed reduction of citral had been investigated, the enzyme was subjected to enzyme engineering in order to invert the natural *S*-selectivity. The often superior selectivities that are achievable by enzyme catalysts rely on their three-dimensional protein structure. The intermolecular forces of this macromolecule usually form a cavity around the site of catalytic action. This cavity, which is known as the active site pocket, constraints the modes of binding that are achievable for a given substrate like citral. The active site residues that form this pocket can therefore have a direct influence on selectivity. Based on the solved crystal structure[81] of NCR, these residues have been identified by selecting all of those amino acids that surround citral in a distance of 5 Å (docking model) with the exception of R261, which lies in 5.5 Å distance, but rounds off the cavity (Figure 29).

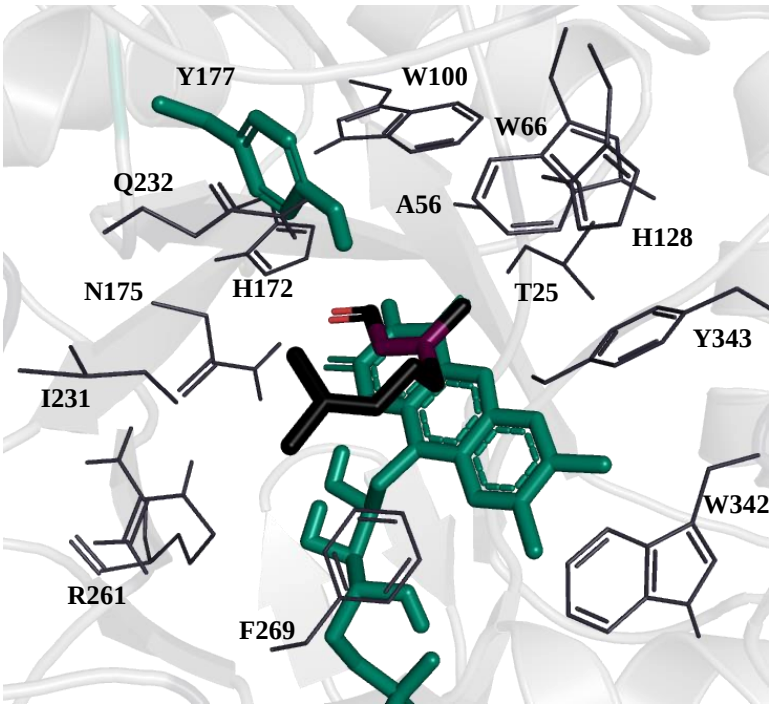

Figure 29: Selection of active site residues in NCR ERED crystal structure (pdb ID: 4A3U) as mutagenesis target sites. Residues (gray) surround citral (black) in a 5 Å distance except for R261, which lies in 5.5 Å vicinity. Citral C=C double bond (purple) and citral oxygen (red) are highlighted as well as the catalytically relevant amino acids Y177 and the prosthetic FMN (green).

In a first mutagenesis approach these residues should be probed to identify residues that influence reaction selectivity directly. For all of the selected 14 active site residues either a smaller (generally A, but G for A) or a larger amino acid (generally F, but W for F or Y) was installed by site-directed mutagenesis except for tryptophan residues that were exchanged against two smaller residues (A and F). This rather small mutant library of 28 enzyme variants was also of reasonable size with respect to the necessary purification of each enzyme to rule out cell-derived alcohol dehydrogenase side reactivity. Also, the rather long analysis time of each sample had to be considered because chiral separation was necessary to assess effects on selectivity. As explained in the introduction, the main challenge of this mutagenesis study was to provide simultaneous *R*-selectivity for the reduction of both isomers of citral. This is complicated by the fact that those isomers usually exert a substrate control effect that guides the reduction to proceed with opposite enantioselectivity. In consequence, all generated enzyme variants in this work were analyzed using the separate isomers, hence *E*-citral and *Z*-citral.

Upon analysis of this first enzyme library, several noteworthy observations were made (Figure 30). First of all, a change of the > 99 % *S*-selective reduction of NCR wild-type was achieved for alterations at positions 25, 56, 66, 100, 172, 175, 177, 231 and 232. In total, 12 of the 28 variations led to different enantioselectivities. However, the impacts of these alterations differed substantially. Especially position 66 catches the eye. Exchange of tryptophan against alanine in variant W66A even inverted the enantiomeric excess in *E*-citral reduction to 46 % *R*, while a wild-type like product formation was maintained. Noticeable changes were also observed by T25F and I231F variations, which in contrast to the W66A exchange were, however, also accompanied by significant decrease of product formation. An unexpected and insightful observation was the completely divergent response of the different citral isomers. While noticeable selectivity alterations were achieved in the reduction of the *E*-isomer, the *Z*-citral reduction selectivity remained ≥ 89 % *S*-selective in all cases. In addition, only seven residues affected the chiral outcome in that case. This isomer differentiation should be regarded in light of the fact that the wild-type enzyme shows the same absolute selectivity (≥ 99 % S) for both citral isomers. Another curious result was that exchange of the ascribed proton donating Y177 was found to influence the selectivity, regardless of an exchange against alanine or tryptophan. Besides, both Y177 variants retained over 50 % wild-type activity. H172 is another catalytically relevant amino acid interacting with the citral carbonyl group that had an influence on selectivity. While exchange against alanine retained more than 30 % of wild-type activity, phenylalanine variation was deleterious in terms of enzyme activity, but also showed greater influence on selectivity than the alanine exchange. As H172, N175 can interact with the substrates electron withdrawing group and this interaction appears to be relevant because alterations decreased product formation at least to an extent of 90 %. However, no influences on the selectivity were observed. Changes at positions 56, 100 and 232 also displayed minor selectivity alterations.

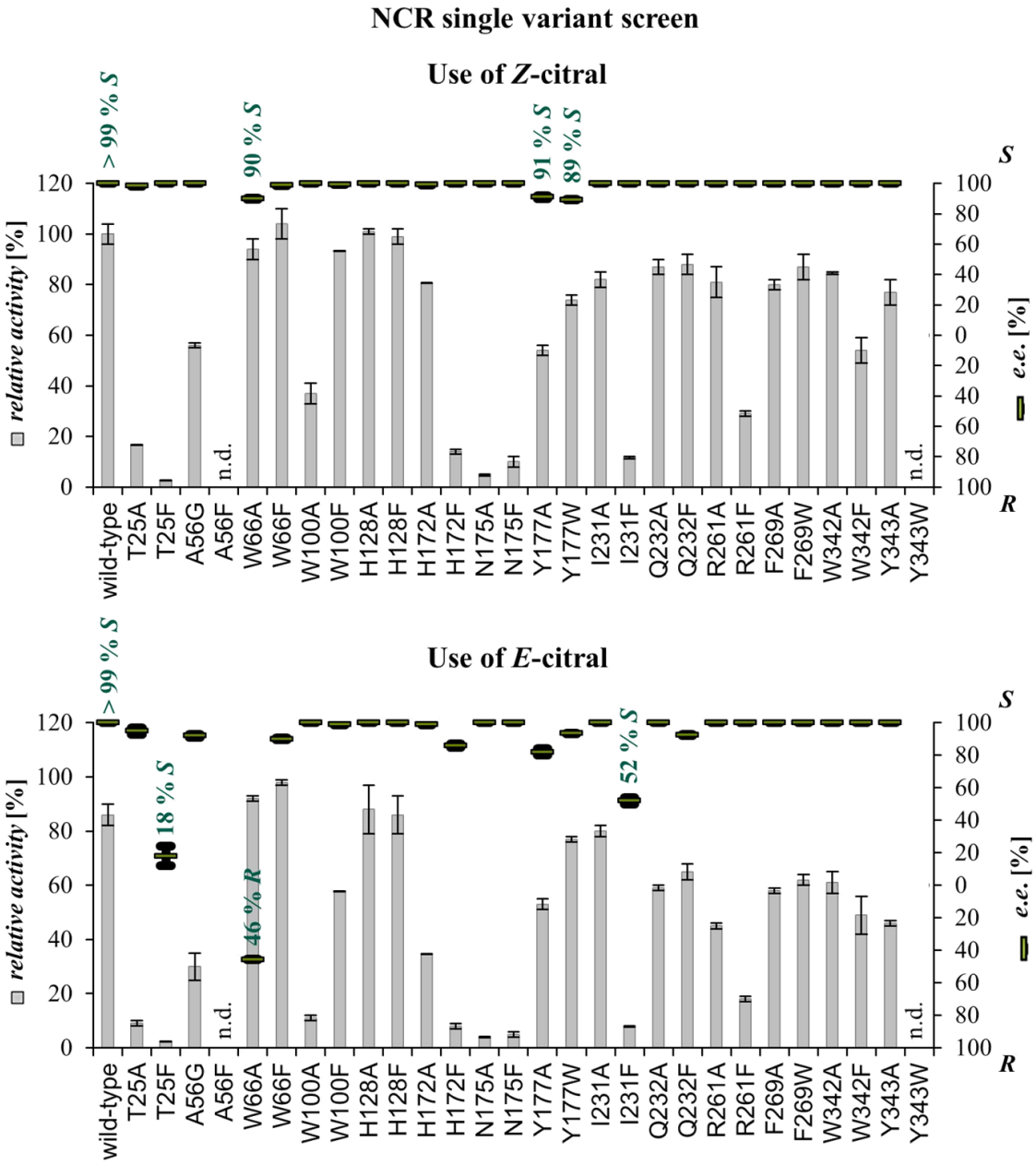

Figure 30: Screening result of *Zymomonas mobilis* NCR ERED active site single variants towards the reduction of either *Z*-citral (above) or *E*-citral (below). Gray bars indicate the relative activity in percent with respect to the product formation resulting from *Z*-citral reduction by NCR wild-type (Primary y axis). Green lines indicate the *e.e.*-value in percent ranging from 100 % *S* to 100 % *R* (Secondary y axis). Variants showing significant enantioselectivity alterations in comparison to wild-type are highlighted by the measured numerical selectivity value; n.d. = not determined. Further details are specified in the appendix (Table Ap. 1).

To sum up the main results of this first round of mutagenesis: i) the citral reduction selectivity of NCR can be altered by single amino acid variants; ii) position 66 is the most relevant target amino acid to alter citral reduction selectivity; ii) enzyme engineering leads to very different selectivity responses with respect to the two citral isomers. Reduction selectivity of *E*-citral is altered more readily.

Screening of double variant library

Based on these findings, it was concluded that the W66A variation is vital to allow opposite enantioselectivity in NCR. A second round of mutagenesis was consequently performed in order to probe if further optimizations are achievable and which amino acids next to W66 might be considered as selectivity hot-spot positions. In this second round of mutagenesis a double variant library was generated based on variant W66A. The same mutagenesis strategy as described before was followed, so 26 variants were generated and screened against reduction of the separate citral isomers (Figure 31).

Analysis of the double variant library revealed further insights. As already observed for NCR W66A and other single variants, a distinct difference in the reduction selectivity of the citral isomers becomes apparent. While nearly all variants retained wild-type selectivity towards *Z*-citral reduction, considerable selectivity switches were observed in the reduction of *E*-citral. However, some variants had mentionable differences in catalytic behavior. Variant W66A/Y177W was the first NCR variant, which significantly influenced the *S*-selectivity of the *Z*-citral conversion, namely the selectivity changed from > 99 *e.e.* % *S* to 44 *e.e.* % *S*, while about 50 % of the wild-type activity was retained. While most double variants remained *R*-selective in the conversion of *E*-citral because of the underlying W66A variation, there were also some variants which restored *S*-selectivity, for example W66A/N175F and W66A/Y343A. Most notably, W66A/N175F qualitatively reverted the selectivity switch introduced by W66A (63 % *S*), but the activity of this enzyme was nearly eliminated as well, while for W66A/Y343A a third of wild-type activity is obtained. Regarding position N175 in combination with W66A, it is furthermore notable that the alanine and phenylalanine variations delivered completely opposite enantioselectivities for *E*-citral as W66A/N175A results an *e.e.*-value of 63 % *R*. This selectivity effect of N175 was not detected by the respective single variants, but rather depended on the W66A variation. However, both variants substantially suppressed catalytic activity. For *E*-citral, in comparison to single variant W66A, two additional double variants led to further selectivity improvements towards *R*, namely W66A/I231A and W66A/F269A. Both retained at least 60 % wild-type activity. Not considering W66A/N175A due to its deleterious effect on catalytic activity, variant W66A/I231A showed the best improvements leading to an *e.e.* value of 63 % *R* from *E*-citral.

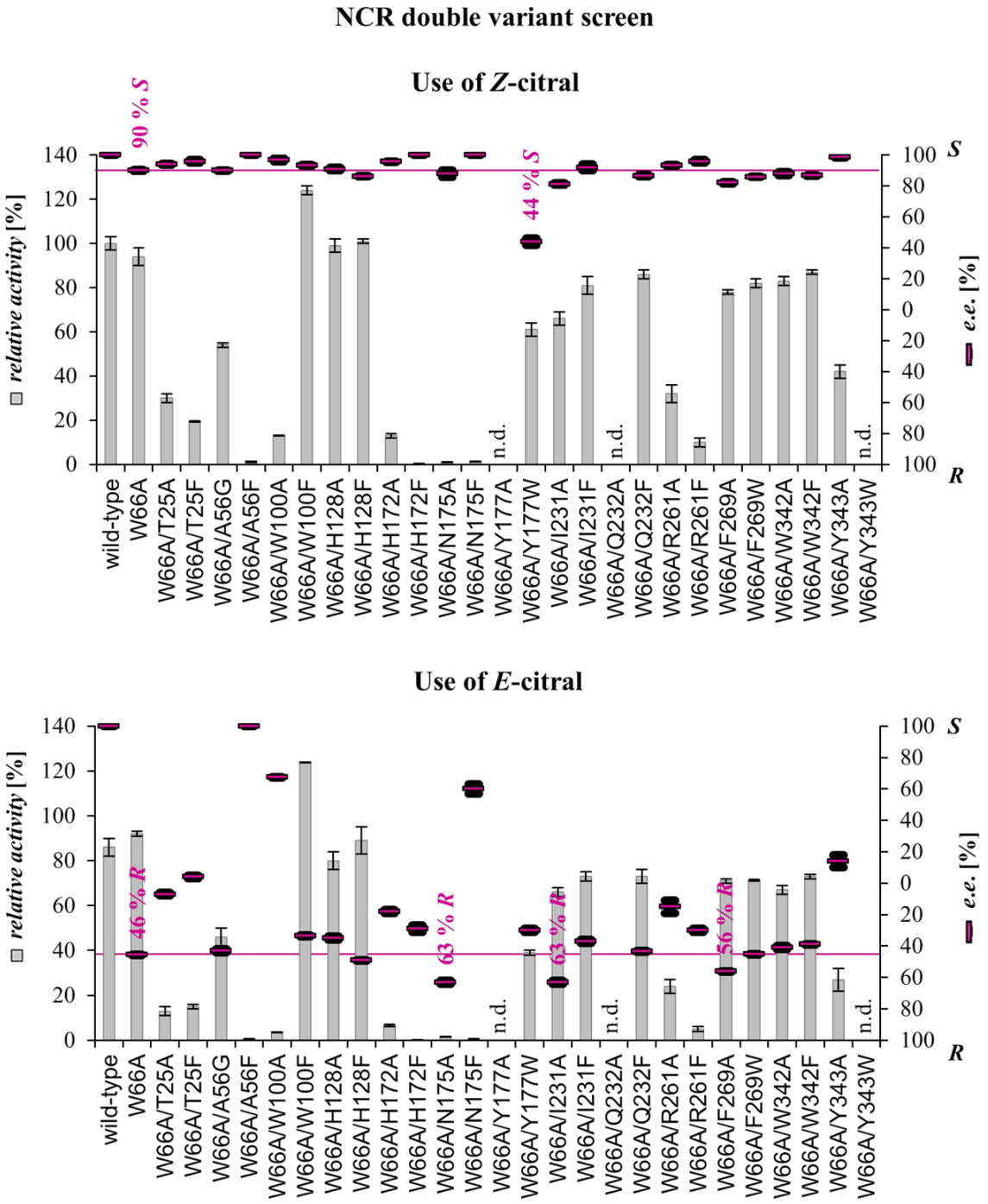

Figure 31: Screening result of *Zymomonas mobilis* NCR ERED active site W66A-based double variants towards the reduction of either *Z*-citral (above) or *E*-citral (below). Gray bars indicate the relative activity in percent with respect to the product formation resulting from *Z*-citral reduction by NCR wild-type (Primary y axis). Magenta lines indicate the *e.e.* values in percent ranging from 100 % *S* to 100 % *R* (Secondary y axis). Variants showing significant enantioselectivity alterations in comparison to wild-type as indicated by the magenta threshold line are highlighted by the measured numerical selectivity values; n.d. = not determined. Further details are specified in the appendix (Table Ap. 2).

Finally, the double variant library demonstrated the improvability of the W66A-introduced selectivity switch and the possibility to change *Z*-citral selectivity as well. Considering the results of the single and double variant libraries, positions 177,

231 and 269 were identified as additional hot-spots that enabled these further optimizations, but at the same time were not deleterious to enzymatic activity.

W66 site-saturation analysis

As the previous mutagenesis approaches emphasized, position 66 seems vital for selectivity control in NCR ERED. Further understanding of this control was generated by site-saturation analysis at this position (Figure 32).

With respect to selectivity, site-saturation mutagenesis showed a correlation to the size of the introduced amino acid at position 66. In Figure 32, the side chain volume decreases from left to right with tryptophan being the largest and glycine the smallest amino acid. Focusing on unpolar amino acid residues (highlighted red), a trend becomes visible. With decreasing side chain volume, the obtained *R*-selectivity increases. However, for instance aspartic acid, which is the fifth smallest amino acid, restores *S*-selectivity. Variants W66A and W66G showed selectivities in the same range, but W66A displayed slightly higher *R*-selectivity. The mentioned trends are mainly observable for *E*-citral because as in the before mentioned mutagenesis approaches, the differences in the reduction of *Z*-citral and *E*-citral become clearly visible in terms of enantioselectivity: most amino acid variations did not affect *Z*-citral reduction selectivity. Most amino acids were well accepted in terms of product formation (60-100 % relative activity). Most prominent exceptions are lysine and proline. Lysine quarters activity and proline variation reduces activity about 100-fold.

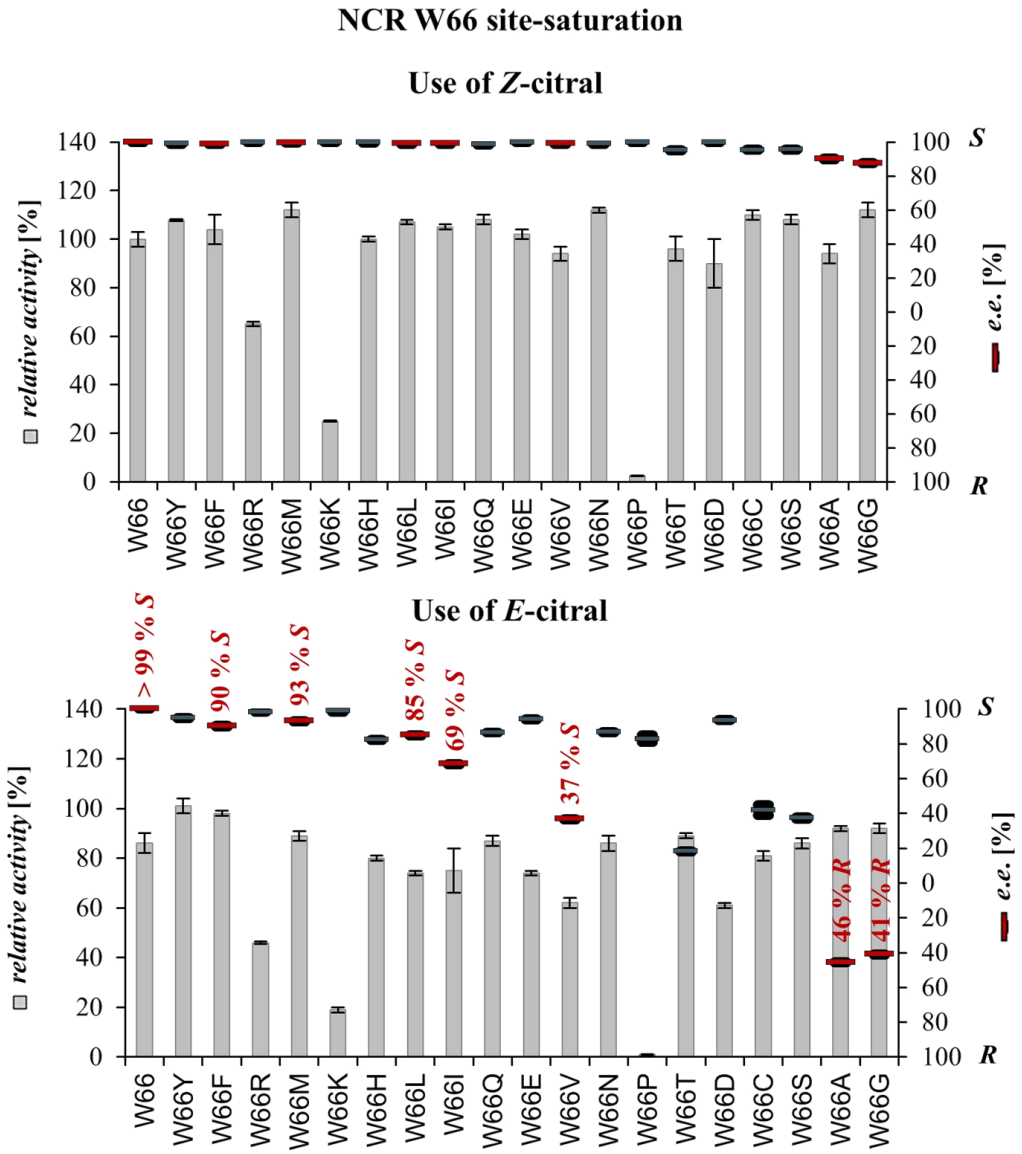

Figure 32: Screening result of *Zymomonas mobilis* NCR ERED W66 site-saturation-based variants towards the reduction of either *Z*-citral (above) or *E*-citral (below). Gray bars indicate the relative activity in percent with respect to the product formation resulting from *Z*-citral reduction by NCR wild-type (Primary y axis). Dark gray or red lines indicate the *e.e.* values in percent ranging from 100 % *S* to 100 % *R* (Secondary y axis). The variants are depicted according to their side chain volume.[161] Enantioselectivity values for less polar amino acid exchanges are highlighted in red. For the purpose of trend highlighting in the case of *E*-citral reduction, enantiomeric excess values are also depicted numerically. Further details are specified in the appendix (Table Ap. 3).

Molecular docking simulation of NCR wild-type and variant W66A

An *in silico* docking simulation was calculated to study the mutational effects of the W66A variant in further detail (Figure 33). Both isomers of citral were comparatively docked into the NCR wild-type and the computationally created W66A variant. With a crystal structure at hand, this is a powerful tool for visualization of the rather complex circumstances in enzyme catalysis. From the different binding modes that are calculated by the applied docking tools, mechanistically relevant binding situations could be selected on the basis of constraints known in literature (chapter 1.3). In this case, the

calculation confirmed the strict *S*-selectivity of the wild-type for citral reduction because all binding modes displayed a pro-*S* prochirality, irrespective of using *E*- or *Z*-citral as docking ligand. This is changed in the variant W66A. For *E*-citral a binding mode with inverted *R*-selectivity was calculated next to the *S*-selective binding mode (not displayed) for *E*-citral, however not for *Z*-citral. This reflects the experimentally achieved results. The calculation visualizes how the large tryptophan residue at position 66 effectively blocks an opposite binding mode. This allows for possible deductions in comparison to the obtained experimental results (chapter 4.1.2).

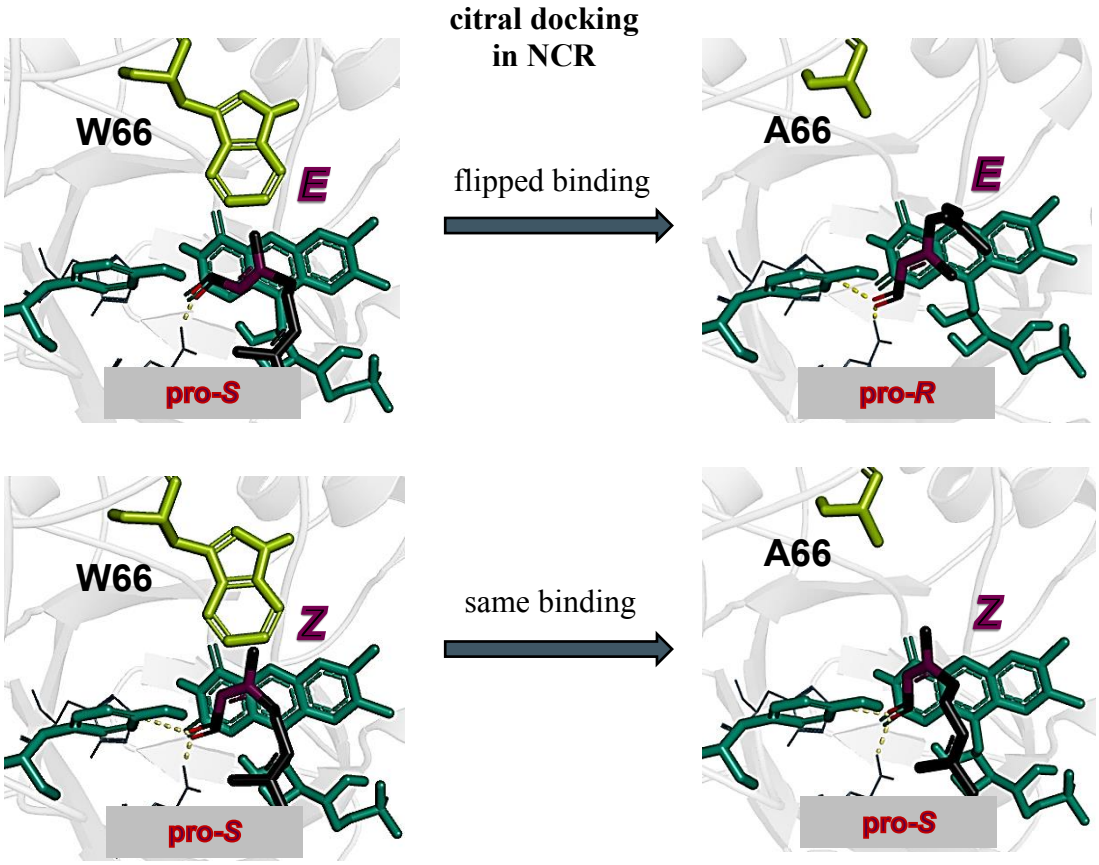

Figure 33: Calculation of binding modes by molecular docking simulation based on the crystal structure of NCR ERED (pdb ID: 4A3U). On the left, docking results of *E*-citral (above) and *Z*-citral (below) in the wild-type are displayed and on the right for the *in silico* generated W66A variant of NCR. The prochirality of calculated binding modes is denoted. For docking of *E*-citral in W66A a pro-*S* binding mode was calculated as well but is not displayed for the sake of clarity. In all structures, the catalytic Y177 residue and the prosthetic FMN (both dark green) are shown alongside H172 and N175 substrate binding residues (blue) as well as position 66 (light green) and the docked citral ligand (black). The reactive double bond in citral is highlighted (purple) and the carbonyl oxygen (red). Calculations used the docking algorithm as implemented in the YASARA software.[155]

3.1.3 Development of whole cell screening reactions

The site-directed mutagenesis strategy described in the previous chapter resulted positions 66, 177, 231 and 269 as potential hot-spots in NCR ERED to enable an inversion of the wild-type *S*-selectivity in the citral reduction. Consequently, these hot-spots should be applied for a less rational combinatorial mutagenesis approach to generate a necessary diversity to identify the desired switch in enantioselectivity. Furthermore, a comparative engineering based on the already partially *R*-selective OYE1 template was assessed as alternative solution. Both approaches were initially limited by the fact that enzyme purification as performed for all previously assessed enzyme variants was impracticable. On the one hand, OYE1 purification by affinity chromatography caused severe losses in catalytic activity (Table Ap. 4). On the other hand, it was unreasonable to purify complete iterative site-saturation libraries. The development of a whole cell reaction system for citral reduction was considered a solution for both approaches and thus conducted.

Evaluation of whole cell reactions

The application of an *E. coli* strain containing the ERED genes was hampered by an alcohol dehydrogenase-catalyzed side reaction (chapter 1.3.3). On the one hand it causes the reduction of citral to nerol and geraniol, which are not further converted by the ERED and are therefore dead-end side products. On the other hand, the reduction of citronellal to citronellol is problematic in light of the envisioned application in the menthol cascade. The SHC cannot convert citronellol to isopulegol. In this work the previously developed *E. coli* strain TG20+ (unpublished results) was successfully applied offering two advantages: i) it contains deletions of the two most unspecific alcohol dehydrogenases (*yahk*$^{-}$ and *yisb*$^{-}$ genes); ii) it contains a deletion of rhamnose isomerase stopping rhamnose metabolism. This enables the efficient application of a rhamnose promotor. This tighter expression system might facilitate folding, which was considered one potential issue during OYE1 gene expression.

Two different whole cell approaches were selected as starting points to identify a suitable reaction system using the *E. coli* TG20+ strain for ERED gene expression (Figure 34). While the first approach, denominated as system A, assumed conditions in a viable cell (resting cell), the second system B approach assumed the opposite case. Essentially, system A contained glucose as carbon source and no additional cofactor

because a viable cell should provide internal NAD(P)H regeneration. In contrast, in the second approach NADH was added. The starting conditions were selected in close accordance to approaches described in literature.[85,162] For all reactions, *E. coli* TG20+ cells containing expressed NCR wild-type gene were washed and resuspended in buffer solution. Supplements were added and biotransformations performed (Figure 34).

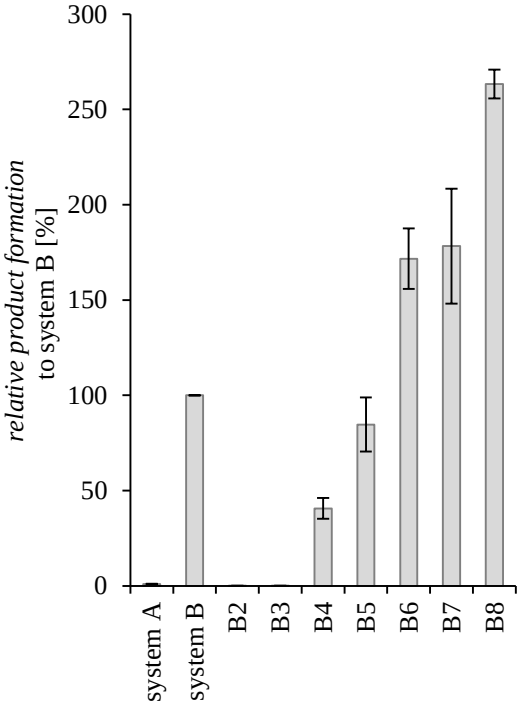

system A:

100 mM KP_i pH 7, 10 mM citral, 50 g_{cww}/L cells, 1 % (*v*/*v*) DMSO, 20 mM glucose

system B:

100 mM KP_i pH 7, 10 mM citral, 5 g_{cww}/L cells, 10 % (*v*/*v*) isopropanol, 12 mM NADH, 5 mM EDTA

changes to system B:

B2	no NADH contained
B3	no NCR ERED
B4	10 % (*v*/*v*) DMSO instead of isopropanol
B5	increase to 50 g_{cww}/L cell use
B6	decrease to 5 % (*v*/*v*) isopropanol
B7	buffer change: 50 mM MES/KOH pH 6.8
B8	no EDTA contained

Figure 34: Evaluation of NCR ERED-catalyzed *E*/*Z*-citral reduction in whole cells to citronellal. Two generally different whole cell systems called A and B as well as deviations from system B were tested as described. *E. coli* TG20+ cells containing NCR ERED were resuspended in buffer solution accordingly. The product formations (in %) relative to system B are displayed. Biotransformations were performed in 1 mL scale for 22 h at 30 °C and 180 rpm as duplicates. Referencing to the sum of educt and product peaks, 39 % chromatographic citronellal yield are obtained for system B.

For system A almost no product formation was obtained (< 1 % relative product formation), while system B resulted in reasonable formation of citronellal product. The approach resulted in 39 % chromatographic citronellal yield. Several alterations of system B were carried out to optimize and simplify the method for a fast screening application. Only a negligible rest activity remained when no NADH was added to system B (B2). A negative control without expressed ERED neither resulted in citronellal formation (B3). The system seemed to be more sensible towards DMSO than isopropanol because exchanging the isopropanol cosolvent with DMSO caused a product formation diminishment of about 50 % (B4). In this case, increasing the cell concentration did not lead to higher citronellal formation (B5). A roughly 1.5-fold improved product formation was achieved by decreasing the volumetric isopropanol

cosolvent proportion from 10 % (*v*/*v*) to 5 % (*v*/*v*) (B6). This increase was also observed for using 50 mM MES/KOH pH 6.8 as alternative buffer system. The reference system B contained the chelator EDTA. It is known that the chelating ligand EDTA can inhibit some alcohol dehydrogenases by competitive binding of divalent zinc.[163–165] The supplement, however, seems to hamper citronellal product formation significantly (B8). The activity of system B without EDTA led to a 2.5-fold citronellal increase. In following experiments, the use of EDTA was desisted from as the *E. coli* TG20+ cells provide a sufficiently lowered ADH side reactivity as will be described in the next experiment.

In a second set of experiments, the findings were used to define a new whole cell reaction system, which was applied in the citral reduction using both, NCR and OYE1 EREDs (Figure 35). For *E. coli* TG20+ NCR a chromatographic citronellal yield of 96 % resulted. For the purpose of evaluation, the *E. coli* TG20+ strain (rha promotor controlled expression on pDHE vector) was compared with the *E. coli* BL21(DE3) strain (T7 promotor controlled expression on pET-28a(+) vector). Both strains contained ERED as biocatalyst and were treated under similar reaction conditions. The comparison of the *E. coli* TG20+ and *E. coli* BL21(DE3) strain clearly shows the effect of the alcohol dehydrogenase deletions in *E. coli* TG20+. In *E. coli* BL21(DE3) a significant ADH activity is observable. It is decreased up to 20-fold in the ADH-deficient strain. ADH activity refers to the sum of terpene alcohol formed by the reduction of either the substrate citral or the product citronellal. The experiment shows that the *E. coli* TG20+ strain enables the use of OYE1 in this system in contrast to the *E. coli* BL21(DE3) strain. In the *E. coli* BL21(DE3) strain almost no citronellal formation was observed, but the formation of citronellol resulting from further reductions by ADHs. In contrast to NCR, the reduction activity of OYE1 towards citral is lower (chapter 3.1.4 provides a comparison of activity towards single isomers). The results also show that a minor residual ADH activity remains in the *E. coli* TG20+ cells.

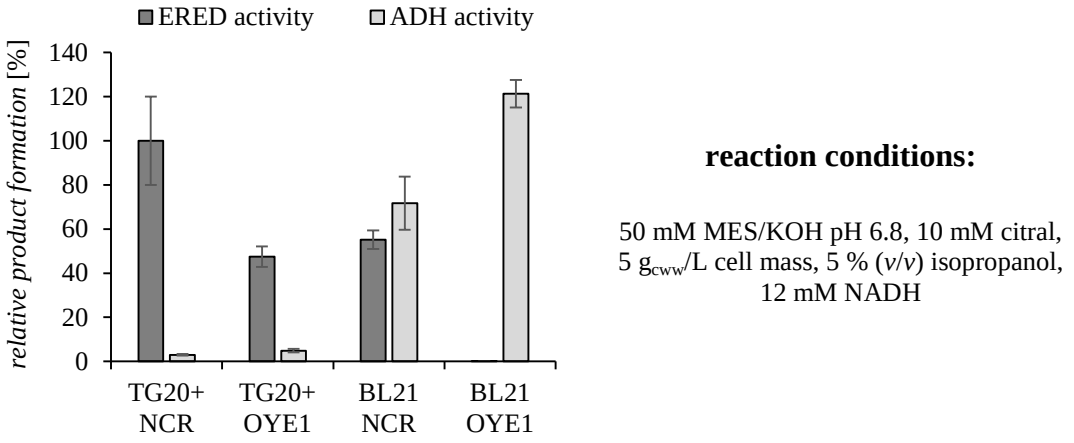

Figure 35: Comparison of ERED-catalyzed *E*/*Z*-citral reduction in *E. coli* TG20+ *vs* *E. coli* BL21(DE3) whole cells to citronellal. Either NCR or OYE1 ERED was applied. Cells were resuspended in buffer solution accordingly. The relative product formation (in %) in relation to the citronellal formation by NCR containing *E. coli* TG20+ strain is displayed. Biotransformations were performed in 1 mL scale for 22 h at 30 °C and 180 rpm as duplicates. The product is either citronellal as consequence of ERED activity or the sum of the alcohols nerol, geraniol and citronellol as consequence of ADH activity. Referencing to the sum of educt and product peaks, 96 % chromatographic yield were obtained for *E. coli* TG20+ NCR.

For key variant NCR W66A, additional experiments were performed comparing enantiomeric excess values obtained using the whole cell system to those using purified enzymes. The reactions were performed under otherwise similar reaction conditions and thus allowed a comparison of these values. Indeed, it was demonstrated that similar selectivity values were obtained. In both cases, 90 *e.e.* % *S* were obtained for *Z*-citral while for *E*-citral 46 *e.e.* % *R* and 48 *e.e.* % *R* were measured for whole cells and purified enzymes, respectively.

Optimizations for mutant library screening

In contrast to the so far applied mutant generation protocol two alterations were required to ensure the formation of at least 95 colonies. They were required to perform the envisioned site-saturation strategy. These were: i) DNA purification using a nitrocellulose membrane for dialysis and ii) cell transformation with mutated DNA using the electroporation procedure, which is known to improve transformation efficiency.[166]

The establishment of a suitable analytical method detecting altered enantioselectivity was vital for variant screening. In literature, for example various spectroscopic methods have been described for selectivity discrimination, but are highly tailored to the specific analytical problem and not generally applicable.[103] In contrast, chiral HPLC and GC analysis is broadly applicable and can suit for the screening of several thousand

mutants. This work focused on optimizing an available chiral gas chromatographic method (~30 min/sample). Due to several optimizations the analysis time was reduced to ~8.5 min/sample (Figure 36). These involved an increase of the isocratic column temperature (90 °C to 100 °C) and the carrier gas flow (30 cm/min to 70 cm/min). Additionally, the method was cut after full citronellal elution causing the substrate peak to be measured in the following sample. Over the course of 100 repeated injections it was found that no overlap of the citral peak with the citronellal peak occurred and that the citronellal signal remained stable. As a trade-off of fast hit identification and accuracy of selectivity determination, the loss of complete base-line separation was accepted.

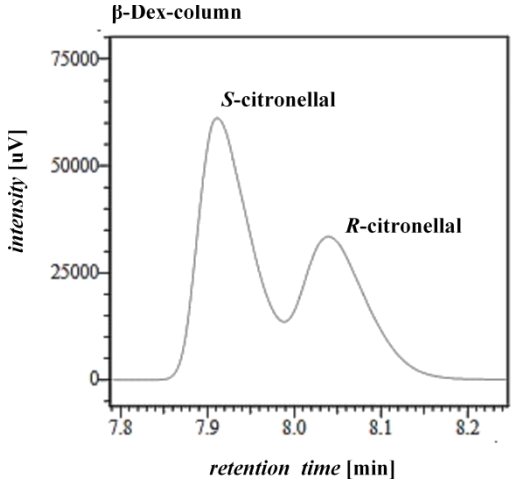

Figure 36: Optimized analytical GC method for fast chiral separation of citronellal. A trade-off between separation quality and method shortage was followed during optimization. Major shortenings can be deduced to an increase of isocratic temperature from 90 °C to 100 °C and an increase of hydrogen carrier gas linear velocity from 30 cm/min to 70 cm/min.

3.1.4 Comparative OYE1 active site engineering

As a complementary approach, OYE1 was also submitted to mutational analysis. Thereby, the potential of this type I citral ERED (chapter 1.3.3) to achieve the desired *R*-selectivity in the reduction of both citral isomers should be evaluated. As the first characterized and most studied ERED in literature, OYE1 was rendered a suitable representative for this comparative probe.[67,69,157,160] The developed whole cell reaction system could be applied for this analysis of OYE1 variants. An active site mutagenesis approach similar to the one presented for NCR ERED was applied. In fact, the mutagenesis targets were selected according to a sequence alignment of both enzymes (Figure Ap. 1). The selection of active site residues in NCR ERED was thus transferred to OYE1. A structural alignment of both enzymes highlights these positions (Figure 37).

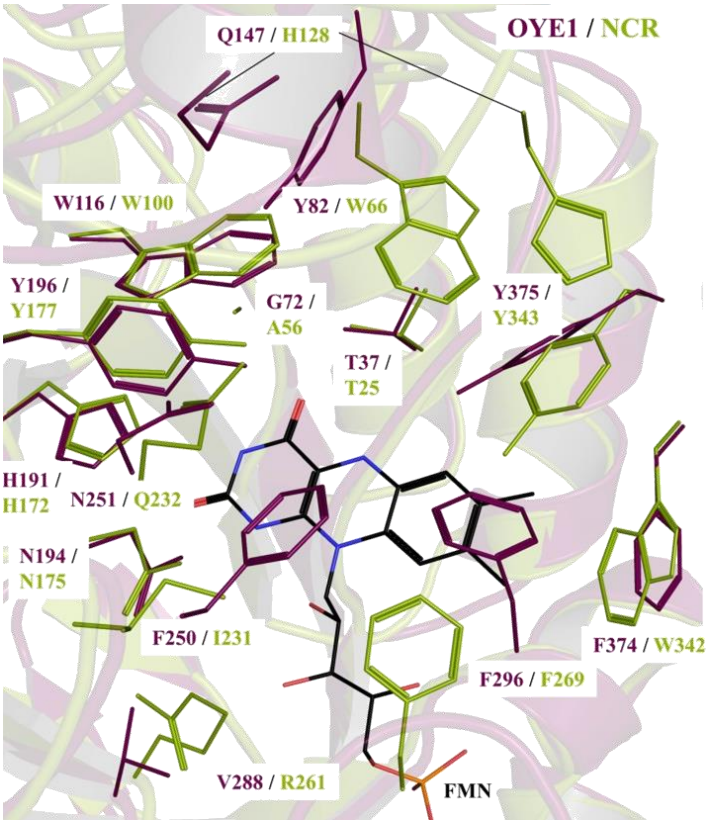

Figure 37: Structural alignment of NCR (green) and OYE1 (purple) EREDs (pdb ID NCR: 4A3U; OYE1: 1OYB). The active site of both enzymes is displayed. Indicated are sequentially similar amino acids in both enzymes subjected to comparative site-directed mutagenesis. For orientation, the prosthetic flavin mononucleotide group is depicted (black). For the selected residues the respective amino acid position in each enzyme as indicated by the color code are presented.

The OYE1 mutagenesis approach was preceded by a comparison of the OYE1 and NCR wild-types in terms of activity and selectivity using the whole cell reaction system (Figure 38). This measurement confirms the type I character of OYE1. The enzyme does naturally display high *R*-selectivity in the reduction of *E*-citral and a significantly less pronounced selectivity towards *Z*-citral. Nevertheless, the outcome was also *R*-selective with an *e.e.* value of 33 %. However, product formations show that citral is a worse substrate for OYE1 than for NCR. While half of NCR activity was achieved for *E*-citral, *Z*-citral is over five-fold lower. This entails an opposite preference for the reduction of *E*-citral. Hence, the question arose whether an optimization of the already present *R*-selectivity would be achievable without further hampering OYE1 activity.

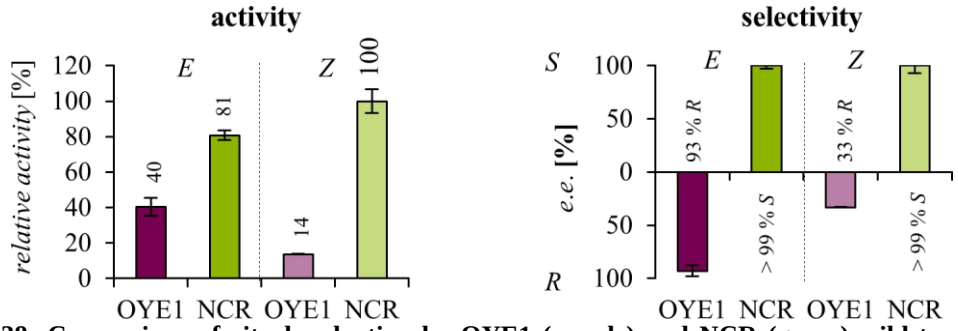

Figure 38: Comparison of citral reduction by OYE1 (purple) and NCR (green) wild-types using whole cells with respect to activity (left) and selectivity (right). Relative activity refers to the product formation as obtained in *Z*-citral reduction by NCR wild-type. The selectivity is expressed as *e.e.* values ranging from 100 % *S* to 100 % *R*. Reduction towards both isomers of citral, *E* (purple) and *Z* (green) have been evaluated. The substrate concentration was 2 mM.

As before, both isomers of citral were evaluated separately in the screen of OYE1 variants (Figure 39). A striking difference to the comparable NCR mutagenesis approach was the high number of OYE1 variants that displayed no activity (10 out of 28). In addition, another 10 of those variants showed relative activities below 10 %. In accordance, variations at the catalytic important amino acids H191 (corresponds to H172 in NCR), N194 (NCR: N175) and Y196 (NCR: Y177) are less well tolerated than in NCR. This demonstrates that citral reduction in OYE1 is more sensitive than in NCR. Alterations of activity and selectivity were observed for both isomers, so no general different effect of mutagenesis can be attributed to the two isomers in this case. With respect to selectivity, many variations altered the selectivity of OYE1, but no amino acid variant resulted in unambiguous further increase of *R*-selectivity. Variants Q147F (NCR: H128) and F374W (NCR: Y343) displayed 40 *e.e.* % *R* in the reduction of *Z*-citral but these increases lie within the measured errors. In contrast, the mutagenesis approach shows that OYE1 selectivity can be reverted to provide *S*-selectivity. For instance, *E*-citral reduction selectivity was inverted to 11 % *S* by variant N194F (NCR: N175) and *Z*-citral reduction selectivity is inverted to 71 % *S* by variant F269W (NCR: F269). It is noticeable that variations at OYE position Y82 (NCR: W66) do not show a mutational effect as pronounced as in NCR W66.

Due to the fact that OYE1 showed a considerably worse mutability than NCR and neither provided distinct starting points for increasing the present OYE1 *R*-selectivity, ongoing mutational studies focused on NCR W66A as engineering target.

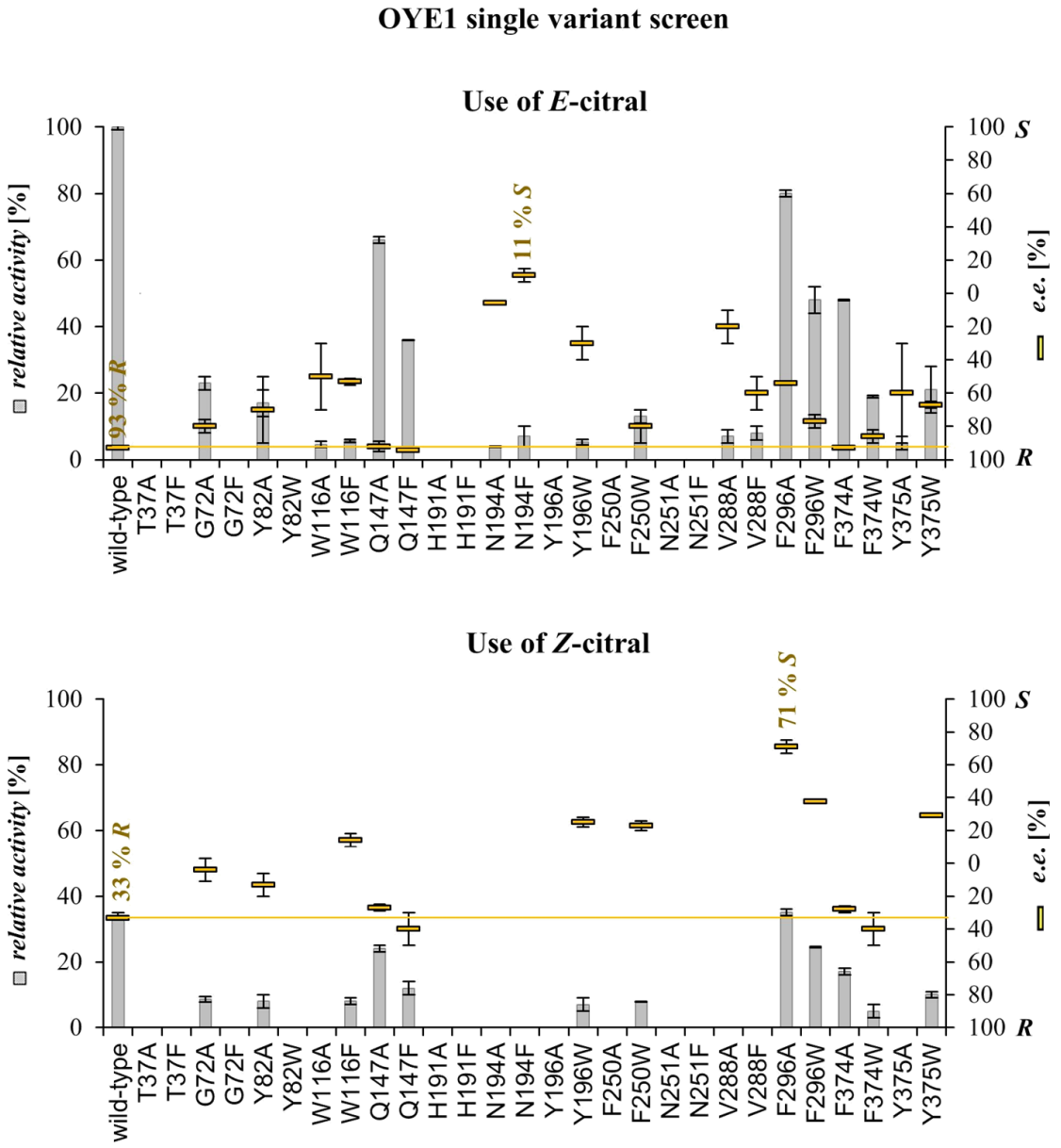

Figure 39: Screening result of *Saccharomyces pastorianus* OYE1 ERED active site single variants towards the reduction of either *E*-citral (above) or *Z*-citral (below) using a whole cell reaction system. Gray bars indicate the relative activity in percent with respect to the product formation resulting from *E*-citral reduction by OYE1 wild-type (Primary y axis). Yellow lines indicate the enantiomeric excess ranging from 100 % *S* to 100 % *R* (Secondary y axis). Variants showing significant enantioselectivity alterations in comparison to wild-type as indicated by the yellow threshold line are highlighted by the measured numerical selectivity value. The results were retrieved from the supervised Bachelor thesis of F. Dehli.[148]

3.1.5 Iterative site-saturation mutagenesis

The preceding site-directed mutagenesis studies on the NCR wild-type proved the feasibility to induce *R*-selectivity in the reduction of citral. Nevertheless, especially for *Z*-citral, the achieved selectivity changes still demanded significant further alterations to provide the desired *R*-selective biocatalyst. The in the previous chapter presented alternative use of OYE1 as mutagenesis target appeared to be unpromising. However,

the successful implementation of the enzymatic citral reduction in a whole cell environment provided the means for creating and analyzing larger enzyme libraries. That allowed combinatorial replacements at hot-spot positions identified in the NCR template. In this work, an iterative site-saturation strategy was followed, motivated by the success in the selectivity engineering of other enzymatic reactions.[101,107,167] For library construction the before applied site-directed mutagenesis approach was expanded by using primers with the degenerate NNK codon (N = A, T, G, C and K = T, G) that encodes all 20 canonical proteinogenic amino acids and thus enabled complete site-saturation. As described before (chapter 2.2.4) 95 colonies per site-saturation were screened for statistical reasons. Therefore, it was convenient to apply 96-DWPs for cell growth, expression and screening reactions (chapter 2.3.1 & 2.4.3). The remaining well was used for buffer negative controls. In order to still allow for screening of both isomers of citral separately, two 96-DWPs containing similar genes were prepared by using the same preculture plate for inoculation. Expression analysis not only proved that ERED genes were expressed under these conditions, but also that the described duplicate plates delivered similar expression levels (Figure Ap. 9). After reaction screening, hot-spot regions with increased *R*-selectivity were selected for gene sequencing. As described in the following, samples with catalytic activities below a defined threshold line were excluded from further analysis, but otherwise activity was no criterion in this screening. In the following, it will be described how the effectivity of the described screening was evaluated.

Evaluation of whole cell screening

The developed whole cell screening should primarily be effective in the identification of variants with increased *R*-selectivity. In light of the existent site-saturation analysis at NCR position 66 that had been performed with purified enzymes (chapter 3.1.2), the effectivity of the screening could be assessed by repeating the site-saturation at position 66 with the whole cell screening as described above. On the one hand, it should be evaluated whether the W66A hit would have been found in the screening and on the other hand how accurately known selectivities would be reproduced. Furthermore, this first evaluation should also prove the principal ability to obtain measurable citral conversions within the wells of the applied DWPs. For this analysis, only *E*-citral was considered as it was known that saturation of position 66 should result in a broad

selectivity distribution for this isomer, while *Z*-isomer reduction selectivity is almost unaffected by variations at position 66.

First, the analysis of the screening resulted in citronellal formation for most samples (12 of 95 reactions did not display measurable citronellal formation), which proved functional ERED production. The buffer negative control resulted in no measurable citronellal formation. Second, a broad distribution of *e.e.* values was obtained ranging from 99 % *S* to 42 % *R* (Figure 40). This hinted that the mutagenesis approach resulted in the generation of different variants including the W66A hit.

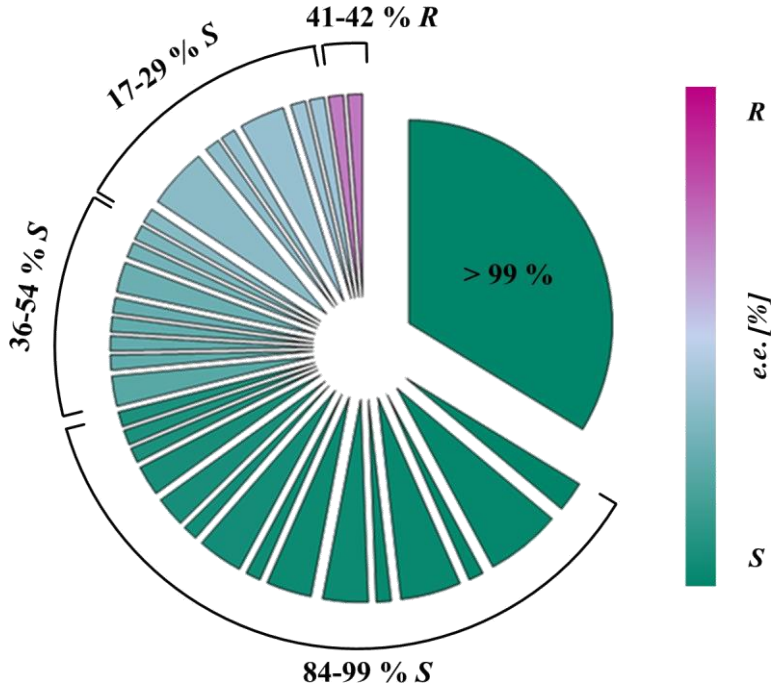

Figure 40: Selectivity distribution obtained after screening *E*-citral reduction by a NCR W66X library, presented as pie chart. Slices correspond to individual color-coded *e.e.* values measured in the library. Slice thickness indicates how often the value was measured. The smallest slice represents one measurement. Next to the prominent > 99 % *S* value, the results are summarized to four regions of measured *e.e.* values as indicated and the numerical values of these regions are depicted. In total, 95 samples of an NCR enzyme library consisting of position 66 variants as obtained by the use of a degenerate NNK codon were screened. W66X indicates a theoretical change against any of the 20 canonical proteinogenic amino acids.

Further insights were generated by sequencing 18 selected samples that mainly displayed different *e.e.* values in the screen. Based on the sequencing results, these values could be compared with the selectivities that were obtained with purified enzymes in the previous site-saturation of position 66 (Table 21).

Table 21: Comparison of NCR W66X *e.e.* values as obtained for purified enzymes in the previous site-saturation approach (previous) with those measured by the whole cell screen for the reduction of *E*-citral in the saturation approach with degenerate codon (screen). 18 samples of a site-saturation library created by the use of a degenerate NNK codon that resulted in various *e.e.* values (screen) were sequenced and then the *e.e.* values were compared to results from a previous site-saturation mutagenesis (previous) created by site-directed mutagenesis and tested with purified enzymes.

e.e. % (screen)	sequenced NCR variant	*e.e.* % (previous)
> 99 *S*	wt	> 99 *S*
> 99 *S*	wt	> 99 *S*
> 99 *S*	wt	> 99 *S*
96 *S*	W66R	96 *S*
87 *S*	W66K	99 *S*
86 *S*	W66H	82 *S*
93 *S*	W66L	85 *S*
88 *S*	W66Q	86 *S*
94 *S*	W66E	94 *S*
28 *S*	W66V	37 *S*
50 *S*	W66V	37 *S*
40 *S*	W66V	37 *S*
85 *S*	W66N	87 *S*
18 *S*	W66T	18 *S*
21 *S*	W66S	37 *S*
23 *S*	W66S	37 *S*
42 *R*	W66A	46 *R*
41 *R*	W66G	41 *R*

The selection of sequenced samples highlighted that the screen succeeded in the identification of the W66A hit and also generated the second *R*-selective W66G variant. Thus, the screening method appeared qualitatively suitable to screen for variants with increased *R*-selectivity for which the screen was primarily designed for. The three samples with > 99 % *S*-selectivity were all identified as wild-type. The relatively large proportion of samples with > 99 % *S*-selectivity (Figure 40) might be derived by residual amount of wild-type genes and therefore, consecutive screens were carried out implementing an extended *Dpn*I restriction digestion. The method was considered to be generally accurate enough as the medium aberration was 6 *e.e.* % (not taking wild-type into account to avoid bias). Regarding activity, the screen has a very limited applicability. As an indicator of activity, the obtained citronellal peak areas (sum of both enantiomers) were related to the highest peak area obtained in one 96-DWP, which gave a relative activity value. From the sequencing results, a triplicate measurement of the wild-type and variant W66V were obtained randomly. The thus calculated relative activities of wild-type and variant W66V were 60 ± 27 % and 35 ± 15 %, respectively.

As activity was initially considered a second criterion, no further optimizations for better reproducibility in activity determination were performed. As a consequence, following screening results only display a zone of activity, which can be regarded as a qualitative assessment. From the 18 selected samples, 13 different amino acids were identified. Without further sequencing of the residual 78 samples, it was assumed that the diversity of the codon degeneracy was generating sufficient variability for the envisioned selectivity improvements. This is supported by the broad selectivity distribution of the screened W66X library (Figure 40).

The site-directed mutagenesis strategy resulted four hot-spot residues in NCR ERED that appeared to have significant influence on the citral reduction selectivity. These were positions 66, 177, 231 and 269. From these identified hot-spot positions, it was decided to randomize three in combination with the W66A variant. As the alanine variant was a crucial leverage variation for opposite NCR enantioselectivity in the citral reduction, it was remained unchanged. This also minimized screening effort. The strategy was to iteratively saturate remaining selectivity hot-spot residues Y177, I231 and F269. In theory, several mutagenesis pathways were thus possible (Figure 41).

Screening of iterative site-saturation libraries

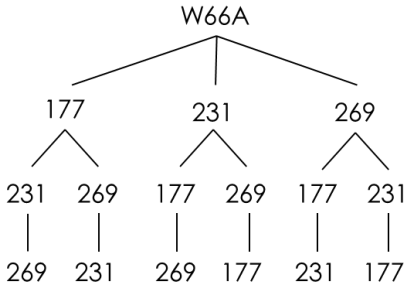

Figure 41: Possible iterative site-saturation pathways for NCR W66A as target. The scheme displays all theoretic combinations in the iterative approach of randomizing one position at a time and selecting a new target gene for further saturation at remaining hot-spot positions.

First, each hot-spot position was randomized separately generating three individual W66A based double variant libraries. Variants with optimized *R*-selectivity were subjected to sequencing. For each library, the variant with highest obtained enantioselectivity was chosen as template for randomization at the residual two positions and so on. In the course of screening, it was identified that it is beneficial to define a threshold activity value of 4 % in the screen (relative activity in comparison to the highest measured product formation within the screen of one library referring to both, the screen towards *E*- and *Z*-citral). Below this value no accurate

enantioselectivity determination was achievable because of the limited ability to concisely integrate small peak areas in a chromatogram. Thus, such samples were not considered further.

The summary of main results of the iterative site-saturation screening starting from the NCR W66A template shows that significant selectivity improvements could indeed be obtained (Figure 42; Table Ap. 5 contains detailed results of sequenced variants). For each randomization, two selected hits with increased *R*-selectivity are displayed. It appears that after position 66, position 231 is most relevant for inducing higher *R*-selectivity. For variant W66A/I231P, *E*-citral reduction was already almost completely *R*-selective (91 *e.e.* % *R*), while herein a selectivity inversion was also achieved for *Z*-citral (32 *e.e.* % *R*). In contrast, the *R*-selectivity enhancing effect of position 269 was less pronounced and produced improvements as already obtained in the site-directed mutagenesis approach of the W66A-based double variant library (chapter 3.1.2). Nevertheless, the combinatorial alteration of position 269 with positions 66 and 231 resulted triple variants with the most promising *R*-selectivity values for both citral isomers. These were for example W66A/I231R/F269V, W66A/I231P/F269V and W66A/I231P/F269P. It is noteworthy that the W66A/I231P/F269V variant was found independently in two different iterative pathways. These variants displayed relatively similar selectivity values. Considering the results of both independent measurements, variant W66A/I231P/F269V resulted for instance an *e.e.* value of 93-96 % *R* for *E*-citral and 63-72 % *R* for *Z*-citral.

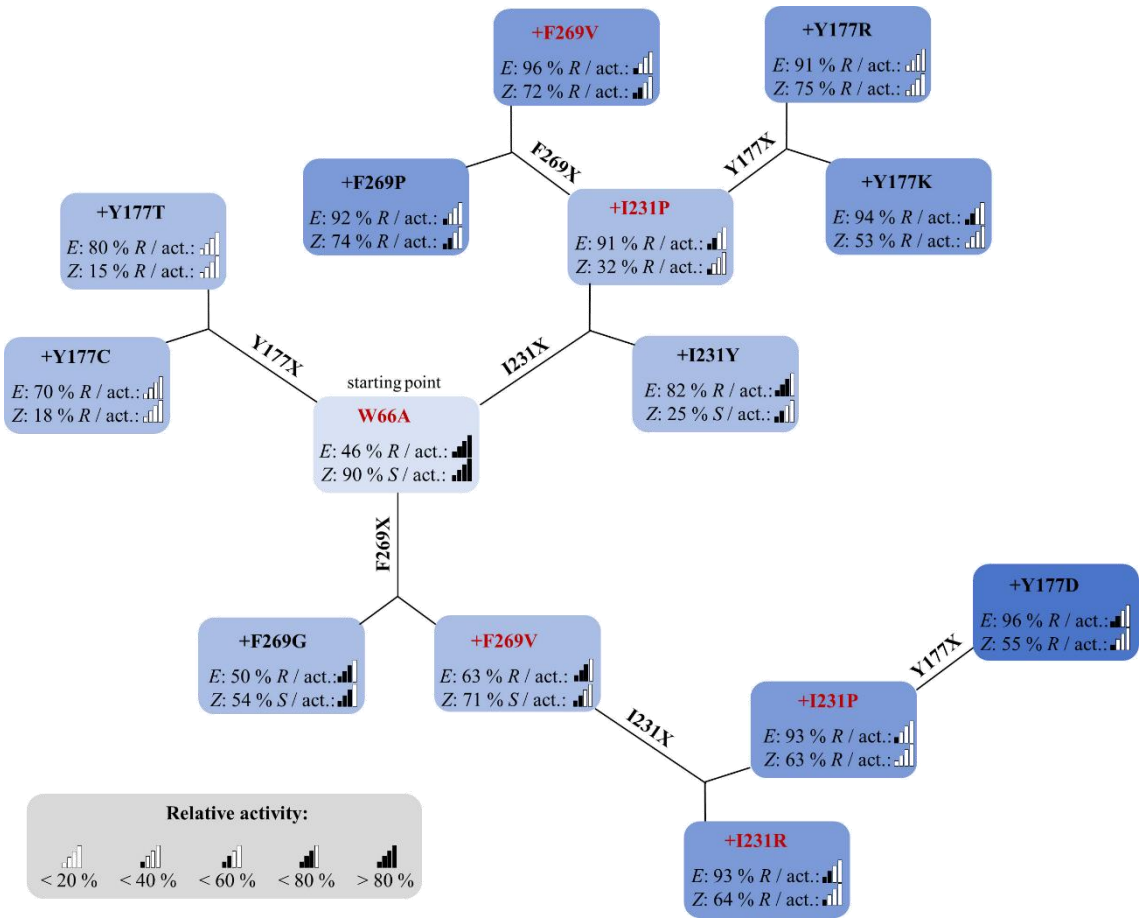

Figure 42: Iterative site-saturation mutagenesis of NCR W66A using a NNK codon degeneracy to allow exchange against all 20 canonical proteinogenic amino acids at displayed target sites. The hot-spot positions Y177, I231 and F269 were randomized separately in a consecutive manner as indicated by "X", e.g. Y177X. From the 95 colonies screened in each saturation step, the best two hits are displayed selected according to improved *R*-selectivity with respect to the underlying template enzyme of the saturation step. Each displayed hit shows the added variation as indicated by "+", i.e. +F269V refers to the variant NCR W66A/F269V. The measured *e.e.* value for each citral isomer (either *E* or *Z*) as % *R* or % *S* and a bar indicator for the related activity (short: act.) are given for each hit. Relative activity values were calculated by comparing the measured citronellal peak area to the highest obtained citronellal peak area within one saturation screen. In consequence, activities need to be compared in reference to the template enzyme. The color depth of the hit's blue background reflects the number of accumulated variations with the lightest blue for the single variant W66A and the darkest blue for the quadruple variant W66A/F269V/I231P/Y177D. The red color indicates the path to hits that were further characterized. Further details of analyzed variants are displayed in the appendix (Table Ap. 5).

In the following description, it is highlighted that the displayed relative activity values can only be regarded in comparison to the template that was used. This is rooted in the calculation method (for example variant W66A/F269V/I231P/Y177D does not display a higher activity than its template W66A/F269V/I231P but rather decreases the activity of the template further). During the screening it was finally decided that following each of the possible iterative site-saturation pathways (Figure 41) was unreasonable due to increasingly severe effects on catalytic activity when alterations at position 177 were included. Previous results from the site-directed mutagenesis approaches had suggested that alterations at the catalytic residue Y177 were accepted in terms of catalytic activity

(chapter 3.1.2). This was, however, contradicted in the presented iterative site-saturation mutagenesis. Randomization of the mechanistically relevant position Y177 mostly resulted in variants with highly diminished catalytic activities when combined with the W66A variant (< 20 % relative activity). The same trend was observed for respective tested triple and quadruple variants containing an alteration at position 177 although also significantly higher selectivities were achieved for example with variant W66A/I231P/Y177R. These losses in activity were regarded too high for further applications and the selectivity of the significantly more active above described triple variants like W66A/I231R/F269V were at least in the range of the most selective Y177X-containing variant.

As an additional observation, it came to attention that some variants also restored NCR's natural *S*-selectivity although those variants all contained the *R*-selectivity inducing W66A variant (Table Ap. 5). For instance, for NCR W66A/I231L *e.e.* values of 95 % *S* and 99 % *S* were obtained for reduction of *E*- and *Z*-citral, respectively.

From the obtained screening results, two candidates were selected for further characterization and potential use in the (-)-menthol cascade. These were NCR variants W66A/I231P/F269V and W66A/I231R/F269V. Both contain additional alterations at position 231, which was found to be crucial in combination with the W66A to achieve significantly higher *R*-selectivities. This was investigated further by molecular dynamics simulations.

Molecular dynamics simulation of NCR W66A/I231P

Next to position 66, position 231 in NCR displayed the greatest effect on citral reduction selectivity within the range of the performed screening. Based on the NCR W66A variant, an additional proline variation at position 231 lifts the selectivity from 46 % *R* to > 90 % *R* in *E*-citral reduction. In an effort to get a further understanding of the mutational effect on this selectivity, a molecular dynamics simulation of NCR variant W66A/I231P with bound *E*-citral has been performed in a time scale of 0 ps to 5000 ps (Figure 43). Comparing different snapshots of the simulation, a noticeable flexibility of asparagine 175 was observed during simulation, which lies in close proximity to the mutated 231 position (Cα distance of amino acids lie between 4-5 Å). Possible deductions from this observation are presented in chapter 4.1.2.

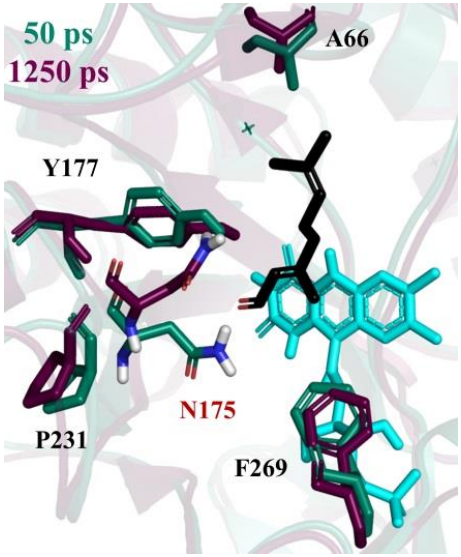

Figure 43: Overlay of two snapshots of a molecular dynamics simulation of NCR variant W66A/I231P after 50 ps (green) and 1250 ps (purple). The four NCR hot-spot positions 66, 177, 231 and 269 are depicted as well as asparagine 175, *E*-citral (black) in *R*-selective binding mode and the FMN prosthetic group (cyan). The snapshot projects the high flexibility of N175 observed during simulation.

Characterization of R-selective citral reductases

For a potential application in the desired (-)-menthol cascade, two NCR-derived candidates from the performed selectivity screen were considered for further characterization, W66A/I231P/F269V and W66A/I231R/F269V. Within the accuracy of the selectivity screen, both variants displayed similarly high *R*-selectivities in the reduction of citral. To provide a more accurate comparison of both variants, citral reduction reactions have been repeated under defined conditions including wild-type NCR for comparison. Both, whole cell reactions (chapter 2.4.2) and reactions using the purified enzyme preparations (chapter 2.4.1) were performed. Purification of the pDHE_*ncr*-derived proteins by affinity chromatography had been enabled due to the insertion of an N-terminal poly-His_6 tag that was introduced in the vector construct by means of Gibson assembly (chapter 2.2.5). It should be noted that both enzymes were readily purified. From an applicative point of view, an interesting observation regarding the use of glycerol stocks was made throughout these experiments. In order to maintain the main line of experiments, these results are described in the appendix (Figure Ap. 10). The summarized characterization results regarding activity and selectivity are derived from biological duplicates (chapter 2.6.1), which were each performed as reaction triplicates (Figure 44).

In the following results description, the enzyme variant NCR W66A/I231R/F269V shall be referred to as Arg variant and the NCR variant W66A/I231P/F269V as Pro variant.

The characterization of these variants under defined conditions reveals distinct differences that were not clearly unraveled during the beforehand screen. The Arg variant displays a clearly better activity towards both isomers of citronellal than the Pro variant, while their selectivity behavior is indeed similar. Consequently, the Arg variant was selected for further application in combination with an SHC for first bienzymatic cascade experiments (chapter 3.2.2).

a) activity

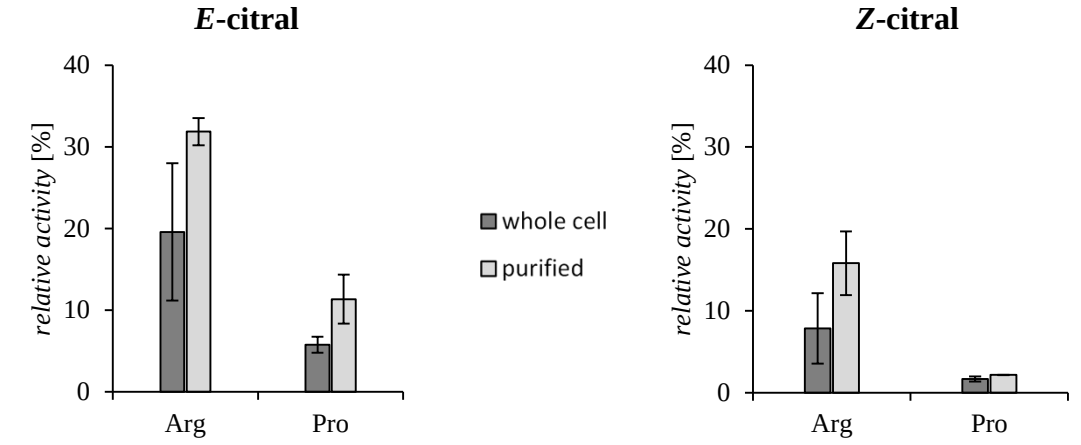

b) selectivity

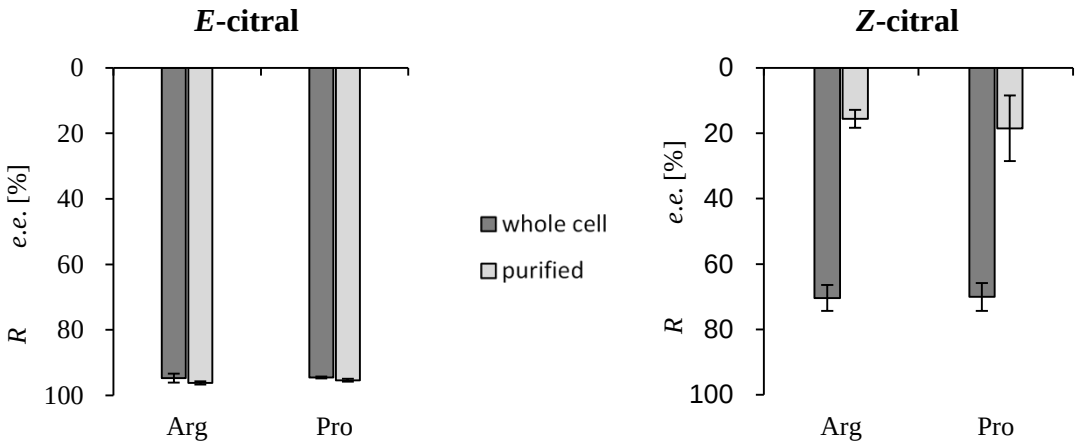

Figure 44: Characterization of the two NCR triple variants Arg (W66A/I231R/F269V) and Pro (W66A/I231P/F269V) as whole cell or purified preparation in the reduction of *E*-citral and *Z*-citral. *E. coli* TG20+ whole cells were applied. All reactions were performed as reaction triplicates of biological duplicates for 4 h at 30 °C and 180 rpm according to chapters 2.4.1 and 2.4.2. a) Obtained *relative activity* values. These refer to the relative product formation in comparison to the reduction of *Z*-citral by purified wild-type NCR ERED. b) Associated measured *e.e.* values. The axis indicates that all reactions were *R*-selective.

In general, whole cell reactions resulted in less product formation than reactions employing purified enzymes. However, it should be noted that the cell amount used was not calibrated to the enzyme concentration in reactions with purified enzymes. These results allowed for a qualitative adjustment. For both variants a clear preference in the

conversion of the *E*-isomer over the *Z*-isomer is visible. The enantioselectivity results were unexpected. Comparing whole cells and purified enzymes, it was surprising to find large selectivity deviations of 50 % in the reduction of *Z*-citral, while the selectivity values obtained for *E*-citral were similar. At this point, it shall be reminded that a previous assessment of the whole cell reaction with variant W66A did not hint at such a behavior because *e.e.* values were satisfactorily reproduced (chapter 3.1.3). But this variant neither displayed a really altered selectivity in the *Z*-citral reduction.

In consequence, consecutive experiments aimed to shed light on this phenomenon. A comparison of the biotransformation with some negative controls focusing on the remaining citral substrate produced valuable information. First, all these experiments and their results will be described. In the respective discussions chapter 4.1.4, a hypothesis is stated from these results trying to explain the enantioselectivity deviations described for whole cell and purified reactions. As before, each experiment considered both isomers of citral separately. However, for this specific experiment, the overall effects were qualitatively similar. For the sake of clarity, here, the results for *Z*-citral are shown (Figure 45). Results for *E*-citral are added in the appendix (Figure Ap. 11).

As can be seen from these experiments, there are significant shifts with respect to the proportion of *E*-citral and *Z*-citral. Comparing a buffer control and a cell control, which have both been treated under reaction conditions; a 94:6 *Z*:*E* proportion is found for the buffer control and a 75:25 *Z*:*E* proportion is found for the cell control. In this regard, it is noteworthy that the purity of the used *Z*-citral is 94 % and thus unchanged in the buffer control. Interestingly, almost the same proportions are obtained for the respective samples, which did contain ERED, irrespective of the parallel reduction to citronellal. A closer look at the overlaid control chromatograms excludes that this shift is solely caused by hypothetical *Z*-citral depletion within the cells. It can be seen that the decrease of the *Z*-citral peak is connected to an increase of the *E*-citral peak.

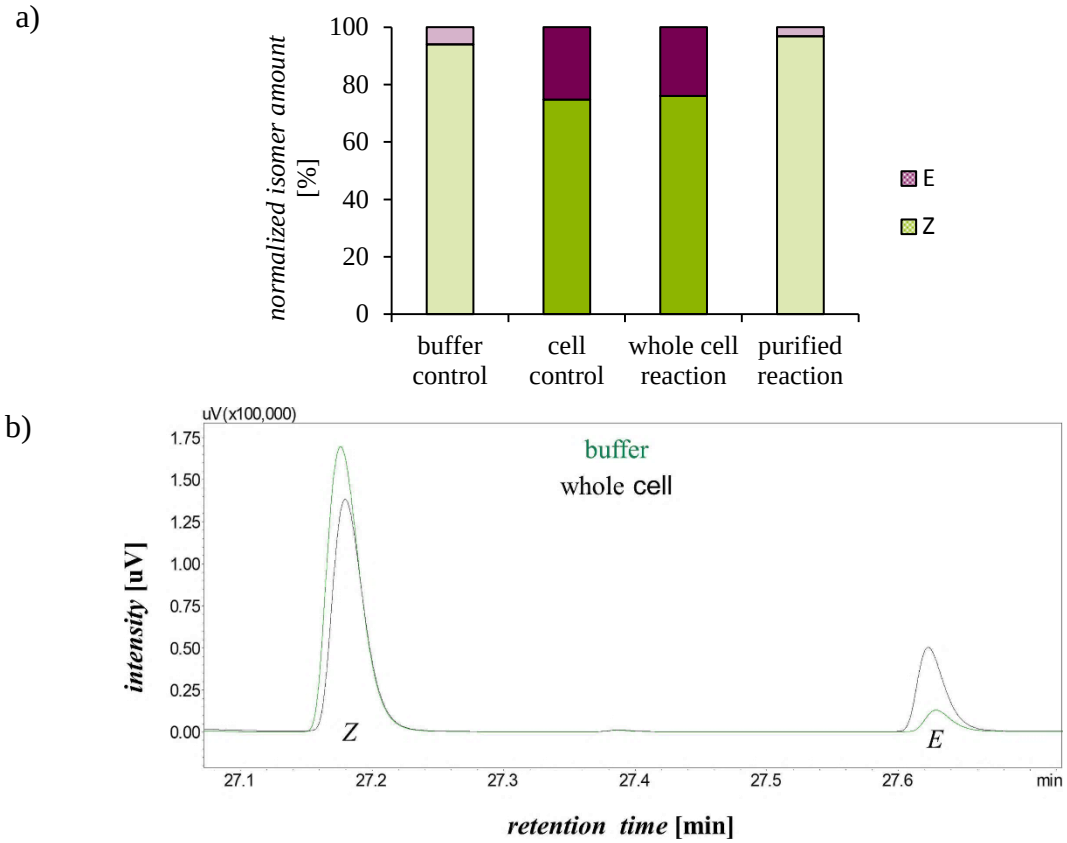

Figure 45: Control experiments with *Z*-citral under reaction conditions. The whole cell and purified reactions using the NCR Arg variant (W66A/I231R/F269V) are compared to buffer control and cell control reactions with regard to the substrate citral. All samples were shaken for 4 h at 30 °C and 180 rpm. Buffer control refers to 12 mM citrate buffer pH 6 with 2 mM *Z*-citral, 1 % (*v*/*v*) DMSO and 2.5 mM NADH added. Cell control refers to 5 g/L empty vector containing *E. coli* TG20+ cells resuspended in 50 mM MES/KOH pH 6.8 with 2 mM *Z*-citral, 5 % (*v*/*v*) isopropanol and 2.5 mM NADH added. Controls did not contain ERED. a) Obtained percental normalized citral isomer amount highlights shifts in the proportion of *E* to *Z*. b) Overlay of control chromatograms focusing on *Z*-citral and *E*-citral peaks. It should be noted that the *Z*-citral standard used for the control reactions contained 6 % *E*-citral.

The evaluation of the temperature-dependence of the NCR Arg variant (W66A/I231R/F269V)-catalyzed citral reduction further contributed to an understanding of this reaction (Figure 46). The reactions were performed as before with reaction temperatures 20 °C, 30 °C and 40 °C.

The data reveal a significant temperature sensitivity of the reaction. At 40 °C, activity is almost extinguished and consequently, selectivity values at this temperature lack accuracy. Lower temperature tends to result in higher activities for *E*-citral, while for *Z*-citral, no preference is visible. Independent of the conditions, similar *e.e*. values were obtained for *E*-citral. As before, significant selectivity alterations are obtained for the substrate *Z*-citral comparing whole cells and purified enzymes. In addition, a temperature-dependence of this deviation is revealed. The enantioselectivity obtained using whole cells at 20 °C is lower compared to 30 °C. In contrast, the same values are

measured for both temperatures when using purified enzymes. Hence, the whole cell-caused deviation is correlated to the reaction temperature. The deviation is lower at the decreased temperature. The different temperatures also influence the ratio of the remaining citral isomers (Figure Ap. 12). For whole cell reactions, the trend for both isomers is: the higher the temperature, the closer the proportion of the citral isomers tends to reflect the thermodynamic equilibrium, which is roughly 60:40 *E*:*Z*. For purified enzymes no trend is visible.

a) temperature-dependent activity

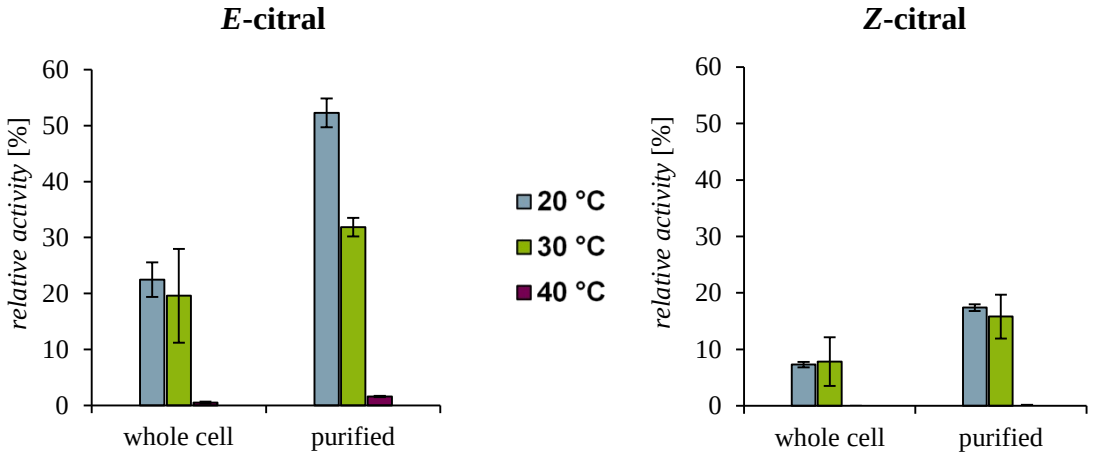

b) temperature-dependent selectivity

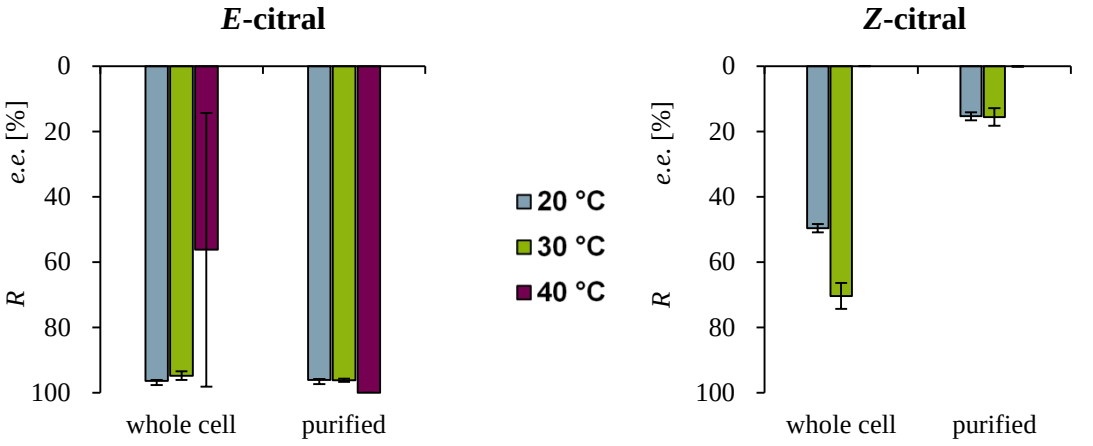

Figure 46: Temperature-dependent reduction of citral isomers by NCR triple variant Arg (W66A/I231R/F269V) as whole cell or purified preparation at 20 °C, 30 °C and 40 °C. *E. coli* TG20+ whole cells were applied. All reactions were performed as reaction triplicates of biological duplicates for 4 h and 180 rpm according to chapters 2.4.1 and 2.4.2. a) Obtained *relative activity* values. These refer to the relative product formation in comparison to the reduction of *Z*-citral by purified wild-type NCR ERED at 30 °C. b) Associated measured *e.e.* values. The axis indicates that all reactions were *R*-selective. For *Z*-citral, no product formation was detectable at 40 °C and no *e.e.* values could be retrieved.

As described in the initial motivation of the presented project, the final goal for application in the later cascade reactions was to use the isomeric mixture of citral.

Therefore, the NCR Arg variant (W66A/I231R/F269V), which was decided to be used in the establishment of this cascade, was also assessed in the reduction of *E*/*Z*-citral (Figure 47).

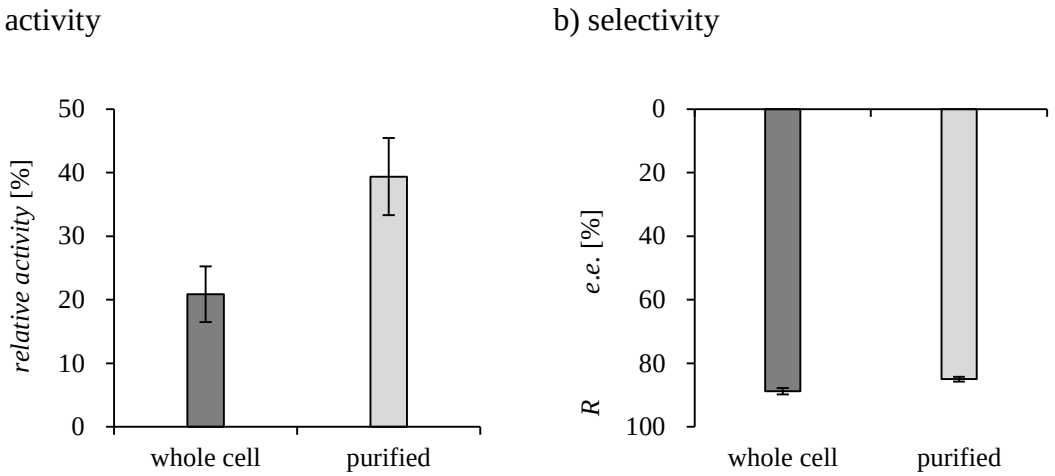

Figure 47: Characterization of the NCR triple variant Arg (W66A/I231R/F269V) as whole cell or purified preparation in the reduction of *E*/*Z*-citral. *E. coli* TG20+ whole cells were applied. All reactions were performed as reaction triplicates of biological duplicates for 4 h at 30 °C and 180 rpm according to chapters 2.4.1 and 2.4.2. a) Obtained *relative activity* values. These refer to the relative product formation in comparison to the reduction of *Z*-citral by purified wild-type NCR ERED. b) Associated measured *e.e*. values. The axis indicates that all reactions were *R*-selective.

For the isomeric mixture of citral, it is also found that in principle, the purified enzymes give higher product amounts; at least under the conditions that were compared. The obtained *e.e*. values for both, whole cells and purified enzymes, were very promising. They were 89 % *R* and 85 % *R*, respectively. Thus, an inversion of selectivity could be achieved proofing that NCR selectivity can be inverted by enzyme engineering. With respect to the observed selectivity anomaly, a hypothesis that explains these observations is deduced in chapter 4.1.4.

3.1.6 Potential of loop engineering

Owing to the structural TIM barrel motif, the active site of EREDs is mainly formed by loop structures. They can be divided into non-flexible structural elements in the inside of the protein on the one hand and flexible surface loops on the other hand forming the entrance to the active site. A structural overlay of NCR from *Zymomonas mobilis* and OYE1 from *Saccharomyces pastorianus* reveals that flexible surface loops are motifs in which these enzymes can differ significantly (Figure 48).[72]

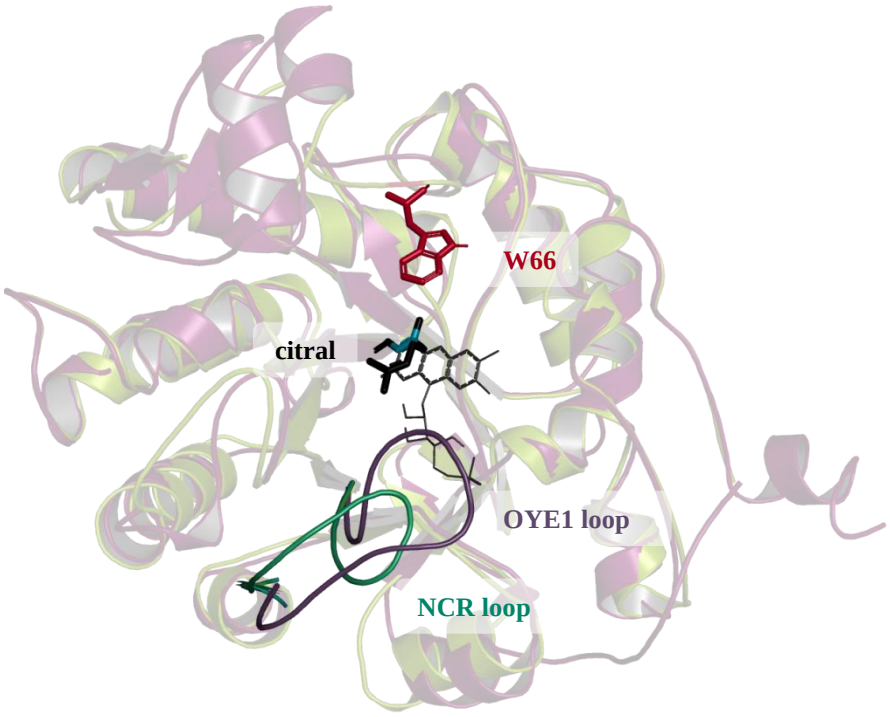

Figure 48: Structural overlay of NCR (green) and OYE1 (purple) ERED highlighting the differences in loop 6 for the respective enzymes (pdb ID NCR: 4A3U; OYE1: 1OYB). For the sake of orientation, selectivity determining W66 is shown in red and citral in bold black with turquois highlighted activated C=C double bond position. Additionally, FMN is displayed as line representation in black.

Previous studies could show that flexible surface loops can also play a significant role in catalysis and enzyme stability.[71–73] In these studies loops from different EREDs had been grafted into the NCR scaffold to assess their influence. Usually, the complete loops starting from helix to β-sheet had been exchanged. However, the structural difference of NCR and OYE1 loop 6 had already inspired an alternative exchange strategy.[74] The OYE1 loop is significantly longer than NCR. Therefore, by structural contemplation, only the visible elongated part of OYE1 was inserted into the NCR loop (Figure 49).

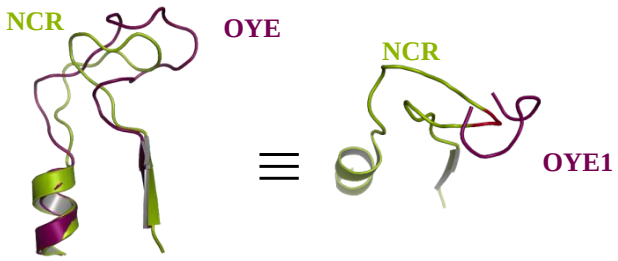

Figure 49: Structural overlay of NCR (green) and OYE1 (purple) loop 6 in two different representations (pdb ID NCR: 4A3U; OYE1: 1OYB). OYE1 loop 6 is significantly longer than in NCR. For the generation of a loop-grafted variant, NCR amino acids T268 and F269 (highlighted red in the right presentation) have been exchanged by displayed OYE1 loop 6 overhang N295-E302.[74]

Precisely, NCR residues T268 and F269 have been exchanged with OYE1 amino acids N295-E302. It is notable that this variant had already shown increased catalytic efficiency in the conversion of another linear aldehyde (2-methyl-2-pentenal).[74] However, none of the loop designs tested had any influence on the citral reduction selectivity. In these studies, the critical W66 function was yet unknown. Consequently, as part of this thesis, the described loop-grafting variant was combined with the W66A variant and assessed with regard to the reduction of both isomers of citral (Table 22).

Table 22: Resulting relative activities *rel. act.* and enantiomeric excess values *e.e.* for analytical reactions comparing NCR ERED and its variants W66A, W66A/F269A and loop 6* W66A in the reduction of *Z*-citral and *E*-citral. Loop 6* refers to an exchange of NCR amino acids T268 and F269 against OYE1 derived loop overhang N295-E302.

	***E*-citral**		***Z*-citral**	
	***rel. act.* [%]**	***e.e.* [%]**	***rel. act.* [%]**	***e.e.* [%]**
NCR WT	88	> 99 *S*	100	> 99 *S*
W66A	66	46 *R*	79	90 *S*
W66A/F269A	71	56 *R*	78	82 *S*
loop 6* W66A	**87**	**60 *R***	**94**	**76 *S***

The here presented combination of the previously described loop-grafting strategy with the W66A variant not only enabled an increase in activity, but also led to an increase in *R*-selectivity in comparison to the W66A variant. Though, the increase of *R*-selectivity was modest, it exceeded optimizations that were for instance achieved by variant W66A/F269A. F269 lies on the addressed loop 6 region. These results are an interesting addition to the potential of engineering loop regions.

3.2 Development of a chemoenzymatic (-)-menthol synthesis

In the previous chapter it was demonstrated that the induction of *R*-selectivity in NCR ERED for the reduction of *E*/*Z*-citral is possible. High *R*-selectivities can be obtained applying the evolved ERED. As a next step, the desired chemoenzymatic cascade to (-)-menthol should be established to demonstrate its feasibility that had not been tested before. The second enzyme of the desired cascade is an SHC from the thermophilic bacterium *Alicyclobacillus acidocaldarius*. Its application in the citral-to-menthol cascade is remarkable because of the underlying chemistry of this enzyme, which was reprogrammed to achieve the Prins monocyclization of citronellal to isopulegol. Naturally, this enzyme catalyzes the cyclization of the roughly three times larger C30 terpene squalene. Siedenburg et al. and Hammer et al. demonstrated that a single amino acid variation in this enzyme enabled the conversion of citral to citronellal by initial protonation of the C=O instead of the terminal C=C double bond.[123,124,128] Next, Bastian et al. could not only show that the selectivity of this reaction can be guided to provide (-)-isopulegol formation from *R*-citronellal, but also that the activity can be increased by mutagenesis and reaction engineering.[117,129] The therein developed *Aac*SHC triple variant A419G/Y420C/G600A could be applied in this work to probe the applicability of such a mechanistically novel enzyme in a valuable cascade reaction. First, it will be described how the previous reaction engineering optimizations of the citronellal cyclization could be further optimized to set a basis for the then performed investigation of the bienzymatic cascade with an ERED. Finally, the preparative scale chemoenzymatic cascade towards (-)-menthol is presented.

3.2.1 SHC-catalyzed Prins monocyclization of *R*-citronellal

Bastian found that reaction engineering was crucial to obtain higher product formation in the cyclization of citronellal.[129] A variation of reaction temperature as well as the nature and concentration of the surfactant were most relevant. Addition of surfactant was required due to the fact that *Aac*SHC is a membrane-bound protein. In this work, the study of Bastian was extended by a combination of these parameters.

A temperature of 20 °C and a Triton X-100 surfactant concentration of 0.1 % (*w*/*v*) were found to increase the activity of *Aac*SHC variants significantly. Twelve different

*Aac*SHC variants had been tested in mentioned previous study including the wild-type and variant D376C, which acts as a negative control because the catalytic aspartic acid D376 has been replaced. In the present work, the same *Aac*SHC variants were tested under the combined optimal conditions (Figure 50).

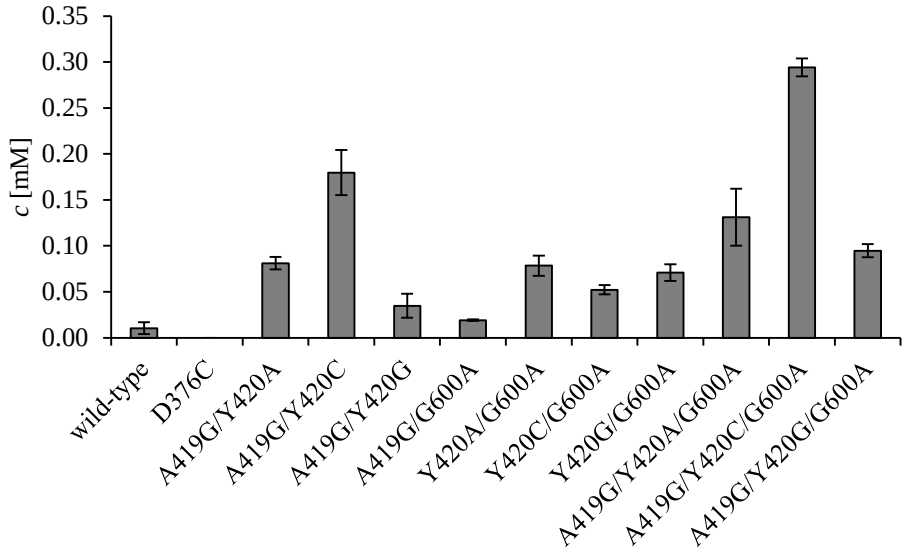

Figure 50: Comparison of different *Aac*SHC variants based on the work of Bastian[129] under combined optimal conditions at 20 °C and Triton X-100 surfactant concentration 0.1 % (*w*/*v*) The total isopulegol product formation in *c* [mM] is displayed. The substrate concentration was 2 mM.

Under the tested conditions *Aac*SHC variant A419G/Y420C/G600A displayed the highest isopulegol formation. In comparison to the wild-type, variant A419G/Y420C/G600A resulted in a 30-fold increase of product formation.

For *Aac*SHC variant A419G/Y420C/G600A, the above mentioned combined conditions were further evaluated by comparison with four other selected conditions (varied temperature and Triton X-100 surfactant conditions) and the diastereoselectivity of these reactions was assessed (Figure 51). These experiments are an extension of the optimizations performed in a previous study.[129]

As described above, previous results suggested a Triton X-100 concentration of 0.1 % (*w*/*v*) and a reaction temperature of 20 °C as suitable conditions for the cyclase-catalyzed citronellal conversion. Within the scope of the comparison experiment, the greatest product formations were obtained for these conditions. A significant impairment in product formation was found for reactions at 40 °C reaction temperature. The measurement of the diastereoselectivity for all tested conditions substantiates the reproducibility of *Aac*SHC A419G/Y420C/G600A selectivity (diastereomeric ratio *d.r.* = 90.6 ± 1.4 %).

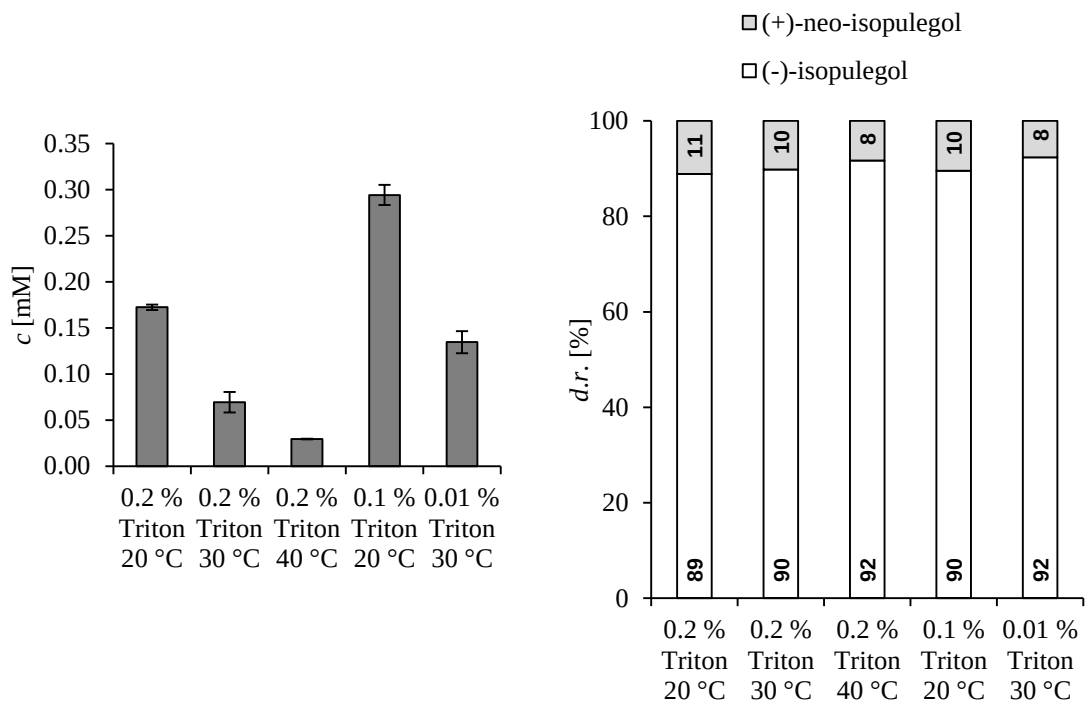

Figure 51: Comparison of citronellal to isopulegol cyclization by *Aac*SHC variant A419G/Y420C/G600A under varying conditions as depicted. a) Activity as total isopulegol product formation in *c* [mM]. b) Obtained diastereoselectivity values presented as diastereomeric ratios *d.r.* in %. Triton X-100 surfactant concentrations refer to % (*w*/*v*). The substrate concentration was 2 mM.

Next to the confirmation of the variant's reported diastereoselectivity, the enantiomer specificity was probed. A test reaction with the *Aac*SHC variant A419G/Y420C/G600A using *S*-citronellal as substrate demonstrated the specificity of this enzyme for *R*-citronellal cyclization (*e.e.* ≥ 99 % *R*) as no isopulegol products were detectable. In addition, chiral isopulegol analysis that was produced from *R*-citronellal by the *Aac*SHC variant confirmed the production of (-)-isopulegol excluding a racemization reaction (Figure Ap. 13 & 14).

3.2.2 Characterization and optimization of bienzymatic ERED-SHC cascade

Initially, the principal compatibility of ERED and SHC catalysis had to be proven, because so far this had not yet been described before. Therefore, initial tests were performed characterizing this bienzymatic cascade. One potential limitation for the bienzymatic cascade lied in the membrane-associated nature of the tested SHC, which *in vitro* requires the addition of surfactants to maintain catalytic function. Besides, the cyclization of citronellal is also a non-natural function of this cyclase and was therefore

expected to be limiting in a bienzymatic cascade. For a very early proof of principle experiment, these considerations accounted for the simple addition of an ERED and NADH to a known cyclase reaction setup. As the experiment was conducted before the identification of an *R*-selective ERED, it was decided to use an alternative *S*-selective version of this cascade. In fact, wild-type NCR was combined with *Aac*SHC I261A, a highly *S*-specific cyclase exclusively producing (-)-*iso* isopulegol (*e.e.* and *d.r.* ≥ 99 %).[124] To a reaction setup as described in chapter 2.4.4, 50 µg/mL NCR and 2.5 mM NADH were added. Citronellal was substituted by citral as substrate and the triplicate reaction was extracted after 70 h. Indeed, (-)-*iso* isopulegol was detected by GC/MS proving the principle compatibility of both enzymes and setting the basis for the below mentioned reaction evaluations. With 2.3 % product formation this initial reaction test offered many options for optimizations of which some were already described for the application of the *R*-specific *Aac*SHC A419G/Y420C/G600A in the previous chapter.

Next to demonstrating the desired cascade reactivity, the experimental exclusion of background reactivity and thus the link to enzymatic catalysis was equally important. This was addressed by scrutiny of several negative controls (Table 23).

Table 23: Conditions for negative controls performed to link the conversion of citral to isopulegol *via* citronellal to the catalytic action of the bienzymatic ERED-SHC cascade.

probed conditions
citral in buffer solution
citronellal in buffer solution
citral and NADH
citronellal and NADH
citral and SHC
citronellal and ERED
citral and *E. coli* cells with empty vector
citronellal and *E. coli* cells with empty vector

As listed above, 500 µL samples in 2.5 mL glass vials contained additives as follows: 5 mM citral or 2 mM citronellal in 12 mM citrate buffer at pH 6 with 5 % (*v*/*v*) isopropanol; 2.5 mM NADH; 2.5 mg/mL *Aac*SHC wild-type; 0.5 mg/mL NCR wild-type; 10 g/L cells both, *E. coli* TG20+ and *E. coli* BL21(DE3) strain were tested separately containing either pDHE or pET-28a(+) empty vectors; all negative controls were incubated for 5 h at 20 °C and 600 rpm as triplicates. Further workup as described in chapter 2.4.6.

The negative controls were selected to test if either citral reduction or citronellal cyclization is observable i) spontaneously in buffer solution, ii) by NADH-induced catalysis, iii) by catalysis of the second enzyme in the cascade meaning reduction by

cyclase or cyclization by the reductase, iv) by *E. coli* cells containing empty vector. For the tested conditions neither ene reduction nor cyclization could be detected by GC/MS. These experiments confirm the functionality of the bienzymatic cascade.

After the principal feasibility of this novel bienzymatic ERED-SHC cascade was shown, basic experiments have been performed to provide an initial characterization. The motivation was to generate a first understanding of the reaction system and to thereby identify crucial parameters that allow for reaction optimization. All of the following investigations have been performed using the combination of the *R*-selective NCR W66A/I231R/F269V variant and the *R*-specific *Aac*SHC A419G/Y420C/G600A variant converting citral to (-)-isopulegol with *R*-citronellal as intermediate. For the following presentation of results these variants are consequently referred to as ERED_*R* and SHC_*R*. If not mentioned otherwise, these experiments have been performed using purified enzymes to provide a better control of the reaction system.

Based on the reaction optimizations described for the separate *Aac*SHC reaction (chapter 3.2.1) and the performance of the engineered NCR variant (chapter 3.1.5), initial reaction conditions for the bienzymatic cascade were chosen (chapter 2.4.5). Further on, these conditions are denoted as “reference conditions” because all evaluated parameters were altered with respect to these conditions to allow comparison. First, it should be evaluated how the reaction proceeds with time. A time course of the reaction was obtained by stopping the reaction after different reaction periods (Figure 52).

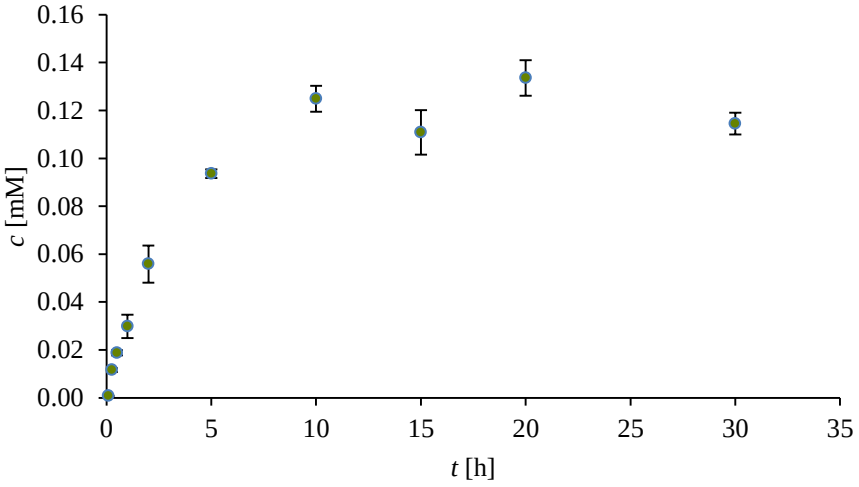

Figure 52: Time course of the ERED_*R* SHC_*R* citral to (-)-isopulegol cascade. The (-)-isopulegol product formation in *c* [mM] is plotted against the reaction time *t* [h]. The time course was determined for the chosen reference conditions as described in chapter 2.4.5. Separate reactions were conducted under reference conditions as described in chapter 2.4.5 and each single reaction was stopped at the depicted time points. The citral substrate concentration was 2 mM.

The time course shows that isopulegol is formed up to a plateau concentration of about 0.13 mM. Within the first hour of the cascade reaction, isopulegol can be detected. However, the production rate declines rapidly. An overlay of chromatograms at different reaction time points highlights that the ene reduction proceeds considerably faster than cyclization (Figure 53). After 5 min, the relative peak area (referred to the sum of educt and product areas) of citronellal already amounts 37 %, whereas isopulegol just starts to be produced (< 1 % relative peak area). The preferred reduction of *E*-citral by NCR_*R* can be confirmed by this measurement (chapter 3.1.5).

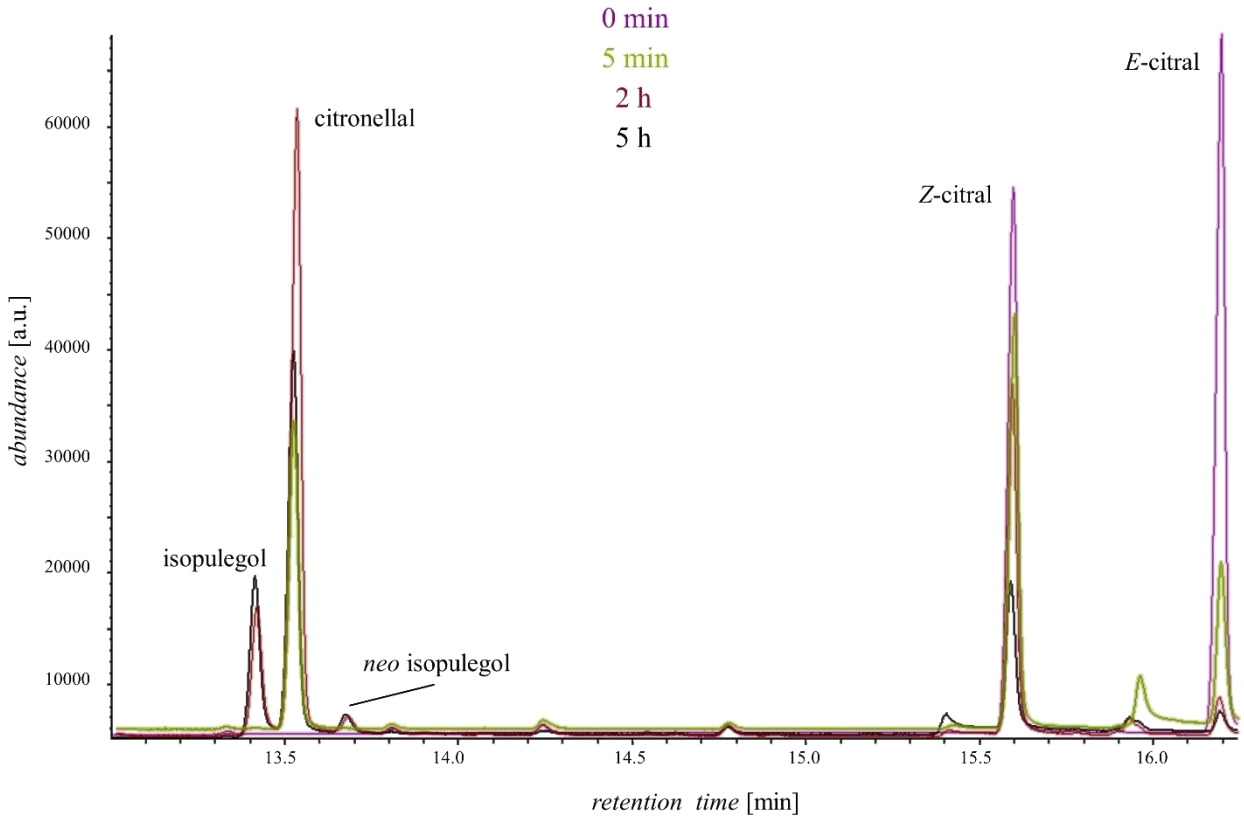

Figure 53: Overlay of chromatograms for bienzymatic cascade reactions employing ERED_*R* and SHC_*R* for conversion of citral at the displayed reaction periods 0 min (purple), 5 min (green), 2 h (red) and 5 h (black). Separate reactions were conducted under reference conditions as described in chapter 2.4.5 and each single reaction was stopped at the depicted time points. The substrate concentration was 2 mM.

In comparison to the separate *Aac*SHC reactions, it seemed that the cascade yields lower product formations. Therefore, both reactions were directly compared in a novel experiment (Figure 54). Both reactions were conducted under similar conditions. In the *Aac*SHC reaction, citral was substituted by citronellal and no NADH and ERED was added. In one additional sample it was tested how the *Aac*SHC reaction proceeds in the presence of additional 1 mM citral.

This experiment confirms that the cascade reaction leads to a roughly four-fold decline in isopulegol product formation. The addition of 1 mM citral also diminishes product formation. However, with a 0.75-fold decrease in product formation, this diminishment is less pronounced.

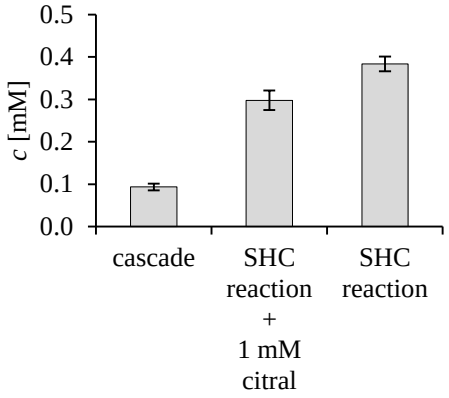

Figure 54: Comparison of bienzymatic cascade reaction with *Aac*SHC reactions. The bienzymatic cascade reaction refers to the reference conditions as described in chapter 2.4.5. The SHC reaction refers to the same conditions without added ERED and *R*-citronellal as substrate instead of citral. The effect of additionally supplementing 1 mM citral to this *Aac*SHC reaction was also evaluated. The obtained product formations are presented as the measured isopulegol concentration *c* [mM]. The substrate concentration was 2 mM.

Further experiments were motivated by finding parameters that might optimize the reactivity (Figure 55). Based on the time course data, a reaction time of 5 h was chosen as suitable reference time point. From the evaluations of ERED and SHC reactions, it was known that the reaction temperature can be a crucial parameter. For both single enzymes a lower temperature of 20 °C was preferable over higher temperatures. For the cascade both, a decrease to 15 °C and an increase to 25 °C led to an about 40 % decrease in isopulegol formation. Next, isopropanol and ethanol were tested as alternative cosolvents in two different concentrations. Isopropanol was selected as it was a viable alternative in the previous work with EREDs and ethanol was selected as alternative polar protic solvent. While ethanol caused a two-fold activity decrease, isopropanol could increase isopulegol formation in the range of 10-30 %. The increase required addition of 5 % (*v*/*v*) isopropanol, because the lower amount of 1 % (*v*/*v*) caused decreased isopulegol formation. The above described time-resolved analysis of the bienzymatic cascade (Figure 53) added to the suggestion that the cyclase is the bottleneck in productivity. A lower (1 mg/mL) and higher (4 mg/mL) enzyme concentration was compared to the reference amount of 2.5 mg/mL. Higher enzyme concentration seems to correlate with higher product formation but the trend does not seem to be linear. While the increase from 1 mg/mL to 2.5 mg/mL optimizes yield by

about 100 %, the further increase to 4 mg/mL only adds 20 %. A similar trend is seen for the substrate concentration. Increases of 60 % and 160 % from 0.5 to 1 mM and from 1 to 2 mM citral were observed, while the use of 10 mM resulted in the same isopulegol amount as 2 mM.

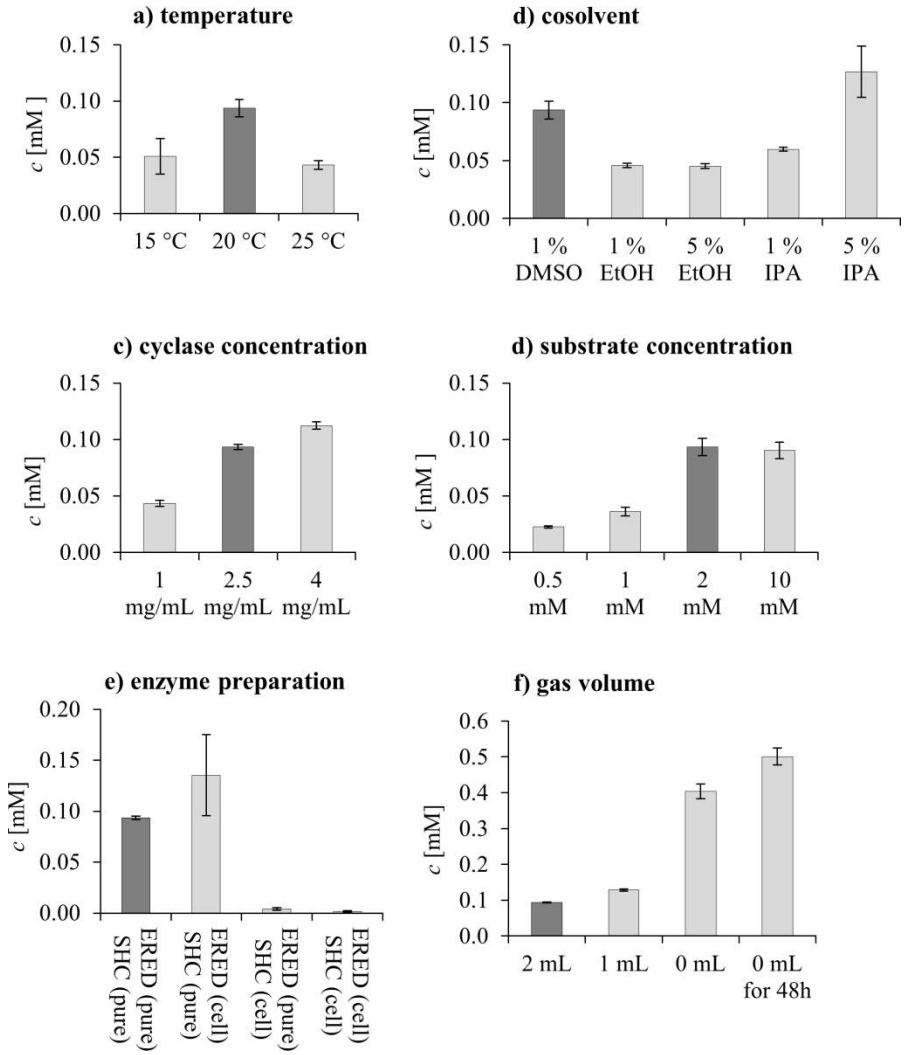

Figure 55: Evaluation of reaction parameters for the bienzymatic cascade of an ERED variant and an *Aac*SHC variant. Each parameter was singly varied with respect to a reaction under reference conditions (dark column) as described in chapter 2.4.5. The obtained product formations are presented as the measured isopulegol concentration *c* [mM]. a) Variation of reaction temperature. b) Variation of added cosolvent used as % (*v*/*v*). c) Variation of cyclase concentration. d) Variation of substrate concentration. e) Variation of enzyme preparation. "Pure" refers to the use of purified enzyme and "cell" to the alternative use of 10 g/L ERED containing *E. coli* TG20+ and 100 g/L *Aac*SHC containing *E. coli* BL21(DE3) cells. f) Variation of the gas volume above the reaction solution. The gas volume variation was achieved as follows: 2 mL by using 500 µL reaction in 2.5 mL vessel; 1 mL by using 500 µL reaction in 1.5 mL vessel and 0 mL by using 1100 µL reaction in 1.1 mL vessels. If not stated otherwise, the citral substrate concentration was 2 mM.

Furthermore, the use of whole cells instead of purified enzymes was evaluated to assess their principle applicability. This work also demonstrated that an increased *R*-selectivity can be achieved if ERED_R is applied as whole cell preparation (Figure 47, chapter 3.1.5). As SHC_*R* is specific for the conversion of *R*-citronellal, it was assumed

that an increased selectivity in the reduction reaction might be reflected by an increased isopulegol formation in the bienzymatic cascade. The results of the combination of purified cyclase and whole cell-based ERED hints to a confirmation of this assumption. However, the obtained concentration value shows a rather large standard deviation. The use of *Aac*SHC-containing *E. coli* BL21(DE3) cells for test purposes suppressed the activity of the bienzymatic cascade reaction almost completely (chapter 4.2.2). Finally, the impact of the gas volume in the samples was tested and found to be crucial for isopulegol detection in the liquid phase. Removing the gas phase by completely filling the reaction vessel with reaction solution increased detected product formation more than four-fold. Further increased product detection could be achieved after elongated reaction time of 48 h, which corresponds to a theoretical yield of 25 % (proportion of measured citronellal concentration to the used citral concentration). Future studies could further evaluate varied ERED concentrations.

Finally, these experiments provide a first identification of relevant parameters and an initial understanding of this novel cascade. The small data set already proves that significant improvements can be achieved. This is a vital basis for future investigations.

3.2.3 Preparative chemoenzymatic (-)-menthol synthesis

In the previous chapters it was described how *R*-selectivity was successfully engineered in the formerly *S*-selective NCR ERED and how this enzyme could be combined with a promiscuous *R*-specific *Aac*SHC variant to synthesize (-)-isopulegol, which is the precursor of (-)-menthol, the target compound of the here presented project. Now, it will be described how chemical hydrogenation can be added to demonstrate the possibility to synthesize (-)-menthol in the chemoenzymatic cascade (Figure 56). A preparative-scale approach was chosen in order to allow for structural product characterization by NMR and IR spectroscopy.

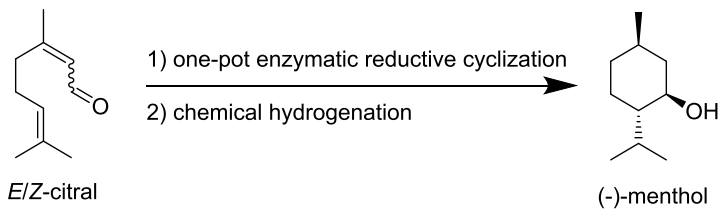

Figure 56: Schematic presentation of the chemoenzymatic cascade synthesis of (-)-menthol from *E*/*Z*-citral. First the one-pot ERED-SHC bienzymatic cascade is performed followed by direct chemical hydrogenation.

For the chemoenzymatic cascade, first the one-pot bienzymatic cascade was performed followed by direct hydrogenation with hydrogen gas over a heterogeneous catalyst. 5 % palladium on charcoal was chosen as a well-studied and robust hydrogenation catalyst that can also exert catalysis at room temperature.[168] In this preparative-scale approach 0.6 mmol citral educt were used, which correlates to a maximum theoretical yield of 93.8 mg menthol. The synthetic scale considered that based on the known performance of the bienzymatic cascade, no complete conversion to the intermediate isopulegol could be expected as well as possible product losses during menthol isolation. The experiences from analytical scale investigations and practical considerations guided the choice of the reaction set-up for the initial bienzymatic cascade (chapter 2.5). 5 mM citral (0.6 mmol) was reacted in a total volume of 120 mL. Because gas phase removal increased product recovery significantly in analytic reactions, 20 mL air-tight headspace vials were used as reaction vessels. Consequently, the total 120 mL approach was splitted to six 20 mL approaches and recombined for subsequent hydrogenation. Each headspace vial was additionally sealed using parafilm. The reaction took place for 22 h at 20 °C and 250 rpm. Reaction progress was probed by GC/MS sampling after 2 h, 5 h and 22 h (Figure 57).

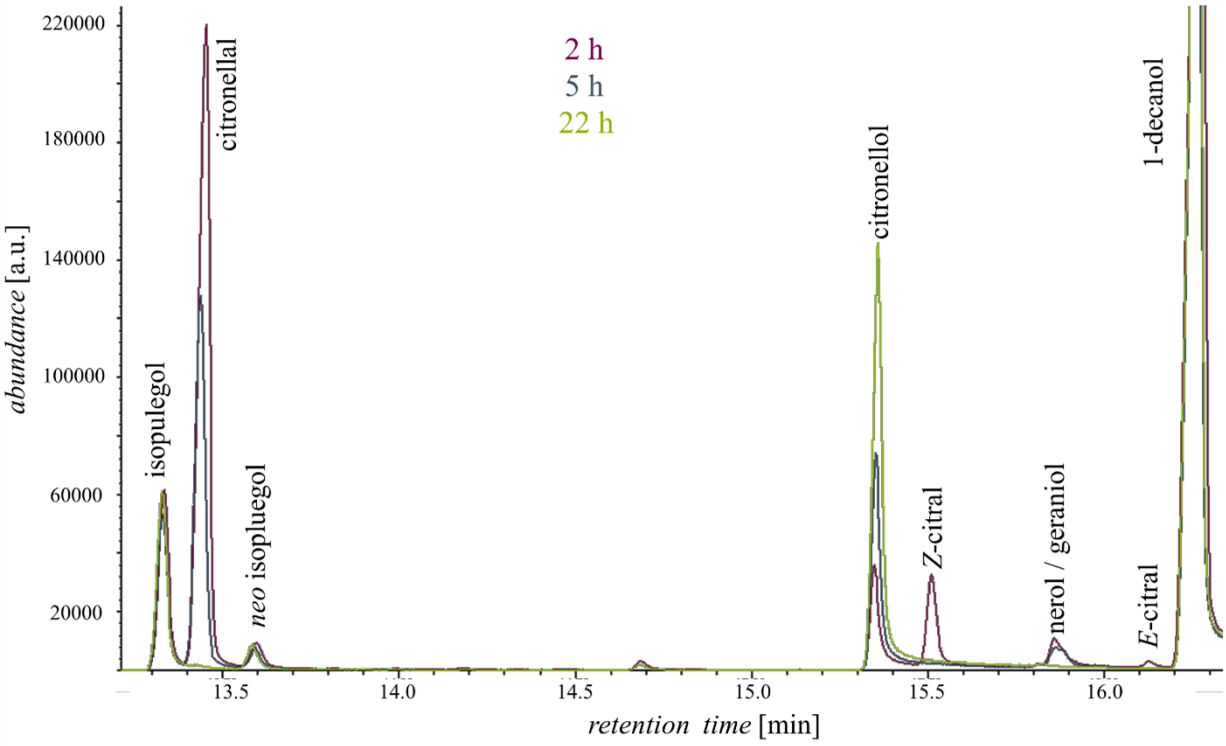

Figure 57: Overlay of 2 h (purple), 5 h (gray) and 22 h (green) sample chromatograms of bienzymatic reaction part of preparative (-)-menthol synthesis. The preparative reaction was performed as described in chapter 2.5. At presented time points 250 µL samples were taken from the same reaction *via* the GC vial septum and extracted (chapter 2.4.6).

The samples show that over time, citral is completely converted. Some nerol/geraniol is detected after 2 h and 5 h, but disappeared after 22 h. The citronellal amount detected after 2 h is clearly diminished after 5 h and is not detectable after 22 h. In reciprocal correlation to citronellal, the citronellol amount increases. In contrast, isopulegol formation did not proceed further after 2 h, but instead the amount of isopulegol remained roughly constant in all measured samples. Referencing to the sum of educt and product peak areas, 32 % isopulegol formation is calculated.

After 22 h, the six 20 mL reaction solutions were combined without further workup, the heterogeneous catalyst (5 % (*w*/*w*) Pd/C) was added and the reaction mixture was stirred in a hydrogen atmosphere at room temperature. Again, samples were taken using a septum to follow the reaction by gas chromatography (Figure 58). Here, the decrease in isopulegol proportion is linked to the increased formation of menthol. After two days no further increase in menthol production was observed. From the final chromatographic sample some conclusions are drawn (Figure Ap. 15). Integrating all educts and products, 31 % menthol are obtained with a diastereomeric ratio of 92 %, while 6 % unreacted isopulegol remain. Furthermore, 63 % 3,7-dimethyloctanol is formed as the only byproduct.

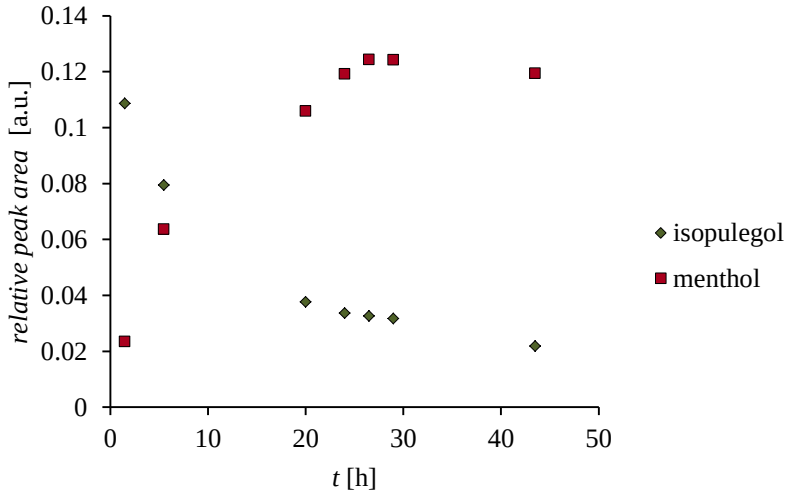

Figure 58: Progress of isopulegol hydrogenation to menthol in the preparative-scale chemoenzymatic cascade approach. The *relative peak area* as obtained by GC/MS is plotted against the sampled reaction time *t* [h]. Peaks areas of substances are referenced to the standard 1-decanol that is contained in the extraction solvent. The hydrogenation reaction was performed as described in chapter 2.5. At presented time points 250 µL samples were taken from the same reaction *via* a septum and extracted (chapter 2.4.6).

First workup steps included filtration and extraction of the menthol-containing reaction solution (chapter 2.5). After removal of the organic phase *in vacuo* a yellow liquid was

obtained. The liquid contained 5 % isopulegol, 29 % menthol and 66 % of the byproduct (relative peak areas). This raw product was separated by flash column chromatography over silica. 6.3 mg of menthol crystals could be isolated after removal of the eluent, which refers to an isolated yield of 6.7 %. During evaporation, menthol could be identified clearly by its characteristic minty smell. As the smell suggested a yield lowering co-evaporation of the menthol product, a trade-off between yield and purity was sought. The characteristic pleasant minty smell with a slight stingy note adhered to the finally obtained transparent crystals. The obtained product was characterized by ^{1}H- and ^{13}C-NMR (Figure Ap. 16 & 17) analysis as well as IR spectroscopy (Figure Ap. 18) confirming the isolation of menthol. By comparison with literature data all ^{1}H signals could be assigned to the respective menthol protons (Figure Ap. 16).[154] However, NMR analysis also revealed residual amounts of isopulegol in the sample. Integration of the characteristic alkene protons in isopulegol in comparison to the menthol proton adjacent to the alcohol function allowed quantifying menthol purity as 93 % (Figure Ap. 19). Chromatographic analysis confirmed the beforehand determined diastereomeric ratio of 92 % and enantiomeric purity of the isolated (-)-menthol. Next to menthol, 15.5 mg (16.3 % isolated yield) of the 3,7-dimethyloctanol byproduct were purified as colourless liquid, which possessed a rose-like scent. The side product was characterized by ^{1}H- and ^{13}C-NMR (Figure Ap. 20-21)

In conclusion, it could be shown as proof of principle that the invented chemoenzymatic cascade enables the synthesis of (-)-menthol. The novel engineered enzymes could be combined and be complemented by chemical synthesis to illustrate an alternative synthetic access to this valuable aroma chemical. However, the yield and purity of the obtained (-)-menthol allow space for further improvements.

4. Discussion

Enzymes are powerful catalytic macromolecules that nature evolved to enable the molecular complexity of life.[1] From a chemical point of view these biocatalysts achieve reactivities and selectivities under ambient conditions that are usually unmatched by 'classical' chemistry.[5,169] Today several reports have shown that enzymes are not restricted to the conversions in nature and provide a valuable novel synthetic alternative or complement to the existent chemical repertoire.[8,17] This is underpinned by the fact that several enzymes are nowadays already used in industrial syntheses.[3,7,170] Nevertheless, the increasing scientific examples of multienzymatic and chemoenzymatic cascades highlight that there is a yet unlocked synthetic potential.[15,16,138,142,144] Moreover, genetic modification of enzymes can provide high adaptability to synthetic needs.[9,17,171,172] However, the current challenge is to study the broader applicability of these techniques to solve various synthetic challenges.

The presented results prove that by exploitation of genetic engineering novel biosynthetic pathways can be established. Though recently various successful combinations of biocatalysts with 'classical' chemical reactions were reported, few examples have actually assessed the even greater opportunities that arise with using enzyme engineering. Herein, this was successfully demonstrated by establishing a novel chemoenzymatic cascade synthesis of the industrially relevant aroma chemical (-)-menthol from *E*/*Z*-citral.

4.1 ERED engineering towards *R*-selective citral reduction

By means of a combination of hot-spot identification through site-directed mutagenesis and subsequent iterative site-saturation mutagenesis at these hot-spots, it was possible to invert the enantiopreference of NCR ERED in the reduction of both isomers of citral. While the wild-type enzyme was exclusively *S*-selective in this conversion, the NCR triple variant W66A/I231R/F269V is *R*-selective achieving up to 89 % enantiomeric excess in the conversion of *E*/*Z*-citral (for purified enzyme 40 % relative product formation in comparison to NCR wild-type). This is relevant for a subsequent reaction sequence that aims to specifically yield the (-)-menthol stereoisomer because for this purpose *S*-citronellal is stereochemically not suited.

Before discussing the details of the engineering strategy that led to the development of this novel catalyst, findings on the mechanism of the NCR ERED-catalyzed citral reductions are evaluated.

4.1.1 Insights on the oxidative half reaction of NCR ERED with citral as oxidant

Different computational methods were applied throughout the herein described thesis to complement or explain the experimental results regarding the engineering of NCR ERED. In a collaboration with Dr. Wolfgang Brandt from the Leibniz Institute of Plant Biochemistry in Halle (Saale), Germany, it was also envisioned to correlate calculated activation barriers of the reduction of citral by NCR variants with altered enantioselectivity. To achieve this, semi-empiric quantum mechanics calculations based on the method PM7 have been performed. Surprisingly, however, this initial motivation couldn't be realized because the mechanism described in literature[77] (here it is called the 'classical mechanism') of the oxidative half reaction of EREDs failed to result in an exergonic reaction, which is a thermodynamic requirement for the reaction to take place by itself.[173] In consequence, alternative reaction paths were sampled computationally. It should be highlighted that because of the simplifications of the applied method, the following results require additional computational and experimental confirmations. Nevertheless, these calculations are insofar significant that they point out several

aspects of the oxidative half reaction in EREDs that we might not have fully understood yet.

The endergonic result of the initial calculation according to the 'classical mechanism' (Figure 13; chapter 1.3.2) is probably caused by a resulting charge separation that results if the hydrogenation of the C=C double bond happens by hydride transfer of the $FMNH_2$ species and a hydrogen transfer from a catalytically active tyrosine (Y177 in NCR). A beforehand neutral constellation is changed to a charge-separated state involving a negatively charged tyrosine and a positively charged flavin. By structural consideration of the NCR enzyme, it was found that an arginine in position 224 could serve as a base that would justify the often assumed $FMNH^{-1}$ species that partially compensates the above-mentioned charge-separation issue and therefore facilitates the hydride transfer (Figure 59). This acid base reaction causes itself a charge separation. However, the reaction will most likely form equilibrium. Moreover, the flavin becomes neutral by the subsequent hydride transfer. And indeed, calculations confirmed that this transformation is likely to happen. To the best of knowledge, this is the first calculation result that confirms such a catalytically relevant function for this arginine. So far, the arginine was reported to be mainly relevant for stabilizing the phosphate moiety of the flavin in the protein structure.[65] However, in the discussion of the crystal structure of the OYE plant homologue OPR1 from *Solanum lycopersicum* such a role of this highly conserved arginine has been hypothesized.[174]

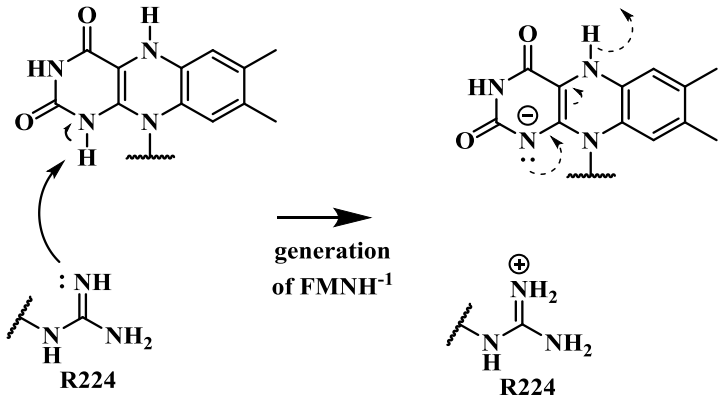

Figure 59: Generation of $FMNH^{-1}$ species due to prior deprotonation of $FMNH_2$ by R224 in NCR ERED. The generated negative charge facilitates a subsequent hydride transfer of the flavin as indicated by dashed arrows.

Furthermore, a potentially alternate reaction path (Figure 28, chapter 3.1.1) was calculated to be energetically feasible within the scope of the applied method. As in the 'classical mechanism' it involves the hydride transfer from the N5 position of the above

justified $FMNH^{-1}$ species, but the initial proton is transferred from a hydrogenated histidine species to form an enol intermediate. It rearranges in the active site and is then transformed by an enzyme-catalyzed keto-enol tautomerization, which involves the tyrosine that is typically described to be catalytically relevant (Y177 in NCR), but also an additional water molecule. In sum, this reaction therefore proceeds non-concerted with respect to hydride and proton addition to the activated C=C double bond. In the following, features of the mechanism and its relevance in comparison to experimental results are discussed.

For the hydride transfer 30.1 kcal/mol was calculated as activation barrier. This high activation barrier is theoretically reasonable in light of the significant hydrogen tunneling contribution that was found experimentally for both, the reductive and the oxidative half reaction in the MR ERED-homologue from *Pseudomonas putida* M10.[82,83]

The assumption of a protonated histidine (H172 in NCR) that results the enol intermediate needs further affirmation. Referring to the histidine side chain pK_a value of about 6, this possibility can be theoretically considered.[175] Moreover, it should be taken into account that the surrounding protein environment influences the actually present pK_a value of the amino acid residue. In contrast, based on an OYE1 crystal structure, it has though been argued as well that the present hydrogen bond network might render the histidine not to function as an acid as described here.[65] Furthermore, NCR variant H172A was shown in this work to possess residual activity in the reduction of citral. However, it should be mentioned that the herein described enol species might in theory also be formed by means of a different hydrogenation pathway.

Especially in light of the found rearrangement and H shift leading to a keto-enol tautomerism, it is interesting to discuss two experimental results, which are not in accordance with the so far described mechanism. For example, several studies have been published reporting on variants of the conserved tyrosine residue (in NCR Y177) that are still fairly active including findings that have been made in this work (chapter 4.1.2).[76,80,81] This is in contrast to initial findings of an inactive OYE1 ERED Y196F variant from *Saccharomyces pastorianus* that substantiated the definition of the role of this tyrosine initially. It appears that this behavior varies among different EREDs. It is relevant that the herein described mechanism also involves this tyrosine and thus confirms a catalytically important function. However, water is also involved in

the hydrogen shift reaction. It has been hypothesized previously in the above-mentioned knock-out studies that water could substitute the role of the tyrosine. The herein described calculations can be understood as a confirmation of such hypothesis. It should be highlighted that a more complex water network, that has not yet been considered, might be involved in the overall reaction. The second experimental finding refers to a study of Brenna et al. investigating the ERED-mediated hydrogenation of tetra-substituted alkenes. In their study they also found evidence for *syn*-addition products for some substrates instead of the generally described *trans*-addition.[176] According to the classically described direct protonation from tyrosine only *trans*-addition products should be formed. In contrast, the herein described rearrangement of the enol intermediate theoretically also allows for the formation of *syn*-addition products.

Despite of the fact that these experiments support the calculated finding that the protonation mechanism in the oxidative half reaction might be more complex, these calculation results stand in contrast to recent QM/MM calculations that studied the oxidative half reaction in the thermophilic ERED YqjM from *Bacillus subtilis* using cyclohexanone as the oxidant. In their study they concluded a confirmation of the proton-donating role of the catalytic tyrosine in the enzyme although they found a non-concerted reaction involving an enolate intermediate.[177] It should be mentioned that this does not affect the findings regarding the potential role of R224 because in their study, an $FMNH^{-1}$ species was assumed in the QM calculation part. As in contrast to semi-empiric calculations, QM/MM calculations consider the protein backbone in the MM part of the calculation, they usually result in more accurate results.[112] Nevertheless, the different experimental outcomes of the reduction of various substrates by different ERED members also underpin the possibility that also mechanistic details differ in different family members. It might be that the calculation results are restricted to the chosen example of citral reduction in NCR. In summary, the herein presented mechanistic results need further investigation, which involves additional experiments and complementary calculative confirmations. For example, variations at position R224 could further elucidate the role of this amino acid for the NCR ERED mechanism.

4.1.2 Implications of the performed mutagenesis study on NCR ERED

During the mutagenic reshaping of NCR ERED for the asymmetric reduction of citral several observations were made and their implications will be discussed step by step.

NCR ERED differs strongly in the enantioselectivity control of the two isomers of citral:

An intriguing property of NCR ERED is its strict enantioconvergent reduction of both isomers of citral, *E* and *Z*, to *S*-citronellal with an *e.e.* > 99 %. Hence, it was a surprising result to find that variants of this enzymes displayed significantly differing selectivity results for the two isomers. This was for example already apparent in the first round of site-directed mutagenesis (chapter 3.1.2). From 28 variants, only seven showed an effect on the enzyme's enantioselectivity using *Z*-citral, while 12 affected the enantiopreference when using *E*-citral. The difference is for example especially illustrative for active site single variant W66A. It's enantioselectivity in *E*-citral reduction is already inverted (46 % *R*), whereas for *Z*-citral a wild-type-like selectivity is observed (90 % *S*). The performed molecular docking study of both isomers into the wild-type crystal structure of NCR ERED (pdb ID: 4A3U) yields a visualization that allows for a possible conformational explanation of this so far not described observation (Figure 60). The simulation verified the *S*-selectivity of the wild-type because no *R*-selective binding modes were calculated. However, this is apparently achieved by a tilted positioning of the enal group.

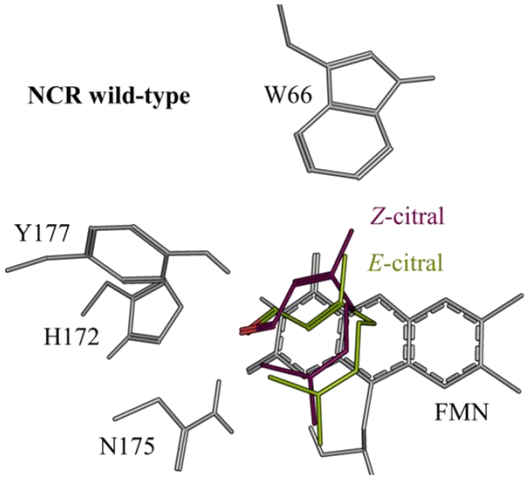

Figure 60: Overlay of molecular docking structures of *Z*-citral (purple) and *E*-citral (green) in NCR wild-type to highlight tilted binding of the isomers. In addition, prosthetic group FMN and amino acid residues W66, H172, N175 and Y177 are presented in gray for orientation. Citral oxygen is shown in red.

NCR W66 acts as a leverage position for inverted citral reduction enantioselectivity:

The present mutagenesis study suggests that initial access to *R*-selective citral reduction by NCR ERED requires variation at position 66. Several findings underpin this hypothesis.

First, position 66 was the only residue to significantly influence NCR ERED citral reduction enantioselectivity in the first round of an active site mutagenesis study. In contrast to all other tested 27 variations, the W66A change alone already caused an inversion of the enantioselectivity in the *E*-citral reduction (from 99 % *S* to 46 % *R*). Interestingly, this variant exhibited retained wild-type-like activity. Furthermore, the performed site-saturation mutagenesis at position 66 discloses the huge effect of alterations at this location on the enantioselectivity in the reduction of citral, especially for *E*-citral conversion. Herein, a focus on mostly unpolar amino acid residues shows a clear correlation to a steric effect at this position (Figure 61).

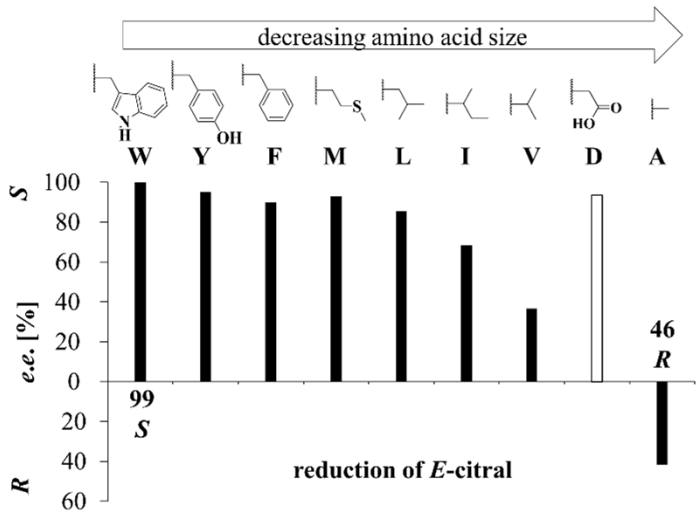

Figure 61: Saturation mutagenesis of NCR position 66 selecting *e.e.* value results for *E*-citral reduction to highlight a steric trend. Mostly unpolar amino acids are depicted according to decreasing amino acid side chain volume.[161] As an exception, the smallest polar amino acid aspartic acid is also displayed. Results are derived from a site-saturation mutagenesis study at position 66 as presented in chapter 3.1.2 (Figure 32).

With decreasing side residue volume, the *R*-selectivity of the enzyme increases. The selected representation of an aspartic acid, however, also highlights that not only steric effects can guide the enzyme's enantioselectivity. The W66D variant is *S*-selective in the reduction of citral, although it is the smallest canonical polar amino acid in terms of side chain volume. This suggests that polar effects can control enantioselectivity as well. In this case it even overrides the steric possibility of an *R*-selective binding mode.

The likely explanation of this observation is a repulsion of the unpolar citral prenyl residue and the polar aspartic acid residue. Finally, a molecular docking simulation using an *in silico* generated NCR W66A variant confirmed the relevance of this variation for inverted citral binding modes that allows *R*-selective conversion of this substrate (chapter 3.1.2, Figure 33). While docking in the NCR wild-type only resulted in *S*-selective binding modes, docking into W66A also gave a flipped substrate orientation in line with measured inverted enantioselectivity for *E*-citral.

When comparing to other ERED selectivity studies, position W116 from OYE1 attracts attention. In the conversion of the monoterpene substrate carvone, alterations at this position caused selectivity inversions.[178] However, it should be noted that W116 in OYE1 corresponds to NCR W100 and not W66. Interestingly, changes at W100 had no significant effect on the citral reduction enantioselectivity in NCR. Nevertheless, taking YqjM ERED from *Bacillus subtilis* as an example, Reetz et al. previously classified position 66 (corresponds to 69 in YqjM) as one of several potential selectivity hot-spots in an exemplary ISM approach.[106] In this first described ISM strategy, enantiocomplementary variants of YqjM in the reduction of cyclopentenone and cyclohexanone derivatives were successfully created. Interestingly, alterations at YqjM position 69 only affected the selectivity significantly when combined with alterations at YqjM position C26 (C26 corresponds to T25 in NCR). This is a difference to the present NCR mutagenesis study towards citral reduction. Here, W66 alone significantly affected enantioselectivity, while combinatorial changes at W66 and T25 were not beneficial and even had a deleterious effect on the activity (chapter 3.1.2). A further relevant study that aimed to engineer selective variants of OYE2.6 ERED from *Scheffersomyces stipitis* CBS 6054 based on an iterative site-saturation approach was described by the Stewart group focusing on Baylis-Hillman adducts.[107] They described a relevant mutagenic and non-additive correlation of residues Y76 and I113 (corresponds to W66 and W100 in NCR) in order to achieve inverted selectivities in OYE2.6 for the tested substrates. In light of the superior importance of W66 in NCR and the fact that no such correlation to W100 was found at all, this underpins again the individuality of mutagenic studies with different enzyme family members on different substrates. In this regard, the findings of the Pietruszka group are insightful.[179] They state that it is generally difficult to predict enantioselectivities on the basis of the protein sequence. Their study contradicted another publication that proposed that this would be possible.[180] Nevertheless, regarding the conversion of the same substrate, Höbenreich

et al. were able to show that in principle, the amino acid alterations in one engineered stereoselective ERED can be transferred to related enzyme family members.[181] Based on the above described study in YqjM they created additional stereocomplementary pairs in *Rm*ER from *Ralstonia metallidurans*, *Dr*ER from *Deinococcus radiodurans*, *Ts*OYE from *Thermus scotoductus* SA-01 and also NCR from *Zymomonas mobilis*. Nevertheless, they conclude that it is generally difficult to predict selective outcomes in EREDs. In this regard, it is worth mentioning a structural study on *Glu*ER from *Gluconobacter oxydans*, which is sequentially and structurally closely related to NCR ERED (~70 % identity) and shares for example the W66 and W100 residues.[182] Among other variations, they tested W66A and W100A single variants in the conversion of carvone and citral, however, without analyzing the stereoselectivity. It is quite surprising that in this closely related enzyme they found completely abolished catalytic activity, which is in contrast to the same variations studied in this work and also contradicts the concept of a general transferability of variations between even closely related enzymes for the conversion of the same substrate.

Synergism of variations at NCR I231 with W66A significantly increases citral reduction R-enantioselectivity via a secondary effect:

In this study it could be shown that next to alterations at NCR W66, additional changes at I231 are crucial to further increase the initially obtained *R*-selectivity in the reduction of citral. For example, in the whole cell screening, the double variant W66A/I231P already displayed an enantiomeric excess of 91 % *R* in the conversion of *E*-citral (chapter 3.1.5).

This result of the iterative site-saturation strategy strongly suggests that the changes at positions 66 and 231 are cooperative in terms of their effect on citral reduction selectivity. The effect of double variations at these positions is greater than the sole sum of the respective single variants. This effect is known as epistasis, which can be seen as a general term to describe non-additive cooperative effects.[99] Here, the special case is that a phenotypic outcome (selectivity enhancing effect by I231 change) is only observable upon introduction of an additional gene variation (W66A). Some functional changes in enzymes rely on specific key amino acids like the here proposed leverage W66 position for the selectivity change in the reduction of citral.

This also characterizes for example observations made for the selectivity effect of NCR N175. The initial first shell mutagenesis strategy that probed single variation in NCR

active site revealed no selectivity function (chapter 3.1.2). However, upon introduction of a W66A variation, the position suddenly affected selectivity strongly. The alanine and phenylalanine variations resulted in opposite selectivities for reduction of *E*-citral (either 63 % *R* or *S*, respectively). It should be noted that position N175 was not considered as a target site in the site-saturation combination screen because all variants proved to be detrimental for the reduction activity. The effect of catalytically important amino acids on the selectivity is discussed later.

Intriguingly, both of these epistatic effects (W66 with I231 and W66 with N175) seem to be intertwined as molecular dynamics simulation suggests (chapter 3.1.5). The simulated W66A/I231P variant revealed a pronounced flexibility of the N175 position. Because of the known selectivity function at position 175, the implication is that alterations at positions 231 exert their function through an influence on position 175. The increased flexibility of N175 might for instance effectively block locations for *S*-selective binding modes (Figure 62). However, the variant is not completely *R*-selective, especially for *Z*-citral. Considering mentioned N175 flexibility this might be reasonable because then, statistically, there would be N175 configurations that do allow for *S*-selective binding. In other words, the flexibility does only decrease the probability of a protein conformation that does allow *S*-selective conversions and hence, some *S*-selective reductions are still observable. Fixing conformations that block *S*-selective binding without hampering the catalytic machinery, is the theoretical solution to a completely *R*-selective enzyme.

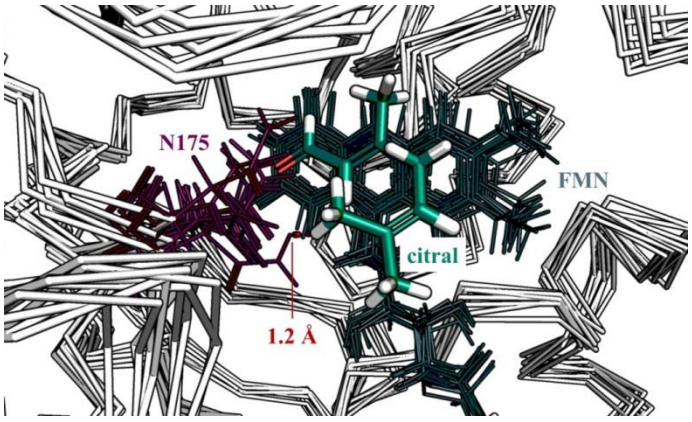

Figure 62: Modelling of *E*-citral binding mode into an overlay of different snapshots of the MD simulation of NCR W66A/I231P variant. The *E*-citral binding mode was obtained from docking into NCR wild-type. The model highlights potential steric clashes between the in the MD simulation calculated highly flexible depicted N175 (purple) and *S*-selective binding of citral (light green with oxygen in red and hydrogens in white). An exemplary distance between citral and one orientation of N175 is measured to 1.2 Å (depicted red). Prosthetic group FMN (dark green) is depicted for orientation and the protein backbone is indicated by ribbon structure. The overlay structure of the MD simulation consists of snapshots after 50, 500, 875, 1250, 1750, 2525, 3475, 4150, 4500 and 4925 ps.

These considerations of epistatic effects that are pivotal for successful engineering of specific traits also point out that the chosen strategy will most likely have missed more beneficial epistatic interactions. This is an inevitable consequence of the selection for a specific library generation method. However, this highlights that enzyme engineering strategies need to be guided by the objectives of the mutational study. What are the resources that one wants to spend on engineering? Is there a suitable screening system? How many features should the optimized enzyme provide? This work and previous studies[106,107] show that simple libraries can also provide significantly improved enzymes.

Furthermore, with regard to the herein found W66 I231 correlation it is interesting to note the finding of another study that an Y78 Y246 pair (corresponds to W66 I231 in NCR) in the plant-derived ERED homologue OPR1 acts as a substrate filter for the ene reduction of a precursor in the biosynthesis of jasmonic acid.[183] Hence, combinatorial specificity controlling effects at these sites are not completely unknown.

Alterations at F269 on a flexible surface loop can fine-tune citral reduction in NCR:

The finally best-performing variant in the *R*-selective reduction of citral was NCR W66A/I231R/F269V. Using the variant as whole cell preparation in the conversion of *E*/*Z*-citral, an enantiomeric excess of 89 % *R* was determined. This is notable in light of the fact that the NCR wild-type converted the mixture with > 99 % *S*. Although mutagenic combinations of W66 and I231 already resulted in pronounced *R*-selective enzymes, additional variations at position 269 were found to be essential to further improve the selectivity. However, in contrast to combinatorial alterations at position 66 and 231, combinations at position 66 and 269 did not result in comparably high improvements of the enzyme's *R*-selectivity (Figure 42, chapter 3.1.5). For example, in the screening, variant W66A showed *e.e.* values of 46 % *R* and 90 % *S* in the conversion of *E*- and *Z*-citral, respectively, and variant W66A/F269V slightly improved this to 63 % *R* and 71 % *S*, while the W66A/I231P variant resulted in the much more pronounced optimization to 91 % *R* and 32 % *R*. Nevertheless, the *Z*-selectivity of 32 % *R* in this W66A/I231P variant was then further increased to 72 % *R* by addition of the F269V alteration. Hence, it is deduced that for the studied example reaction, variations at position 269 act as a fine-tuning element for altered citral reduction enantioselectivity. It is furthermore interesting that many very different alterations at

this position led to such a fine-tuning effect. For example, in the W66A/I231P/F269X screen (X represents one of the 20 possible canonical proteinogenic amino acid residues), amino acids H, P, Q, V, and Y were all identified as possible residues at this position that led to further increased *R*-selectivity (Table Ap. 5). A potential explanation for this fine-tuning effect might be correlated to the highly dynamic nature of the surface loop 6 on which this position is located (Figure 48, chapter 3.1.6). This large flexibility was described in various previous studies. In one example, the flexibility of this loop in NCR was recognized by the high B-factor of this structural element and the information was used to create truncated loop variants with increased solvent tolerance and thermostability.[71] In another structural study with *Cm*OYE from *Corynebacterium aquaticum* it was found that this loop can adopt an open and closed conformation, which is relevant for substrate recognition.[184] From these data it is hypothesized that alterations at position 269 result in a remodeled flexibility of loop 6 in NCR, which might explain the fine-tuning effect on the enantioselectivity. This hypothesis is underpinned by the fact that the combination of the selectivity-defining W66A variation with a defined grafting of loop 6 derived from OYE1 also resulted in such a fine-tuned selectivity (chapter 3.1.6). Surprisingly, this more direct loop remodeling even resulted in increased product formations. NCR variant loop 6* W66A showed up to 32 % enhanced activity compared to the NCR W66A single variant (Table 22). In this work, it was the only variant that restored some of the wild-type reduction activity in the citral reduction because usually the increased selectivity was accompanied by a decreased product formation. This highlights the huge potential that lies in the direct engineering of loops, which recently is increasingly realized.[185] Herein, the specific loop-grafting was restricted to a structural extension of OYE1 loop 6 in comparison to NCR, which was added to NCR loop 6 (Figure 49). In light of the fact that OYE1 already is *R*-selective in the reduction of the *E*-isomer of citral, it can be argued that this overhang is involved in controlling this selectivity and that the loop-grafting could partially transfer this feature.

Catalytically relevant NCR amino acids H172, N175 and Y177 exhibit a selectivity-controlling effect:

Amino acids H172, N175 and Y177 in NCR ERED are highly conserved in the OYE enzyme family and are known to be catalytically relevant.[54] This reasons why these amino acids are usually not addressed in mutagenesis studies.[106] Nevertheless, due to

the general active site approach that was chosen in this work to select for potential target sites, these amino acids have not been excluded from mutagenesis (chapter 3.1.2). This allows discussing how such alterations affected enzyme catalysis in the reduction of citral. It was found that alterations at all of these sites resulted in altered enantioselectivity. NCR single variants at positions Y177 and H172 already affected enantioselectivity to a small extent (up to 18 % decreased *S*-enantioselectivity). In this light it is notable that only eight of the 14 tested active site amino acids showed any direct influence on the citral reduction enantioselectivity. Moreover, only considering the *Z*-isomer, in this initial site-directed mutagenesis study variant Y177W even showed the highest influence on enantioselectivity (89 % *S*). As discussed in the previous discussion chapter, a great selectivity influence of position N175 was observed when combined with a W66A variation. Alanine and phenylalanine exchanges resulted for *E*-citral conversion in *e.e*. values of 63 % *R* and 63 % *S*, respectively. The W66A-based double variant library confirmed the selectivity influence of positions H172 and Y177. Especially the W66A/Y177W variant was the first to result in significantly decreased *S*-selectivity in the reduction of *Z*-citral. Therefore, position Y177 was also considered for the consecutive iterative site-saturation mutagenesis strategy. These findings suggest that to some extent, these residues, which are known for their catalytic function, do also play a distinct function in controlling the citral reduction selectivity in NCR ERED.

This is in confirmation to a site-saturation study at homologous positions H181 and H184 (correspond to H172 and N175 in NCR) in PETNR ERED from *Enterobacter chloacae* PB2 investigating the reduction of *E*-2-aryl-1-nitropropene.[186] It was found that the enantioselectivity of the conversions was affected by variants of the site-saturation libraries and even a regioselectivity switch to nitro-reduction could be observed. With selected variants of these enzyme libraries they could also observe a slight *e.e*. shift from 93 % *S* (PETNR wild-type) up to 82 % *S* (H184T) in the reduction of citral.

Apart from discussing these influences on selectivity, it may be generally regarded surprising that these variants indeed showed catalytic activity considering their ascribed catalytic functions. Nevertheless, pronounced negative effects on reduction activity were finally observed for all of these positions. The severity of this deleterious effect differed between H172, N175 and Y177 also depending on the number of total amino acid variations. While single alterations at H172 and Y177 retained up to 81 % and

77 % relative activity, respectively, N175-based single variants resulted in 4-10 % relative activity. When combined with the W66A variation, additional changes at H172 also became critical (0.2-13 % relative activity), while changes at Y177 still remained acceptable in terms of relative activity to the wild-type (39-61 %). However, variations at Y177 then also proved deleterious when added in triple and quadruple variants (chapter 3.1.5). From the data it is inferred that NCR N175 is especially important for citral reduction activity, followed by H172 and Y177. Residues N175 and H172 both interact with electron withdrawing groups of ERED substrates. The results suggest that the substrate stabilization by only one of those residues suffices to promote reduction activity. Similar observations were described in the above mentioned PETNR study.[186] Position Y177 is the discussed proton donor in the oxidative half reaction of the NCR enzyme. However, the retained activity suggests that alternative proton sources like water might substitute Y177 as described in the previous discussion chapter.

4.1.3 Comparison to OYE1 ERED as alternative engineering target

As described in the introduction (chapter 1.3.3), OYE1 and NCR ERED can be regarded as two principally different types of citral reductases. The type I citral reductase OYE1 is already *R*-selective in the reduction of *E*-citral but not in the reduction of *Z*-citral, while the type II citral reductase NCR catalyzes an enantioconvergent reduction of both isomers to *S*-citronellal. This behavior known in literature[85] was confirmed in this work (chapter 3.1.4). It could also be shown that the citral reduction activity of NCR is up to five times higher compared to OYE1. The previous discussion of the mutagenesis studies on NCR ERED showed that *R*-selectivity can be engineered in this enzyme. The engineering was based on an initial active site mutagenesis study (chapter 3.1.2). As a comparative approach, a similar active site mutagenesis approach was adapted to OYE1 ERED in order to evaluate if the already present *R*-selectivity can especially for *Z*-citral be further improved. However, none of the tested variants resulted in higher *R*-selectivities than the wild-type already displayed. To the contrary, some variants induced *S*-selectivity in OYE1. For example, variant F296A changed the *Z*-citral reduction enantioselectivity from 33 % *R* to 71 % *S* while no change in activity was observed compared to the OYE1 wild-type. It is interesting to mention that this position corresponds to F269 in NCR ERED, which was one of the selectivity hot-spots in NCR that was required to be alternated in order to generate the

herein most *R*-selective NCR variant W66A/I231R/F269V. Therefore, this residue on loop 6 might be of general relevance for citral reduction control in EREDs. However, while in NCR only a fine-tuning effect was observed, in OYE1 the mutational effect on this position is much more pronounced, which also underpins the mutational differences in these two enzymes. Another significant difference of the mutational approaches were the huge deviations in mutability as most of the OYE1 variants were either catalytically inactive or their activity was critically impaired. Apart from alterations at position 269, no variants altered the selectivity without almost completely impairing catalytic activity. This was for example also the case for variants bearing alterations at position 116, which is known as a position to control the enantioselectivity in carvone reduction.[178] Up to 10-fold decrease in activity resulted for W116 variation. The effect on reduction selectivity could be confirmed (up to 47 % changed *e.e.*), but was less pronounced as reported for carvone reduction. From these results it was concluded that the citral reduction in OYE1 is highly delicate and therefore, no further variations were considered.

Conversion of NCR ERED to a type I citral reductase:

By means of a further comparison of OYE1 ERED and the best NCR hit variant W66A/I231R/F269V additional deductions are possible. In fact, the NCR mutagenesis study introduced many traits that are akin to the observations made for citral reduction with OYE1. Both of these enzymes are highly *R*-selective in the reduction of *E*-citral and exhibit a distinctly higher activity in the reduction of *E*-citral over *Z*-citral. However, they differ in the reduction of *Z*-citral. While for OYE1 an *e.e.* of 33 % *R* was obtained, the generated best NCR variant displayed 70 % *R*. These values were obtained for reactions with the developed whole cell reaction system. However, as will be discussed later on, the whole cell reaction leads to higher enantioselectivities than in reactions with the purified EREDs. For the same best NCR variant only 16 % *R* is then obtained for the reduction of *Z*-citral. This means further efforts are required to create a completely enantioconvergent *R*-selective ERED. In the present work the use of whole cells, though, provided an alternative solution to achieve high *R*-selectivity in the reduction of both citral isomers.

Taking all these considerations into account, it can be consequently argued that the herein described mutagenesis approach converted NCR ERED from a type II into a type I citral reductase. This can be further underpinned by a structural comparison of

OYE1 and NCR (Figure 63). The overlaid structures focus on those residues that have been identified as selectivity hot-spots in NCR and were addressed in the herein described ISM strategy (chapter 3.1.5). In NCR these were W66, Y177, I231 and F269 and in OYE1 they correspond to Y82, Y196, F250 and F296, respectively. While the three-dimensional location of the tyrosine seems to be unchanged, it attracts attention that the other three hot-spots adopt significantly differing locations. This is even more significant considering that from the 14 addressed active site amino acids only one additional residue shows such a structurally differing positioning (NCR/OYE: H128/Q147) due to a very different loop localization in the two distinct crystal structures. In consequence, unconsciously the initial NCR site-directed mutagenesis study led to the selection of exactly those structurally differing positions. This infers that a huge proportion of the difference between these type I and type II citral reductases is rooted in the alternative location of these three positions. Furthermore, this indicates that the positions could have been selected rationally by such a structural comparison.

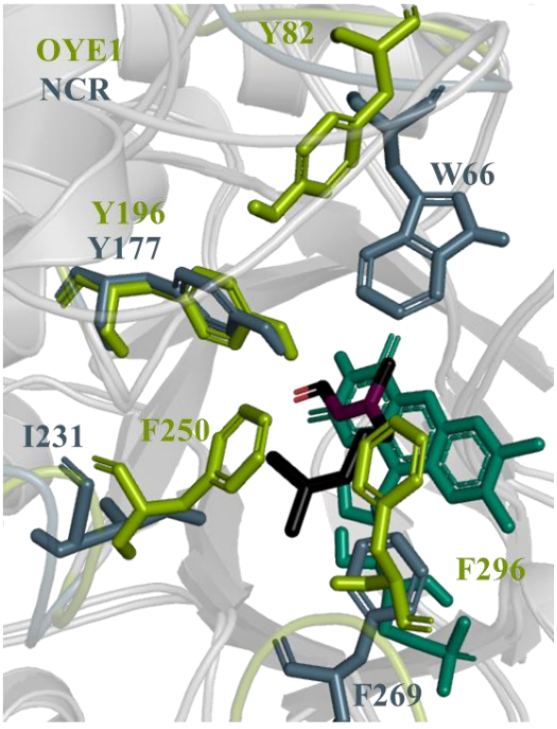

Figure 63: Structural overlay of OYE1 (pdb ID: 4A3U) and NCR (pdb ID: 1OYB) ERED highlighting the hot-spot positions in the active site pocket that have been addressed for iterative site-saturation mutagenesis in NCR. OYE1 residues are depicted in light green, NCR residues in gray, prosthetic group FMN shown in dark green and citral in black with indicated activated C=C double bond in purple and carbonyl oxygen in red.

4.1.4 Citral reduction by EREDs in whole cell environment

The development of a reaction system that allows for citral reduction biotransformations in whole cells was vital in this work (chapter 3.1.3). Primarily it allowed for faster screening of mutant libraries, which was required to perform the herein performed ISM study (chapter 3.1.5). Furthermore, it allowed for the analysis of a comparative OYE1 mutagenesis approach because functional OYE1 enzyme purification was unsuccessful (chapter 3.1.4).

In the following, some features of the described whole cell system are discussed. Two essentially different whole cell systems were initially compared, which were adapted from literature.[85,162] In one system, a setup was chosen to promote viable cell conditions, therefore glucose was added to stimulate cell metabolism, but no NADH was added assuming that cell metabolism would constantly supply the redox equivalent. In contrast, in a second system, no glucose was added, but NADH instead. The second system also contained 5 % (*v*/*v*) isopropanol to facilitate citral solubilization. Reduction activity was only observed with the second system. Leaving out external NADH supply in this system extinguished the activity, which confirms the assumption that the conditions are unviable. In the viable cell approach the absence of enzymatic activity might for example derive from a possible toxicity of citral or the inability of the substrate to cross the cell wall to come in contact with the reductase. However, this has not been analyzed further. Moreover, it can only be speculated that in the unviable cell approach the presence of citral and isopropanol cause a partial disintegration of the cell membrane allowing access to the reducing enzymes. This could have been clarified by further viability experiments, but in this work the objective of the whole cell approach was to provide ERED activity overcoming the so far necessary time-consuming enzyme purification. This could be achieved and also an increased product formation in comparison to the initially chosen reaction system was achieved by variation of reaction parameters (Figure 34 & 35, chapter 3.1.3).

Another objective in the development of this whole cell reaction system was to suppress a reduction of the aldehyde to an alcohol by dehydrogenases in the cells. Previous studies showed that employing EREDs for citral reductions in whole cell systems results in the formation of citronellol.[89] Furthermore, the additional aldehyde reduction of the substrate citral to nerol and geraniol can lower the obtainable product yield because the alcohols are not further converted by EREDs. Therefore, the *E. coli* strain

TG20+ lacking two of the most active non-specific ADH enzymes in *E. coli* was utilized. It was shown successfully that in comparison to the *E. coli* strain BL21(DE3) this undesired side reactivity is decreased up to 20-fold (Figure 35). Only a small residual activity (~2 %) of aldehyde reduction remained. Overcoming citronellol formation was furthermore useful for possible application in the (-)-menthol cascade because citronellol is not converted to (-)-isopulegol by the consecutively applied *Aac*SHC.

An unexpected finding was that the whole cell system unconsciously allowed for highly *R*-selective reductions with the citral isomers (Figure 44, chapter 3.1.5). In the characterization of the two most *R*-selective hit variants NCR W66A/I231R/F269V and NCR W66A/I231P/F269V, a comparison of reactions performed in whole cells with those performed with the purified enzymes revealed significant deviations in enantioselectivity (e.g. 16 % *R* for purified enzyme and 70 % *R* for whole cells). However, this was only found for *Z*-citral because when using *E*-citral the enantioselectivity was reproducibly high in both reaction systems (95 % *R*). Additional experiments have therefore been conducted to understand this apparent anomaly (Figure 45 & 46). By comparison of buffer and cell negative controls with either *E*- or *Z*-citral as substrate it was for example found that the cells cause a shift in the ratios of the citral isomers from which it was inferred that the cells cause an isomerization reaction (Figure 45 & Figure Ap. 11). This was underpinned by the finding that the depletion of one isomer was always accompanied by the increase of the other isomer. Furthermore, the found temperature-dependence of this process also favors this isomerization assumption (Figure 46). From literature it is for example known that proteins can catalyze citral isomerization.[94] However, this isomerization was described to primarily occur at basic conditions while here, slightly acidic conditions were chosen. Hence, the exact source of this isomerization remains obscure and further experiments are necessary to shed light on this. As an alternative, it is for example also conceivable that a specific *E. coli* enzyme catalyzes such an isomerization reaction. Nevertheless, the results of these experiments allow for stating a hypothesis explaining the beforehand surprising selectivity aberrations (Figure 64). For the continuing discussion it is noted that due to thermodynamic reasons, a system that allows for isomerization will generally strive to reach an equilibrium state, which for citral is a 3:2 mixture of *E*/*Z* at standard conditions.

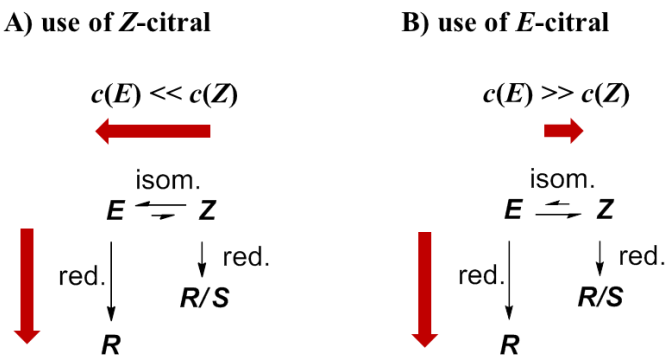

Figure 64: Schematic representation of ERED reaction (red.) using for example NCR W66A/I231R/F269V and parallel *cis-trans* isomerization (isom.) in *E. coli* whole cell system for applying either *Z*-citral (A) or *E*-citral (B) as substrate. The whole cells cause an isomerization of the citral isomers towards an equilibrium state (60 % *E* and 40 % *Z*). At the same time *E*-citral is reduced selectively to the product *R*-citronellal, while *Z*-citral is reduced with about half activity to racemic *R*/*S*-citronellal. These citral conversions to citronellal disturb the isomerization rates that would be obtained without this parallel process as indicated by the red arrows. A) When using *Z*-citral with $c(E) << c(Z)$, isomerization rate towards *E*-citral is enhanced due to the parallel reduction reaction pulling *E*-citral out of the equilibrium faster than *Z*-citral. This results in an accumulation of *R*-citronellal. B) When using *E*-citral with $c(E) >> c(Z)$, isomerization rate towards *Z*-citral is decreased because the faster reduction of *E*-citral to *R*-citronellal pulls out *E*-citral from the equilibrium anyway. Therefore, no significant alteration of enantioselectivity is caused.

The hypothesis that explains the observed enantioselectivity differences relies on the deliberation that the isomerization rates observed for using either enriched *Z*- or *E*-citral will be disturbed by the parallel conversion of both isomers to citronellal. A further key aspect is the fact that the reaction velocity of this parallel NCR variant-catalyzed reduction reaction differs significantly and also results in different enantioselectivities. For the discussed triple variants, it was found that *E*-citral is converted rapidly and selectively to *R*-citronellal (Figure 44, chapter 3.1.5)). In contrast, reactions with purified enzymes showed that *Z*-citral is converted considerably slower (25-50 % activity relative to *E*-citral conversion) yielding racemic citronellal (Figure 44). With these considerations in mind, the consequent different situations for either isomer can be discussed:

- Using *Z*-citral as substrate (Figure 64 A), the ERED whole cell reaction causes continuous isomerization to *E*-citral. However, due to the parallel reduction reaction *E*-citral is pulled out of the isomerization equilibrium faster than *Z*-citral. In consequence, the isomerization rate will increase in comparison to the undisturbed system. Hence, in comparison to a reduction reaction with purified ERED the system contains considerably more *E*-citral that is converted selectively to *R*-citronellal, which explains the huge enantioselectivity deviations.

- Using *E*-citral as substrate (Figure 64 B), the ERED whole cell reaction causes continuous isomerization to *Z*-citral. As described above, *E*-citral is, though, pulled out of the isomerization equilibrium faster than *Z*-citral due to the parallel reduction reaction. Hence, the effect on the isomerization rate, in contrast to the use of *Z*-citral as substrate, is opposite and thus, the isomerization rate will decrease in comparison to the undisturbed system. In consequence, reactions with whole cells and reactions with purified ERED behave similar explaining why in this case no enantioselectivity deviations were observed.

It is interesting to note that these deliberations will also affect conversions with OYE1 because this enzyme shows comparable selectivity and activity behaviors towards the different citral isomers like the described NCR variant. Hence, for purified OYE1 it might be expected that likewise a more *S*-selective outcome would be expected in the conversion of *Z*-citral. As no successful purification was achieved, though, this remains to be proven.

In summary, it is shown that an isomerization process is so far required to ensure the high *R*-selectivities achieved for *E*/*Z*-citral reduction. Intriguingly, this is comparable to a chemical solution for this reaction described by Hori et al. using a palladium catalyst and auxiliary 2-(diphenyl)methylpyrrolidine forming an *in situ* iminium that leads to an isomerization of citral.[53] So far, both systems achieve *e.e.* values up to 89 % *R*. However, it can be expected that further rounds of evolution will optimize the enzymatic approach further if desired. For example, a recent research project that was based on the results of the herein described thesis could successfully show that both, selectivity and activity of an NCR-based reductase were improved further.[187] In that work it was shown that Q232 can be another hot-spot for selectivity reaching up to 60 % *R* for converting *Z*-citral when using purified enzymes instead of the whole cell approach and alterations at H128 were found to restore wild-type like activity.

In the following it will be discussed how the development of this ERED catalyst could be implemented in a novel chemoenzymatic cascade for (-)-menthol synthesis.

4.2 Development of a chemoenzymatic (-)-menthol synthesis

The herein described chemoenzymatic cascade reaction sequence is adapted from a currently industrially applied (-)-menthol synthesis from citral.[19,22] A noteworthy expansion of the current method is the direct use of an isomeric mixture of citral because so far the isomers need to be separated by laborious distillation prior to their use.[19] The reduction of citral to citronellal followed by Prins cyclization to isopulegol are the reaction steps defining the chiral information in the final menthol product that is obtained by additional unselective reduction of the isopulegol (Figure 65). In consequence, the chemoenzymatic approach is hence suited to investigate i) the potential of engineered enzymes to add synthetic value and ii) the opportunity of combining such novel biocatalysts with well-established chemical methods.

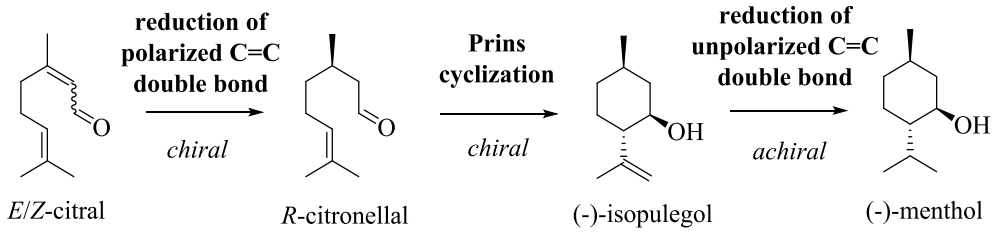

Figure 65: Conceptual reaction pathway for (-)-menthol synthesis from *E*/*Z*-citral. First, two chiral reaction steps convert citral in a reduction of a polarized C=C double bond to *R*-citronellal and then in a Prins cyclization to (-)-isopulegol. Secondly, (-)-menthol can be obtained by final achiral reduction of the remaining unpolarized C=C double bond.

4.2.1 Optimization of SHC-catalyzed *R*-citronellal formation

After the development of a suitable *R*-selective ERED for the desired novel (-)-menthol synthesis, this enzymatic reaction should be combined with a previously developed[117,129] enzymatic Prins cyclization using a *Aac*SHC to demonstrate the potential of selective enzyme catalysis. First, this only recently engineered enzyme was reevaluated and previous optimizations on the single *R*-citronellal to (-)-isopulegol conversion were expanded.

Surfactant and temperature are crucial parameters for SHC-catalyzed isopulegol formation

In this work, previously described optimizations for the SHC-catalyzed citronellal cyclization could be expanded.[129] The results confirmed that *Aac*SHC variant

A419G/Y420C/G600A leads to notable improvements in both activity and diastereoselectivity in the conversion of *R*-citronellal to (-)-isopulegol (Figure 50 & 51, chapter 3.2.1). Furthermore, it was confirmed that the adaption of surfactant concentration and reaction temperature are crucial parameters to achieve higher product formation. For the triple variant, the tested conditions differed up to ten-fold in product formation (Figure 51). It may be regarded surprising that a lowering in reaction temperature leads to improved product yields if one compares to the identified optimal temperature region of 50-60 °C in the conversion of squalene using this thermophilic *Aac*SHC.[188] This observation can be explained by evaporation in the herein performed analytical reactions (chapter 4.2.2). Increased temperature favors faster evaporation and thus, lower temperatures caused higher measurable product formations under the test conditions. Further experiments under evaporation-avoiding conditions at varying temperatures would be necessary to reevaluate the influence. However, from a practical point of view, the herein found productive conditions at lower temperatures harmonized well with the desired previous ERED catalysis.

4.2.2 Implementation of bienzymatic ERED-SHC cascade

ERED and SHC catalysis are compatible:

To the best of knowledge, ERED and SHC biocatalysts have not yet been applied together in a cascade reaction, especially not engineered variants of these enzymes. Therefore, it was initially not clear if both enzymatic systems would be compatible in a common reaction system. Specifically, it was for example unclear whether the presence of a surfactant that is required for the SHC conversion would significantly hamper the ERED activity. Nevertheless, the described results demonstrate that both enzymatic systems are compatible and can be optimized. Negative controls confirmed that the cascade activity did not derive from background reactivities (Table 23, chapter 3.2.2).

The SHC-catalyzed Prins cyclization is a non-natural activity. From the known results for the separate conversions of citral by ERED variants and citronellal by *Aac*SHC variants, it was expected that the cyclization to isopulegol would be the limiting conversion. For example, time-resolved investigations of the bienzymatic cascade were in favor of this deliberation (Figure 53, chapter 3.2.2). Already after 5 min reaction, considerable amounts of citronellal have been formed (~37 %), while isopulegol was hardly detectible yet.

The bienzymatic cascade offers optimization potential

Several parameters were initially evaluated in small sets of experiments to characterize influential parameters on this novel cascade reaction (Figure 55, chapter 3.2.2). It was shown that temperature, choice and concentration of the cosolvent, the cyclase concentration and the substrate concentration influence the bienzymatic cascade performance. Moreover, EREDs can be used in purified form or as whole cell preparation. As described before, using ERED in a whole cell environment leads to a higher *R*-selectivity in the reduction of citral (Figure 47, chapter 3.1.5). This increases the amount of convertible substrate for the consecutively active cyclase, which is specific for the *R*-enantiomer (*e.e.* > 99 %). Indeed, the obtained product formation seems to be higher in this case. However, the experimental error for this measurement was relatively high. Although the *Aac*SHC was expressed in the ADH-containing *E. coli* BL21(DE3) strain, the direct application of SHC-containing cells was also evaluated and resulted in a loss of activity. As in analogy to the reactions with purified enzyme, a higher amount of SHC-containing cells was applied, it was confirmed that this results in a fast accumulation of terpene alcohols that are not converted by the cyclase. In future, it might therefore be of value to clone the *shc* gene in a pDHE vector that allows subsequent expression in the ADH-deficient *E. coli* strain TG20+. As a final parameter, suppressing evaporation proofed to be crucial for detecting significantly higher product formation. For example, this caused a four- to five-fold increase in detectable product formation. In sum, this initial parameter evaluation allowed for improvement of the initially measured 2.3 % product formation to around 25 %. This result not only encourages further improvements for this cascade by using more elaborate optimization strategies, but also an increasing application of the versatile chemistry of SHCs in combination with other enzymatic systems.

Influence of evaporation on reactions using volatile terpenes:

The above discussed evaluation of the bienzymatic cascade already highlighted that evaporation is a physical property that is relevant for the in this work analyzed conversions of terpenes into one another. This relevance has already been considered for initial characterization experiments for the NCR ERED-catalyzed reduction of citral to citronellal (chapter 3.1.1). In the following, the influence of evaporation especially on analytical-scale reactions performed in this work are generally discussed on the basis of herein performed experiments.

As described in the introduction (chapter 1.2.1), evaporation is a surface effect happening below the boiling point.[42] It can be significant as shown for citronellal although its boiling point is as high as 208 °C.[189] Initially, the effect came to attention due to the clearly observable loss of citronellal at longer times of a time-resolved citral to citronellal reduction analysis (Figure 25). The performed experiments suggest that evaporation is the mainly relevant source of this loss in contrast to theoretically possible alternative explanations like an interaction of the terpenes with the reaction vessel – to name an example: i) qualitative curve analysis of the citronellal loss fits to the theory of evaporation in a closed vessel (Figure Ap. 22). In a closed vessel, evaporation will cause proceeding citronellal loss in solution until equilibrium concentration in liquid and gas phase is achieved and the closer the system gets to this equilibrium, the slower the evaporation rate will become.[190] For clarification purposes, the measured data points can for example be relatively well fitted to logarithmic decay. This highlights that over time the decay process slows and can thus be connected to evaporation; ii) headspace measurement confirmed citronellal in the gas phase; iii) experiments with changed gas volume revealed a direct correlation of the citronellal loss in solution and respective chosen gas volume (chapter 3.1.1 & Figure Ap. 7).

To evaluate the relevance of evaporation for a typical analytical reaction performed in this work, the ideal gas equation can be used to roughly compare the theoretical amount of citronellal in a saturated gas phase and the amount of citronellal that has been added to the liquid phase. The ideal gas equation connects the amount of substance n with the given partial pressure p of the evaporating substance for a given temperature T, a given gas volume V_{Gas} and the ideal gas constant R, which is 8.314 $J \cdot mol^{-1} \cdot K^{-1}$. The correlation is $n = p \cdot V_{Gas} \cdot T^{-1} \cdot R^{-1}$. Considering a standard analytical reaction, V_{Gas} amounts 1 mL. The partial pressure of citronellal at 25 °C (T = 298.15 K) is 33.3305 Pa.[191] Using the ideal gas equation, the amount of citronellal in a saturated gas phase can be estimated to $n = 1.3 \cdot 10^{-5}$ mol. In comparison, after full conversion, the 2 mM reaction approaches in 1 mL can maximally contain $n = 2 \cdot 10^{-6}$ mol citronellal. While a quantitative analysis of these numbers might be hampered by the simplifications of the ideal gas equation, it is qualitatively evident that the amounts of substance are in a similar range. Hence, evaporation has a huge impact on these analytical conversions and furthermore, no equilibrium between liquid and gas phase is achieved in the time-span of these reactions. According to literature it is rather complex to mathematically model such non-equilibrium states.[192] Furthermore, evaporation is

influenced by many parameters in a non-linear fashion like the surface area of the liquid, the heat of evaporation, temperature, outside pressure, solubility of the evaporating molecule, gas volume, fluid and gas dynamics (e.g. influenced by shaking of reaction vessels) and colligative effects.[192,193]

These considerations explain the huge impact on the product formations measured in the cascade reactions when the gas phase was deleted. At larger reaction scales, the amount of substance in the reaction solution will usually exceed the amount of substance that is needed for gas phase saturation and then, the analytical impact of evaporation should decrease. If evaporation can be expected to be problematic for product recovery, it has been shown that removal of the gas phase is a possible solution. As an alternative, evaporation can be suppressed by increased outside pressure, for example in an autoclave.

Alcohols are formed as side products in the cascade reactions:

Investigations on the single ERED-catalyzed reduction of citral to citronellal successfully showed that ADH activity is largely suppressed (Figure 35). Notwithstanding, considerable alcohol side products were detected in the bienzymatic cascade reactions (Figure 57, chapter 3.2.3), especially after longer reaction periods (e.g. 22 h). Two causes might be considered explaining this observation: i) a residual ADH activity was still detectable for whole cell reactions using the *E. coli* TG20+ strain. After longer reaction times this might cause gradually increasing alcohol formation; ii) the *Aac*SHC purification involved a heat-shock treatment and ion exchange chromatography, however, the enzyme still contained detectable impurities and thus, the cyclase preparation might have contained residual amount of active non-specific ADH enzymes (Figure Ap. 23). As mentioned above, SHC enzymes might be produced in an ADH-deficient strain as well or further measures might be investigated to suppress ADH activity. Nevertheless, increasing the efficiency of the cascade would very likely be a preferable solution because then, the slower side reaction will probably be of minor relevance.

The enzymatic cyclization is inhibited in the bienzymatic cascade:

Several experiments in this work suggest a putative cyclase inhibition as a so far limiting factor of the bienzymatic cascade: i) the maximally achievable isopulegol formation after the herein described initial optimizations stopped roughly at 25 %; ii)

time-resolved investigation of the bienzymatic cascade revealed a boundary of product formation after 10 h (Figure 52, chapter 3.2.2); iii) in the chemoenzymatic cascade it was shown that already after 2 h of the bienzymatic cascade reaction part, most of the achievable isopulegol was formed (Figure 57, chapter 3.2.3); iv) further on, it was clear that the performance of the *Aac*SHC reaction is diminished in the bienzymatic cascade (Figure 54, chapter 3.2.2). The addition of 1 mM citral to a separate *Aac*SHC reaction approach slightly decreased the resulting product formation. This shows that concurrent citral presence already results some inhibition, but does not fully explain the product formations observed in a comparable cascade experiment. Thus, a promising approach to increase the efficiency of this reaction sequence might focus on further revealing the nature of this inhibition, which might allow for developing solutions overcoming this inhibition. A comparison to recent literature regarding conversions using the *Aac*SHC allows further discussion of this observation. Seitz describes various inhibition effects in her thesis on SHC-catalyzed reactions, for example referring to the *Aac*SHC-catalyzed conversion of the sesquiterpene homofarnesol to (-)-ambrox.[194] She not only revealed that higher substrate concentration inhibited the reaction, but also showed that the reaction is inhibited in the presence of the ambroxan product and also that the much more productive natural cyclization of the triterpene squalene is inhibited in the presence of either homofarnesol or ambroxan. These results support that the herein obtained results for citronellal cyclization are hampered by comparable inhibition effects. So far, it is unclear if such an inhibition would be of allosteric or competitive nature. However, it is likely that theoretically all of the different monoterpenes present in the reaction mix of the bienzymatic cascade will fit in the large hydrophobic active site of the cyclization biocatalyst and might add to such inhibitions.

Further on, a theoretical systems biology calculation on this bienzymatic cascade that was performed in collaboration with Allgöwer et al. supports the inhibition deliberation and also offers a potential solution by reaction engineering.[195] For these calculations, time-resolved data of the in this work described ERED-catalyzed citral reduction were fed in the calculation and reaction parameters of the cyclase were assumed. The calculations suggested that a compartmentalization of both reactions could lead to increased product yields. The mathematical model might be expanded with additional experimental data to predict a possibly suitable reactor system for further evaluation.

4.2.3 Proof of principle of the chemoenzymatic cascade synthesis of (-)-menthol

The previously discussed achievements should finally be exploited to show as a proof of principle that this novel synthetic concept can be used in a preparative approach to isolate (-)-menthol. Indeed, after purification it was possible to characterize the finally achieved product as (-)-menthol by mass spectrometry, NMR and IR analysis. The product was obtained in 7 % isolated yield with an *e.e.* of 99 % and a *d.r.* of 92 % in a purity of 93 %. In the following, some details of the chosen synthesis approach are further discussed.

In this 100 mL-scale approach, first the one-pot bienzymatic cascade was performed to produce (-)-isopulegol. Then, a heterogeneous palladium on charcoal catalyst was added directly to the crude reaction mixture and the final reduction to (-)-menthol was started in a hydrogen atmosphere. A complete one-pot reaction was herein not considered because the unspecific nature of this reduction would have negatively interfered with the first two reaction steps. Furthermore, the presence of the palladium catalyst and the hydrogen atmosphere might have hampered the performance and stability of the enzymes.

Both, the bienzymatic cascade and the final hydrogenation were followed by analyzing small reaction samples after different reaction times. Combining so far best suited conditions of the bienzymatic cascade, it was found that in the closed vessel after 22 h reaction 32 % isopulegol formation could be achieved (Figure 57, chapter 3.2.3). However, it was either observed that most of the product has already been formed after 2 h and alcohol side products like citronellol were also observable after longer reaction times (chapter 4.2.2). No citral or citronellal have been detected in the reaction mixture after 22 h. It is important to note that the results suggest that herein formed isopulegol was not primarily limited by the later observed alcohol formation. In contrast, further isopulegol formation seemed to stop after reaching a certain plateau concentration in the reaction mixture and therefore remaining citronellal was finally reduced to citronellol. Cyclase inhibition was discussed as a likely cause in the previous discussion chapter. These findings suggest that overcoming this inhibition should also suppress alcohol formation. For the following hydrogenation it could be successfully shown that catalysis proceeded continuously in the presence of the crude aqueous reaction mixture and after 44 h no further menthol was produced. This confirms that such hydrogenations can be

well performed in the presence of biological matrices as has been previously described in other chemoenzymatic cascades.[16,145] The gradual increase of menthol formation could be correlated to the loss of isopulegol (Figure 58, chapter 3.2.3). Finally, 31 % menthol was detected in the final reaction sample after 44 h.

The following product isolation was also accompanied by a significant loss of product as after extraction, flash column chromatography and final solvent removal at the evaporator, 7 % isolated yield were obtained (6.3 mg). It is very likely that during solvent removal, also a lot of product evaporated because of the volatile nature of this terpene. The distinctly observable minty smell during this purification step underpins this assumption. Nevertheless, the solvent removal was continued until transparent crystals were formed. A trade-off of product purity and yield should be achieved and therefore, NMR analysis revealed that the final product did not contain remaining solvent. However, residual amounts of the isopulegol educt were detectable.

Nevertheless, the main side product, 3,7-dimethyloctanol, could be separated successfully from the desired menthol and no traces of this side product were detectable in the final menthol sample. This side product results as a final hydrogenation product of the previous byproducts of the bienzymatic cascade, hence, nerol, geraniol and citronellol (Figure 66). After flash column-chromatography, 15.5 mg of 3,7-dimethyloctanol were isolated in a separate fraction (16.3 % yield). Due to the *R*-selective ERED reduction, mainly the *R*-enantiomer of this side product will have been formed. However, it is interesting to note that the opposite *S*-enantiomer of 3,7-dimethyloctanol might be interesting as aroma chemical ingredient itself because it is described to possess a '[…] floral odour like clean rose […]' scent.[196] Using wild-type NCR ERED in a whole cell approach with following chemical hydrogenation, this aroma chemical should be synthesised quantitatively with absolute enantiopurity.

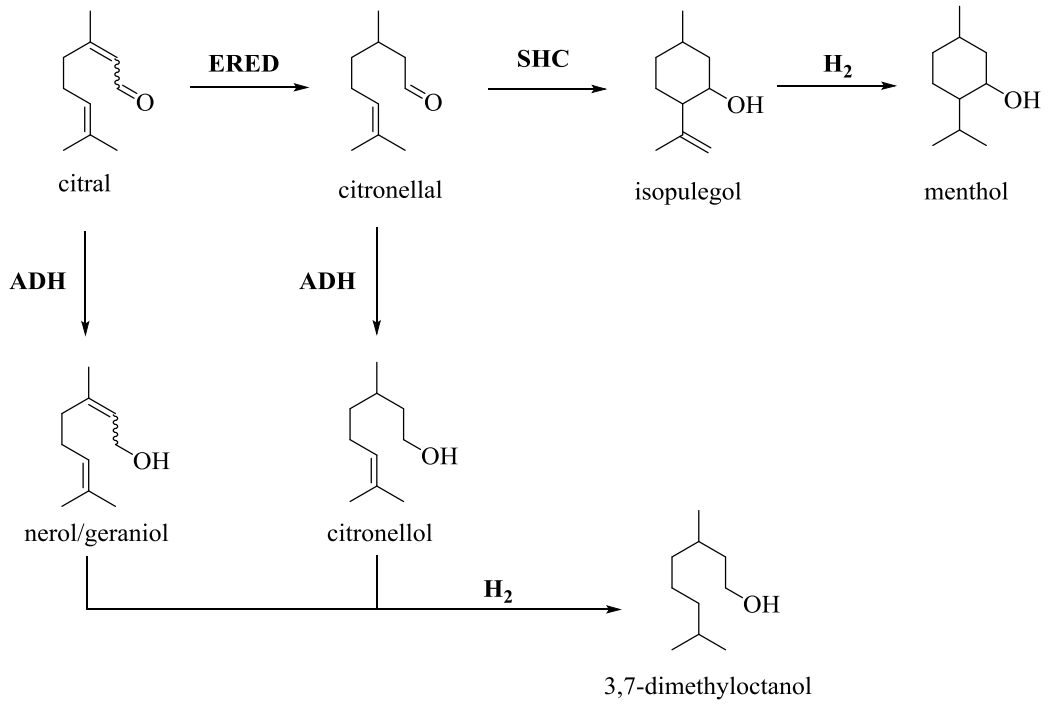

Figure 66: Reaction scheme explaining obtained products in the herein described chemoenzymatic cascade reaction. The desired reaction path involved citral reduction by an ERED biocatalyst, followed by citronellal cyclization by an SHC biocatalyst and final reduction of isopulegol to menthol by hydrogen. However, especially after longer reaction times, remaining residual ADH activity resulted in the formation of small amounts of nerol and geraniol and larger amounts of citronellol because of the incomplete cyclization of citronellal to isopulegol. These alcohols were all fully reduced to 3,7-dimethyloctanol by hydrogen, which accumulated as only byproduct of the reaction.

Finally, this work successfully demonstrates that the initially envisioned chemoenzymatic cascade could be assembled successfully to synthesize (-)-menthol. Potential inhibition effects in the bienzymatic cascade and necessary improvements in product purification were identified as potential bottlenecks of this approach. Hence, there still exists a large optimization potential to create a potentially efficient synthetic method. Although the herein described synthetic concept is due to its novelty still in an early developmental phase, it might be advantageous for a potential hypothetical application. Essentially, in particular the enzymatic reduction of citral and the following citronellal cyclization could be regarded as a 'biocatalytic upgrade' to the existent menthol production from citral. The advantages of these biocatalysts like the possible redundancy of a prior citral isomer separation might therefore initially be easier adapted in existent synthetic networks in contrast, for example, to a fermentative biotechnological procedure that is based on other resources than citral. Most recently, it was for example reported that a so far missing isomerase has been identified that should enable the transfer of the plant menthol biosynthesis in a by comparison better to handle *E. coli* strain.[29] Hence, such a fermentative menthol production based for example on a resource like glucose might be demonstrated in future. This would make a very different

in vivo approach in contrast to the herein described *in vitro* approach accessible. Both approaches have general advantages and disadvantages regarding for example operability, cost of catalyst and process workup that would need to be evaluated against each other in terms of economic and ecologic needs (chapter 1.6).[142] In detail, this can be a complex endeavor, which with respect to current situations can also vary over time. From a scientific point of view, it is, however, generally an asset to demonstrate the frontiers of our synthetic capabilities as broadly as possible.

Exploiting biological and mechanistic diversity to create new enzymes:

Next to the potential synthetic benefits of the chemoenzymatic synthesis that has been developed in this work, the chosen example serves to generally highlight how new enzymatic functions can be developed for a given synthetic challenge. While it is nowadays well known that enzymatic properties can be changed by genetic engineering, an important aspect is to find a suitable starting point for such an engineering.[197] This work demonstrates that novel enzymatic functions can be developed from two conceptually different starting points (Figure 67).

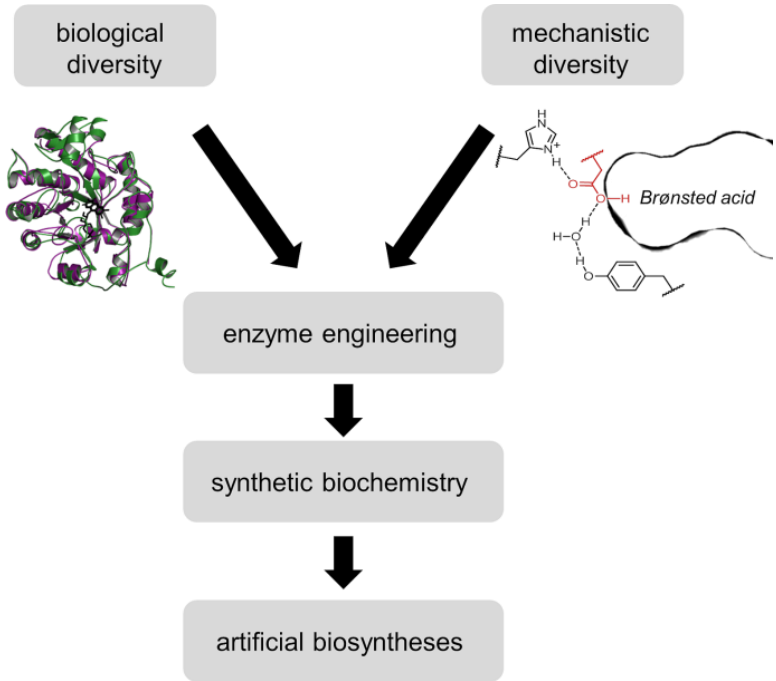

Figure 67: Conceptual strategy to find enzyme engineering targets by exploiting either biological or mechanistic diversity for application in synthetic biochemistry to enable the assembly of novel artificial biosyntheses. In this work, such a strategy is showcased by engineered ERED and SHC enzymes that have been combined with a chemocatalyst to create a novel synthetic route to (-)-menthol. The figure has been adapted according to a previously published article.[197] The SHC active site depiction was also reported previously.[128]

These different concepts can be distinguished by the exploitation of biological diversity on the one hand, and mechanistic diversity on the other hand. In the case of the altered enantioselectivity of NCR ERED, it was shown that the biologically present valuable reductase function could be diversified to adopt a novel selectivity. In contrast, the herein applied engineered *Aac*SHC does not resemble its natural cyclization activity of the triterpene squalene, but rather exploits the inherent mechanistic diversity of its underlying Brønsted acid chemistry in a different type of chemical reaction.[117,129] Interestingly, although these starting points are very different, the methods for engineering the ERED and SHC enzyme towards their novel functions were quite similar. Both strategies identified potential hot-spot positions in the active sites of the respective enzymes and introduced new combinations that enabled the novel function. Finally, this work represents a valuable showcase that such conceptually different derived novel enzymatic functions can not only be combined on the multienzymatic level, but also with ‘classical’ chemical reaction steps in a chemoenzymatic cascade reaction. This strategy should motivate to regard enzyme catalysis as a complementary opportunity in retrosynthetic analysis.

5. Outlook

This work successfully demonstrated that tailored reductase and cyclase biocatalysts and a chemocatalyst can be combined to create a novel synthetic route towards the valuable aroma chemical, (-)-menthol. This sets a basis for further investigations and optimizations that are required to overcome remaining challenges.

For a start, the herein applied engineered biocatalysts need to be further improved in terms of activity and productivity. It should be emphasized that the engineering of NCR ERED and the previously described engineering of *Aac*SHC[117,124,128,129] exploited a limited set of alterations in the active sites of those proteins. Hence, these studies could be expanded by further rounds of combinatorial and random mutagenesis. Thereby, selectivities might be increased even further and also the catalytic activity might be elevated. For example, a concomitant mutational study on NCR ERED based on the herein described findings could show that variations at NCR H128 restored activity in *R*-selective NCR variants without influencing the enantioselectivity.[187] Moreover, enzyme engineering might be expanded outside the active site pocket. In this work, it was shown that loop engineering is a very promising complementary approach to tailor enzymatic functions.

With respect to the *R*-selective citral reduction, it was observed that a cell-induced citral isomerization increases the enantiopurity of *R*-citronellal product. Further experiments are required to identify the nature of this isomerization. It could be an unspecific process catalyzed by amino acids at protein surfaces or by cell metabolites or a specific enzyme-dependent reaction. Several further negative controls and the analysis of *E. coli* fractions could shed a light on this. The findings could enable the set-up of a more controlled isomerization, which might be beneficial for process design. Another approach could be the addition of chemical auxiliaries like various amines to promote such isomerizations.

With regard to the optimizations of the biocatalysts, an additional alternative is to screen for even better template enzymes. This work describes a classification of EREDs towards citral reduction based on well-characterized enzyme family members. However, the unexplored sequence space remains enormous and might contain promising catalysts. Furthermore, a screening of alternative SHC enzymes might

provide an enzyme with a better starting activity for the cyclization of citronellal. For example, *Zmo*SHC enzymes showed promising results with respect to catalytic activity[122], but so far mutational studies[123] could not provide selectivities comparable to the most selective *Aac*SHC variants.

Due to the use of an NADH-dependent oxidoreductase, future studies will furthermore need to maintain low catalytic concentrations of this costly cofactor or to overcome its application completely. For example, many enzymatic cofactor regeneration systems have been described and can be applied.[198] Usually an orthogonal enzymatic reaction like the oxidation of glucose to gluconolactone by glucose dehydrogenase restores the required amount of reducing equivalents. As an alternative, it has been shown that cheaper cofactor mimics can be applied.[199] It has been reported that such mimics can increase citral conversions by EREDs.[200] Moreover, further efforts might enable the application of the cascade reaction under viable whole cell conditions allowing for internal cofactor regeneration.

It was described that inhibition of the cyclase is a major limitation of the investigated synthetic cascade. Detailed kinetic studies are necessary to shed a light on this observation and could guide measures to overcome such inhibition. In this regard, reaction engineering will play a crucial role. For example, two-phase systems of an aqueous phase and a non water-miscible solvent might help to maintain a limited mass transport in the aqueous phase to overcome catalyst inhibition.[201] In such a system, though, enzyme stability and solvent tolerance will also need to be evaluated. It has been shown that enzyme stabilities can for example be increased by enzyme immobilization to a carrier[202], protein-crosslinking[203] or specific protein engineering strategies[204]. In order to increase product yield further, systems biology calculations on the bienzymatic cascade suggested application of compartmentalization for the two enzymatic reactions.[195] With respect to the realization of such compartmentalization and the avoidance of enzyme inhibition, it might be interesting to evaluate the use of continuous-flow microreactors.[205,206] They might allow a custom-made design of several compartments and could also include the chemical hydrogenation. Recently, a proof of concept study demonstrated the combinability of continuous flow hydrogenation and enzymatic catalysis.[207] Next to microreactors, compartmentalization might be achieved by various alternative strategies like the application of virus capsids or protein cages.[208]

In general, a combinatorial approach of kinetic modelling and experimental data acquisition for specific cascade reaction approaches can be a straightforward strategy.[209,210] Experimental data could be fed back into model systems to refine them. Moreover, various crucial parameters of the present cascade like catalyst, cofactor and substrate concentrations, nature and proportion of cosolvent and surfactant, reaction temperature, pressure and time will likely be optimized crucially in a statistical design of experiment approach.[211,212] A combination of the suggested reaction engineering approaches might finally allow for an efficient process with high product titers.

List of references

1. Sumner, J. B. Enzymes, the Basis of Life. *J. Chem. Educ.* **29,** 114–118 (1952).
2. Wolfenden, R. & Snider, M. J. The Depth of Chemical Time and the Power of Enzymes as Catalysts. *Acc. Chem. Res.* **34,** 938–945 (2001).
3. Nestl, B. M., Nebel, B. A. & Hauer, B. Recent progress in industrial biocatalysis. *Curr. Opin. Chem. Biol.* **15,** 187–193 (2011).
4. Clouthier, C. M. & Pelletier, J. N. Expanding the organic toolbox: a guide to integrating biocatalysis in synthesis. *Chem. Soc. Rev.* **41,** 1585–1605 (2012).
5. Torrelo, G., Hanefeld, U. & Hollmann, F. Biocatalysis. *Catal. Letters* **145,** 309–345 (2015).
6. Hughes, G. & Lewis, J. C. Introduction: Biocatalysis in Industry. *Chem. Rev.* **118,** 1–3 (2018).
7. Choi, J., Han, S. & Kim, H. Industrial applications of enzyme biocatalysis : Current status and future aspects. *Biotechnol. Adv.* **33,** 1443–1454 (2015).
8. Nestl, B. M., Hammer, S. C., Nebel, B. A. & Hauer, B. New Generation of Biocatalysts for Organic Synthesis. *Angew. Chem. Int. Ed.* **53,** 3070–3095 (2014).
9. Bornscheuer, U. T. *et al.* Engineering the third wave of biocatalysis. *Nature* **485,** 185–194 (2012).
10. Bornscheuer, U. T. The fourth wave of biocatalysis is approaching. *Philos. Trans. A. Math. Phys. Eng. Sci.* **376: 20170,** 1–7 (2018).
11. Nicolaou, K. C. & Chen, J. S. The art of total synthesis through cascade reactions. *Chem. Soc. Rev.* **38,** 2993–3009 (2009).
12. Nicolaou, K. C., Edmonds, D. J. & Bulger, P. G. Cascade Reactions in Total Synthesis. *Angew. Chem. Int. Ed.* **45,** 7134–7186 (2006).
13. Metallo, C. M. & Vander Heiden, M. G. Understanding metabolic regulation and its influence on cell physiology. *Mol. Cell* **49,** 388–398 (2014).
14. Keasling, J. D. Manufacturing Molecules Through Metabolic Engineering. *Science* **330,** 1355–1358 (2010).
15. Ricca, E., Brucher, B. & Schrittwieser, J. H. Multi-Enzymatic Cascade Reactions : Overview and Perspectives. *Adv. Synth. Catal.* **353,** 2239–2262 (2011).
16. Rudroff, F. *et al.* Opportunities and challenges for combining chemo- and biocatalysis. *Nat. Catal.* **1,** 12–22 (2018).
17. Renata, H., Wang, Z. J. & Arnold, F. H. Expanding the Enzyme Universe: Accessing Non-Natural Reactions by Mechanism-Guided Directed Evolution. *Angew. Chem. Int. Ed.* **54,** 3351–3367 (2015).
18. Schmidt-Dannert, C. & Lopez-Gallego, F. A roadmap for biocatalysis – functional and spatial orchestration of enzyme cascades. *Microb. Biotechnol.* **9,** 601–609 (2016).
19. Schäfer, B. Menthol. *Chemie unserer Zeit* **47,** 174–182 (2013).

20. Leffingwell, J. C. & Shackelford, R. E. Leavo-menthol – syntheses and organoleptic properties. *Cosmet. Perfum.* **89,** 69–78 (1974).

21. Croteau, R. B., Davis, E. M., Ringer, K. L. & Wildung, M. R. (-)-Menthol biosynthesis and molecular genetics. *Naturwissenschaften* **92,** 562–577 (2005).

22. Hopp, R. & Lawrence, B. M. Natural and Synthetic Menthol. in *Mint - The genus Mentha* 371–398 (Taylor & Francis Group, 2007).

23. Lange, B. M. Biosyntehsis and Biotechnology of High-Value p-Menthane Monoterpenes, Including Menthol, Carvone and Limonene. *Adv. Biochem. Eng. Biotechnol.* **148,** 319–353 (2015).

24. McCoy, M. Hot Market For A Cool Chemical. *Chem. Eng. News* **88,** 15–16 (2010).

25. Kayser, O. & Averesch, N. *Technische Biochemie: Die Biochemie und industrielle Nutzung von Naturstoffen*. (Springer Spektrum, 2015).

26. Marienhagen, J. & Bott, M. Metabolic engineering of microorganisms for the synthesis of plant natural products. *J. Biotechnol.* **163,** 166–178 (2013).

27. O'Connor, S. E. *Methods in Enzymology - Synthetic Biology and Metabolic Engineering in Plants and Microbes Part A: Metabolism in Microbes*. (Zoe Kruze, Elsevier, 2016).

28. Toogood, H. S. *et al.* Enzymatic Menthol Production: One-Pot Approach Using Engineered *Escherichia coli*. *ACS Synth. Biol.* **4,** 1112–1123 (2015).

29. Currin, A. *et al.* Engineering the 'Missing Link' in Biosynthetic (–)-Menthol Production: Bacterial Isopulegone Isomerase. *ACS Catal.* **8,** 2012–2020 (2018).

30. Lokotsch, W., Fritsche, K. & Syldatk, C. Resolution of D,L-menthol by interesterification with triacetin using the free and immobilized lipase of *Candida cylindracea*. *Appl. Microbiol.* **31,** 467–472 (1989).

31. Vorlová, S. *et al.* Enantioselective Hydrolysis of D,L-Menthyl Benzoate to L-(-)-Menthol by Recombinant *Candida rugosa* Lipase LIP1. *Adv. Synth. Catal.* **344,** 1152–1155 (2002).

32. Trasarti, A. F., Marchi, A. J. & Apesteguía, C. R. Highly selective synthesis of menthols from citral in a one-step process. *J. Catal.* **224,** 484–488 (2004).

33. Mäki-Arvela, P. *et al.* One-pot citral transformation to menthol over bifunctional micro- and mesoporous metal modified catalysts: Effect of catalyst support and metal. *J. Mol. Catal. A Chem.* **240,** 72–81 (2005).

34. Trasarti, A. F., Marchi, A. J. & Apesteguía, C. R. Design of catalyst systems for the one-pot synthesis of menthols from citral. *J. Catal.* **247,** 155–165 (2007).

35. Plößer, J., Dedeaga, F., Lucas, M. & Claus, P. The effect of catalyst preparation conditions on the synthesis of menthol from citronellal on Ru/H-BEA. *Appl. Catal., A* **516,** 100–108 (2016).

36. Leffingwell, J. & Leffingwell, D. Chiral chemistry in flavours & fragrances. *Spec. Chem. Mag.* **3,** 30–33 (2011).

37. Fleischer, J., Bauer, K. & Hopp, R. Verfahren zur Abtrennung von optisch reinem D- und L-menthol. *DE2109456B2* (1971).

38. Noyori, R. *Les Prix Nobel. The Nobel Prizes 2001*. (Nobel Foundation, 2002).

39. Pophof, B., Stange, G. & Abrell, L. Volatile Organic Compounds as Signals in a

Plant-Herbivore System: Electrophysiological Responses in Olfactory Sensilla of the Moth *Cactoblastis Cactorum*. *Chem. Senses* **30,** 51–68 (2005).

40. Blöde, K. A. *Lehrbuch der Chemie - übersetzt nach der zweiten schwedischen Originalausgabe von J. Jakob Berzelius*. (J. J. Mäcken'sche Buchhandlung, 1821).
41. Beach, C. B. & McMurry, F. M. *The New Student's Reference Work - Volume II*. (F. E. Compton and Company, 1914).
42. Silberberg, M. S. *Chemistry: The Molecular Nature of Matter and Change*. (McGraw-Hill Education, 2015).
43. Marques, A. M. & Kaplan, M. A. C. Preparative isolation and characterization of monoterpene isomers present in the citral-rich essential oil of *Pectis brevipedunculata*. *J. Essent. Oil Res.* **25,** 210–215 (2013).
44. Jäkel, C. & Paciello, R. The Asymmetric Hydrogenation of enones - Access to a New L-Menthol Synthesis. in *Asymmetric Catalysis on Industrial Scale: Challenges, Approaches and Solutions* (eds. Blaser, H.-U. & Federesel, H.-J.) (WILEY-VCH Verlag GmbH & Co. KGaA, 2010).
45. Schäfer, B. *Natural Products in the Chemical Industry*. (Springer-Verlag, 2014). doi:10.1007/978-642-54461-3
46. Cunningham, A. D., Ham, E. Y. & Vosburg, D. A. Chemoselective Reactions of Citral: Green Syntheses of Natural Perfumes for the Undergraduate Organic Laboratory. *J. Chem. Educ.* **88,** 322–324 (2011).
47. Stolle, A., Gallert, T., Schmöger, C. & Ondruschka, B. Hydrogenation of citral: a wide-spread model reaction for selective reduction of α,β-unsaturated aldehydes. *RSC Adv.* **3,** 2112–2153 (2013).
48. Jäkel, C. & Paciello, R. Method for the production of optically active carbonyl. *US7534921B2* (2009).
49. Miyashita, A. *et al.* Synthesis of 2,2'-Bis(diphenylphosphino)-1,1'-binaphthyl (BINAP), an Atropisomeric Chiral Bis(triaryl)phosphine, and Its Use in the Rhodium(I)-Catalyzed Asymmetric Hydrogenation of α-(Acylamino)acrylic Acids. *JACS* **102,** 7932–7934 (1980).
50. Lipshutz, B. H. & Servesko, J. M. CuH-Catalyzed Asymmetric Conjugate Reductions of Acyclic Enones. *Angew. Chem. Int. Ed.* **42,** 4789–4792 (2003).
51. Dang, T.-P., Aviron-Violet, P., Colleuille, Y. & Varagnat, J. Catalyse d'hydrogenation en phase homogene des aldehydes α-β insatures. Application a la synthese asymetrique du citronellal. *J. Mol. Catal.* **16,** 51–59 (1982).
52. Chapuis, C., Barthe, M. & Laumer, J.-Y. de Saint. Synthesis of Citronellal by RhI-Catalysed Asymmetric Isomerization of N,N-Diethyl- Substituted Geranyl and Nerylamines or Geraniol and Nerol in the Presence of Chiral Diphosphino Ligands, under Homogeneous and Supported Conditions. *Helv. Chim. Acta* **84,** 230–242 (2001).
53. Maeda, H., Yamada, S., Itoh, H. & Hori, Y. A dual catalyst system provides the shortest pathway for L-menthol synthesis. *Chem. Commun.* **48,** 1772 (2012).
54. Toogood, H. S., Gardiner, J. M. & Scrutton, N. S. Biocatalytic Reductions and Chemical Versatility of the Old Yellow Enzyme Family of Flavoprotein Oxidoreductases. *ChemCatChem* **2,** 892–914 (2010).

55. Durchschein, K., Hall, M. & Faber, K. Unusual Reactions Mediated by FMN-Dependent Ene- and Nitro-Reductases. *Green Chem.* **15,** 1764–1772 (2013).

56. Scholtissek, A., Tischler, D., Westphal, A. H., van Berkel, W. J. H. & Paul, C. E. Old Yellow Enzyme-Catalysed Asymmetric Hydrogenation: Linking Family Roots with Improved Catalysis. *Catalysts* **7,** 130 (2017).

57. Brown, G., Moody, T. S., Smyth, M. & Taylor, S. J. C. Almac: An Industrial Perspective of Ene Reductase (ERED) Biocatalysis. in *Biocatalysis: An Industrial Perspective* 229–256 (CPI Group (UK) Ltd, 2017).

58. Swiderska, M. A. & Stewart, J. D. Stereoselective enone reductions by *Saccharomyces carlsbergensis* old yellow enzyme. *J. Mol. Catal. B Enzym.* **42,** 52–54 (2006).

59. Müller, A., Stürmer, R., Hauer, B. & Rosche, B. Stereospecific Alkyne Reduction: Novel Activity of Old Yellow Enzymes. *Angew. Chem. Int. Ed.* **46,** 3316–8 (2007).

60. French, C. E., Nicklin, S. & Bruce, N. C. Aerobic Degradation of 2,4,6-Trinitrotoluene by *Enterobacter cloacae* PB2 and by Pentaerythritol Tetranitrate Reductase. *Appl. Environ. Microbiol.* **64,** 2864–2868 (1998).

61. Durchschein, K. *et al.* Unusual C=C Bond Isomerization of an α,β-Unsaturated γ-Butyrolactone Catalysed by Flavoproteins from the Old Yellow Enzyme Family. *ChemBioChem* **13,** 2346–2351 (2012).

62. Mueller, N. J., Stueckler, C., Hall, M., Macheroux, P. & Faber, K. Epoxidation of conjugated C=C-bonds and sulfur-oxidation of thioethers mediated by NADH:FMN-dependent oxidoreductases. *Org. Biomol. Chem.* **7,** 1115–1119 (2009).

63. Weitz, E. & Scheffer, A. Über die Einwirkung von alkalischem Wasserstoffsuperoxyd auf ungesättigte Verbindungen. *Berichte der Dtsch. Chem. Gesellschaft (A B Ser.*) **54,** 2327–2344 (1921).

64. Mangan, D., Miskelly, I. & Moody, T. S. A Three-Enzyme System Involving an Ene-Reductase for Generating Valuable Chiral Building Blocks. *Adv. Synth. Catal.* **354,** 2185–2190 (2012).

65. Fox, K. M. & Karplus, P. A. Old Yellow Enzyme at 2-Angstrom Resolution - Overall Structure, Ligand-Binding, and Comparison with Related Flavoproteins. *Structure* **2,** 1089–1105 (1994).

66. Williams, R. E. & Bruce, N. C. 'New uses for an Old Enzyme' – the Old Yellow Enzyme family of flavoenzymes. *Microb.* **148,** 1607–1614 (2002).

67. Warburg, O. & Christian, W. Ein zweites sauerstoffübertragendes Ferment und sein Absorptionsspektrum. *Naturwissenschaften* **20,** 688 (1932).

68. Haas, E. Isolierung eines neuen gelben Ferments. *Biochem. Z.* **298,** 378–390 (1938).

69. Stott, K., Saito, K., Thiele, D. J. & Massey, V. Old Yellow Enzyme - The Discovery of Multiple Isozymes and a Family of Related Proteins. *J. Biol. Chem.* **268,** 6097–6106 (1993).

70. Fischer, F. G. & Wiedemann, O. Über die Hydrierung ungesättigter α-Ketosäuren, Aldehyde und Alkohole durch gärende Hefe. *Ann. der Chemie* **513,** 260–280 (1934).

71. Reich, S., Kress, N., Nestl, B. M. & Hauer, B. Variations in the stability of NCR ene reductase by rational enzyme loop modulation. *J. Struct. Biol.* **185,** 228–233 (2014).

72. Reich, S. Studies on variable surface loop regions of the ene reductase NCR from *Zymomonas mobilis*. *PhD thesis* (University of Stuttgart, 2014).

73. Reich, S., Nestl, B. M. & Hauer, B. Loop-Grafted Old Yellow Enzymes in the Bienzymatic Cascade Reduction of Allylic Alcohols. *ChemBioChem* **17,** 561–565 (2016).

74. Kreß, N. Loop Grafting Studies on Old Yellow Enzymes. *Master thesis* (University of Stuttgart, 2014).

75. Xu, D., Kohli, R. M. & Massey, V. The role of threonine 37 in flavin reactivity of the old yellow enzyme. *Proc. Natl. Acad. Sci.* **96,** 3556–3561 (1999).

76. Messiha, H. L., Munro, A. W., Bruce, N. C., Barsukov, I. & Scrutton, N. S. Reaction of Morphinone Reductase with 2-Cyclohexen-1-one and 1-Nitrocyclohexene. *J. Biol. Chem.* **280,** 10695–10709 (2005).

77. Kohli, R. M. & Massey, V. The Oxidative Half-reaction of Old Yellow Enzyme. *J. Biol. Chem.* **273,** 32763–32770 (1998).

78. Brown, B. J., Deng, Z., Karplus, P. A. & Massey, V. On the Active Site of Old Yellow Enzyme - Role of Histidine 192 and Asparagine 194. *Biochemistry* **273,** 32753–32762 (1998).

79. Amato, E. D. & Stewart, J. D. Applications of protein engineering to members of the old yellow enzyme family. *Biotechnol. Adv.* **33,** 624–631 (2015).

80. Opperman, D. J. *et al.* Crystal structure of a thermostable Old Yellow Enzyme from *Thermus scotoductus* SA-01. *Biochem. Biophys. Res. Commun.* **393,** 426–431 (2010).

81. Reich, S., Hoeffken, W., Rosche, B., Nestl, B. M. & Hauer, B. Crystal Structure Determination and Mutagenesis Analysis of the Ene Reductase NCR. *ChemBioChem* **13,** 2400–2407 (2012).

82. Basran, J., Harris, R. J., Sutcliffe, M. J. & Scrutton, N. S. H-tunneling in the Multiple H-transfers of the Catalytic Cycle of Morphinone Reductase and in the Reductive Half-reaction of the Homologous Pentaerythritol Tetranitrate Reductase. *J. Biol. Chem.* **278,** 43973–43982 (2003).

83. Pang, J., Hay, S., Scrutton, N. S. & Sutcliffe, M. J. Deep tunneling dominates the biologically important hydride transfer reaction from NADH to FMN in morphinone reductase. *JACS* **130,** 7092–7097 (2008).

84. Meisner, J. & Kästner, J. Atom Tunneling in Chemistry. *Angew. Chem. Int. Ed.* **55,** 5400–5413 (2016).

85. Müller, A., Hauer, B. & Rosche, B. Asymmetric Alkene Reduction by Yeast Old Yellow Enzymes and by a Novel *Zymomonas mobilis* Reductase. *Biotechnol. Bioeng.* **98,** 22–29 (2007).

86. Hall, M. *et al.* Asymmetric Bioreduction of C=C Bonds using Enoate Reductases OPR1, OPR3 and YqjM: Enzyme-Based Stereocontrol. *Adv. Synth. Catal.* **350,** 411–418 (2008).

87. Mueller, N. J. *et al.* The Substrate Spectra of Pentaerythritol Tetranitrate Reductase, Morphinone Reductase, N-Ethylmaleimide Reductase and Estrogen-

Binding Protein in the Asymmetric Bioreduction of Activated Alkenes. *Adv. Synth. Catal.* **352,** 387–394 (2010).

88. Bougioukou, D. J., Walton, A. Z. & Stewart, J. D. Towards preparative-scale, biocatalytic alkene reductions. *Chem. Commun.* **46,** 8558–60 (2010).

89. Müller, A., Hauer, B. & Rosche, B. Enzymatic reduction of the α,β-unsaturated carbon bond in citral. *J. Mol. Catal. B Enzym.* **38,** 126–130 (2006).

90. Richter, N., Gröger, H. & Hummel, W. Asymmetric reduction of activated alkenes using an enoate reductase from *Gluconobacter oxydans*. *Appl. Microbiol. Biotechnol.* **89,** 79–89 (2011).

91. Yanto, Y. *et al.* Asymmetric Bioreduction of Alkenes Using Ene-Reductases YersER and KYE1 and Effects of Organic Solvents. *Org. Lett.* **13,** 2540–2543 (2011).

92. Sheng, X., Yan, M., Xu, L. & Wei, M. Identification and characterization of a novel Old Yellow Enzyme from *Bacillus subtilis* str.168. *J. Mol. Catal. B Enzym.* **130,** 18–24 (2016).

93. Adalbjörnsson, B. V. *et al.* Biocatalysis with Thermostable Enzymes: Structure and Properties of a Thermophilic 'ene'-Reductase related to Old Yellow Enzyme. *ChemBioChem* **11,** 197–207 (2010).

94. Wolken, W. A. M., ten Have, R. & van der Werf, M. J. Amino Acid-Catalyzed Conversion of Citral: cis-trans Isomerization and Its Conversion into 6-Methyl-5-hepten-2-one and Acetaldehyde. *J. Agric. Food Chem.* **48,** 5401–5405 (2000).

95. Reetz, M. T., Kahakeaw, D. & Lohmer, R. Addressing the Numbers Problem in Directed Evolution. *ChemBioChem* **9,** 1797–1804 (2008).

96. Bornscheuer, U. T. & Pohl, M. Improved biocatalysys by directed evolution and rational protein design. *Biocatal. Biotransformation.* **5,** 137–143 (2001).

97. Davids, T., Schmidt, M., Böttcher, D. & Bornscheuer, U. T. Strategies for the discovery and engineering of enzymes for biocatalysis. *Curr. Opin. Chem. Biol.* **17,** 215–220 (2013).

98. Arnold, F. H. Design by Directed Evolution. *Acc. Chem. Res.* **31,** 125–131 (1998).

99. Miton, C. M. & Tokuriki, N. How mutational epistasis impairs predictability in protein evolution and design. *Protein Sci.* **25,** 1260–1272 (2016).

100. Chica, R. A., Doucet, N. & Pelletier, J. N. Semi-rational approaches to engineering enzyme activity: Combining the benefits of directed evolution and rational design. *Curr. Opin. Biotechnol.* **16,** 378–384 (2005).

101. Reetz, M. T. & Carballeira, J. D. Iterative saturation mutagenesis (ISM) for rapid directed evolution of functional enzymes. *Nat. Protoc.* **2,** 891–903 (2007).

102. Sun, Z. *et al.* Reshaping an Enzyme Binding Pocket for Enhanced and Inverted Stereoselectivity: Use of Smallest Amino Acid Alphabets in Directed Evolution. *Angew. Chem. Int. Ed.* **54,** 12410–12415 (2015).

103. Reetz, M. T. An Overview of High-Throughput Screening Systems for Enantioselective Enzymatic Transformations. in *Directed Enzyme Evolution - Screening and Selection Methods* (eds. Arnold, F. H. & Georgiou, G.) 259–282 (Humana Press, 2003).

104. Acevedo-Rocha, C. G., Agudo, R. & Reetz, M. T. Directed evolution of

stereoselective enzymes based on genetic selection as opposed to screening systems. *J. Biotechnol.* **191,** 3–10 (2014).

105. Reetz, M. T. Gerichtete Evolution stereoselektiver Enzyme : Eine ergiebige Katalysator-Quelle für asymmetrische Reaktionen Angewandte. *Angew. Chem.* **123,** 144–182 (2011).
106. Bougioukou, D. J., Kille, S., Taglieber, A. & Reetz, M. T. Directed Evolution of an Enantioselective Enoate-Reductase : Testing the Utility of Iterative Saturation Mutagenesis. *Adv. Synth. Catal.* **351,** 3287–3305 (2009).
107. Walton, A. Z., Sullivan, B., Patterson-Orazem, A. C. & Stewart, J. D. Residues Controlling Facial Selectivity in an Alkene Reductase and Semirational Alterations to Create Stereocomplementary Variants. *ACS Catal.* **4,** 2307–2318 (2014).
108. Romero-Rivera, A., Garcia-Borràs, M. & Osuna, S. Computational tools for the evaluation of laboratory-engineered biocatalysts. *Chem. Commun.* **53,** 284–297 (2017).
109. Huang, P.-S., Boyken, S. E. & Baker, D. The coming of age of *de novo* protein design. *Nature* **537,** 320–327 (2016).
110. Yunta, M. J. R. Docking and Ligand Binding Affinity: Uses and Pitfalls. *Am. J. Model. Optim.* **4,** 74–114 (2016).
111. Rester, U. Dock around the Clock - Current Status of Small Molecule Docking and Scoring. *QSAR Comb. Sci.* **25,** 605–615 (2006).
112. Werner, H.-J. & Kästner, J. *An Introduction to Computational Chemistry*. (University of Stuttgart, 2013).
113. Meng, X.-Y., Zhang, H.-X., Mezei, M. & Cui, M. Molecular Docking: A powerful approach for structure-based drug discovery. *Curr. Comput. Aided Drug Des.* **7,** 146–157 (2011).
114. Osuna, S., Jiménez-Osés, G., Noey, E. L. & Houk, K. N. Molecular Dynamics Explorations of Active Site Structure in Designed and Evolved Enzymes. *Acc. Chem. Res.* **48,** 1080–1089 (2015).
115. Stewart, J. J. P. Optimization of parameters for semiempirical methods VI: More modifications to the NDDO approximations and re-optimization of parameters. *J. Mol. Model.* **19,** 1–32 (2013).
116. Hoshino, T. & Sato, T. Squalene–hopene cyclase: catalytic mechanism and substrate recognition. *Chem. Commun.* 291–301 (2002). doi:10.1039/b108995c
117. Bastian, S. A., Hammer, S. C., Kreß, N., Nestl, B. M. & Hauer, B. Selectivity in the Cyclization of Citronellal Introduced by Squalene Hopene Cyclase Variants. *ChemCatChem* **9,** 4364–4368 (2017).
118. Wendt, K. U., Poralla, K. & Schulz, G. E. Structure and Function of a Squalene Cyclase. *Science* **277,** 1811–1815 (1997).
119. Wendt, K. U., Schulz, G. E., Corey, E. J. & Liu, D. R. Enzyme Mechanisms for Polycyclic Triterpene Formation. *Angew. Chem. Int. Ed.* **39,** 2812–2833 (2000).
120. Wendt, K. U. Enzyme Mechanisms for Triterpene Cyclization: New Pieces of the Puzzle. *Angewandte Chemie - International Edition* **44,** 3966–3971 (2005).
121. Gao, Y., Honzatko, R. B. & Peters, R. J. Terpenoid synthase structures: a so far incomplete view of complex catalysis. *Nat. Prod. Rep.* **29,** 1153 (2012).

122. Siedenburg, G. *et al.* Activation-Independent Cyclization of Monoterpenoids. *Appl. Environ. Microbiol.* **78,** 1055–1062 (2012).

123. Siedenburg, G. & Breuer, M. Prokaryotic squalene-hopene cyclases can be converted to citronellal cyclases by single amino acid exchange. *Appl. Microbiol. Biotechnol.* **97,** 1571–1580 (2013).

124. Hammer, S. C., Marjanovic, A., Dominicus, J. M., Nestl, B. M. & Hauer, B. Squalene hopene cyclases are protonases for stereoselective Brønsted acid catalysis. *Nat. Chem. Biol.* **11,** 121–126 (2015).

125. Seitz, M., Nestl, B. M., Hammer, S. C., Syrén, P.-O. & Hauer, B. Squalene hopene cyclases : highly promiscuous and evolvable catalysts for stereoselective C–C and C–X bond formation. *Curr. Opin. Chem. Biol.* **17,** 293–300 (2013).

126. Seitz, M. *et al.* Synthesis of Heterocyclic Terpenoids by Promiscuous Squalene-Hopene Cyclases. *ChemBioChem* **14,** 436–439 (2013).

127. Syrén, P. O., Henche, S., Eichler, A., Nestl, B. M. & Hauer, B. Squalene-hopene cyclases - evolution, dynamics and catalytic scope. *Curr. Opin. Struct. Biol.* **41,** 73–82 (2016).

128. Hammer, S. C. Zur Anwendbarkeit von Squalen-Hopen-Zyklasen als chirale Brønsted-Säuren in der asymmetrischen Katalyse. *PhD thesis* (University of Stuttgart, 2014).

129. Bastian, S. Stereoselektive enzymatische Brønsted-Säure-Katalyse unter Verwendung einer Squalen-Hopen-Cyclase. *PhD thesis* (University of Stuttgart, 2016).

130. Racolta, S., Juhl, P. B., Sirim, D. & Pleiss, J. The triterpene cyclase protein family: A systematic analysis. *Proteins Struct. Funct. Bioinforma.* **80,** 2009–2019 (2012).

131. Christianson, D. W. Structural and Chemical Biology of Terpenoid Cyclases. *Chem. Rev.* **117,** 11570–11648 (2017).

132. Gandour, R. D. On the Importance of Orientation in General Base Catalysis by Carboxylate. *Bioorg. Chem.* **10,** 169–176 (1981).

133. Vandichel, M. *et al.* Insight in the activity and diastereoselectivity of various Lewis acid catalysts for the citronellal cyclization. *J. Catal.* **305,** 118–129 (2013).

134. Dreimann, J., Vorholt, A. J., Skiborowski, M. & Behr, A. Removal of Homogeneous Precious Metal Catalysts via Organic Solvent Nanofiltration. *Chem. Eng. Trans.* **47,** 343–348 (2016).

135. da Silva, K. A. *et al.* Cyclization of (+)-citronellal to (-)-isopulegol catalyzed by $H_3PW_{12}O_{40}/SiO_2$. *Catal. Commun.* **5,** 425–429 (2004).

136. Hart-Cooper, W. M., Clary, K. N., Toste, F. D., Bergman, R. G. & Raymond, K. N. Selective Monoterpene-like Cyclization Reactions Achieved by Water Exclusion from Reactive Intermediates in a Supramolecular Catalyst. *JACS* **134,** 17873–17876 (2012).

137. Sigrist, R., Costa, B. Z. da, Marsaioli, A. J. & de Oliveira, L. G. Nature-inspired enzymatic cascades to build valuable compounds. *Biotechnol. Adv.* **33,** 394–411 (2015).

138. Sperl, J. M. & Sieber, V. Multienzyme Cascade Reactions—Status and Recent Advances. *ACS Catal.* **8,** 2385–2396 (2018).

139. Schrittwieser, J. H., Velikogne, S., Hall, M. & Kroutil, W. Artificial Biocatalytic Linear Cascades for Preparation of Organic Molecules. *Chem. Rev.* **118,** 270–348 (2018).

140. Peters, C. *et al.* Identification, Characterization, and Application of Three Enoate Reductases from *Pseudomonas putida* in *In Vitro* Enzyme Cascade Reactions. *ChemCatChem* **6,** 1021–1027 (2014).

141. Oberleitner, N. *et al.* An Enzymatic Toolbox for Cascade Reactions: A Showcase for an *In Vivo* Redox Sequence in Asymmetric Synthesis. *ChemCatChem* **5,** 3524–3528 (2013).

142. France, S. P., Hepworth, L. J., Turner, N. J. & Flitsch, S. L. Constructing Biocatalytic Cascades: *In Vitro* and *in Vivo* Approaches to *de Novo* Multi-Enzyme Pathways. *ACS Catal.* **7,** 710–724 (2017).

143. Liu, W. & Wang, P. Cofactor regeneration for sustainable enzymatic biosynthesis. *Biotechnol. Adv.* **25,** 369–384 (2007).

144. Gröger, H. & Hummel, W. Combining the 'two worlds' of chemocatalysis and biocatalysis towards multi-step one-pot processes in aqueous media. *Curr. Opin. Chem. Biol.* **19,** 171–179 (2014).

145. Makkee, M., Kieboom, A. P. G., Van Bekkum, H. & Roels, J. A. Combined Action of Enzyme and Metal Catalyst, applied to the Preparation of D-Mannitol. *J. Chem. Soc. Chem. Commun.* 930–931 (1980). doi:10.1039/c39800000930

146. Kraußer, M. *et al.* Combination of C=C Bond Formation by Wittig Reaction and Enzymatic C=C Bond Reduction in a One-Pot Process in Water. *ChemCatChem* **3,** 293–296 (2011).

147. Denard, C. A. *et al.* Development of a One-Pot Tandem Reaction Combining Ruthenium-Catalyzed Alkene Metathesis and Enantioselective Enzymatic Oxidation To Produce Aryl Epoxides. *ACS Catal.* **5,** 3817–3822 (2015).

148. Dehli, F. Vergleichende Mutagenese in OYE1 und NCR En-Reduktase. *Bachelor thesis* (University of Stuttgart, 2016).

149. Green, M. R. & Sambrook, J. *Molecular cloning - A Laboratory Manual*. *Zool. Res.* **33,** (Cold Spring Harbor Laboratory Press, 2012).

150. Pugh, S., McKenna, R., Halloum, I. & Nielsen, D. R. Engineering *Escherichia coli* for renewable benzyl alcohol production. *Metab. Eng. Commun.* **2,** 39–45 (2015).

151. Stumpp, T., Wilms, B. & Altenbuchner, J. Ein neues, L-Rhamnose-induzierbares Expressionssystem. *BioSpektrum* **1,** 33–36 (2000).

152. Stürmer, D. R., Hauer, P. D. B., Rosche, D. B. & Müller, A. Verfahren zur enzymatischen Reduktion von Alkinderivaten. *EP1894999A1* (2008).

153. Bradford, M. M. A Rapid and Sensitive Method for the Quantitation Microgram Quantities of Protein Utilizing the Principle of Protein-Dye Binding. *Anal. Biochem.* **72,** 248–254 (1976).

154. Kwan, E. E. & Huang, S. G. Structural Elucidation with NMR Spectroscopy: Practical Strategies for Organic Chemists. *Eur. J. Org. Chem.* **2008,** 2671–2688 (2008).

155. Krieger, E. & Vriend, G. YASARA View - molecular graphics for all devices - from smartphones to workstations. *Bioinformatics* **30,** 2981–2982 (2014).

156. Pollard, D. J. & Woodley, J. M. Biocatalysis for pharmaceutical intermediates: the future is now. *Trends Biotechnol.* **25,** 66–73 (2007).

157. Theorell, H., Yagi, K., Ludwig, G. D. & Egami, F. Effect of Flavin Monosulphate on Old Yellow Enzyme. *Nature* **180,** 922–923 (1957).

158. Cronan, J. E. *Escherichia coli as an Experimental Organism*. (WILEY-VCH, 2014). doi:10.1002/9780470015902.a0002026.pub2

159. Kitzing, K. *et al.* The 1.3 Å Crystal Structure of the Flavoprotein YqjM Reveals a Novel Class of Old Yellow Enzymes. *J. Biol. Chem.* **280,** 27904–27913 (2005).

160. Kohli, R. M. & Massey, V. The Oxidative Half-reaction of Old Yellow Enzyme. *Am. Soc. Biochem. Mol. Biol.* **273,** 32763–32770 (1998).

161. Esque, J., Oguey, C. & de Brevern, A. G. A Novel Evaluation of Residue and Protein Volumes by Means of Laguerre Tessellation. *J. Chem. Inf. Model.* **50,** 947–960 (2010).

162. Scheps, D. *et al.* Synthesis of ω-hydroxy dodecanoic acid based on an engineered CYP153A fusion construct. *Microb. Biotechnol.* **6,** 694–707 (2013).

163. Anthony, C. & Zatman, L. J. The Microbial Oxidation of Methanol. *Biochem J* **96,** 808–812 (1965).

164. Magonet, E., Hayen, P., Delforge, D., Delaive, E. & Remacle, J. Importance of the structural zinc atom for the stability of yeast alcohol dehydrogenase. *Biochem. J.* **287,** 361–5 (1992).

165. Chinnawirotpisan, P. *et al.* Purification and Characterization of Two NAD-Dependent Alcohol Dehydrogenases (ADHs) Induced in the Quinoprotein ADH-Deficient Mutant of *Acetobacter pasteurianus* SKU1108. *Biosci. Biotechnol. Biochem.* **67,** 958–965 (2003).

166. Dower, W. J., Miller, J. F. & Ragsdale, C. W. High efficiency transformation of E. coli by high voltage electroporation. *Nucleic Acids Res.* **16,** 6127–45 (1988).

167. Reetz, M. T., Prasad, S., Carballeira, J. D., Gumulya, Y. & Bocola, M. Iterative Saturation Mutagenesis Accelerates Evolution of Enzyme Stereoselectivity : Rigorous Comparison with Traditional Methods. *JACS* **132,** 9144–9152 (2010).

168. Peter, K., Vollhardt, C. & Schore, N. E. *Organische Chemie*. (WILEY-VCH, 2011).

169. Grogan, G. Biotransformations. *Annu. Rep. Prog. Chem. Sect. B: Org. Chem.* **105,** 206–231 (2009).

170. Schmid, A. *et al.* Industrial biocatalysis today and tomorrow. *Nature* **409,** 258–259 (2001).

171. Toogood, H. S. & Scrutton, N. S. Enzyme engineering toolbox – a ‘catalyst’ for change. *Catal. Sci. Technol.* **3,** 2182 (2013).

172. Bommarius, A. S., Blum, J. K. & Abrahamson, M. J. Status of protein engineering for biocatalysts: how to design an industrially useful biocatalyst. *Curr. Opin. Chem. Biol.* **15,** 194–200 (2011).

173. Atkins, P. & de Paula, J. *Physical chemistry, 8th edition*. (Oxford University Press, 2006).

174. Straßner, J., Fürholz, A., Macheroux, P., Amrhein, N. & Schaller, A. A Homolog of Old Yellow Enzyme in Tomato. *J. Biol. Chem.* **274,** 35067–35073 (1999).

175. Campbell, M. K. & Farrell, S. O. Amino Acids and Peptides. in *Biochemistry* 70 (Cengage Learning, 2012).

176. Brenna, E., Gatti, F. G., Monti, D., Parmeggiani, F. & Serra, S. Stereochemical Outcome of the Biocatalysed Reduction of Activated Tetrasubstituted Olefins by Old Yellow Enzymes 1–3. *Adv. Synth. Catal.* **354,** 105–112 (2012).

177. Lonsdale, R. & Reetz, M. T. Reduction of α,β-Unsaturated Ketones by Old Yellow Enzymes: Mechanistic Insights from Quantum Mechanics/Molecular Mechanics Calculations. *JACS* **137,** 14733–14742 (2015).

178. Padhi, S. K., Bougioukou, D. J. & Stewart, J. D. Site-Saturation Mutagenesis of Tryptophan 116 of *Saccharomyces pastorianus* Old Yellow Enzyme Uncovers Stereocomplementary Variants. *JACS* **131,** 3271–3280 (2009).

179. Classen, T., Pietruszka, J. & Schuback, S. M. Revisiting the Enantioselective Sequence Patterns in Enoate Reductases. *ChemCatChem* **5,** 711–713 (2013).

180. Oberdorfer, G., Steinkellner, G., Stueckler, C., Faber, K. & Gruber, K. Stereopreferences of Old Yellow Enzymes: Structure Correlations and sequence Patterns in Enoate Reductases. *ChemCatChem* **3,** 1562–1566 (2011).

181. Nett, N., Duewel, S., Richter, A. A. & Hoebenreich, S. Revealing Additional Stereocomplementary Pairs of Old Yellow Enzymes by Rational Transfer of Engineered Residues. *ChemBioChem* **18,** 685–691 (2017).

182. Yin, B., Deng, J., Lim, L., Yuan, Y. A. & Wei, D. Structural insights into stereospecific reduction of α,β-unsaturated carbonyl substrates by old yellow enzyme from *Gluconobacter oxydans*. *Biosci. Biotechnol. Biochem.* **79,** 410–421 (2015).

183. Breithaupt, C. *et al.* Structural Basis of Substrate Specificity of Plant 12-Oxophytodienoate Reductases. *J. Mol. Biol.* **392,** 1266–1277 (2009).

184. Horita, S. *et al.* An Engineered Old Yellow Enzyme that Enables Efficient Synthesis of (4*R*,6*R*)-Actinol in a One-Pot Reduction System. *ChemBioChem* **16,** 440–445 (2015).

185. Nestl, B. M. & Hauer, B. Engineering of Flexible Loops in Enzymes. *ACS Catal.* **4,** 3201–3211 (2014).

186. Toogood, H. S. *et al.* A Site-Saturated Mutagenesis Study of Pentaerythritol Tetranitrate Reductase Reveals that Residues 181 and 184 Influence Ligand Binding, Stereochemistry and Reactivity. *ChemBioChem* **12,** 738–749 (2011).

187. Reil, D. Enzym Engineering der NCR En-Reduktase hinsichtlich der (*R*)-selektiven Reduktion von Citral. *Master thesis* (Universität Stuttgart, 2018).

188. Füll, C. & Poralla, K. Conserved Tyr residues determine functions of Alicyclobacillus acidocaldarius squalene-hopene cyclase. *FEMS Microbiol. Lett.* **183,** 221–224 (2000).

189. O'Neil, M. J. *The Merck index: An encyclopedia of Chemicals, Drugs and Biologicals*. (Merck, 2006).

190. Lister, T. & Renshaw, J. *Understanding Chemistry for Advance Level*. (Stanley Thornes Ltd, 2000).

191. Pubchem. Chemical and Physical Properties of Citronellal. Available at: https://pubchem.ncbi.nlm.nih.gov/compound/citronellal#section=Chemical-and-Physical-Properties. (Accessed: 30th January 2018)

192. Librovitch, B. V., Nowakowski, A. F., Nicolleau, F. C. G. A. & Michelitsch, T. M. Non-equilibrium evaporation/condensation model. *arXiv:1707.01497 [cond-mat, physics:physics]* 1–20 (2017).

193. Giebler, E. & Knechtel, W. Abhängigkeit der Verdunstung aus galvanotechnischen Prozess- und Spüllösungen. *Galvanotech. - Eugen G. Leuze Verlag* **11,** 2630–2869 (2009).

194. Seitz, M. Characterization of the substrate specificity of squalene - hopene cyclases (SHCs). *PhD thesis* (University of Stuttgart, 2012).

195. Halter, W. *et al.* Yield-Analysis of Different Coupling Schemes for Interconnected Bio-Reactors. in *2015 Proceedings of the Conference on Control and its Applications* 384–391 (Society for Industrial and Applied Mathematics, 2015). doi:10.1137/1.9781611974072.53

196. Yamamoto, T. *et al.* Olfactory study on optically active citronellyl derivatives. *Flavour Fragr. J.* **19,** 121–133 (2004).

197. Kreß, N. & Hauer, B. Enzymdiversität als Basis für die Entwicklung artifizieller Biosynthesen. *BioSpektrum* **23,** 836–838 (2017).

198. Zhao, H. & Van Der Donk, W. A. Regeneration of cofactors for use in biocatalysis. *Curr. Opin. Biotechnol.* **14,** 583–589 (2003).

199. Knaus, T. *et al.* Better than Nature: Nicotinamide Biomimetics That Outperform Natural Coenzymes. *JACS* **138,** 1033–1039 (2016).

200. Löw, S. A., Löw, I. M., Weissenborn, M. J. & Hauer, B. Enhanced Ene-Reductase Activity through Alteration of Artificial Nicotinamide Cofactor Substituents. *ChemCatChem* **8,** 911–915 (2016).

201. Carrea, G. Biocatalysis in water-organic solvent two-phase systems. *Trends Biotechnol.* **2,** 102–106 (1984).

202. Sheldon, R. A. & van Pelt, S. Enzyme immobilisation in biocatalysis: why, what and how. *Chem. Soc. Rev.* **42,** 6223–6235 (2013).

203. Li, H., Xiao, W., Xie, P. & Zheng, L. Co-immobilization of enoate reductase with a cofactor-recycling partner enzyme. *Enzyme Microb. Technol.* **109,** 66–73 (2018).

204. Lehmann, M. & Wyss, M. Engineering proteins for thermostability: The use of sequence alignments versus rational design and directed evolution. *Curr. Opin. Biotechnol.* **12,** 371–375 (2001).

205. Swarts, J. W., Kolfschoten, R. C., Jansen, M. C. A. A., Janssen, A. E. M. & Boom, R. M. Effect of diffusion on enzyme activity in a microreactor. *Chem. Eng. J.* **162,** 301–306 (2010).

206. Krühne, U. *et al.* Biocatalytic process development using microfluidic miniaturized systems. *Green Process. Synth.* **3,** 23–31 (2014).

207. Fink, M. J., Schön, M., Rudroff, F., Schnürch, M. & Mihovilovic, M. D. Single Operation Stereoselective Synthesis of Aerangis Lactones: Combining Continuous Flow Hydrogenation and Biocatalysts in a Chemoenzymatic Sequence. *ChemCatChem* **5,** 724–727 (2013).

208. Schmidt, S., Castiglione, K. & Kourist, R. Overcoming the Incompatibility Challenge in Chemoenzymatic and Multi-Catalytic Cascade Reactions. *Chem. - A Eur. J.* **24,** 1755–1768 (2018).

209. Zhang, Y. & Hess, H. Toward Rational Design of High-efficiency Enzyme Cascades. *ACS Catal.* **7,** 6018–6027 (2017).

210. Dvorak, P. *et al.* Maximizing the Efficiency of Multienzyme Process by Stoichiometry Optimization. *ChemBioChem* **15,** 1891–1895 (2014).

211. Demming, R. M., Otte, K. B., Nestl, B. M. & Hauer, B. Optimized Reaction Conditions Enable the Hydration of Non-natural Substrates by the Oleate Hydratase from *Elizabethkingia meningoseptica*. *ChemCatChem* **9,** 758–766 (2017).

212. Fricke, J. *et al.* Designing a fully automated multi-bioreactor plant for fast DoE optimization of pharmaceutical protein production. *Biotechnol. J.* **8,** 738–747 (2013).

213. Li, W. *et al.* The EMBL-EBI bioinformatics web and programmatic tools framework. *Nucleic Acids Res.* **43,** W580–W584 (2015).

214. McWilliam, H. *et al.* Analysis Tool Web Services from the EMBL-EBI. *Nucleic Acids Res.* **41,** 597–600 (2013).

215. Rice, P., Longden, I. & Bleasby, A. EMBOSS: The European Molecular Biology Open Software Suite. *Trends Genet.* **16,** 276–277 (2000).

216. Hao, H., Sun, J. & Dai, J. Dose-dependent behavioral response of the mosquito *Aedes albopictus* to floral odorous compounds. *J. Insect Sci.* **13,** 127 (2013).

Appendix

```
NCR         1 -------------MPSLFDPIRFGAFTAKNRIWMAPLTRGRATR-DHVPT     36
                          ..:||.||:.|.....:|..:.||||.||.. .::|.
OYE1        1 MSFVKDFKPQALGDTNLFKPIKIGNNELLHRAVIPPLTRMRALHPGNIPN     50

NCR        37 EIMA-EYYAQRAS--AGLIISEATGISQEGLGWPYAPGIWSDAQVEAWLP     83
              ...| |||.|||.  ..:||:|...||.:..|:..|||:||:.|:..|..
OYE1       51 RDWAVEYYTQRAQRPGTMIITEGAFISPQAGGYDNAPGVWSEEQMVEWTK    100

NCR        84 ITQAVHDAGGLIFAQLWHMG-RMVPSNVS--GMQPVAPSASQAPGLGHTY    130
              |..|:|:...:.:.|||.:| ...|.|::  |::..:.|.:.........
OYE1      101 IFNAIHEKKSFVWVQLWVLGWAAFPDNLARDGLRYDSASDNVFMDAEQEA    150

NCR       131 DGKKPYDVARALRLDEIPRLLDDYEKAARHALKAGFDGVQIHAANGYLID    180
              ..||..:...:|..|||.:.:.:|.:||::::.||.|||:||:||||::
OYE1      151 KAKKANNPQHSLTKDEIKQYIKEYVQAAKNSIAAGADGVEIHSANGYLLN    200

NCR       181 EFIRDSTNHRHDEYGGAVENRIRLLKDVTERVIATIGKERTAVRLSPNGE    230
              :|:...:|.|.|||||::|||.|...:|.:.::..||.|:..:||||.|.
OYE1      201 QFLDPHSNTRTDEYGGSIENRARFTLEVVDALVEAIGHEKVGLRLSPYGV    250

NCR       231 IQGTVDSHPEQVFIPAAKMLSDLD--------IAFLGMREGAVDGTF---    269
              ..........:....|.:..:|:         :||:.:.|..|...|
OYE1      251 FNSMSGGAETGIVAQYAYVAGELEKRAKAGKRLAFVHLVEPRVTNPFLTE    300

NCR       270 -------GKTDQPKLSPEIRKVFKPPLVLNQDYTFETAQAALDSGVAD--    310
                    |..|      .:..::|.|::  :...|.....:...|.|
OYE1      301 GEGEYEGGSND------FVYSIWKGPVI--RAGNFALHPEVVREEVKDKR    342

NCR       311 -AISFGRPFIGNPDLPRRFFEKAPLTKDVIETWYTQTPKGYTDYPLLGD-    358
               .|.:||.||.|||||..|..:..||.|...:|:|..:..||.|||...:
OYE1      343 TLIGYGRFFISNPDLVDRLEKGLPLNKYDRDTFYQMSAHGYIDYPTYEEA    392

NCR       359 --------

OYE1      393 LKLGWDKK 400
```

Figure Ap. 1: Sequence alignment of NCR and OYE1 ERED. NCR active site residues and their OYE1 sequential analogues subjected to site-directed mutagenesis are highlighted bold red. The genes share a sequence identity of 29.4 % and a sequence similarity of 46.3 %. The pairwise sequence alignment was generated by the EMBOSS needle algorithm as provided online (‘https://www.ebi.ac.uk/Tools/psa/emboss_needle/’) by the European Bioinformatics Institute EMBL-EBI.[213–215]

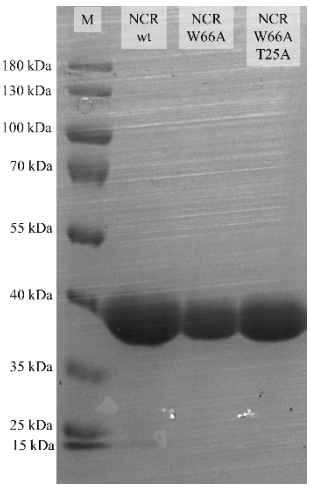

Figure Ap. 2: Exemplary developed SDS-PAGE gel of purified NCR EREDs. After Poly-His_6 tag-based affinity chromatography, NCR EREDs were obtained with a purity of at least > 90 % as indicated by the bands at 40 kDa.

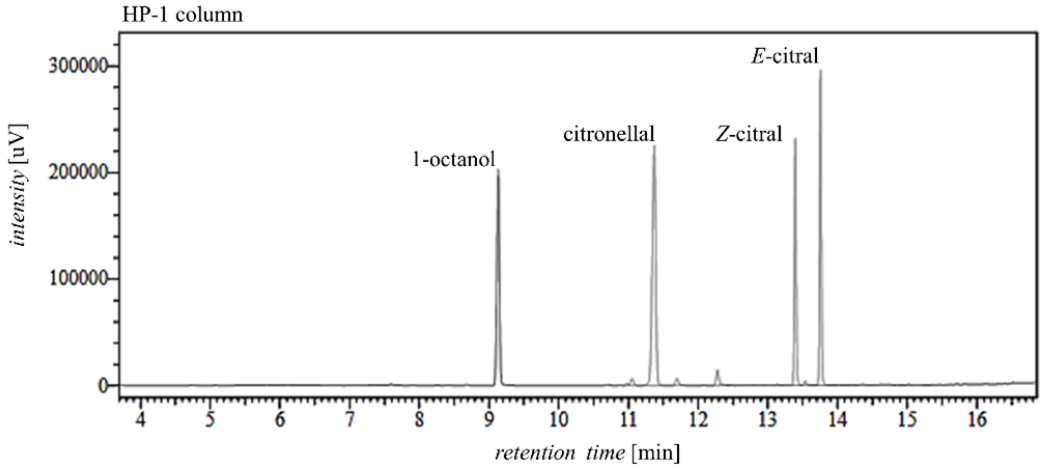

Figure Ap. 3: Gas chromatogram displaying peak positions and retention times for 1-octanol (9.13 min), citronellal (11.37 min), *Z*-citral (13.39 min) and *E*-citral (13.76 min) for achiral measurements on HP-1 column using an FID detector. The related method is described in chapter 2.6.1. Smaller peaks in the background are impurities from the citral samples.

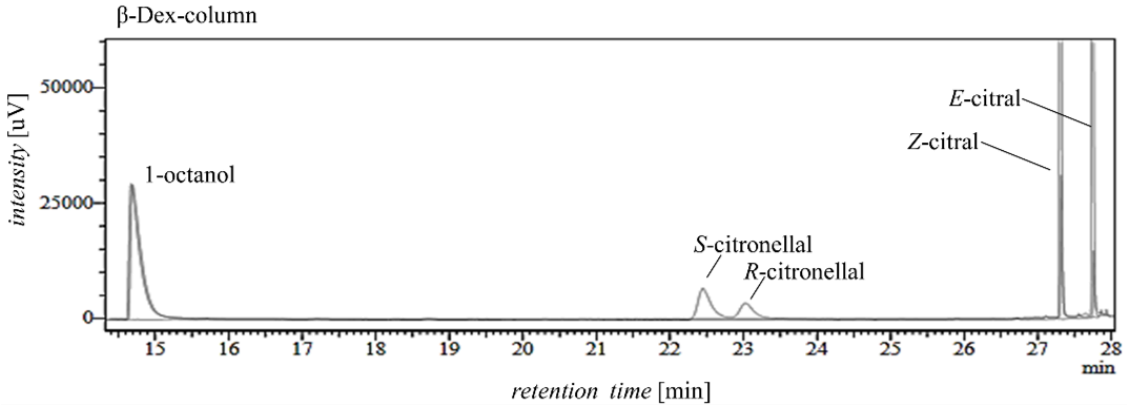

Figure Ap. 4: Gas chromatogram displaying peak positions and retention times for 1-octanol (14.70 min), *S*-citronellal (22.45 min), *R*-citronellal (23.03 min), *Z*-citral (27.31 min) and *E*-citral (27.74 min) for chiral measurements on β-Dex column using an FID detector. The related method is described in chapter 2.6.1. For reasons of clarity, chromatogram was zoomed accordingly, which causes the citral peaks to be partly cut.

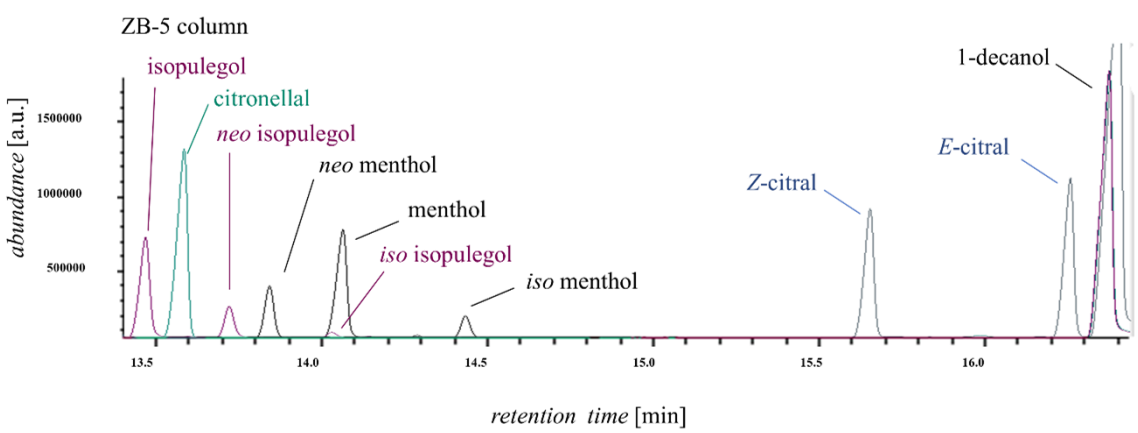

Figure Ap. 5: Gas chromatogram displaying peak positions and retention times for isopulegol (13.48 min), citronellal (13.60 min), *neo* isopulegol (13.73 min), *neo* menthol (13.86 min), *iso* isopulegol (14.04 min), menthol (14.08 min), *iso* menthol (14.44 min), *Z*-citral (15.66 min), *E*-citral (16.26 min) and 1-decanol (16.38 min) for achiral measurements on ZB-5 column using an FID/MS detector. The related method is described in chapter 2.6.1. The overlaid extracted standards are indicated by color, namely isopulegol in magenta, citronellal in green, menthol in black and citral in blue. The mode of zooming does not show *neoiso* isopulegol (14.24 min) and *neoiso* menthol (14.30 min) because except for standards these diastereomers where not formed in any reaction analyzed in this thesis. Menthol and *iso* isopulegol peak overlap was uncritical as chosen enzyme variant for menthol cascade did not form *iso* isopulegol.

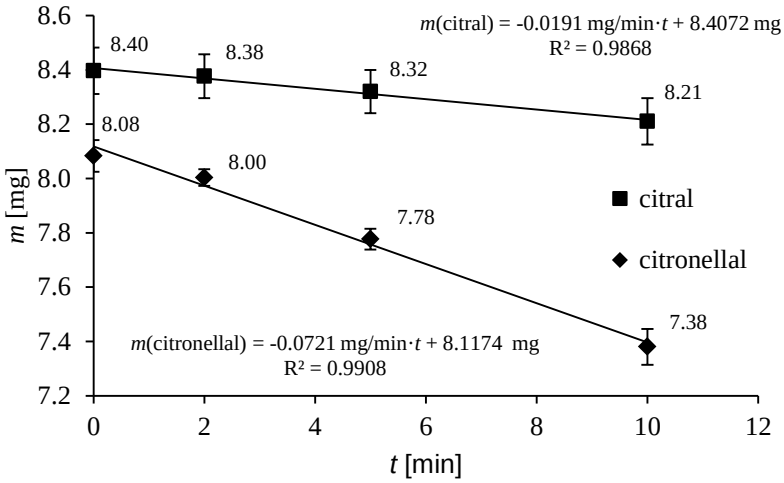

Figure Ap. 6: Evaporation rate comparison of citral and citronellal in an open system. In triplicates, the weight loss of 10 µL citral or citronellal soaked on a filter paper at 25 °C in an open system was followed for 10 min. By linear regression, evaporation rates were calculated. They are shown as the slope of the linear regression. For citral 0.0191 ± 0.0016 mg/min and for citronellal 0.072 ± 0.005 mg/min was calculated. The method was adopted as described elsewhere.[216]

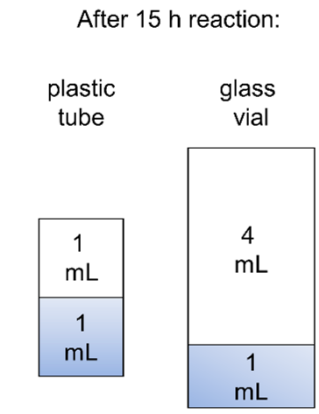

c(citronellal) [mM]	
0.376 ± 0.020	0.093 ± 0.014

Figure Ap. 7: Comparison of NCR ERED-catalyzed reduction of citral in 2 mL plastic tubes and 5 mL glass vial after 15 h. 1 mL reactions using 10 µg/mL NCR wild-type and 2 mL *E*/*Z*-citral were performed in triplicates as described in chapter 2.4.1. The residual citronellal concentration in the liquid was determined. The four-fold gas volume increase correlates to a four-fold citronellal decrease in the liquid.

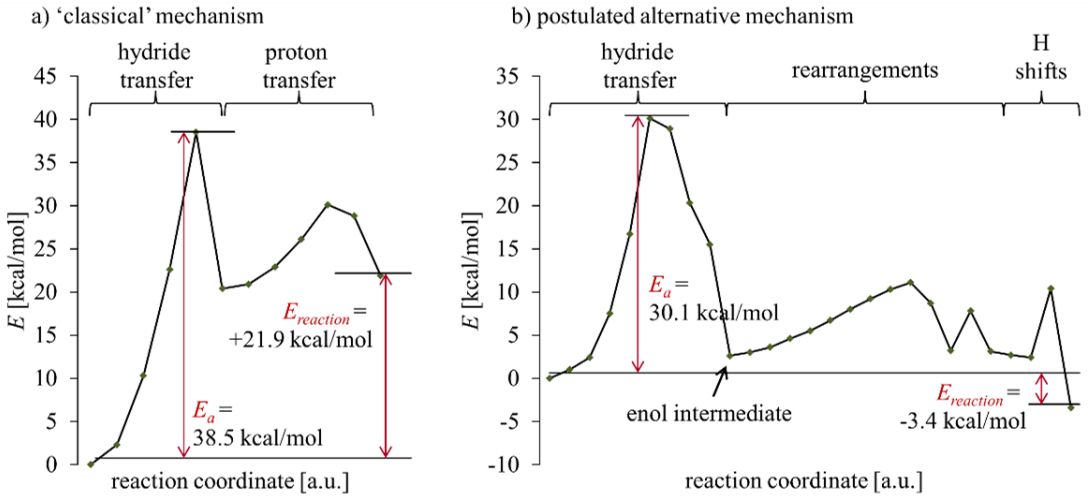

Figure Ap. 8: Calculated reaction pathways for two different assumed mechanisms for the NCR ERED-catalyzed reduction of citral. a) Result for the 'classical' mechanism derived from literature[54,77] involving hydride transfer from an $FMNH^{-1}$ species and concurrent protonation from Y177. The calculated mechanism is endergonic ($E_{reaction}$ = 21.9 kcal/mol) and the activation barrier of the hydride transfer is E_a = 38.5 kcal/mol. b) Result for a postulated alternative mechanism. The hydride transfer is similar but the protonation mechanism differs involving a protonated H172 and a catalytically active water molecule as described in chapter 3.1.1 & 4.1.1. The reaction is exergonic ($E_{reaction}$ = -3.4 kcal/mol) and the activation barrier of the hydride transfer is E_a = 30.1 kcal/mol. The semi-empiric PM7 method implemented in MOPAC was used for calculation.

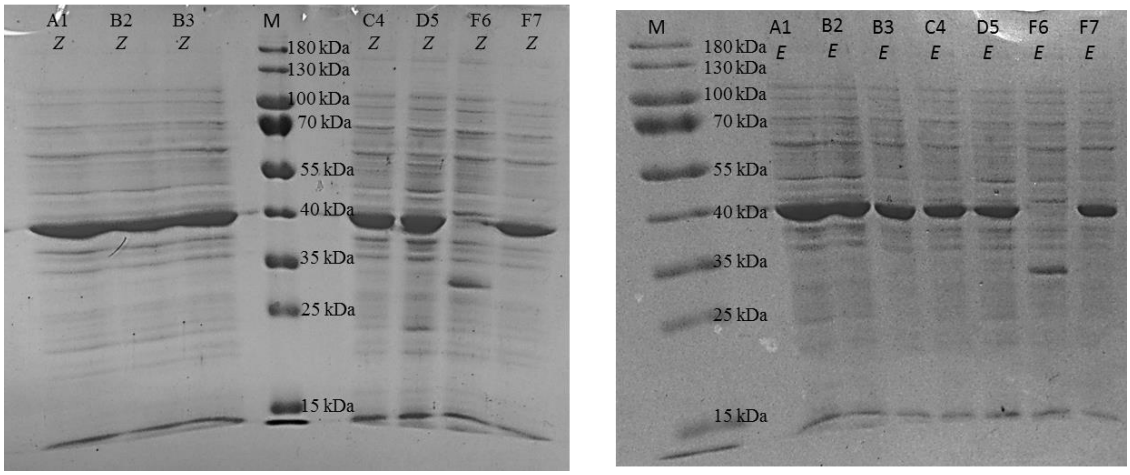

Figure Ap. 9: Evaluation of NCR ERED gene expression in 96-DWPs and comparison of plate duplicates by means of SDS-PAGE. The samples are derived from a site-saturation mutagenesis at position 231 using a degenerate NNK codon on the template NCR W66A. The denotations at individual bands correspond to the selected positions. Each plate consists of A to H rows and 1 to 12 lines. The plates were duplicates that were inoculated from a similar "preculture 96-DWP" and for SDS-PAGE samples from correspondent wells were taken. Denotations *Z* and *E* refer to the use of the duplicate plates for reduction screening of one of the two citral isomers. The chosen marker M indicates gene expression of a 40 kDa protein, which coincides with the protein weight of NCR ERED. The expression levels of both duplicates are similar. All well positions qualitatively display similar levels of gene expression. Position F6 contained an expressed gene with decreased weight due to the insertion of a stop codon.

Applicability of glycerol stocks

While setting up experiments to characterize obtained NCR hits, another noteworthy observation was made regarding the applicability of glycerol stocks for whole cell reactions (Figure Ap. 10). It proved to be necessary to freshly transform cells with respective ERED genes rather than inoculating media with a glycerol stock when intending to perform whole cell reactions. For whole cell reactions, product formation decreased about 10-fold when using glycerol stocks. However, purified EREDs from both cellular sources had essentially the same catalytic efficiencies.

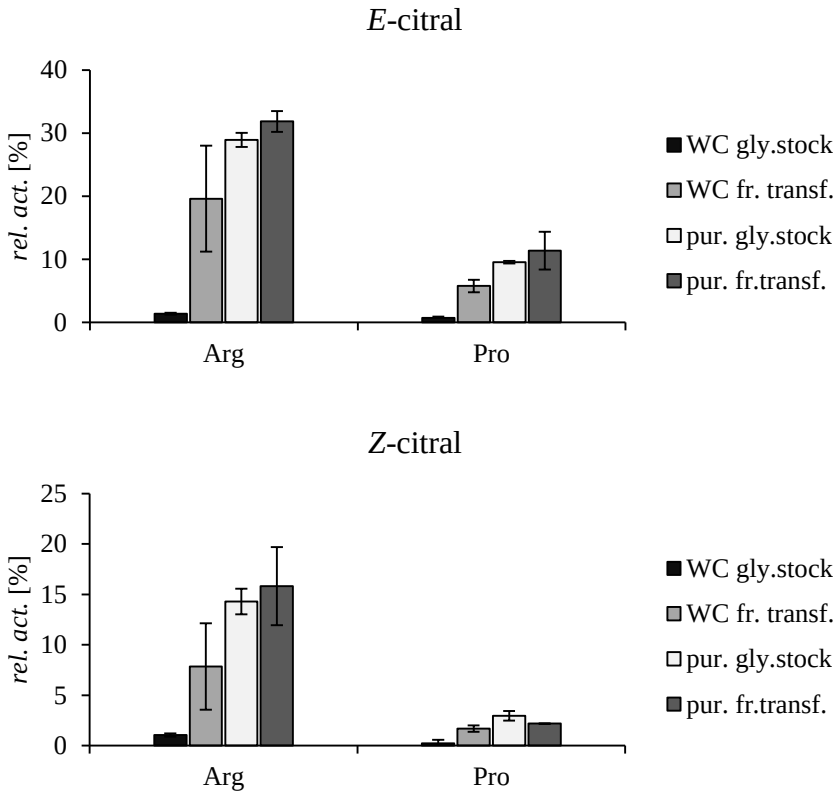

Figure Ap. 10: Comparison of whole cell (wc) reactions and reactions with purified enzymes (pur.) with enzymes derived from glycerol stock inoculated cells (gly. stock) or from inoculation with freshly transformed cells (fr. transf.). The data refers to the reduction of either *E*-citral (above) or *Z*-citral (below) by NCR ERED-derived triple variants Arg (W66A/I231R/F269V) and Pro (W66A/I231P/F269V). *E. coli* TG20+ whole cells were applied. All reactions were performed as reaction triplicates of biological duplicates for 4 h at 30 °C and 180 rpm according to chapters 2.4.1 and 2.4.2. The obtained relative activity (*rel*. *act*.) values refer to the relative product formation in comparison to the reduction of *Z*-citral by purified wild-type NCR ERED (derived from freshly transformed cells).

a)

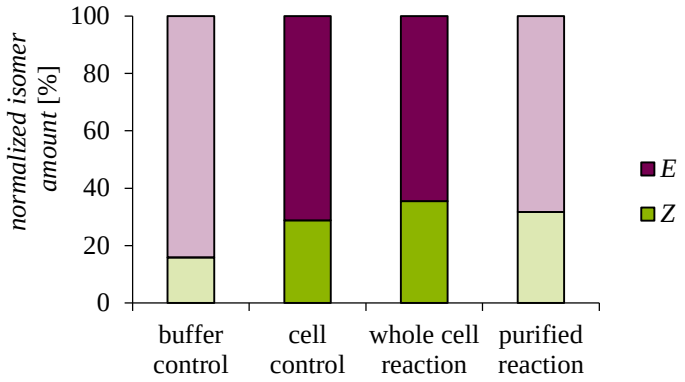

b)

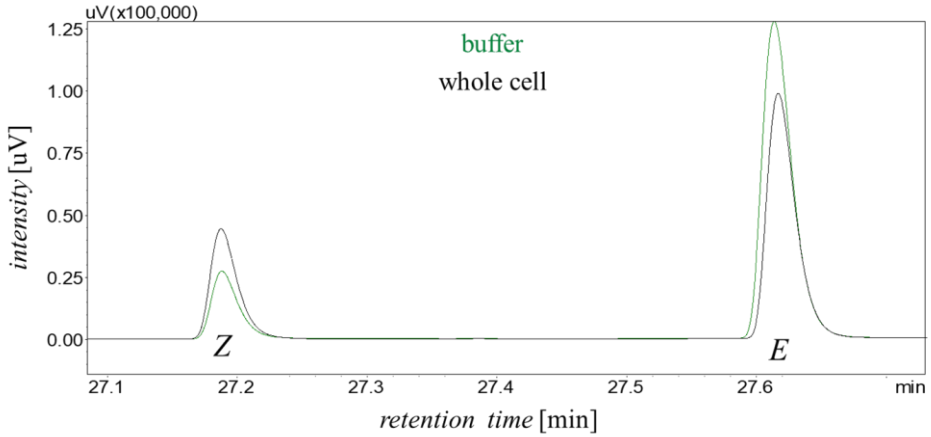

Figure Ap. 11: Control experiments with *E*-citral under reaction conditions. The whole cell and purified enzyme reactions using the NCR Arg variant (W66A/I231R/F269V) are compared to buffer control and cell control reactions with regard to the substrate citral. All samples were shaken for 4 h at 30 °C and 180 rpm. Buffer control refers to 12 mM citrate buffer pH 6 with 2 mM *E*-citral, 1 % (*v*/*v*) DMSO and 2.5 mM NADH added. Cell control refers to 5 g/L empty vector containing *E. coli* TG20+ cells resuspended in 50 mM MES/KOH pH 6.8 with 2 mM *E*-citral, 5 % (*v*/*v*) isopropanol and 2.5 mM NADH added. Controls did not contain ERED. a) Obtained percental normalized citral isomer amount highlights shifts in the proportion of *E* to *Z*. b) Overlay of control chromatograms focusing on *Z*-citral and *E*-citral peaks.

a) *E*-citral

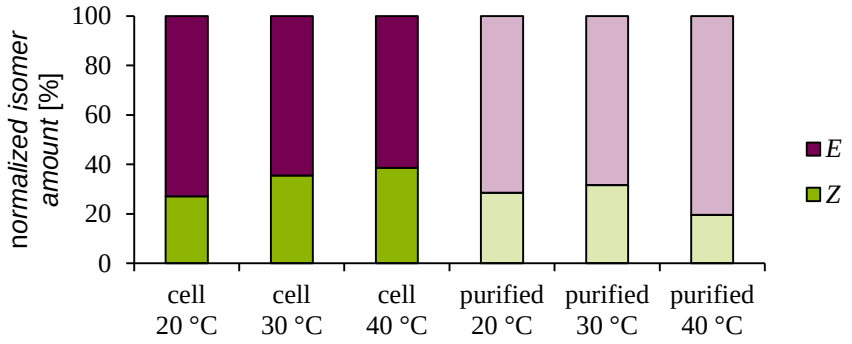

b) *Z*-citral

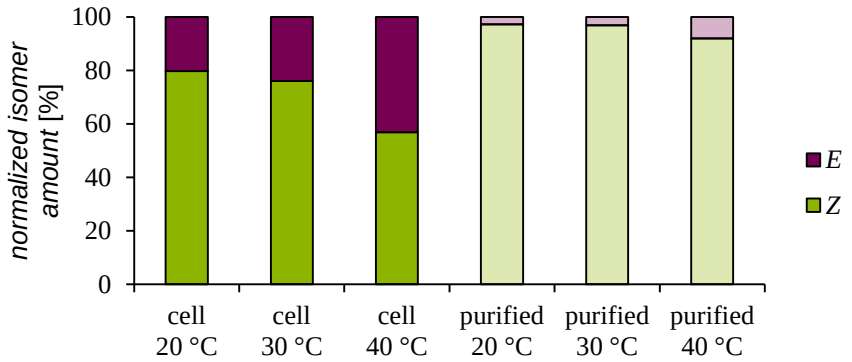

Figure Ap. 12: Temperature-dependent normalized proportion of citral isomers in the reduction of citral by NCR triple variants Arg (W66A/I231R/F269V) as whole cell or purified preparation at 20 °C, 30 °C and 40 °C. *E. coli* TG20+ whole cells were applied. All reactions were performed as reaction triplicates of biological duplicates for 4 h and 180 rpm according to chapters 2.4.1 and 2.4.2. Here, the obtained percental normalized citral isomer amount is shown to highlight shifts in the proportion of *E* to *Z*. a) Results for using *E*-citral in the reduction reactions. b) Results for using *Z*-citral in the reduction reaction.

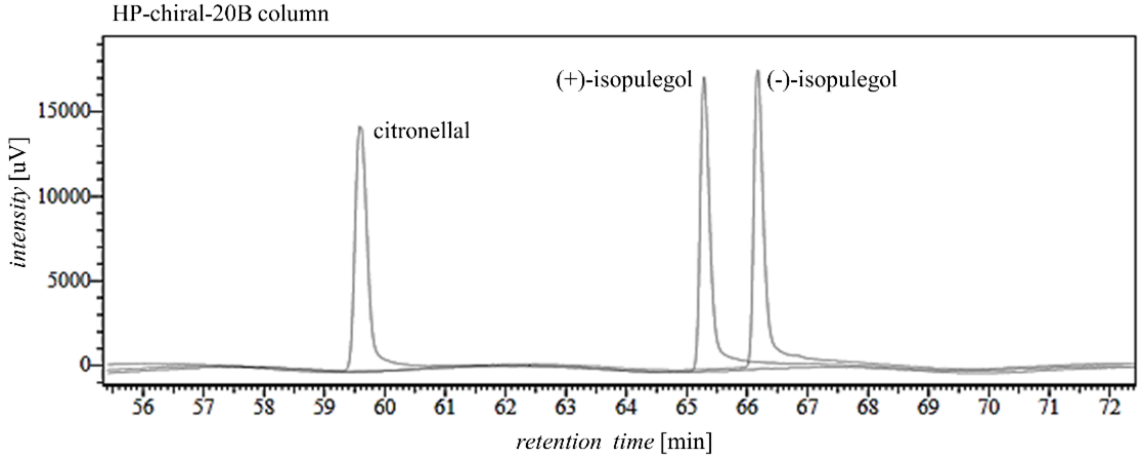

Figure Ap. 13: Gas chromatogram displaying peak positions and retention times for citronellal (59.58 min), (+)-isopulegol (65.29 min) and (-)-isopulegol (66.18 min) for chiral measurements on HP-chiral-20B column using an FID detector. The related method is described in chapter 2.6.1. The method was solely used to determine cyclase enantioselectivity. While enantioselective separation of isopulegol could be achieved, citronellal chirality remained unresolved under chosen conditions.

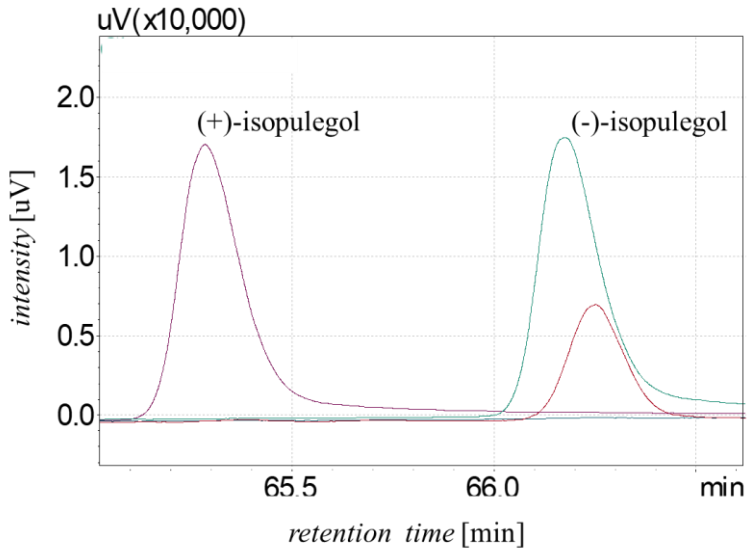

Figure Ap. 14: Test of *Aac*SHC variant A419G/Y420C/G600A specificity in the citronellal cyclization. Conversions of *S*-citronellal (blue baseline) and *R*-citronellal (red) with the *Aac*SHC variant were analyzed on a chiral HP-chiral-20B column. The possible isopulegol product was probed by comparison with standards for (+)-isopulegol (purple; 65.29 min) and (-)-isopulegol (green; 66.18 min).

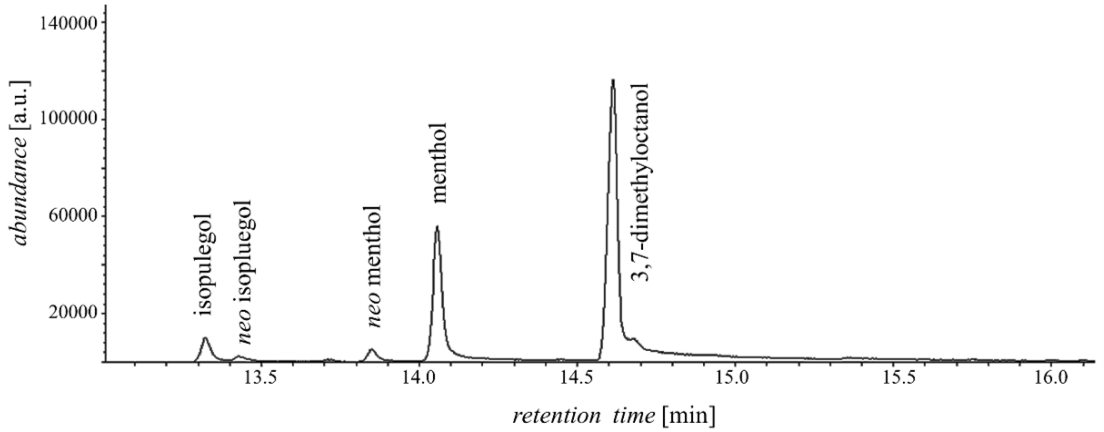

Figure Ap. 15: Chromatogram of isopulegol hydrogenation after 44 h as part of the preparative (-)-menthol synthesis. The hydrogenation reaction was performed as described in chapter 2.5. At the presented time point, a 250 µL sample were taken from the same reaction *via* a septum and extracted (chapter 2.4.6).

a) ^{1}H-NMR spectrum of isolated (-)-menthol in this work

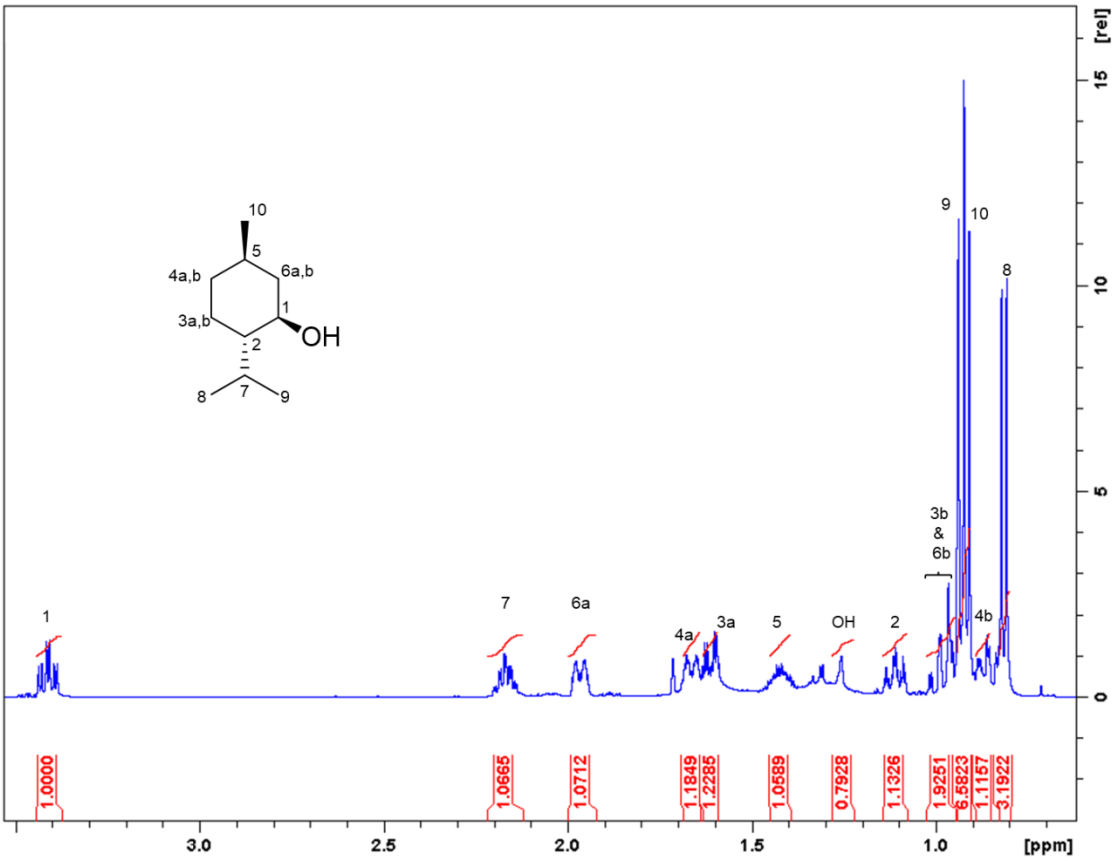

b) Reference literature ^{1}H-NMR spectrum of menthol

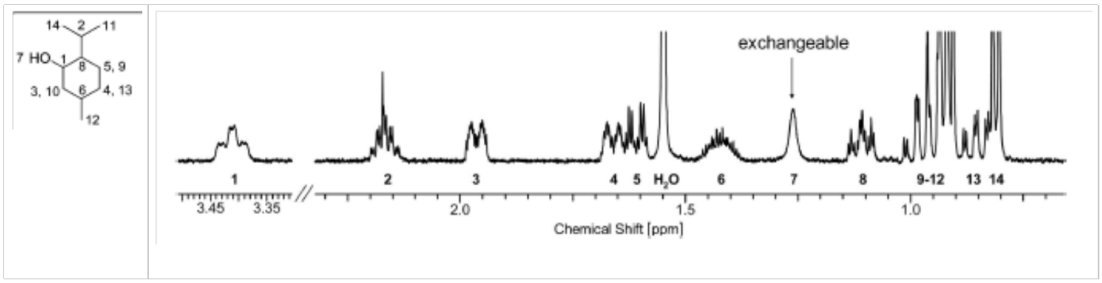

Figure Ap. 16: ^{1}H-NMR spectrum of (-)-menthol. a) Measured 500 MHz spectrum of (-)-menthol synthesized in this work. The protons are assigned accordingly. b) Reference spectrum from literature that was used to assign NMR peaks to protons.[154]

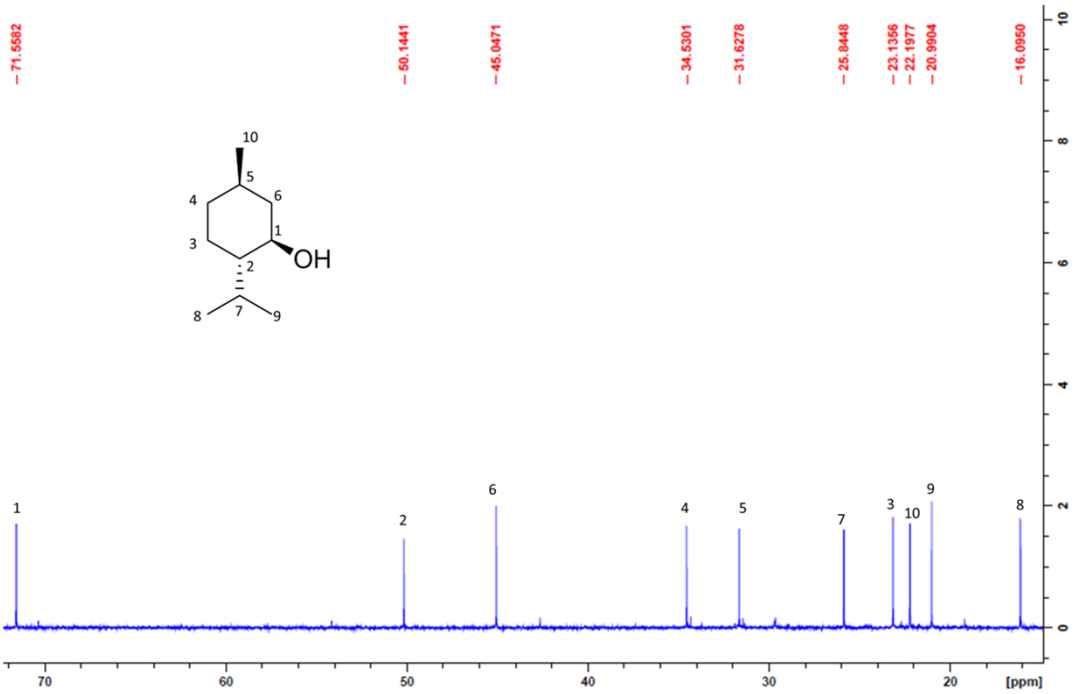

Figure Ap. 17: ^{13}C-NMR spectrum of (-)-menthol. Measured 126 MHz spectrum of (-)-menthol synthesized in this work. The peaks are assigned accordingly.

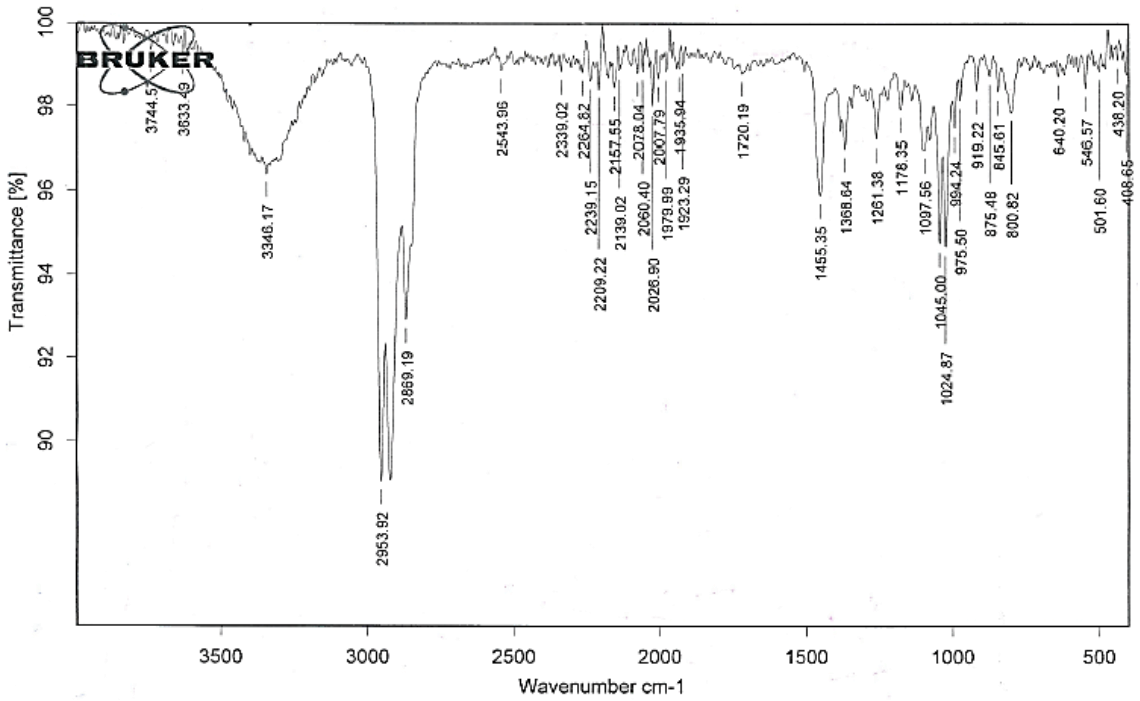

Figure Ap. 18: IR spectrum of isolated (-)-menthol as obtained from the chemoenzymatic cascade in this work.

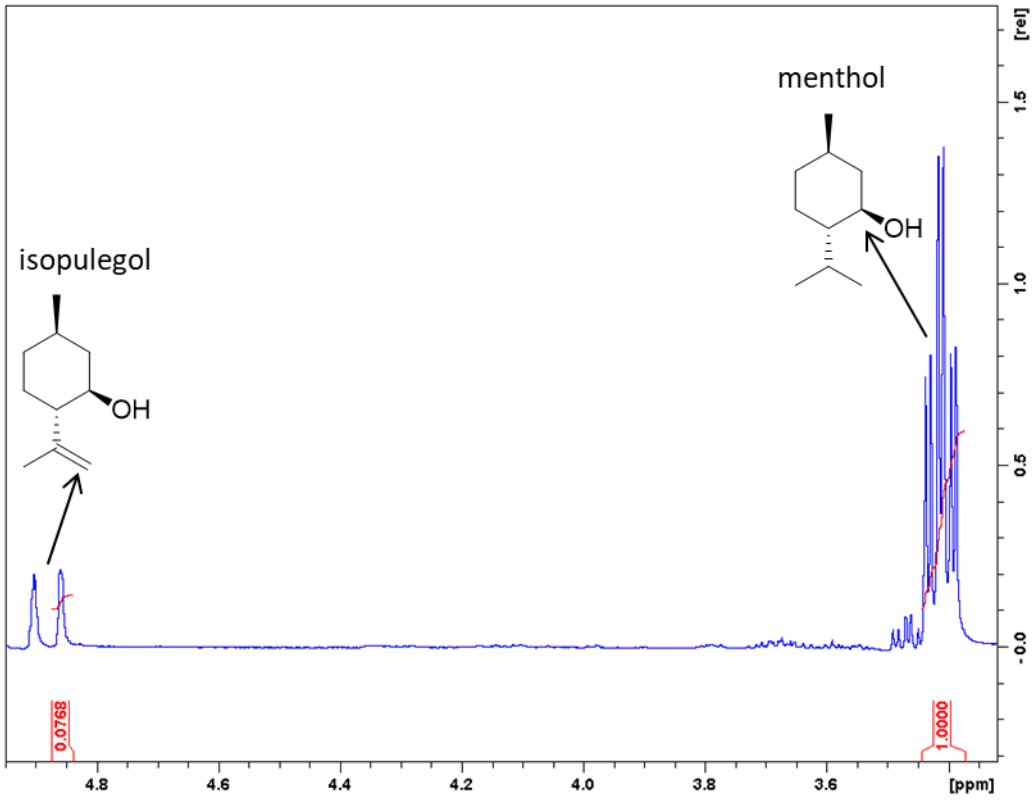

Figure Ap. 19: Quantification of isolated (-)-menthol by ^{1}H-NMR. Integration of the characteristic alkene shifts in (-)-isopulegol with the (-)-menthol proton signal adjacent to its hydroxyl group was used to quantify the purity of the isolated (-)- menthol.

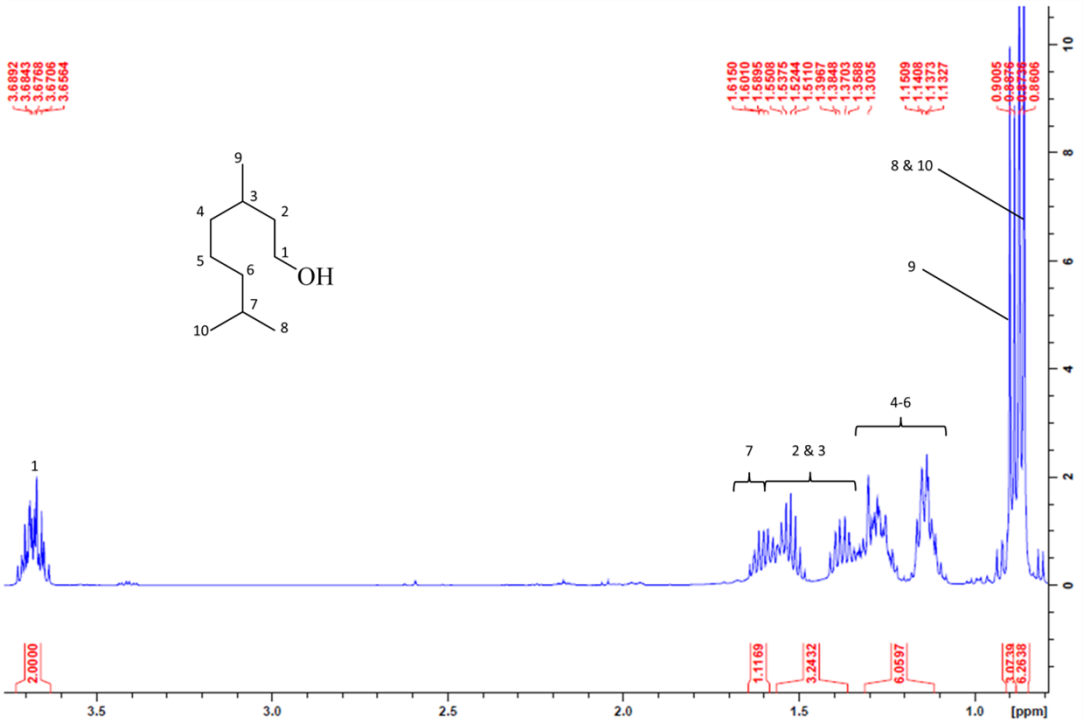

Figure Ap. 20: ^{1}H-NMR spectrum of 3,7-dimethyloctanol. Measured 500 MHz spectrum of 3,7-dimethyloctanol synthesized as byproduct in this work. The protons are assigned accordingly.

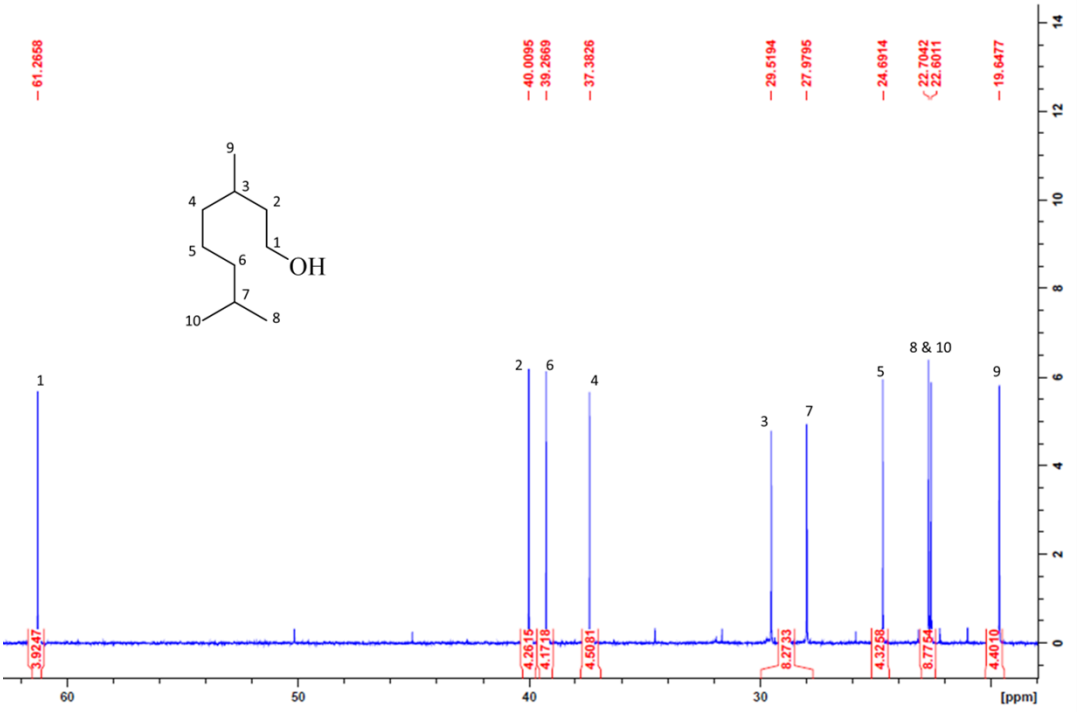

Figure Ap. 21: ^{13}C-NMR spectrum of 3,7-dimethyloctanol. Measured 126 MHz spectrum of 3,7-dimethyloctanol synthesized as byproduct in this work. The peaks are assigned accordingly.

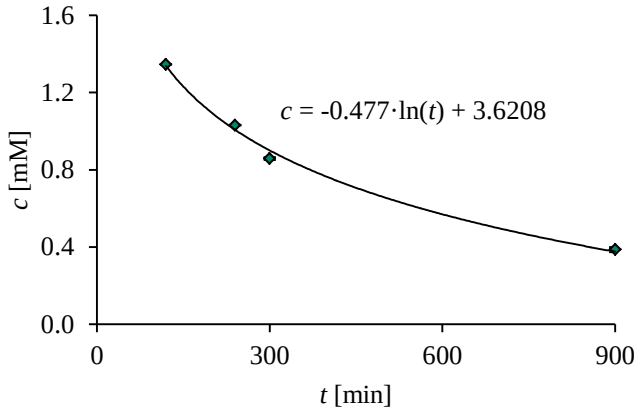

Figure Ap. 22: Citronellal decay from buffer solution in a closed vessel after complete reduction of *E*/*Z*-citral by NCR wild-type. The curve can for example be well fitted by logarithmic decay. Analytical reactions as described in chapter 2.4.1 were performed as triplicates for each displayed time point. The calculated concentrations *c* [mM] of citronellal are plotted against the time *t* [min].

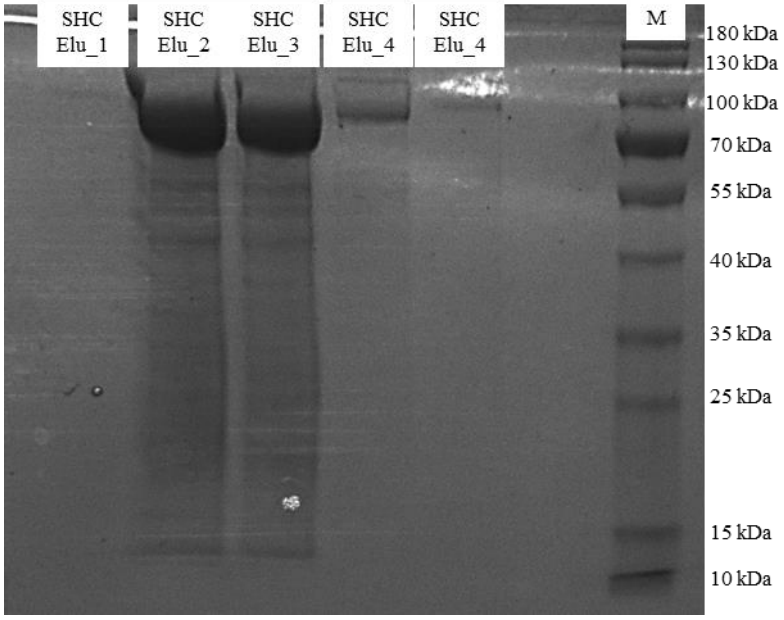

Figure Ap. 23: Exemplary developed SDS-PAGE gel of *Aac*SHC samples after heat-shock and ion exchange chromatography purification with protein marker M. In this example, the enrichment of *Aac*SHC variant A419G/Y420C/G600A at ~70 kDa in different consecutive 2 mL elution (Elu) fractions was visualized. It can be seen that the protein is enriched significantly, but still contains some residual protein impurities. The protein purity is estimated to be > 80 %.

Table Ap. 1: Screening results of *Zymomonas mobilis* NCR ERED active site single variants towards the reduction of either *E*-citral or *Z*-citral. Obtained enantiomeric excess *e.e.* and relative activity *rel. act.* values are depicted with respective standard deviation. All activities are calculated relative to the citronellal product formation resulted from the conversion of *Z*-citral by NCR wild-type. Purified enzymes were applied (chapter 2.4.1).

NCR variant	*Z*-citral		*E*-citral	
	***e.e.* [%]**	***rel. act.* [%]**	***e.e.* [%]**	***rel. act.* [%]**
wild-type	> 99 *S*	100 ± 4	> 99 *S*	86 ± 4
T25A	98.5 ± 0.3 *S*	16.71 ± 0.02	95 ± 2 *S*	9 ± 1
T25F	> 99 *S*	2.6 ± 0.1	18 ± 6 *S*	2.4 ± 0.1
A56G	> 99 *S*	56 ± 1	92 ± 1 *S*	30 ± 5
A56F	n.d.*	n.d.*	n.d.*	n.d.*
W66A	90.1 ± 0.4 *S*	94 ± 4	45.6 ± 0.2 *R*	92 ± 1
W66F	98.9 ± 0.2 *S*	104 ± 6	90.1 ± 0.4 *S*	98 ± 1
W100A	> 99 *S*	37 ± 4	> 99 *S*	11 ± 1
W100F	99.3 ± 0.2 *S*	93.423 ± 0.003	98.9 ± 0.1 *S*	57.79 ± 0.03
H128A	> 99 *S*	101 ± 1	> 99 *S*	88 ± 9
H128F	> 99 *S*	99 ± 3	> 99 *S*	86 ± 7
H172A	99.1 ± 0.2 *S*	80.69 ± 0.07	98.9 ± 0.2 *S*	34.747 ± 0.003
H172F	> 99 *S*	14 ± 1	86 ± 1 *S*	8 ± 1
N175A	> 99 *S*	4.7 ± 0.3	> 99 *S*	4.0 ± 0.2
N175F	> 99 *S*	10 ± 2	> 99 *S*	5 ± 1
Y177A	91 ± 1 *S*	54 ± 2	82 ± 2 *S*	53 ± 2
Y177W	89.3 ± 0.3 *S*	74 ± 2	93.5 ± 0.2 *S*	77 ± 1
I231A	> 99 *S*	82 ± 3	> 99 *S*	80 ± 2
I231F	> 99 *S*	11.7 ± 0.5	52 ± 2 *S*	7.9 ± 0.2
Q232A	> 99 *S*	87 ± 3	> 99 *S*	59 ± 1
Q232F	> 99 *S*	88 ± 4	92.4 ± 0.3 *S*	65 ± 3
R261A	> 99 *S*	81 ± 6	> 99 *S*	45 ± 1
R261F	> 99 *S*	29 ± 1	> 99 *S*	18 ± 1
F269A	> 99 *S*	80 ± 2	> 99 *S*	58 ± 1
F269W	> 99 *S*	87 ± 5	> 99 *S*	62 ± 2
W342A	> 99 *S*	84.5 ± 0.4	> 99 *S*	61 ± 4
W342F	> 99 *S*	54 ± 5	> 99 *S*	49 ± 7
Y343A	> 99 *S*	77 ± 5	> 99 *S*	46 ± 1
Y343W	n.d.*	n.d.*	n.d.*	n.d.*

*n.d.: not determined.

Table Ap. 2: Screening results of *Zymomonas mobilis* NCR ERED active site double variants based on the W66A single variant towards the reduction of either *E*-citral or *Z*-citral. Obtained enantiomeric excess *e.e.* and relative activity *rel. act.* values are depicted with respective standard deviation. All activities are calculated relative to the citronellal product formation resulted from the conversion of *Z*-citral by NCR wild-type. Purified enzymes were applied (chapter 2.4.1).

NCR variant	*Z*-citral		*E*-citral	
	***e.e.* [%]**	***rel. act.* [%]**	***e.e.* [%]**	***rel. act.* [%]**
wild-type	> 99 *S*	100 ± 3	> 99 *S*	86 ± 4
W66A/T25A	94.1 ± 0.4 *S*	30 ± 2	7 ± 1 *R*	13 ± 2
W66A/T25F	96 ± 1 *S*	19.5 ± 0.3	4 ± 1 *S*	15 ± 1
W66A/A56G	90 ± 0.1 *S*	54 ± 1	43 ± 1 *R*	46 ± 4
W66A/A56F	> 99 *S*	1.2 ± 0.2	> 99 *S*	0.5 ± 0.1
W66A/W100A	97 ± 1 *S*	13.21 ± 0.01	67.4 ± 0.2 *S*	3.72 ± 0.02
W66A/W100F	93.3 ± 0.4 *S*	124 ± 2	33.5 ± 0.3 *R*	123.8 ± 0.2
W66A/H128A	91 ± 1 *S*	99 ± 3	35 ± 1 *R*	80 ± 4
W66A/H128F	86.3 ± 0.1 *S*	101 ± 1	48.97 ± 0.04 *R*	89 ± 6
W66A/H172A	95.8 ± 0.1 *S*	13 ± 1	18 ± 1 *R*	6.7 ± 0.5
W66A/H172F	> 99 *S*	0.2 ± 0.1	29 ± 2 *R*	0.22 ± 0.03
W66A/N175A	88 ± 2 *S*	1.0 ± 0.1	63 ± 1 *R*	1.6 ± 0.1
W66A/N175F	> 99 *S*	1.2 ± 0.1	60 ± 3 *S*	0.6 ± 0.1
W66A/Y177A	n.d.*	n.d.*	n.d.*	n.d.*
W66A/Y177W	44 ± 2 *S*	61 ± 3	30 ± 1 *R*	39 ± 1
W66A/I231A	81.3 ± 0.5 *S*	66 ± 3	63 ± 1 *R*	66 ± 2
W66A/I231F	92 ± 2 *S*	81 ± 4	37 ± 1 *R*	73 ± 2
W66A/Q232F	86.6 ± 0.5 *S*	86 ± 2	43.4 ± 0.2 *R*	73 ± 3
W66A/R261A	93.4 ± 0.4 *S*	32 ± 4	15 ± 4 *R*	24 ± 3
W66A/R261F	96 ± 1 S	10 ± 2	30 ± 1 *R*	5 ± 1
W66A/F269A	82.2 ± 0.5 *S*	78 ± 1	56.0 ± 0.1 *R*	71 ± 1
W66A/F269W	86.0 ± 0.2 *S*	82 ± 2	45.3 ± 0.3 *R*	71.3 ± 0.3
W66A/W342A	88 ± 1 *S*	83 ± 2	41 ± 1 *R*	67 ± 2
W66A/W342F	86.8 ± 0.2 *S*	87 ± 1	38.8 ± 0.1 *R*	73 ± 1
W66A/Y343A	98.6 ± 0.1 *S*	42 ± 3	14 ± 4 *S*	27 ± 5
W66A/Y343W	n.d.*	n.d.*	n.d.*	n.d.*

*n.d.: not determined.

Table Ap. 3: Screening results of *Zymomonas mobilis* NCR ERED W66A site-saturation variants towards the reduction of either *E*-citral or *Z*-citral. Obtained enantiomeric excess *e.e.* and relative activity *rel. act.* values are depicted with respective standard deviation. All activities are calculated relative to the citronellal product formation resulted from the conversion of *Z*-citral by NCR wild-type. Purified enzymes were applied (chapter 2.4.1).

NCR variant	*Z*-citral		*E*-citral	
	***e.e.* [%]**	***rel. act.* [%]**	***e.e.* [%]**	***rel. act.* [%]**
wild type	> 99 *S*	100 ± 3	> 99 *S*	86 ± 4
W66Y	99.2 ± 0.1 *S*	107.8 ± 0.4	95.07 ± 0.03 *S*	101 ± 3
W66F	98.9 ± 0.2 *S*	104 ± 6	90.1 ± 0.4 *S*	98 ± 1
W66R	> 99 *S*	65 ± 1	98.48 ± 0.05 *S*	46.0 ± 0.5
W66M	99.38 ± 0.03 *S*	112 ± 3	93.0 ± 0.1 *S*	89 ± 2
W66K	> 99 *S*	25.0 ± 0.3	99.0 ± 0.5 *S*	19 ± 1
W66H	99.78 ± 0.05 *S*	100 ± 1	82.37 ± 0.04 *S*	80 ± 1
W66L	98.96 ± 0.04 *S*	107 ± 1	85.1 ± 0.1 *S*	74 ± 1
W66I	99.2 ± 0.1 *S*	105 ± 1	68.5 ± 0.1 *S*	75 ± 9
W66Q	98.85 ± 0.01 *S*	108 ± 2	86.45 ± 0.01 *S*	87 ± 2
W66E	> 99 *S*	102 ± 2	94.3 ± 0.1 *S*	74 ± 1
W66V	98.97 ± 0.09 *S*	94 ± 3	36.7 ± 0.3 *S*	62 ± 2
W66N	99.06 ± 0.04 *S*	112 ± 1	86.97 ± 0.03 *S*	86 ± 3
W66P	> 99 *S*	2.47 ± 0.08	83 ± 2 *S*	1.09 ± 0.01
W66T	95.39 ± 0.07 *S*	96 ± 5	18.4 ± 0.1 *S*	89 ± 1
W66D	> 99 *S*	90 ± 10	93.6 ± 0.2 *S*	61 ± 1
W66C	95.48 ± 0.1 *S*	110 ± 2	42 ± 3 *S*	81 ± 2
W66S	95.61 ± 0.2 *S*	108 ± 2	37.4 ± 0.4 *S*	86 ± 2
W66A	90.1 ± 0.4 *S*	94 ± 4	45.6 ± 0.2 *R*	92 ± 1
W66G	87.5 ± 0.2 *S*	112 ± 3	41.0 ± 0.2 *R*	92 ± 2

Table Ap. 4: Comparison of *Z*-citral and *E*-citral conversions by purified NCR and OYE1 wild-types. Reactions were performed for 2.5 h under conditions described in chapter 2.4.1. However, no standard was added to the extraction solvent and the product formations were determined by percental comparison of educt and product peak area. For comparison, NCR and OYE1 conversions in whole cell reactions are depicted in Figure 38.

	***product formation* [%]**	
	***Z*-citral**	***E*-citral**
NCR WT	97.4 ± 0.3	94 ± 4
OYE1 WT	0.76 ± 0.02	2.6 ± 0.8

Table Ap. 5: Screening results of iterative site-saturation libraries for the NCR ERED-catalyzed reduction of *E*- and *Z*-citral. Enantiomeric excess *e.e.* and relative activity *rel. act.* values of selected hit variants are presented. Relative activity values were calculated by comparison to the highest obtained citronellal peak area within one screening (including both citral isomers). Occurrence frequency of amino acids and number of inactive variants in one screen is stated. Where possible, standard deviations were calculated.

occurrence frequency	NCR variant	*Z*-citral		*E*-citral	
		***e.e.* [%]**	***rel. act.* [%]**	***e.e.* [%]**	***rel. act.* [%]**
W66A/I231X		inactive: 18			
6x	I231P	27 ± 6 *R*	36 ± 15	89.5 ± 2.1 *R*	46 ± 6
3x	I231R	39 ± 4 *S*	50 ± 3	80 ± 4 *R*	57 ± 13
2x	I231W	2 ± 5 *R*	8.3 ± 2.5	90 ± 3 *R*	3.7 ± 1.2
2x	I231Y	25 ± 4 *S*	43 ± 4	81.8 ± 0.4 *R*	61.3 ± 2.1
1x	I231K	34 *S*	26	65 *R*	29
1x	I231D	33 *S*	47	80 *R*	67
1x	I231H	47 *S*	78	80 *R*	50
1x	I231L	99 *S*	29	95 *S*	32
W66A/Y177X		inactive: 34			
3x	Y177A	14 ± 11 *R*	4.5 ± 0.6	70.4 ± 0.6 *R*	8.7 ± 2.0
3x	Y177T	15 ± 12 *R*	6 ± 4	80 ± 5 *R*	8.4 ± 3.0
2x	Y177N	0 ± 9 *R*/*S*	5.6 ± 2.9	66.5 ± 1.6 *R*	7.2 ± 2.8
2x	Y177H	36 ± 5 *S*	15 ± 8	70.9 ± 0.7 *R*	32 ± 4
2x	Y177D	21 ± 20 *R*	1.4 ± 1.4	75 ± 8 *R*	3.4 ± 1.2
1x	Y177M	58 *S*	5	53 *R*	21
1x	Y177C	18 *R*	7	70 *R*	9
W66A/F269X		inactive 2			
2x	F269S	74.4 ± 0.4 *S*	75 ± 13	60.10 ± 0.20 *R*	40 ± 6
2x	F269C	68 ± 10 *S*	63 ± 23	60.3 ± 0.7 *R*	39 ± 4
2x	F269L	71.20 ± 0.12 *S*	57 ± 10	61.6 ± 0.4 *R*	71 ± 5
1x	F269K	74 *S*	70	60 *R*	59
1x	F269V	71 *S*	54	63 *R*	76.8
1x	F269G	54 *S*	71	50 *R*	68
W66A/I231P/F269X		inactive: 28			
2x	F269V	72.0 ± 1.5 *R*	32 ± 4	95.6 ± 0.6 *R*	43 ± 8
1x	F269H	71 *R*	14	96 *R*	46
1x	F269Q	72 *R*	40	94 *R*	40
1x	F269P	74 *R*	20	92 *R*	43
1x	F269Y	73 *R*	33	95 *R*	40
W66A/I231P/Y177X		inactive: 129			
1x	Y177R	75 *R*	3	91 *R*	5
1x	Y177K	53 *R*	17	94 *R*	40
1x	Y177F	51 *R*	13	91 *R*	17
W66A/F269V/I231X		inactive: 15			
4x	I231R	64 ± 8 *R*	28 ± 3	92.9 ± 0.6 *R*	45 ± 13
5x	I231P	63 ± 3 *R*	15 ± 5	92.7 ± 0.9 *R*	24.5 ± 2.0
W66A/F269V/I231P/Y177X		inactive: 91			
1x	Y177D	55 *R*	38	96 *R*	56

Table Ap. 6: List of the 20 canonical proteinogenic amino acids with respective 3-letter and 1-letter code abbreviations.

amino acid	3-letter code	1-letter code	amino acid	3-letter code	1-letter code
alanine	Ala	A	leucine	Leu	L
arginine	Arg	R	lysine	Lys	K
asparagine	Asn	N	methionine	Met	M
aspartic acid	Asp	D	phenylalanine	Phe	F
cysteine	Cys	C	proline	Pro	P
glutamine	Gln	Q	serine	Ser	S
glutamic acid	Glu	E	threonine	Thr	T
glycine	Gly	G	tryptophan	Trp	W
histidine	His	H	tyrosine	Tyr	Y
isoleucine	Ile	I	valine	Val	V